

RTD-TDR-63-3096, Vol. II

RTI
63
Y

AD 627597

DESIGN PROCEDURES FOR SHOCK ISOLATION SYSTEMS OF UNDERGROUND PROTECTIVE STRUCTURES

Volume II

Structure Interior Motions Due to Directly Transmitted Ground Shocks

F. Finlayson
L. E. Fugelson
Y. Shulman

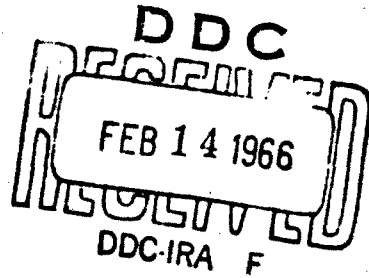
**General American Transportation Corporation
Niles, Illinois
Contract AF29(601)-6253**

TECHNICAL REPORT NO. RTD-TDR-63-3096, Volume II

December 1965

AIR FORCE WEAPONS LABORATORY
Research and Technology Division
Air Force Systems Command
Kirtland Air Force Base
New Mexico

20050323149



RTD-TDR-63-3096, Vol. II

Research and Technology Division
AIR FORCE WEAPONS LABORATORY
Air Force Systems Command
Kirtland Air Force Base
New Mexico

When U. S. Government drawings, specifications, or other data are used for any purpose other than a definitely related Government procurement operation, the Government thereby incurs no responsibility nor any obligation whatsoever, and the fact that the Government may have formulated, furnished, or in any way supplied the said drawings, specifications, or other data, is not to be regarded by implication or otherwise, as in any manner licensing the holder or any other person or corporation, or conveying any rights or permission to manufacture, use, or sell any patented invention that may in any way be related thereto.

This report is made available for study with the understanding that proprietary interests in and relating thereto will not be impaired. In case of apparent conflict or any other questions between the Government's rights and those of others, notify the Judge Advocate, Air Force Systems Command, Andrews Air Force Base, Washington, D. C. 20331.

Distribution of this document is unlimited.

REVISIONS TO	
SPRT	WHITE SECTION <input checked="" type="checkbox"/>
SRS	BUFF SECTION <input type="checkbox"/>
UNAMENDED	
JULY 1970	
FMS	
DISTRIBUTION/AVAILABILITY CODES	
DIR.	AVAIL AND/or SPECIAL
/	

RTD TDR 63-3096, Vol. II

DESIGN PROCEDURES FOR SHOCK ISOLATION SYSTEMS
OF UNDERGROUND PROTECTIVE STRUCTURES

Volume II

Structure Interior Motions Due to Directly Transmitted Ground Shock

F. Finlayson

L. E. Fugelso

Y. Shulman

General American Transportation Corporation
Niles, Illinois
Contract AF29(601)-6253

TECHNICAL REPORT NO. RTD TDR 63-3096, Volume II

Distribution of this document
is unlimited.

FOREWORD

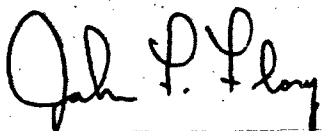
This report was prepared by the General American Transportation Corporation, MRD Division, Niles, Illinois, under Contract AF29(601)-6253. The work was performed under Program Element 7.60.06.01.5, Project 5710, Subtask 13.167, and was funded by the Defense Atomic Support Agency (DASA). Inclusive dates of research were November 1963 to January 1965. The report was submitted 12 November 1965 by the AFWL Project Officer, Lt John F. Flory (WLDC).

This report is one of five volumes presenting the results of a series of studies carried out by General American Transportation Corporation and Newmark, Hansen and Associates. The five volumes are organized as follows:

- Vol. I Structure Interior Motions Due to Air Blast Induced Ground Shock
- Vol. II Structure Interior Motions due to Directly Transmitted Ground Shock
- Vol. III Response Spectra of Single-Degree-of-Freedom Elastic and Inelastic Systems
- Vol. IV Response Spectra of Two-Degree-of-Freedom Elastic and Inelastic Systems
- Vol. V Response Spectra of Multi-Degree-of-Freedom Elastic Systems

The authors wish to thank Mr. M. R. Johnson for his guidance throughout the project and Mr. A. A. Arentz, Jr., for his criticism of the work and this report. Mr. R. K. Waddick was responsible for the computer program.

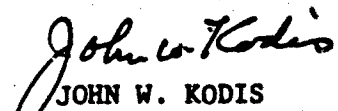
This report has been reviewed and is approved.



JOHN F. FLORY
1Lt USAF
Project Officer



FREDRICK W. KORFICZ, JR.
Lt Colonel, USAF
Chief, Civil Engineering Branch



JOHN W. KODIS
Colonel USAF
Chief, Development Division

ABSTRACT

This volume presents a method for estimating the motions on the interior of a buried cylindrical shell resulting from directly-induced ground shock caused by the detonation of a nuclear device to aid in the preliminary design of shock isolation equipment.

Various theoretical models for calculating the free-field waveform are reviewed and the acoustic model is recommended for this purpose. The reasons for this recommendation are enumerated and the methods for applying it are given. Methods for solving the structure-medium-interaction problem are discussed and the normal-mode analysis of the response of an elastic cylindrical shell in an acoustic medium to a specified input pulse is reviewed in detail.

A discussion of ranges of parameters appropriate to realistic problems is included. A thorough explanation of the results of computer solutions for the shell response is presented, and a large number of graphs illustrating the results are included. The results are analyzed to determine the relative influence of the parameters on interior shell motion.

The application of the method developed is explained and illustrated by sample problems. An appendix contains a Duhamel-integral computer program that can be used to generate results for cases not included in this volume. ()
↑

This page intentionally left blank.

CONTENTS

<u>Section</u>		<u>Page</u>
1	INTRODUCTION	1
1.1	Objectives	1
1.2	Method of Approach	2
1.3	Recommendations for the Shock-Isolation Engineer	3
1.4	Recommendations for Future Work	5
2	FREE-FIELD MOTION	6
2.1	Theoretical Prediction of Ground Motion	9
2.2	Empirical Data	20
2.3	Calculation of Free-Field Waveform in the Directly Transmitted Ground Shock Region	22
3	STRUCTURE-MEDIUM-INTERACTION ANALYSIS	25
3.1	Methods for Solving the Structure-Medium- Interaction Problem	25
3.2	Normal Mode Analysis of the Response of an Elastic Cylindrical Shell in an Acoustic Medium to a Specified Input Pulse	31
3.3	Parameters	33
4	DISCUSSION OF RESULTS	41
4.1	Shell Response to Step-Wave Input	43
4.2	Response to Rectangular Pulse	50
4.3	Response to Exponentially Decaying Pulse	65
4.4	Summary of Shell Response to Step, Rectangular and Exponentially-Decaying Pulses	69
4.5	General Response to Change in Shell and Medium Properties for Other Waveshapes	70

CONTENTS (Continued)

<u>Section</u>	<u>Page</u>
4.6 Influence of Variations in Waveform on Response for Given Medium and Shell Properties	72
4.7 Ranking of Parameters	83
4.8 Influence of Deviations in Parametric Values on Shell Response	89
5 DESIGN METHODS FOR ESTIMATING STRUCTURE MOTION IN DIRECTLY-TRANSMITTED REGION	177
5.1 Selection of Pulse Shape	177
5.2 Parametric Values	178
5.3 Estimation of Response	179
5.4 Numerical Example	181
APPENDIX A - DUHAMEL INTEGRAL COMPUTER PROGRAM	191
APPENDIX B - TERMINAL VELOCITIES OF RIGID-BODY-MODE RESPONSE	193
REFERENCES	195

SYMBOLS

B	= bulk modulus of medium = $\rho_m c^2$
c	= longitudinal wave velocity or acoustic velocity in medium
E	= $\frac{E_s}{1 - \nu^2}$
E_s	= Young's modulus of shell material
F	= point force divided by 2π
$f()$	= function of ()
g	= acceleration due to gravity
\tilde{g}_n	= assumed constant coefficient (see Ref. 21)
H	= shell thickness to radius ratio = h/R
h	= shell thickness
$I_{n\theta}(z)$	= incomplete modified Bessel function of the first kind $= \frac{1}{\pi} \int_0^{\tilde{\theta}} \cos n\theta e^z \cos d\theta \dots \text{ for } \tau \leq 2$ $I_n(z)$ - complete Bessel function . . . for $\tau \geq 2$
L	= range distance = $(r^2 + \zeta^2)^{1/2}$ (see Figure 4)
l	= dimensionless pulse length = $\frac{X}{R}$
m	= mass per unit area of shell
m_n	= $(\frac{l + n^2}{2}) m$
n	= mode number
P	= pressure in the medium
P_o	= pressure amplitude in the medium (see Figures 10 and 11)
P_i	= defined in Figures 10 and 11

Q_n	= dimensionless modal displacement = $\frac{q_n}{q_{st}}$
$Q_{elastic}$	= dimensionless root-mean-square value of displacement
$\tilde{Q}_{elastic}$	= dimensional value of $Q_{elastic}$
Q_{total}	= total displacement = $Q_{elastic} + Q_1$
$(Q_1)_{T=2}$	= dimensionless first mode displacement at $T=2$
q_n	= dynamic deflection of the nth mode
q_{st}	= zeroeth mode static displacement of shell = $\frac{PR}{EH_s}$
R	= radius of shell
r	= radial coordinate
t	= time
t_A	= time of arrival of front of pulse
t_B	= time of arrival of back of pulse
u	= particle velocity in the medium
V_n	= dimensionless modal velocity = $\frac{dq_n}{d\tau}$
$V_{elastic}$	= dimensionless root-mean-square value of velocity
$\tilde{V}_{elastic}$	= dimensional values of $V_{elastic}$
V_n peak	= peak value of V_n
V_{total}	= total velocity = $V_{elastic} + V_1$
W	= yield of weapon in megatons
X	= pulse length (see Figure 9)
x_1	= defined in Figure 9
x_2	= defined in Figure 9
z	= complex root
β	= decay rate of exponentially decaying wave = $\frac{5}{l}$

γ	= decay factor = $\frac{\sigma_n}{2}$
δ	= Dirac delta function
ζ	= vertical coordinate in the medium (see Figure 4)
θ	= angular coordinate
$\tilde{\theta}$	= $\cos^{-1} (1 - \tau)$
λ	= ct
μ	= density ratio of shell to medium = $\frac{\rho_s}{\rho_m}$
ν	= Poisson's ratio
ξ_n	= dimensionless parameter = $\frac{m_n}{\rho_m R}$
ρ	= mass density
σ_n	= dimensionless parameter = $\frac{E}{B} H^3 \frac{(1 - n^2)^2}{12}$
τ	= dimensionless time parameter = $\frac{ct}{R}$
Ω	= $\frac{1}{2} \sqrt{l_4 \sigma_n \tilde{g}_n - \sigma_n^2}$

I subscript =	incident
m subscript =	medium
n subscript =	mode
p subscript =	peak in medium
R subscript =	radiated or reflected
r subscript =	radial of shell
s subscript =	shell
ζ subscript =	vertical in medium

This page intentionally left blank.

SECTION I

INTRODUCTION

This is the second volume of a five-volume work directed toward the improvement of design procedures for shock-isolation systems for underground protective structures. Volume I dealt with motions imparted to the interior of a structure by the air-blast-induced ground shock from a nuclear detonation. This volume deals with the region where the ground motions transmitted directly from the crater predominate over the air-blast-induced motions.

Motions appearing at the interior of an underground protective structure are predicted. They may be used as inputs to the response spectra given in Volumes III, IV, and V for the design of specific shock isolation systems.

In comparison with the state of knowledge of air-induced ground shock, there is a decided lack of empirical data concerning directly-induced ground shock. For this reason, the program reported herein was more analytic than its predecessor.

1.1 Objectives

The objectives of the program reported in this volume were threefold. The first was to establish the relation between arbitrary free-field ground motions and motions which appear at the interior of an underground protective structure. The second objective was to rank the site, weapon, and dynamic-structure-medium-interaction parameters which influence the interior motions of a structure in order of their physical importance. The third objective

was to develop preliminary design methods for estimating shock-isolation requirements based on the most important parameters.

1.2 Method of Approach

The first effort was the study of directly-induced ground motion. The results of this portion of the study are reported in Section 2. Existing theories of predicting the free-field motions caused by directly transmitted ground shock were reviewed in terms of consideration of physical aspects of the problem, input-data requirements, computation difficulties, and applicability of the end product as input to the next phase. The theories were compared on these bases, and the best approach for this program was chosen.

The next phase of the program was to determine the best method for predicting interior structure motions since these are the input required by the designer to estimate shock-isolation requirements. Interior motions will be due to both the free-field motions of the surrounding medium and the motions caused by the structure-medium interaction. In this study, it was of particular importance to compare the motions of each of these phenomena. Prediction of structure motion was obtained by means of an existing structure-medium interaction solution which was selected from several that were studied. This solution was extended for application to the problems peculiar to this study. The selection of the method was based on considerations of ease of computation and ability to give physical insight to the

structure motion. The structural configuration chosen for the program was a horizontal cylinder, because it appeared to be more universally applicable to existing or planned structure shapes than any other.

The ranges of the parameters pertinent to the problem were then chosen on the bases of the physical aspects of the problem and the limitations of the solution. A computer program was then prepared and a large number of cases was run. The results were then plotted, compared, and evaluated. Based on this evaluation, the parameters were ranked according to their relative importance in influencing interior shell motion. The effects of errors in estimating these parameters on the shell motion were also considered. The presentation of this portion of the program is contained in Sections 3 and 4.

Section 5 presents preliminary design methods for estimating shock-isolation requirements and includes numerical examples illustrating application of the method.

1.3 Recommendations for the Shock-Isolation Engineer

The shock-isolation engineer is concerned with the design of a system which will both support an item in a structure and mitigate the shock motions between the point of support on the structure and the item. The first step in the design of a shock-isolation system is to predict the input motions on the wall of the structure at points where the shock isolation system is to be attached.

Techniques for predicting the displacement and velocity histories are presented in this report. They show that the most important displacement which must be considered is the free-field displacement of the medium surrounding the structure, as this is practically identical to the first mode or "rigid-body" displacement of the structure. In most situations, this displacement will far exceed the deformational displacements caused by the stress-wave interaction with the shell. (In the case of the cylinder, these displacements are the zeroeth, second, third, etc., modes.) Therefore, the shock-isolation engineer should pay particular attention to the free-field displacement caused by the directly-transmitted ground-shock wave.

The input-velocity history must also be considered in the design of a shock-isolation system. In this study, it has been found that the peak input velocities due to the first or rigid-body displacement mode and the structure-deformation modes are comparable. Therefore, when considering the effect of the input velocity on the design of a shock-isolation system, both the rigid-body and deformational modes of the structure should be carefully studied.

Once the input motions on the wall of the structure have been predicted, the response spectra presented in Volumes III, IV, and V may be used to determine shock-isolation requirements for items within the structure. These response spectra are for one-and-two degree-of-freedom elastic and inelastic systems and multi-degree-of-freedom elastic systems. Responses to several

different input waveforms are included in these volumes. The input waveform which most closely corresponds to the input motions predicted by the methods outlined in this report should be used.

1.4 Recommendations for Future Work

The results presented in this study should be considered as an interim guide to the prediction of motions which must be considered in the design of shock-isolation systems. There are two reasons for this. First, the formulas for predicting free-field motions from a surface explosion which are presented in this report are based on an acoustic model for the medium. It is to be expected that work now in progress and future research will yield improved predictions of directly-transmitted ground shock caused by surface nuclear explosions.

The second reason is that only one class of structure-medium interaction problems is considered in this report, namely that of the circular cylindrical shell with an acoustic medium. It was chosen because it is the only class of interaction problem studied thus far which lends itself to the convenient calculation of motions using a wide variation of parameters. It is recommended that interaction analyses be conducted for additional models of the medium and for different types of structures. Structural types should include circular cylinders with soft liners between the medium and structure. Also other structural shapes such as the sphere should be studied. The elastic medium is the type of medium which should be considered next.

SECTION 2

FREE-FIELD MOTION

Specification of the free-field ground motion caused by a nuclear burst is prerequisite to the determination of the motions of a structure placed in the soil. For this study, the ground motion has been estimated for the regions where the directly transmitted ground shock predominates over the air-induced ground shock.

When a nuclear device is exploded at the surface or slightly above the surface of the earth, a crater is formed. The typical crater consists of a hole in the ground and highly-fractured and permanently-deformed regions in the soil surrounding this hole. Figure 1 shows a typical crater from a 1-MT surface burst. This figure represents a description of the residual

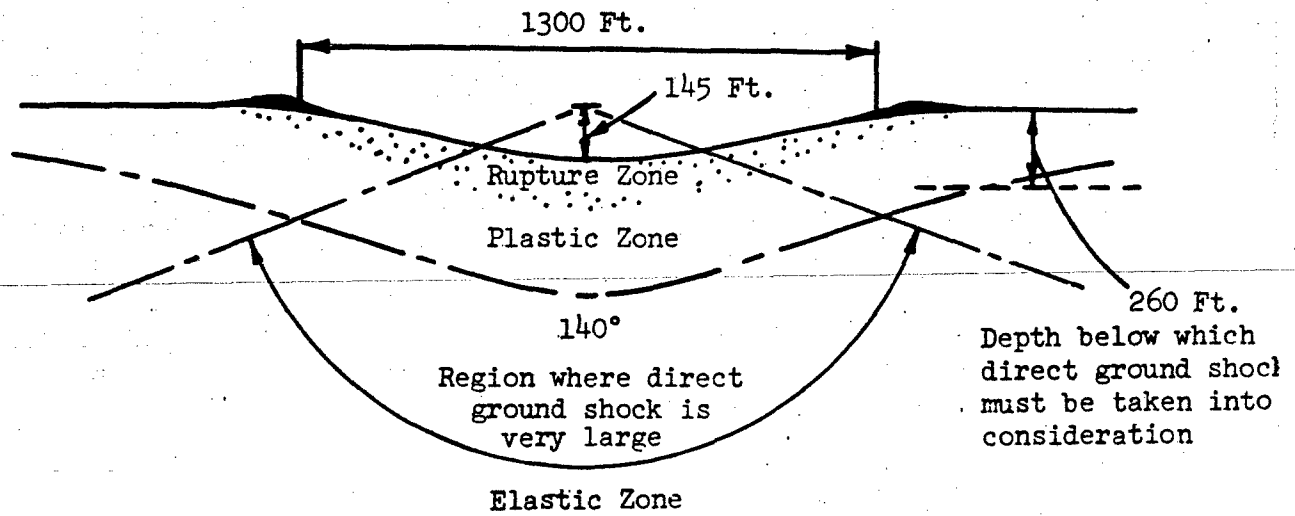


Figure 1 CRATER FROM A 1 MT SURFACE BURST ^{1*}

*Numbers refer to references at end of report.

configuration of a crater. Time-varying pressures in the soil lead to the formation of the crater and the deformed regions surrounding it. When a nuclear device is exploded at the surface of the soil, shock waves are propagated in the air and soil.

Ground-shock effects stem from two sources. The first is stress waves transmitted through the soil from the immediate region of the burst point where cratering action takes place. These stress waves are called directly-transmitted ground shock. The second source is the air-blast wave moving across the surface of the ground. This gives rise to stress waves called air-blast-induced ground shock. At the present time, it is impossible to define exactly the region where directly-transmitted ground shock predominates, the region where air-blast-induced ground shock predominates and the relative effects of each in the region where both are important. For the purpose of defining the region where the results of this report are applicable, it is adequate to use the definition given in Reference 2 which states that the region of space involved in directly-transmitted ground-shock effects is a cone with the apex located at ground zero and with an apex angle of approximately 140 degrees.

The limitations on the knowledge of the stress waves in the directly transmitted-ground-shock region are also given in Reference 2.

"Present knowledge of direct-transmitted shock effects is substantially less extensive than the knowledge of air-induced effects. This situation is a result of a number of factors, principal among which are the following: (1) Field test data for direct shock effects are far less extensive than for air-induced effects. (2) Field test data that are available, with only a few exceptions, are from buried high explosive detonations. Extrapolation from high explosive shock effects

to nuclear shock effects requires the introduction of a yield equivalence factor, about which some uncertainties exist.

(3) Extrapolation from the effects produced by buried charges to effects produced by surface charges requires the introduction of another yield equivalence factor to estimate the percentage of the energy in a surface burst which is propagated directly into the ground. (4) The test data that are available, even from high explosive detonations, produce very little information concerning the variation with time of the direct transmitted shock pulses. In general, only maximum values of strain or acceleration were measured."

Several theoretical models for the prediction of the free-field ground motion in the directly-transmitted region are available. Each of the theoretical approaches is dependent on the values of various soil parameters. The determination of stresses at a point in the soil also requires the knowledge of the yield and point of detonation of the delivered weapon. Neither the soil parameters nor the delivery parameters are ever known very accurately. Rather, a range of delivery parameters and a range of possible soil parameters may be specified.

In view of the uncertainty of the various parameters in the problem, only the simplest model giving an adequate representation of the deformation processes is justified. Elaborate theory and elaborate computational work whose end product is only a refinement of secondary effects, are not warranted.

In this section, several theoretical models of stress-wave propagation in soils are discussed and the pertinent physical quantities associated with each are listed. From the theoretical models of stress-wave propagation in soils that are presented, a waveform is synthesized. This waveform contains the pertinent features of the stresses propagated from a surface nuclear burst.

In particular, the synthesized wave yields:

1. Magnitude of the stress as a function of position
2. Time duration of the stress pulse
3. Approximations of the waveshape

The synthesized waveform is not an exact description of the actual stress wave in any given soil. It gives reasonable descriptions of all the free-field phenomena required for specifying the input for the interaction problem in the region where directly transmitted ground shock is predominant and presents quantitative estimates for these parameters in a simple and usable form. Formulas for the velocities and pressures are presented.

2.1 Theoretical Prediction of Ground Motion

No single consistent theory for the several elements of ground motion in real soil has been generated. Several approximate solutions of the problem are in the literature. Existing theories fall into these categories:

1. Numerical calculations based on analysis which treats the soil as a fluid undergoing finite deformation
2. Analytical and numerical solutions of the stress-wave propagation in a linear-elastic half-space
3. Analytical solutions for the stress-wave propagation in an acoustic or linear-hydrodynamic half-space
4. Analytical solutions to combined models of the above

2.1.1 Hydrodynamic Calculations

Brode and Bjork³ have calculated a numerical example of the ground motion due to a very-high-yield weapon detonated on the surface. The solution for the pressures and particle velocities in the very-high-pressure region was accomplished by numerical integration of the equations of motion. The pressures were computed for a soil whose equation of state was represented by a single pressure term which was a function of density and temperature. It was assumed that, in the close-in region, the soil could be represented as a fluid. The equations of motion were solved for a 1-MT device exploded on a semi-infinite half-space containing tuff. An analytical fit to the equation of state for tuff was made from experimental data.

The results of this calculation may be summarized by the following observations:

The pressure pulse obtained in the tuff was essentially rectangular. The bulk of the energy and momentum transferred to the soil propagated in the vertical direction. In the very close regions (less than 10 meters from the point of detonation) the peak pressure decayed as the inverse cube of the distance from the burst and was independent of orientation. At greater distances, the peak pressure decayed inversely with the square of the distance from the burst and showed an angular dependence (approximately sinusoidally with the angle from the normal to the free surface). (See Figure 2) The peak radial and vertical velocities decay similarly. (See Figure 3)

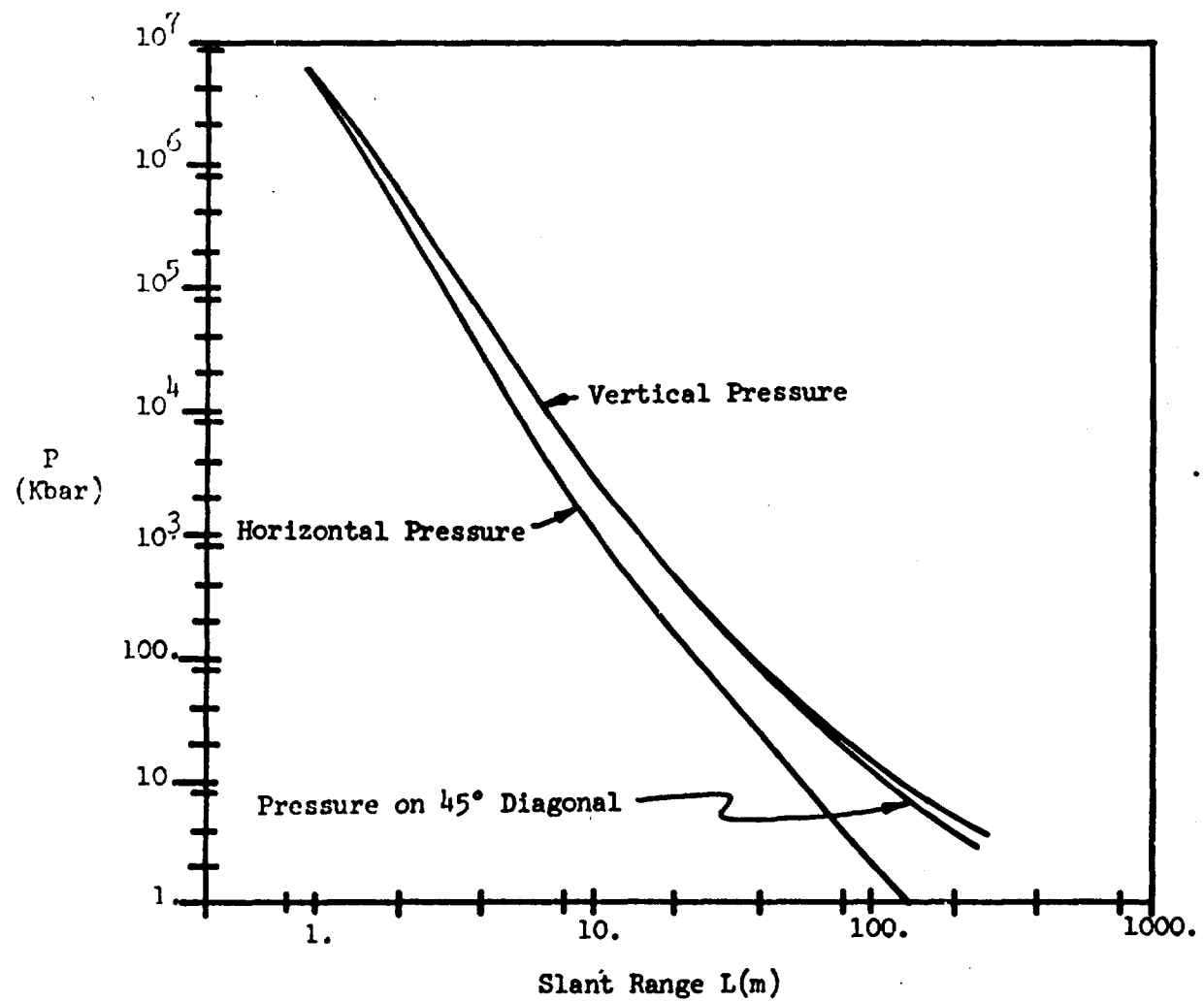


Figure 2 DECAY OF PRESSURE WITH DISTANCE FROM SURFACE BURST
(1 MT) IN TUFF³

V_v = Vertical velocity along vertical axis

V_h = Vertical velocity along surface

U_v = Horizontal velocity along vertical axis

U_h = Horizontal velocity along surface

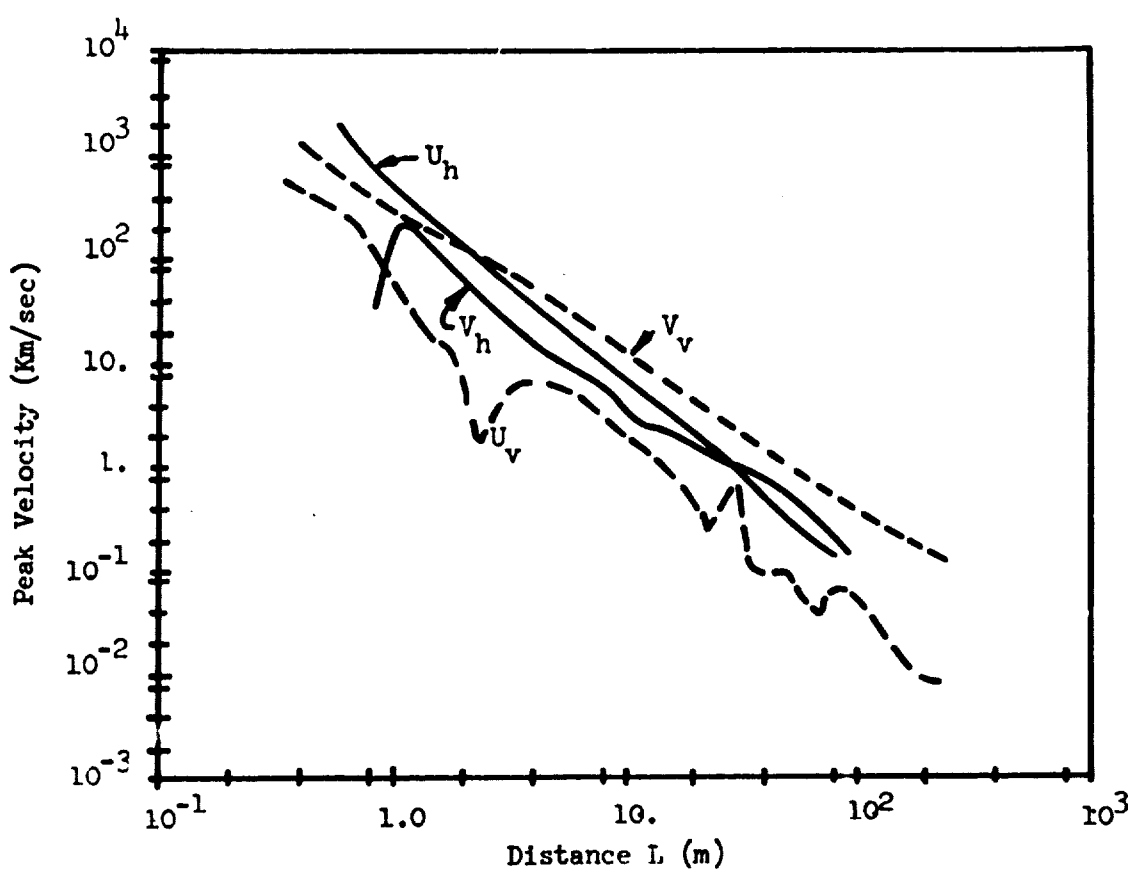


Figure 3 DECAY OF VERTICAL AND HORIZONTAL VELOCITY WITH DISTANCE
FROM A 1 MT SURFACE BURST³

2.1.2 Acoustic Calculations

The simplest of all analytical models representing the free-field is the linear-compressible-hydrodynamic or acoustic model. This is the linear-elastic model with the shear modulus set equal to zero. In this case, a closed-form solution for the pressure and velocity may be obtained.⁴

A point force of magnitude $2\pi F$ is applied at the surface of a semi-infinite half space at time $t = 0$ and maintained for a period Δt .

The problem may be considered as two-dimensional because of symmetry.
(See Figure 4)

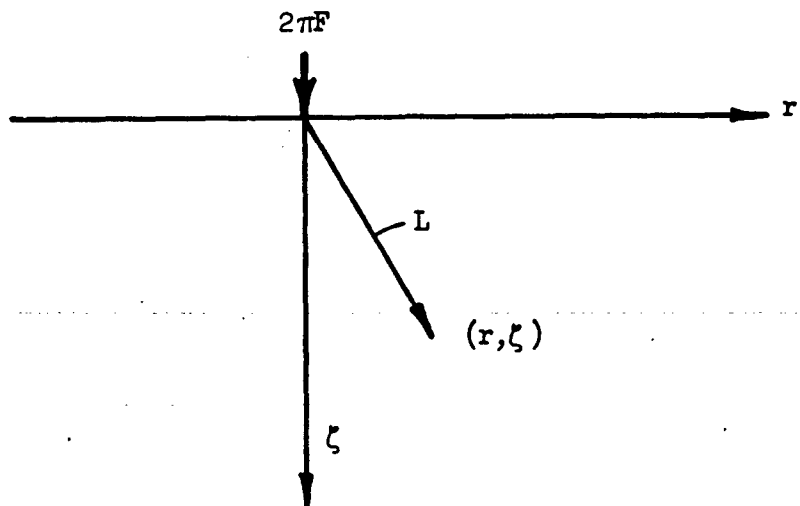


Figure 4 COORDINATES FOR ACOUSTIC SOLUTION

The resultant pressure and particle velocities are:

Pressure:

$$\frac{P(r, \zeta, \lambda)}{F} = \frac{\zeta}{L^3} \left[1(\lambda - L) - 1(\lambda - L - \Delta\lambda) \right] + \frac{\zeta}{L^2} \left[\delta(\lambda - L) - \delta(\lambda - L - \Delta\lambda) \right] \quad (1)$$

Radial Velocity:

$$\begin{aligned} \frac{\rho_m c}{F} u_r(r, \zeta, \lambda) &= \frac{\zeta r}{L^3} \left[\delta(\lambda - L) - \delta(\lambda - L - \Delta\lambda) \right] \\ &+ \frac{3\zeta r}{L^4} \left[\frac{\lambda}{L} 1(\lambda - L) - \frac{\lambda - \Delta\lambda}{L} 1(\lambda - L - \Delta\lambda) \right] \end{aligned} \quad (2)$$

Vertical Velocity:

$$\begin{aligned} \frac{\rho_m c}{F} u_\zeta(r, \zeta, \lambda) &= \frac{\zeta^2}{L^3} \left[\delta(\lambda - L) - \delta(\lambda - L - \Delta\lambda) \right] \\ &+ \frac{2\zeta^2 - r^2}{L^4} \left[\frac{\lambda}{L} 1(\lambda - L) - \frac{\lambda - \Delta\lambda}{L} 1(\lambda - L - \Delta\lambda) \right] \end{aligned} \quad (3)$$

where $\delta(x)$ denotes the Dirac delta function

$1(x)$ denotes the Heaviside step function

$$1(x) = 1 \quad x > 0$$

$$1(x) = 0 \quad x < 0$$

$$L^2 = r^2 + \zeta^2$$

$$\lambda = ct$$

At $\lambda = L + \Delta\lambda$, the pressure undergoes a jump equal and opposite to the initial jump and thereafter the pressure is zero. The velocity components also have jump characteristics at $\lambda = L + \Delta\lambda$. An idiosyncrasy of this model is that the velocities do not return to zero after the passage of the second wave front, but continue at a constant value. Therefore, the model should not be used after passage of the wave.

The vector sum of the horizontal and vertical components of velocity equals $P/\rho_m c$ immediately behind the wavefront. To a first approximation this particle velocity may be considered constant for the duration of the rectangular pressure pulse.

The delta-function singularities are an idealization of the rapid variations near the wavefront. These variations are damped out by nonlinearity of the wave propagation and only the rectangular pressure pulse gets through. Even the rectangular pulse is distorted by propagation through real soils. The change of pulse shape by percycle damping has been reported by R.S. Weiner⁵ and by T. G. Morrison and L. M. Weiner.⁶

The rectangular pulse closely matches Brode's numerical solution as a function of position. The solution does not match the time coordinates, however, as the sonic velocity here is a constant. The identification with Brode's calculations³ requires that the point force divided by 2π be:

$$F = 10^6 \cdot W^{1/3} \text{ kilobars - ft}^2 (\text{MT})^{-1/3}$$

Figure 5 compares the acoustic solution and Brode's numerical solution.

The pressure pulse is applied for a duration Δt which is proportional to the cube root of the weapon yield.

$$\Delta t = \Delta t_1 W^{1/3} \quad (4)$$

Again, using Brode's solution for 10 MT,

$$\Delta t \approx 0.10 \text{ sec for } 10 \text{ MT}$$

thus

$$\Delta t_1 \approx 0.05 \text{ sec}/(\text{MT})^{1/3}$$

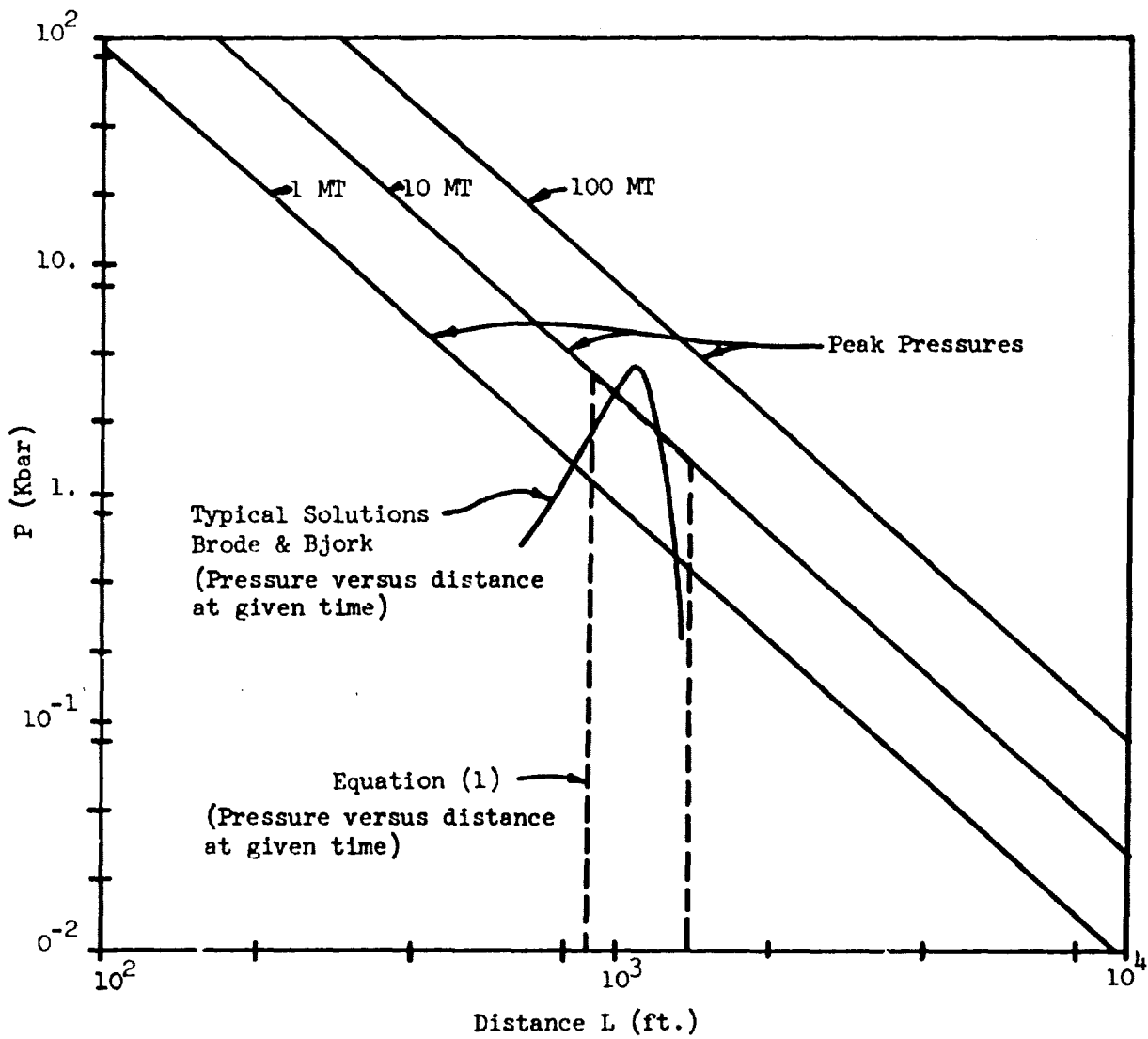


Figure 5 PEAK PRESSURE VS. DISTANCE FROM DETONATION POINT FOR A SURFACE BURST, ACOUSTIC APPROXIMATION

This gives a means for estimating the wavelength of the pulse, since

$$\Delta \lambda = c\Delta t$$

2.1.3 Linear-Elastic Solutions

The problem of wave propagation in an elastic half-space from a time-dependent surface load has attracted the attentions and efforts of many authors in the past 50 years.

Cagnaird⁷ has solved the stress-wave propagation in a linear-elastic half space due to a point pressure suddenly applied and maintained on the axis of symmetry. Pekeris⁸ has solved the same problem for a point vertical stress suddenly applied and maintained on the axis of symmetry. Knopoff⁹ has generated algebraic solutions for the displacements at the wave front in Pekeris' problem.

The general solutions for the displacements and stresses in this problem are usually in integral form. A general closed-form solution is not available. Portions of Cagnaird's solutions are algebraic, but the remainder of his solution and Pekeris' solution are in the form of contour integrals or numerical tables.

Love¹⁰ generated a closed-form solution for the propagation of stress waves in an infinite space due to a point force suddenly applied and maintained.

Pekeris and Lifson¹¹ have calculated the vertical and horizontal displacements on the surface from a suddenly applied concentrated vertical stress.

Baron, Bleich, and Weidlinger⁴, by application of the dynamic-reciprocal theorem, have used the Pekeris and Lifson results to generate displacements and vertical strain in the region of the semi-infinite half space ($\sqrt{2r} \leq \zeta$)

under the point of application of the force. The loading was a force moderately applied at a point and thereafter maintained.

From their solution, the vertical strain (which is the largest component of strain along the vertical axis) may be used to deduce the behavior of the stress in this model. The stresses in the linear elastic model have the following features:

1. A spike, the magnitude of which decays inversely with distance from the source.
2. An almost rectangular pulse, the magnitude of which decays as the inverse square of the distance from the source.
3. Permanent stress, the magnitude of which also decays as the inverse square of the distance from the source.

2.1.4 Combined Models

A recent study¹² has developed two approaches to the problem of analyzing ground motion in an elastic medium due to the energy delivered directly to the ground by a nuclear weapon. One of these approaches treats the elastic region as a cratered half-space, where the hemispherical boundary of the crater is subjected to the pressure history exerted by a hydrodynamic region within the crater. The other approach treats the elastic region as a complete half space, a portion of which has initial motion and pressures corresponding to the state of the hydrodynamic region at some instant when its behavior is becoming more nearly elastic than hydrodynamic.

Exact analytic expressions were obtained for the stresses at the wave-front for the cratered-half-space approach, and numerical results were produced. For the complete-half-space approach, analytic expressions alone were presented.

2.1.5 Wavefront Attenuation

In both the linear elastic model of wave propagation in a half-space and the acoustic model of wave propagation in a half-space, the main part of the stress wave decays as the inverse square of the distance from the source of the detonation. There is a short-duration pulse at the beginning of the disturbance which decays as the inverse of the distance from the detonation. In a real soil, there are a number of mechanisms which will reduce or attenuate this spike.

1. The elastic stress-strain curve is nonlinear. If the slope of the stress-strain curve increases with stress level, the shock wave that is propagated downward will be similar in some features to a one-dimensional shock wave. In particular, the shock wave will be subsonic in comparison with the sonic velocity behind it¹³. Rarefaction waves generated at the surface will overtake and degrade the shock front.
2. Real soils are dissipative. Internal friction will degrade and attenuate the high-frequency components of the wave, particularly in regions where the stresses are high. A simple calculation of the properties of stress waves in a linear visco-elastic¹⁴ or linear visco-plastic material^{15,16} shows that the stress jump at the wave front is sharply attenuated.

3. Real soils are inhomogeneous. If the sonic velocity, elastic constants, or density are randomly inhomogeneous, the high-frequency components of the stress wave will be reflected internally and the sharp wavefront will be attenuated¹⁷.

Estimates of the amounts of damping and attenuation (and their attendant effects on the magnitude and shape of the propagated wave pulse) have been obtained by the methods of percyclic damping. Using the percyclic-damping formulas for the decay of a rectangular pulse developed by Weiner⁵, the change in shape of a rectangular pulse would be as shown in Figure 6.

2.2 Empirical Data

Reference 2 summarizes the few experimental data available on the directly-transmitted ground shock. The only experimental data on nuclear bursts for displacements, velocities, and accelerations directly transmitted through soil and/or rock are from a sequence of deeply buried, low-yield explosions. These data do not relate directly to the problem of predicting directly-transmitted ground shock from the surface burst of a nuclear weapon. Therefore, in this report the use of the acoustic model for predicting directly-transmitted ground shock (see Section 2.1.2) is recommended. The pertinent formulae are summarized in the following subsection. One could use, of course, some other prediction method or free-field data. The presentation of interaction data in the later sections of this report is adequate to accommodate many different forms of predicted incoming ground shock.

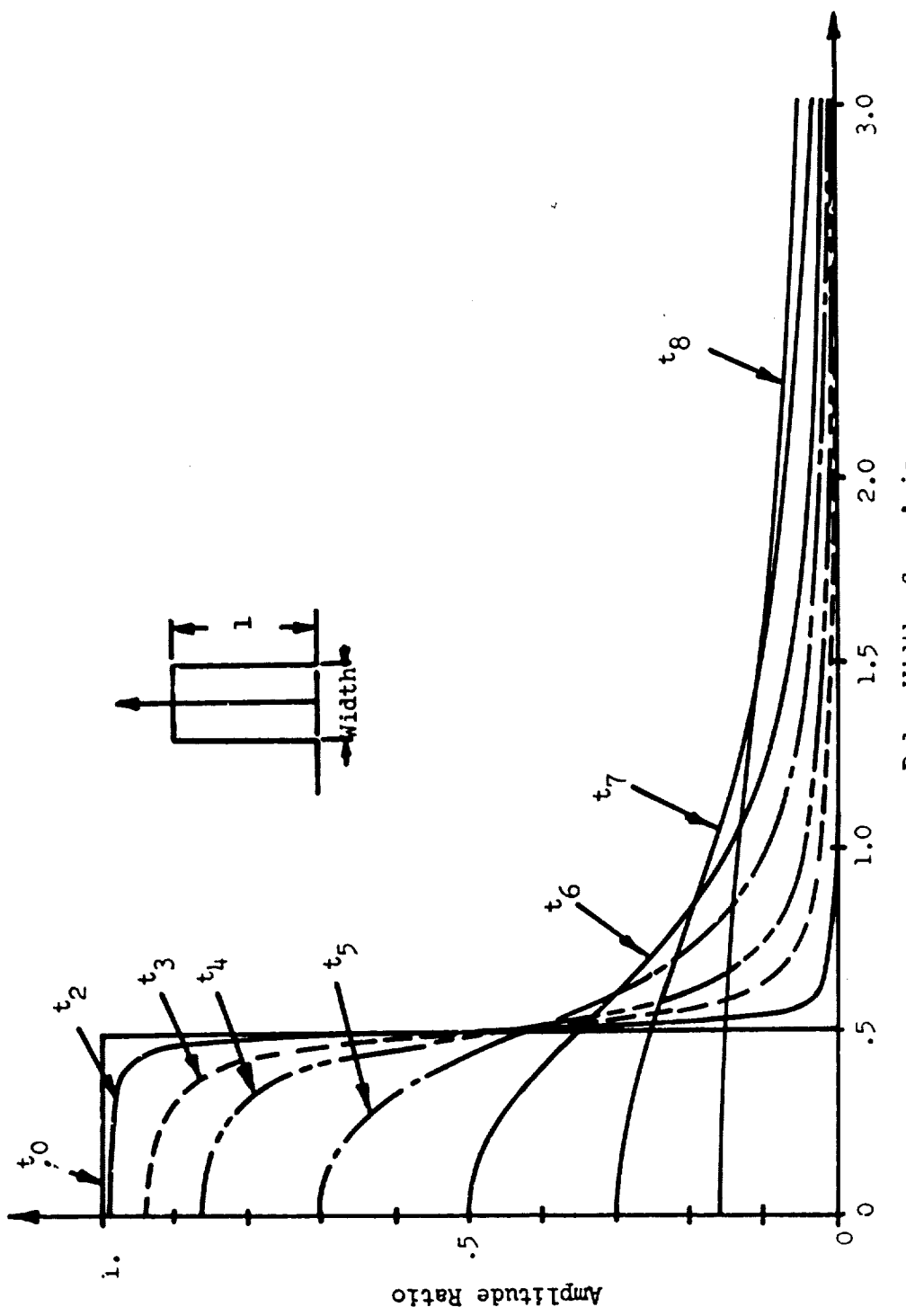


Figure 6 DAMPING OF RECTANGULAR PULSE

2.3 Calculation of Free-Field Waveform in the Directly Transmitted Ground Shock Region

The dominant stress and velocity for the linear-elastic model and the acoustic model decay as the inverse square of the distance from the burst. The pressure spike, which decays inversely as distance from the source, is further attenuated by various mechanisms that exist in a real soil. In the region of interest for this program, it can be assumed that the spike has decayed sufficiently to be ignored.

The order of magnitude of the stresses and displacements calculated from either the elastic or acoustic models is the same for the same surface loading. The variations of stress with angle are of less concern to the designer than the magnitude, and this magnitude is most easily estimated by the acoustic model.

The acoustic model of the soil will be used for prediction of the waveform. This simplification of the free-field studies is made for the following reasons:

1. The dominant long-period pressures computed in the hydrodynamic numerical calculations, the linear elastic, and the acoustic models all show the same dependence on distance and approximately the same dependence on the angle from the source.
2. The acoustic model has a simple analytic closed-form expression.

The basic waveform suggested is a rectangular pulse, whose magnitude is a function of position in the soil with respect to the detonation point and of

the yield of the weapon. The duration of the pulse is a function of the yield of the weapon.

The basic rectangular pressure pulse may be obtained then from the acoustic model. The pressure that may be expected at a point (r, ζ) from a surface burst is given by (lbs/ft^2):

$$\frac{P(r, \zeta, \lambda)}{F} = \frac{\zeta}{L^3} \quad (5)$$

where

$$F = 1.45 \cdot 10^{10} \cdot W^{1/3} \text{ ft}^2 \cdot \text{psi/MT}^{1/3}$$

The particle velocity (ft/sec) behind the wavefront is:

$$u = \frac{P}{\rho c} \quad (6)$$

The pressure and velocity are held for time Δt . The upper and lower bounds on Δt are

$$\Delta t_{\text{upper}} = L/2c \text{ sec.}$$

$$\Delta t_{\text{lower}} = 0.05 W^{1/3} \text{ sec/MT}^{1/3}$$

For $L < 0.1 c W^{1/3}$ ft., the lower bound should be used.

The waveshape that propagates through a real soil is altered from an ideal shape. As has been mentioned, several mechanisms tend to smooth out the wave. This attenuation and alteration of the waveform may be represented mathematically using the theory of percycle damping.

The mathematical form of the altered wave, after application of the percycle damping formulas, is quite complicated. Other mathematically simpler curves may be used as approximations to the altered rectangular pulse. These waveshapes are presented and discussed in Section 3.

SECTION 3

STRUCTURE-MEDIUM-INTERACTION ANALYSIS

The problem of interaction of a moving pressure pulse with an infinitely long cylinder of finite circular cross-section immersed in an infinite acoustic medium was investigated. The pressure pulse was considered to be traveling through the medium with its front parallel with the axis of the cylinder. In the subsequent analysis of the problem, the shell response of the elastic cylinder was considered to be of prime importance, and the analysis was restricted to determining displacements and velocities of the shell in response to a variety of input pulse shapes. Since the primary motive of the investigation was to obtain information beneficial to the design of shock-isolation systems within the structure, the influence of the shell on the motion of the medium was not investigated.

The problem is basically a two-dimensional one and may be represented, with its defining variables, as shown in Figure 7.

3.1 Methods for Solving the Structure-Medium-Interaction Problem

A great deal of work has been done on the subject of the interaction of waves propagating through various media and diffracting about specific structures. There is an essential similarity in all kinds of wave behaviors whether the waves are transverse or longitudinal, elastic or electric. This means that even methods developed for treatment of certain special cases of wave propagation have wide application. Thus, a wealth of information exists concerning the wave diffraction problem.

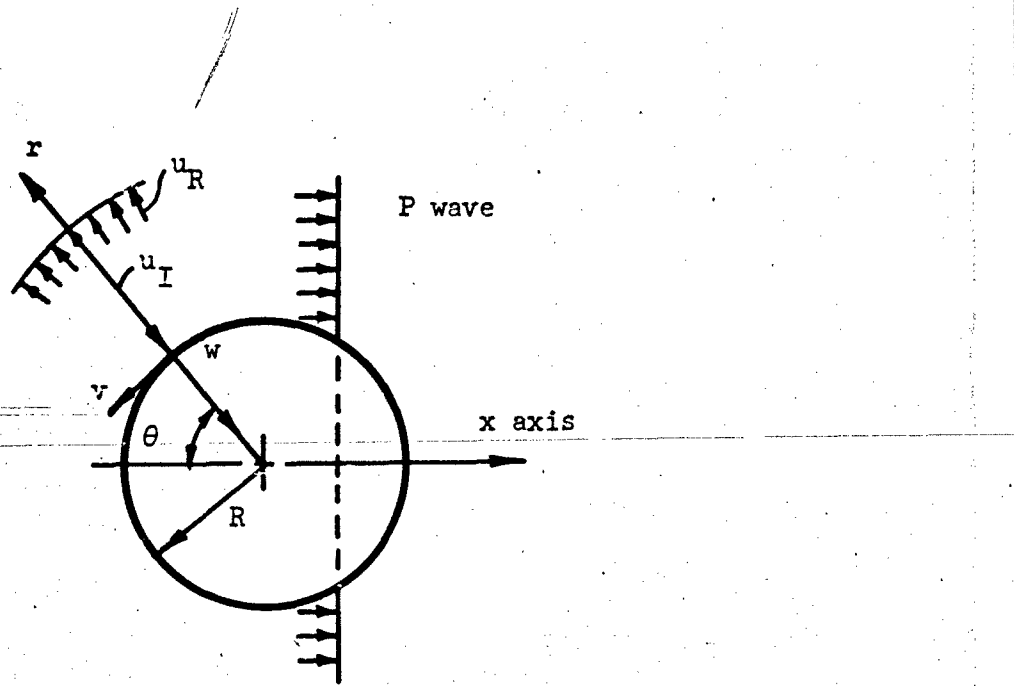


Figure 7 INTERACTION OF MOVING PRESSURE PULSE WITH CYLINDER

Essentially, three basic methods exist by which solutions have been obtained to the wave-diffraction process about cylindrical objects, the normal-mode method, the double-transform method, and the geometrical method. The first two methods require the differential equations of motion of the problem be separable in their independent variables; the third method does not require separability of variables, thus giving it wider applicability to cylinders of arbitrary cross section. The first two methods are by far the most widely used and, in terms of work on the subject of wave interaction with elastic cylinders, have a certain chronological pre-eminence over the geometric method.

3.1.1 The Normal-Mode Method

In the normal-mode method, displacements of the elastic shell are given in terms of the normal modes of vibration of the shell. The angular coordinate, θ , describing the shell and medium, is expanded in a Fourier series.

3.1.1.1 Acoustic Media

Historically, the first attempts to obtain the solution of the problem of wave diffraction about an elastic cylinder were made by the normal-mode method. The first work on the problem was done for an acoustic medium by Carrier¹⁸ in 1951. In 1953, Mindlin and Bleich¹⁹ simplified Carrier's method by assuming that each element of the cylindrical surface could be considered as a flat plate in reflecting and radiating the acoustic wave. This approximation should be valid in principle for short times with respect to the development of the shell motion, but the resulting series obtained for the radial acceleration was not uniformly convergent. In 1954, Baron²⁰ used the same plane-wave approximation in work with the acoustic-medium problem, but used a more sophisticated shell model. It was Haywood²¹ who, in 1958, succeeded in representing the reflected and radiated waves in cylindrical form, permitting a significantly greater time period to be accurately represented with the normal-mode technique.

3.1.1.2 Elastic Media

The first attempts to apply the normal-mode method to the interaction of elastic waves with an elastic cylinder was made by Baron who, in company with several other authors, has written a number of papers on the

subject in the period from 1960-1962. The most recent and inclusive of this series of Baron's reports is that of Baron and Parnes²². Some of the others who have contributed to the development of the normal-mode approach to the elastic-wave problem are Soldate and Hook²³ (1960), Paul and Robinson²⁴ (1963), and Yoshihara, Robinson, and Meritt²⁵ (1963).

3.1.2 Integral-Transform Method

The normal-mode technique for solution of the shell-medium-interaction problem has some difficulties. Perhaps the principal problem is that, while theoretically correct, the Fourier-series expansion of the angular coordinate results in series expressions for the solution of the problem which do not always converge rapidly enough for convenience in numerical computation.

The double-transform technique was developed to meet this problem. Historically, the method evolved over a period of many years. Perhaps the earliest use of the basic techniques of the method was made by Sommerfeld²⁶ in 1896 in his study of the problem of the diffraction of light by a wedge of arbitrary angle. Sommerfeld solved the problem by the method of images regarding the xy -plane of Figure 7 as a multiple-sheeted Riemann surface, and treating separately each of the infinitely many sources which comprise the actual θ -periodic distribution of sources. The multiple-sheeted-Riemann-surface concept was applied to the wave-cylinder interaction problem by Friedlander²⁷ in 1954. Using this technique, Friedlander was able to describe wave motion occurring on the surface of the cylinder, not only during its first passage about the cylinder (in the physical plane of the angular coordinate θ , where $-\pi \leq \theta \leq \pi$) but also in repeated passages of the wave about the cylinder where θ was

described on Riemann surfaces whose sheets were given by $(2m - 1)$
 $\pi \leq \theta \leq (2m + 1)\pi$ for $m = \dots, -1, 0, +1, +2, \dots$. With this technique,
it is possible to take the infinite Fourier transform of the dependent
variable of the problem with respect to the angular coordinate, θ .

The technique was not immediately exploited to its full potential.
It was used by Payton²⁸ in 1960 to obtain exact expressions for the shell
and fluid motion during the diffraction process for an acoustic medium.
In 1963, Peralta²⁹ applied the method to the acoustic-medium problem using
an elastic shell which was filled with acoustic medium other than that en-
closing the shell.

The problem of the interaction of an elastic wave with a cylindrical
shell using the infinite-Riemann-sheet method together with a double trans-
form (a Laplace transform over the time variable, t , and a Fourier transform
over the angular coordinate, θ) was presented by Gilbert and Knopoff³⁰ in
1959 and Soldate and Hook³¹ in 1962. The method can be described with dis-
arming simplicity, but problems evolve during inversion of the formal solution
when attempting to attain the actual expressions for the untransformed vari-
ables. In practice, although a formal closed-form solution may be obtained
by application of the transform-inversion integrals, integration of the
expressions must almost invariably be performed numerically.

3.1.3 Geometrical Method

Credit for the initial development of the geometrical method must be
given to Friedlander. In his book Sound Pulses³², he developed the technique
for an acoustic medium. The technique was applied to an elastic medium by

Soldate and Hook³¹. The method yields solutions in the form of power series in time. The primary drawback is that the calculation of successive terms in the time series is exceedingly complicated. However, the leading terms are relatively easy to obtain and provide a means of finding short-time solutions as a complement, perhaps, to one of the other methods of solution described.

3.1.4 Choice of Method

The method chosen for use in solving the structure-medium-interaction problems for this program was the normal-mode method, as adapted by Haywood²¹.

Because of the inherent difficulties attendant in the numerical inversion of transforms required in applying the integral-transform method, this technique was rejected. Likewise, the complication involved in computing successive terms of the time series as required in using the geometrical method led to its rejection. Neither of these methods gives the physical insight into the motion of the structure that the normal-mode method provides.

The normal-mode solution of the acoustic problem by Haywood²¹ represents a very powerful and relatively straightforward tool for determination of shell response to various input forcing functions. In view of the state of the art of the prediction of the free-field motion as previously stated, the assumption of an acoustic medium surrounding the cylinder is felt to be justified. The resulting simplification in the description of the medium can be used to permit sophisticated waveforms to be treated in the interaction problem itself. It is further felt that a thorough understanding of the acoustic-medium-structure-interaction problem is an absolute necessity as a foundation upon which to consider and compare more complicated and sophisticated soil models.

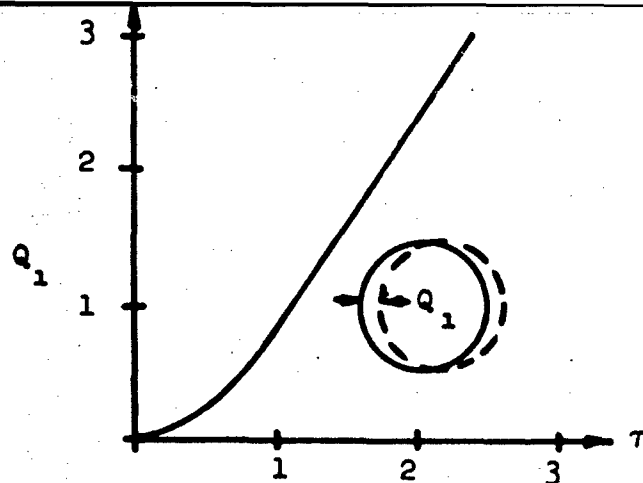
The method used in this program, then, is an extension of Haywood's to a complete solution of the acoustic-medium-cylinder-interaction problem.

3.2 Normal Mode Analysis of the Response of an Elastic Cylindrical Shell in an Acoustic Medium to a Specified Input Pulse

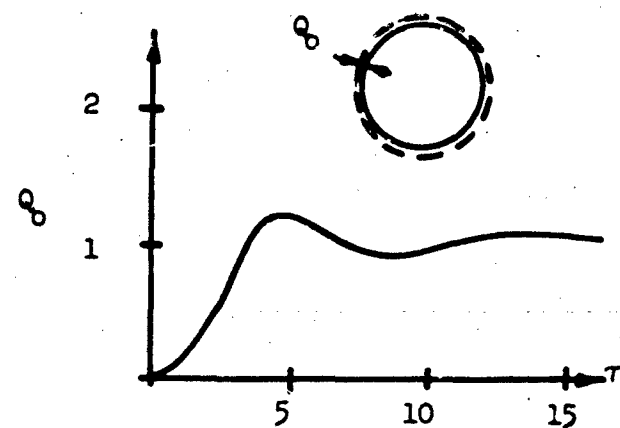
Using a modal analysis, the motion of the structure can be separated into two essentially separate portions, the rigid-body motion of the shell and the elastic shell response. The latter response includes the dilatational (breathing or zeroeth-mode response) and bending-mode response. It can be shown that the rigid-body motion of the shell has the same general shape as the free-field ground motion except for its modification due to the effect of the breathing and bending-mode motion.

A typical response of a cylinder to a step pulse is shown in Figure 8. Perhaps, the most distinctive feature of the rigid-body response of a shell to a step pulse is the terminal velocity which the shell attains at long times. The magnitude of the shell's terminal velocity depends upon the properties of the shell and the medium. The inertia of the structure causes a gradual initial acceleration to take place during the early time history of the shell motion until the structure reaches the rigid-body terminal velocity. In the dilatational mode, the shell is compressed initially to a displacement generally somewhat greater than the displacement which would be attained under an identical hydrostatic load. The shell then oscillates in a rapidly decaying manner about the static displacement which it approaches for long times.

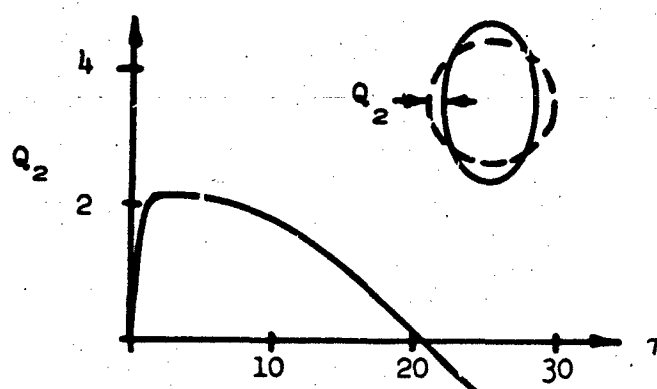
In general, the response in the first bending mode ($n = 2$ in the Fourier-series expansion) as indicated in Figure 8(c), is the most significant of any



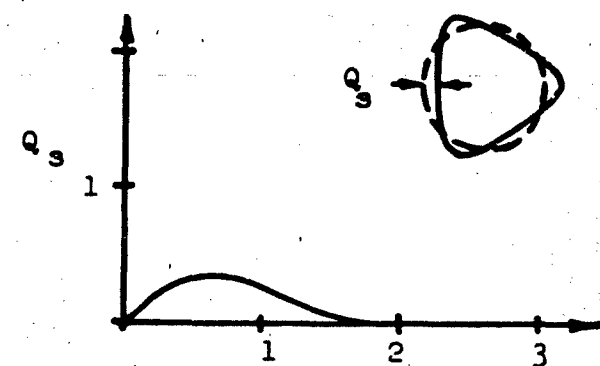
(a) RIGID-BODY MODE ($n=1$)



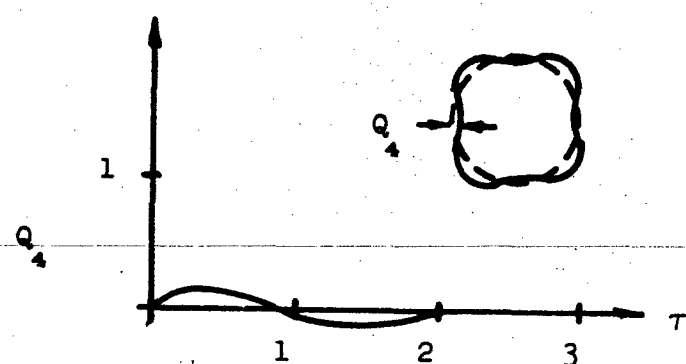
(b) DILATATIONAL MODE ($n=0$)



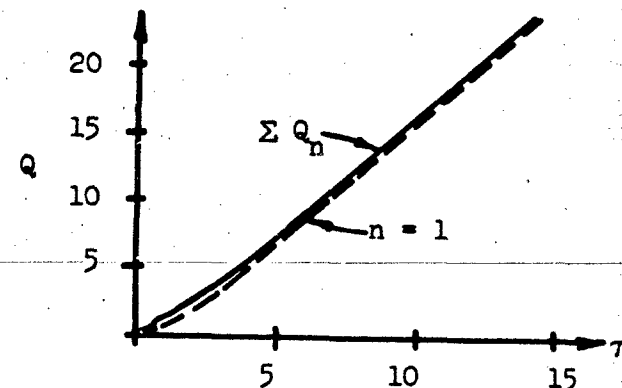
(c) FIRST BENDING MODE
($n=2$)



(d) SECOND BENDING MODE ($n=3$)



(e) THIRD BENDING MODE ($n=4$)



(f) TOTAL RESPONSE AT $\theta = 0^\circ$

Figure 8 TYPICAL RESPONSE OF CYLINDER IN ACOUSTIC MEDIUM TO A STEP PULSE

of the elastic modes ($n = 0, 2, 3, 4, \dots$). The predominant long-time oscillatory motion of this mode of the shell may be shown to take place at a frequency which is directly proportional to the ratio of the square of the natural frequency of the shell in vacuum to the bulk modulus of the soil. The response of the shell in higher modes decreases rapidly as the order of the mode increases. For these higher modes, the motion takes place only during the period when pressure wave moves over the shell. After engulfment, the higher modes are essentially quiescent and the motion of the shell when subjected to a step pressure pulse is then confined to only the rigid-body mode and the dilatation and first bending modes. The total displacement response at the position $\theta = 0^\circ$, the point at which the wave first makes contact with the cylinder, is given in Figure 8(f). For the step pulse, the most important modifications to the rigid-body motion made by the elastic modes occur during the early transient response-period of motion.

3.3 Parameters

Observations of the formal and complete solutions to the acoustic-medium-structure interaction problem, as outlined in the previous section, indicate that a relatively small number of dimensional parameters govern the shell response to a given input forcing function. These parameters are contained within the two dimensionless parameters, ξ_n and σ_n (these correspond to λ_n and σ_n , respectively, in Ref. 21). Both of these parameters are involved in the general mass-dependent response of the shell and must certainly be considered in the rigid-body motion of the shell ($n = 1$). If the mass of the shell can be neglected, only σ_n influences the shell motion and consequently

the number of parameters is reduced. The constants ξ_n and σ_n are defined as:

$$\xi_n = \frac{m_n}{\rho_m R} = \mu H \left(\frac{1 + n^2}{n^2} \right) \quad (8)$$

$$\sigma_n = \frac{E}{B} H s \frac{(1 - n^2)^2}{12} \quad (9)$$

Thus, in general, each modal response of the shell depends upon the parameters μ , H , E , and B . In general, all four of these parameters are required to specify completely the solution for the shell displacement. In this program, however, it was necessary to use only three of the four at any one time for the reasons stated below.

Except for very small times, the mass of the shell may be neglected in determining the elastic modes of shell motion ($n = 0, 2, 3, 4, \dots$). Hence, $\xi_n \approx 0$ and only the parameters involved in the constant σ_n are of importance to the problem, i.e., E , B , and H .

For the case of the rigid-body motion of the shell ($n = 1$) $\sigma_1 = 0$, and the parameters required for definition of the shell motion are μ , H , and B . The term B , although not contained with ξ_1 , is contained in the general expression for the solution of the problem. However, it enters the equation simply as a multiplication constant.

Data presented in this section are given in terms of the dimensionless displacement, Q_n , and velocity, V_n . It should be noted that the displacements in all modes are made dimensionless by means of the zeroeth-mode static displacement. This provides a uniform base for direct comparison of relative displacements among modes. Because of singularities in the short-time

solutions for the dimensionless velocity, V_n , it was not possible to obtain the maximum acceleration values, since they appear to occur at very short times in the development of the motion. Consequently, accelerations are not presented in the results which follow. The inability to present acceleration values was disappointing, but the investigation of the overall shock-isolation problem indicated that knowledge of maximum values of displacement and velocity was sufficient to define shock-isolation requirements for protective structures. Hence, description of response properties was limited to displacement and velocity results.

The final parameter of importance in the problem is the wavelength of the incoming wave. The incoming wave is illustrated in Figure 9.

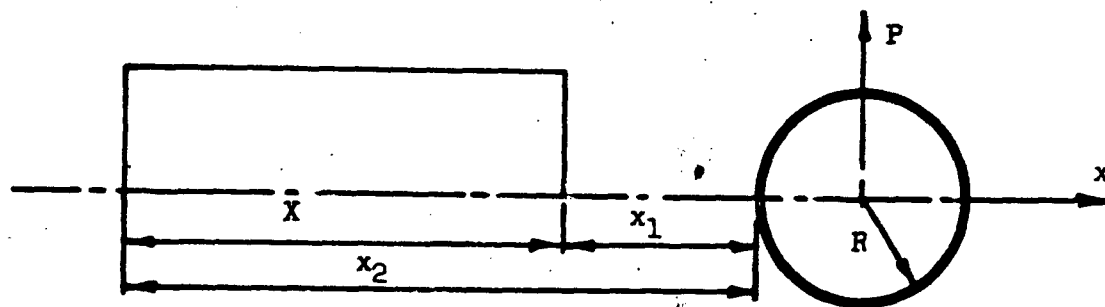


Figure 9 INCOMING PRESSURE WAVE

The positive-pressure phase of the wave is defined nondimensionally as

$$\ell = \frac{x}{R} = \frac{1}{R} (x_2 - x_1) = \frac{c}{R} (t_B - t_A) = \tau_B - \tau_A \quad (10)$$

It should be noted that τ_A and τ_B are simply the arrival time and clearing time of the positive-pressure phase of the incoming wave, respectively, in dimensionless form. The wavelength of the incoming wave is an extremely important parameter. Physically, it is directly related to the weapon yield.

3.3.1 Waveforms of Incoming Pulse

As indicated in Section 2, the incoming wave may be represented as a rectangular pulse. For such a wave, the range of estimates of appropriate values for the wavelength of the positive phase, X , were taken as

$$300 \text{ ft.} < X < 750 \text{ ft. for } W = 1 \text{ MT}$$

The range is an allowance for variations in types of soils. Based on the above estimate of the wavelength of the incoming pulse, nondimensional wavelengths, ℓ , were investigated within the range

$$0 < \ell < 30$$

In some cases, the range was extended to investigate interesting phenomena.

In addition to the investigation of shell response to a rectangular waveform, it was felt that a number of other basic waveshapes should be investigated. Examination of the literature indicated that a wide variety of waveforms have been observed in experimental investigations of free-field motion. To cover as broad a range of waveforms as possible and to investigate the effect of perturbations of some of the fundamental waveshapes, the following waveforms were investigated: (1) the rectangular pulse, (2) a rectangular pulse with an exponentially decaying spike superimposed upon it (various decay rates were investigated), (3) a half sine, (4) a haversine, (5) a sine wave with discontinuous first derivatives at its initiation and termination,

and (6) a modified sine.* These are illustrated in Figures 10 and 11. The wave-shapes discussed above were all investigated throughout the entire range of wavelengths as given above.

3.3.2 Shell Parameter Ranges

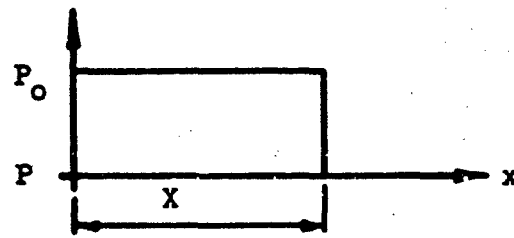
Only steel shells were investigated because in the region of interest of ground shock stress, namely, $1000 \text{ psi} < P < 10,000 \text{ psi}$, concrete shells might not survive. The value of E selected was $E = \frac{E_s}{1 - \nu^2} = 33 \times 10^6 \text{ psi}$.

As a first estimate of the order of magnitude of shell thickness-to-radius ratios to be used in the investigations, a static design for the shell was made. After ruling out the use of concrete, it was estimated that steel shells would withstand the ground shock of interest with thickness-to-radius ratios of the order of .01 to .1. It was decided to investigate the values of thickness-to-radius ratios of $H = .01, .04, \text{ and } .08$.

3.3.3 Medium Parameter Ranges

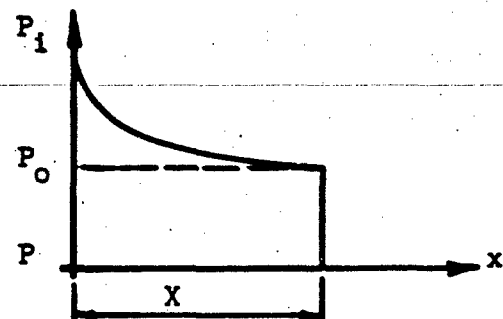
The problem of determining an appropriate range for the parameter B of the medium is complicated by one of the basic assumptions in the solution to the problem. The assumption is made that the motions of the shell can be described in a Fourier series in the angular coordinate, θ . This assumption implies that all points on the circumference of the shell respond simultaneously to a force exerted at any point on the shell. In a real shell, when a load is applied locally, the signal from the load is not felt instantaneously throughout the entire shell, but is transmitted as a wave motion either through the shell or through the medium, whichever route provides the most rapid path.

*For the origin of this waveshape, see Volume III of this report.



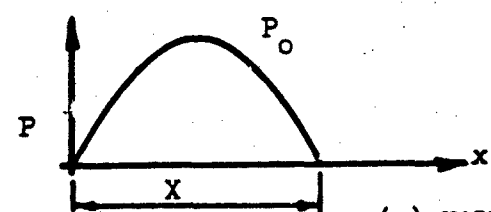
$$P = \begin{cases} 0, & x < 0 \\ P_0, & 0 \leq x \leq X \\ 0, & x > X \end{cases}$$

(a) RECTANGULAR PULSE



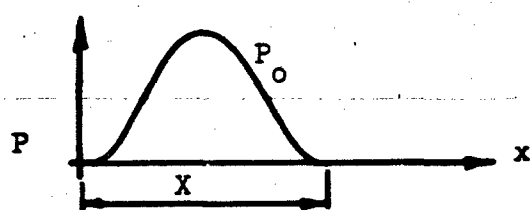
$$P = \begin{cases} 0, & x < 0 \\ P_0 + (P_1 - P_0)e^{-\beta x}, & 0 \leq x \leq X \\ 0, & x > X \end{cases}$$

(b) EXPONENTIALLY DECAYING PULSE



$$P = \begin{cases} 0, & x < 0 \\ P_0 \sin \frac{\pi x}{X}, & 0 \leq x \leq X \\ 0, & x > X \end{cases}$$

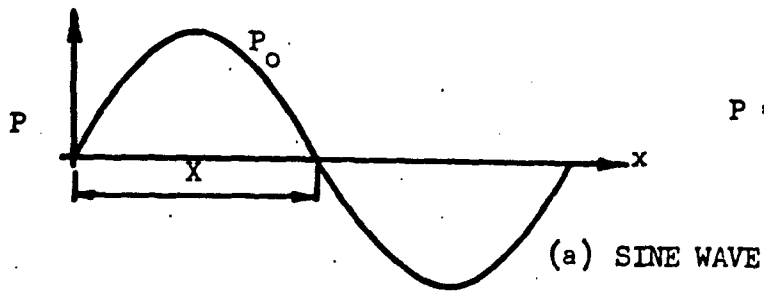
(c) HALF SINE PULSE



$$P = \begin{cases} 0, & x < 0 \\ P_0 \sin^2 \frac{\pi x}{X}, & 0 \leq x \leq X \\ 0, & x > X \end{cases}$$

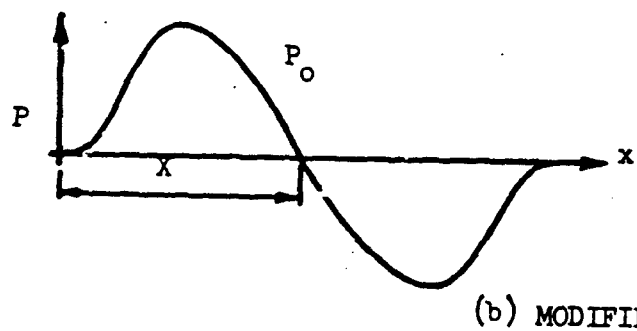
(d) HAVERSINE PULSE

Figure 10 PRESSURE PULSE FORMS



$$P = \begin{cases} 0 & , x < 0 \\ P_0 \sin \frac{\pi x}{X}, & 0 \leq x \leq 2X \\ 0 & , x > 2X \end{cases}$$

(a) SINE WAVE



$$P = \begin{cases} 0 & , x < 0 \\ P_0 \sin \frac{2\pi x}{X}, & 0 \leq x < \frac{X}{2} \\ P_0 \sin \frac{\pi x}{X}, & \frac{X}{2} \leq x < \frac{3X}{2} \\ -P_0 h v \sin \frac{2\pi x}{X}, & \frac{3X}{2} \leq x \leq 2X \\ 0 & , x > 2X \end{cases}$$

(b) MODIFIED SINE WAVE

Figure 11 PRESSURE WAVE FORMS

Since it is assumed that the forcing function on the shell is represented by a traveling wave, the propagation of the signal in the shell must be much greater than the signal propagation in the medium if the assumption of the Fourier series expansion of the shell motion is to be valid. To insure the validity of this assumption, it was necessary to choose values of wave propagation velocities in the medium in ranges which were below that of the acoustic velocity of steel.

Even with such stringent requirements, it was found possible to make the range of the parameter B embrace a large variety of materials. A low and high-modulus soil were selected with a range of B of 0.4×10^6 to 2.0×10^6 psi. The low-modulus medium is representative of the value of the modulus which one might obtain from a typical clay or a slow sandstone.³³ The upper limit of the soil modulus is representative of a typical limestone or a slow granite.³³ Thus, a wide variety of potential media may be considered while still remaining within the requirements of the solution of the problem.

Once the range of the modulus of the medium has been selected, the selection of the density ratios becomes nearly automatic. To provide the widest range in the density ratio, the density extremes for the media corresponding to the limits of the range of the bulk modulus of the medium were selected. The values of the density ratio used were:

$$\mu = 4 \text{ when } B = .4 \times 10^6 \text{ psi}$$

$$\mu = 3 \text{ when } B = 2.0 \times 10^6 \text{ psi}$$

The value of $\mu = 4$ corresponds to the ratio of the density of steel to that of a typical water-saturated clay. The density ratio $\mu = 3$ corresponds to ratio of the density of steel to that of granite. A range of this size adequately covers practically all media of interest.

SECTION 4

DISCUSSION OF RESULTS*

Because of the many combinations of parametric variations that were necessary to explore the relative influence of these parameters on the structure response, a great number of cases were computed.

The usual custom of distributing the graphs throughout the written text was departed from in this section because it would be too disruptive of overall continuity and many of the graphs have application in several parts of the discussion. Therefore, the graphs are all located at the end of the section.

The discussion of results is long because of the many relationships which must be considered. Standards of comparison must be developed and explained. It is important to note that the quantities plotted in the figures are nondimensional. Most of the following discussion compares nondimensional displacements and velocities. When comparing specific parameters for specific situations, the quantities should be brought back to dimensional form.

Major subdivisions of the discussion are based on the shape of the input pulse or wave, beginning with the step pulse and continuing with the rectangular pulse and other waveforms. The discussion of both the step pulse and rectangular pulse is rather extensive since these form the bases of comparison for the influence of other waveshapes.

*Designers of shock isolation systems interested only in applying the data to specific situations need not read the beginning of this section, but may proceed directly to Subsection 4.4 on page 69 without loss of continuity.

Discussion within each major subdivision is ordered according to modal response, beginning with the zeroeth mode and progressing in sequence to the third and fourth modes. Within each of the modes, displacement response and velocity response are considered.

Following this, the general shell response to changes in shell and medium properties for all waveshapes is presented. Then the influence of variation in waveform on shell response for various media and shell properties is discussed.

Finally, the parameters are ranked according to their influence on displacement and velocity response, and the effects of errors in estimating values of parameters on prediction of response are presented.

To present complete displacement and velocity-time histories for all cases considered for this program would make the report too large. Moreover, since an estimate of the response of interior articles to be shock isolated can be made on the basis of values of peak displacement and velocity alone, presentation of the modal response of the shell to various waveforms will, in general, be limited to discussion of the peak positive and negative values of the modal shell response. In order that the results of this study may be considered completely described herein, the Duhamel-integral computer routine used for determination of the response of the shell to any given input waveform is included in Appendix A. When coupled with the response of the shell to the unit-step pressure pulse described in detail in subsection 4.1, the Duhamel integral routine will provide complete time-history solutions to other

waveforms which one may wish to investigate. Therefore, after the discussion of the step-pulse response, this section will consist primarily of a discussion of the modal response peaks.

4.1 Shell Response to Step-Wave Input

The response of the shell to the unit-step-pressure-pulse input is reported in this section. Modal shell displacement response to the unit step wave is shown in Figures 12 through 22. The velocity response is shown in Figures 23 to 32.

4.1.1 Zeroeth Mode Response ($n = 0$)

In Figure 12, the zeroeth or "breathing" mode response of the shell in low-modulus ($B = .4 \times 10^6$ psi) soil is shown. The results shown in Figure 12 are unique in that the type of response shown was not found in any other medium or mode investigated. It will be noted that for the thin shell ($H = .01$) the shell responds rapidly, its displacement increasing until approximately $\tau = 5$, at which time the displacement has exceeded the static displacement. The peak displacement response is approximately $Q_0 = 1.1$. After reaching its peak value, the zeroeth-mode displacement decreases towards its static value, about which it oscillates with rapidly decaying amplitude. The displacement may be considered to have reached the static value by the time $\tau = 20$.

The thicker shells investigated do not exhibit this same type of displacement response. As the shell thickness increases, the displacement no longer overshoots its static value, but remains below it, approaching the static displacement asymptotically. This type of response is very similar in appearance to that of a damped spring-mass system. The thin shells have

the appearance of an underdamped system in which the displacement overshoots its equilibrium position and then oscillates about it with a decaying amplitude. The thicker shells, conversely, have the appearance of being overdamped, so that no oscillation is apparent in their response.

Because there is such similarity to damped oscillatory motion, it becomes interesting to investigate conditions under which a response similar to critical damping is obtained. Examination of the conditions which cause this type of response shows that it is connected with the change of the poles of the integrand (See Equation 6.1 in Reference 21) from complex to real. For complex poles, the motion is similar to that of the under-damped system. When the poles become real, the response behaves like an over-damped system. It is reasonable to conclude that critical damping will occur as the poles change from complex to real. As Equation 6.1 in Reference 21 is a quadratic equation in z , the transition from complex to real roots of z will occur as the discriminant, D , goes to zero. Where

$$D = \sigma_n^2 - 4\sigma_n \tilde{g}_n \quad (11)$$

D equals zero for two cases. In the only nontrivial case,

$$\begin{aligned} H &= 4 \tilde{g}_o \frac{B}{E} \\ &= 1.71 \times 10^{-2} \quad \text{for } B = 0.4 \times 10^6 \text{ psi} \\ &= 34.2 \times 10^{-2} \quad \text{for } B = 2.0 \times 10^6 \text{ psi} \end{aligned} \quad (12)$$

Thus, it can be seen that motion corresponding to the case of critical damping is obtained for the case described in Figure 12 where $H = .0171$. For thickness-to-radius ratios less than this value, the solution yields complex roots and

corresponds to the under-damped case, as indicated when $H = .01$. For $h > .0171$, the solution yields real roots and the shell response corresponds to an over-damped case, having an appearance similar to that indicated for the values $H = .04$ and $.08$.

It is interesting to note that for the case of the high-modulus medium ($B = 2 \times 10^6$ psi) the roots remain complex for $H < .342$. Values of the thickness-to-radius ratio of this magnitude exceed the limits of thin-shell theory. It may be observed that the response curves for all indicated values of H in Figure 13 resemble the under-damped case. It should also be noted that as H increases the response of the shell becomes more rapid, the initial velocities of the shell being greater for thicker shells in a given medium than they are for thin shells.

In the zeroeth-mode-displacement response for the high-modulus medium (Figure 13), the characteristic under-damped motion of the shell may be observed. It should be noted however, that the peak values of the displacement are considerably larger for the high-modulus medium than for the low one. Whereas the maximum value of the displacement for the low-modulus medium was $Q_0 = 1.1$ for $H = .01$, the peak value of the displacement for the high-modulus medium is $Q_0 = 1.35$ for $H = .01$. The increase in the peak values of the zeroeth-mode displacement is also accompanied by more pronounced oscillation of the shell about the static displacement. There is an apparent direct connection between the magnitude of the discriminant D (Equation (11)) and the damping of the zeroeth-mode response. As the imaginary part of the complex root of z increases, the damping of the zeroeth-mode displacement decreases. Hence, peak responses increase under such conditions and it may be concluded that

oscillatory motion will become more predominant as well; the motion will decay to the static displacement value more gradually as the magnitude of the imaginary part of the root of z increases. This indicates that for values of the bulk modulus of the medium exceeding those presented here, peak shell response would continue to increase with increasing values of the modulus and damping would be expected to decrease.

4.1.2 Rigid-Body Response - First Mode ($n = 1$)

The rigid-body-displacement response of the shell to a unit step pulse is shown in Figures 14 and 15. The velocity response to the step pulse is shown in Figures 25 and 26. The most striking feature of the rigid-body response to a step pulse is the terminal velocity which the shell attains. The shell is accelerated until it reaches its characteristic terminal velocity. This acceleration period is relatively short. (However, for example, see Figures 25 and 26 where terminal velocity is essentially reached before $\tau = 5$.)

Figures 14, 15, 25 and 26 indicate that terminal velocity is a function of both B and H . Actually, in dimensional units the terminal velocity is independent of H and depends only on B ; it is identical to the free field particle velocity associated with the stress wave. The H dependence indicated in the figure is due solely to the manner in which the nondimensional variables were formulated.

4.1.3 Second Mode Response ($n = 2$)

The second mode response to a unit step pulse is shown for relatively short times in Figures 16 and 17. The long-time response is shown to a different scale in Figures 20, 21, and 22. The second-mode response develops the largest

variations in displacement of any of the elastic modes, $n = 0, 2, 3, 4 \dots$

This is particularly true for the low-modulus soil. The peak displacement response for a given shell thickness is nearly five times as great for the low-modulus soil as it is for the high modulus.

The effect of shell thickness on the second-mode response is quite significant. Figures 16 and 17 show that Q_2 is nearly directly proportional to shell thickness. It is only for the very largest displacement response, i.e., thick shell and low modulus medium where this direct relationship breaks down. This effect may be quite misleading. Since the static displacement, q_{st} , is actually inversely proportional to the shell thickness, this effect and the increasing of Q_2 with shell thickness tend to cancel each other. Thus the actual dimensional displacement in the second mode, q_2 , would be nearly the same for all shell thicknesses, except for the case of thick shells in a low-modulus medium where q_2 would be somewhat less than that of a thin shell in the same medium.

Consider now the gross motion of the shell in the second mode. Comparing the curves of the displacement, Figures 16 and 17, with those of the velocity, Figures 27 and 28, it can be observed that the peak values of velocity occur as the front of the wave passes over the shell, i.e., $0 \leq T \leq 2$. In all cases, the peak is reached during this very short period. In general, one can also observe that an abrupt change in shell velocity occurs after the passage of the wave over the shell. The essence of this activity during the engulfment period is contained in the contribution of the incomplete Bessel Function, $I_{n\theta}(z)$, which is a time-dependent factor during the passage of the wave across the shell.

Its value is dependent upon the value of the angle, $\Theta = \cos^{-1}(1 - \tau)$, which describes the position of the wavefront in terms of the angle swept out by a radius vector to the shell surface at the wavefront and the x-axis of the shell. The incomplete Bessel function becomes an ordinary Bessel function when the wavefront has traversed the shell $\Theta = \pi$ or $\tau \geq 2$, and thereafter is no longer time dependent. Thus, following the engulfment of the shell by the wavefront, the motion of the shell is entirely a function of the two exponential terms of the equation, $e^{z_1(\tau-1)}$ and $e^{z_2(\tau-1)}$. But since z_1 and z_2 are the two roots of a quadratic equation which, in the case of the second mode, may be shown to always be complex for the entire range of variables investigated for this problem, z_1 and z_2 are simply complex conjugates of one another. Letting

$$z_1 = \gamma \pm i\Omega, \quad (13)$$

the two time-dependent exponential terms become

$$e^{-\gamma(\tau-1)} : e^{i\Omega(\tau-1)} \quad (14)$$

The first term of (14) contributes an exponential decay to the magnitude of the modal shell displacement, while the second term gives the response a time harmonic oscillatory motion with frequency Ω . It can be shown that γ and Ω may be represented as

$$\gamma = \frac{\sigma_n}{2}; \quad \Omega = \frac{1}{2} \sqrt{4\tilde{\sigma}_n \tilde{\epsilon}_n - \sigma_n^2} \quad (15)$$

In the second mode, the magnitude of σ_2 is very small with a range of $1.2 \times 10^{-4} \leq \sigma_2 \leq 3.07 \times 10^{-2}$

Thus, the exponential decay term $e^{\gamma(\tau - 1)}$ is very small and, at the lower limits of σ_2 , becomes almost negligible. Conversely, Ω is directly proportional to $\sqrt{\sigma_2}$. Hence, the order of magnitude of the frequency of the shell oscillatory motion is several times greater than that of the decay factor, γ . For this reason, a distinct time-harmonic oscillation of the shell, about the zero point of the displacement may be seen in the long-time response of the shell in the second mode, as shown in Figures 20 through 22. Little or no evidence of any exponential decay can be observed for the high-modulus medium, but the decay rate of the low modulus medium is apparent as might be expected, since the largest values of σ_2 are associated with the low-modulus medium.

4.1.4 Higher-Mode Response (n = 3, 4)

Response of the shell in the higher modes is shown in Figures 18 and 19 for the displacement and Figures 29 through 32 for the velocities. The displacement response in the higher modes decreases rapidly with increasing modal order. Although there are some relatively large fluctuations in displacement during the engulfment period, the shell motion in the higher modes is nearly negligible in terms of long-time motion. One would expect that the long-time motion of the shell in the higher modes should be very similar to that of the second mode in that it should exhibit the same type of oscillatory motion about the zero value of the modal displacement with a frequency Ω which is proportional to $\sqrt{\sigma_n}$ while the magnitude of the oscillations should decay exponentially in time with a decay factor $\gamma = \frac{\sigma_n}{2}$. However, the magnitude of the displacement which remains at $\tau = 2$ is negligible

and the oscillatory motion is imperceptible. The decay factor γ is substantially larger for the higher modes as well, being of order one for thick shells and low-modulus soils. Thus, even if the motion were apparent, it would decay rapidly with time and be of little significance following the passage of the wave over the shell. During the engulfment of the thicker shell, however, some fairly substantial peak positive and negative displacements are obtained for the low-modulus medium (Figure 18). Since they are of relatively high frequency, their effect on items of equipment to be shock-isolated may not be negligible.

Although the peak positive and negative displacements for the higher modes decrease much more rapidly than do the velocities as the modal number increases, observation of the velocity-time curves for the shells (shown in Figures 29 through 32) indicates that the peak velocities decrease fairly rapidly with increasing modal number. Thus, both the displacements and the velocities are negligible after engulfment, and it is unnecessary to carry the investigation of the modal response of the shell beyond the fourth mode.

4.2 Response to Rectangular Pulse

The peak positive and negative values of displacement response of a shell are shown in Figures 33, 39, 45, 46, 57 and 59, for the zeroeth, first, second, third, and fourth modes, respectively. Peak modal velocity response to a rectangular-pulse input are shown in Figures 61, 67, 73, 80, 81, 82 and 83, again for the zeroeth, first, second, third, and forth modes, respectively. All the above curves are plotted in terms of peak response versus dimensionless pulse wavelength, λ , as a function of thickness to radius ratio, H , and bulk

modulus of the medium, B. Response-time histories for shell response to a rectangular pulse may be obtained by direct superposition of a step pulse response curve initiated at time τ_A (see Figure 10) and a negatively directed step pulse response curve of equal magnitude initiated at the time τ_B , the delay corresponding to the desired input wavelength. Thus, the results obtained for the peak response curves may be inferred directly by observation of appropriate step-wave curves. Typical modal response-time curves for the case of rectangular-pulse interaction are shown in Figure 84.

4.2.1 Zeroeth-Mode Response

Description of the zeroeth-mode displacement response to a rectangular pulse is made more tractable by distinguishing between relatively short and relatively long pulse lengths. For relatively short pulse durations, the shell displacement is characterized by increasing absolute values of the peak positive and peak negative response with increasing wavelengths. As the duration of the rectangular pulse increases, however, the peak positive and negative displacement response curves reach constant values which are not exceeded thereafter regardless of how long the pulse length is made. For relatively large pulse lengths, increasing the shell thickness decreases both the peak positive and negative displacement response of the shell. For short pulse lengths, the situation is reversed, and increasing shell thickness causes increased peak positive values of the displacement response. As the soil bulk modulus increases in magnitude, the magnitude of the peak positive and negative shell response increases also. In the paragraphs which follow, an explanation of these response features is given.

From a comparison of the curves of Figure 33 with those of Figures 12 and 13, it is apparent that if the pulse duration is less than the time required for the shell displacement to reach its peak response to the step pulse, the maximum value of the response will be that value of the displacement which the shell has attained at the moment the tail of the wave reaches the shell, and the negatively directed step-pulse curve is initiated (i.e., when $\tau = \ell$). Thus, the peak positive values indicated in Figure 33 follow the pressure-time curve for the step pulse as shown in Figures 12 and 13 exactly until the peak value of the response to the step pulse is reached. When positive duration of the pulse is longer than the time required to reach the maximum for the step pulse, the maximum value remains constant at the peak value obtained with the step pulse.

The peak negative values obtained for the zeroeth mode are much smaller in absolute magnitude than those of the peak positive response. That peak negative values are obtained at all is simply the result of the fact that the displacement response to the step wave may overshoot the static displacement. If this occurs, then regardless of when the negatively directed portion of the pulse is initiated, there will be a time at which its absolute magnitude will exceed that of the earlier starting positive phase of the wave. This will then provide the peak negative response of the shell. If, in the step-pulse response, the response does not overshoot the static displacement value but acts as though it were overdamped, approaching the static displacement value from below, then there can be no peak negative value for any rectangular pulse. This will be true regardless of the length of the rectangular pulse. An example of this is

shown in Figure 33 for the low-modulus soil and shell thicknesses of .04 and .08. The curve indicates that there are no peak negative displacement values for such shells. On the other hand, the thinner shell ($H = .01$) behaves as an under-damped mass-spring system, overshooting the static displacement value before returning to it.

Attention should be called to the fact that positively and negatively directed displacement response is simply a function of sign convention. According to the shell displacement sign convention, negative displacements are directed outward, in the direction of increasing values of r . Thus, increasingly negative values of the displacement indicate actually increasing absolute values of the outwardly directed displacement. That is to say, large absolute values of negative displacements are actually just large outward displacements. In the following sections when large peak negative values of the response are mentioned, it should be understood that large absolute values are implied.

Returning to the discussion of zeroeth mode response to a rectangular pulse, it should be noted that the peak negative response obtained in the zeroeth mode for the rectangular pulse remains constant after the pulse length has reached a certain value. For example, in the high-modulus thin-shelled case, the response of the shell to a step pulse appears to have little damping and oscillates noticeably about the static displacement, but with decaying amplitude. For such a case, the constant value of the peak negative response which the shell attains for large pulse lengths may not, in fact, be the maximum value of the peak negative response of the shell. Examining the particular case illustrated in Figure 33, it is observed that the largest absolute value of the

negative response is obtained at a pulse length of about $\ell = 14$. Comparing this result with the displacement-time history shown for the step-pulse response of a shell-medium system with the same properties, as shown in Figure 13, it may be observed that this corresponds to the initiation of the negatively directed pulse at a time such that its maximum absolute value will occur at the time when the lowest point of the first oscillation of the positively directed pulse about the static displacement is obtained. Such a case provides the maximum peak negative value of the response.

It is interesting to observe that in the zeroeth mode, as the shell thickness increases, the peak positive value of the shell displacement response decreases for long pulse durations. On the other hand, for pulse lengths less than that required for the attaining of the maximum peak positive values for each of the shell thicknesses considered, the opposite condition holds. That is, under such circumstances, thick shells will have larger dynamic displacements than a thin shell. This phenomenon appears to hold true regardless of the bulk modulus of the medium.

In the case of the peak negative displacement values, the absolute value of the shell response is always greater for thin shells than for thick shells, regardless of wavelength and medium properties.

The effect of variation in medium modulus on the shell response is similar to that for the step pulse. That is, as the modulus of the soil increases, the maximum and minimum displacements of the shell increase also.

In summary, the results of variation of shell and medium parameters on zeroeth mode shell displacement response to a rectangular-pulse yield the

following information:

(1) For relatively large pulse lengths, increasing the shell thickness decreased both the peak positive and negative displacement response of the shell.

(2) For short pulse lengths, the situation is reversed, and increasing shell thickness causes increased peak positive values of the shell.

(3) As the soil modulus increases in magnitude, the magnitudes of the shell peak positive and negative response increase also.

Moreover, the response of the shell in the higher-modulus soil is more sluggish than in a lower-modulus soil. This is shown by the fact that larger times, hence greater pulse lengths, are required to obtain both the maximum values of the peak positive and negative response in the higher-modulus soil.

Results for the velocity response to the rectangular pulse are more straightforward than those of the displacement. The velocity response-time curves for a rectangular pulse may be obtained by superposition from step-pulse velocity-time curves in an identical fashion to those for the displacement.

Comparing Figures 23 and 24 for step-pulse velocities with Figure 61 for the rectangular-pulse peak positive and negative velocities, it can be seen that maximum velocities for the step pulse are obtained very rapidly. Consequently, the pulse lengths required to obtain the maximum-peak-positive values of the velocity (Figure 61) are very short. It is physically impossible to exceed the maximum-peak-positive velocity values obtained for the step pulse regardless of

rectangular-pulse lengths. Similar results are obtained for the peak-positive-velocity response as a function of pulse length regardless of shell or medium parameters.

The peak-negative values of shell response do not have the same response characteristics which are found in the peak-positive values. In considering the effect of the step-pulse velocity response on the rectangular-pulse response, it may be observed from the step-pulse response curves (Figures 23 and 24) that the peak velocity increases with increasing shell thickness. However, the duration of the velocity response and the variation in shell motion is greater for the thinner shells. As the soil modulus increases (hence, as observed previously, damping of the shell motion decreases) variation in velocity-time curves and duration of response increases. Thus, for the thinnest shell in the high-modulus medium, a well-defined peak negative value of the velocity occurs in the velocity-time history of the response to the step-pulse. This minimum value of the velocity occurs at a time of approximately $\tau = 17.5$. If the length of the rectangular pulse is chosen such that in superposition, the negatively directed peak velocity associated with the tail of the wave is made to coincide with the appropriate value of time at which the positively directed phase associated with the head of the wave is experiencing the above described minimum, a peak-negative-velocity value whose absolute magnitude is greater than that of the peak-positive value will occur. This accounts for the rather peculiar looking bulges occurring in the peak-negative-velocity-response curves shown for the high-modulus medium in Figure 61. It will be noticed that the maximum value of the peak-negative response,

in absolute value, exceeds the maximum response for the peak-positive velocity for the equivalent thickness. In particular, the pulse length at which the maximum-peak negative velocity is obtained corresponds to about $\ell = 13$ when $H = .01$, $\ell = 7$ when $H = .04$, and $\ell = 7$ when $H = .08$, for the high-modulus soil. At pulse lengths greater than these indicated values, the peak-negative velocity response decreases in absolute magnitude until, for long pulses, the peak positive and negative responses for the shell velocity are identical. Similar results, though not so pronounced, are observable for the thin-shell, low-modulus soil case. The thicker shells do not exhibit this same characteristic for the low-modulus soil. The velocity responses of these shells approach zero rapidly without a change in direction.

It should be noted that the development of maximum values of peak negative response of equal or greater absolute value than the peak-positive maximum occurs at much larger pulse lengths than those required to obtain constant maximum values of the peak-positive velocity. The required pulse length to obtain maximum values of the peak-negative-velocity response decreases as the shell thickness increases. As an example, observe that pulse lengths on the order of $\ell \leq 1/2$ are required for the maximum-peak-positive-velocity response to be attained for the low-modulus soil. To obtain the maximum-peak-negative response for the thick shell, a pulse length of $\ell \geq 4$ is required. For a thin shell in the same medium, a wavelength of approximately $\ell \geq 7$ is required before the magnitude of the peak-negative response becomes equal to or exceeds that of the maximum peak-positive response. Similar results are obtained for the high-modulus medium.

The peak positive and negative absolute values of velocity response increase with increasing shell thickness for all pulse lengths. For the low-modulus soil, the range of the maximum velocity values is .41 for $H = .01$, .88 for $H = .04$, and 1.25 for $H = .08$.

As the modulus of the soil increases, the same general relationship between the maximum velocities and shell thickness continues to hold true. However, as the soil modulus increases, the absolute value of the peak positive and negative response is decreased. For example, the corresponding values of velocity maxima in the high-modulus soil to those shown above for equal shell thickness in the low-modulus soil are .17 for $H = .01$, .37 for $H = .04$, and .56 for $H = .08$. Thus, the magnitude of the velocity response has been reduced to a value less than half that of the low-modulus soil-shell system. For the high-modulus soil the magnitude of the maximum-peak-negative velocity exceeds that of the maximum-peak-positive response for the corresponding shell thickness in every case. The representative values of the maximum-peak-negative velocity being .24 for $H = .01$, .42 for $H = .04$, and .59 for $H = .08$. The absolute values of the peak-negative velocity maxima will exceed corresponding values of the peak-positive maxima in every case where the medium-shell system exceeds the requirements for critical damping and becomes underdamped.

Summarizing the variation in zeroeth-mode velocity response with medium and shell parameters, it is noted that:

- (1) The maximum-peak-positive velocities associated with rectangular-pulse shell response are developed very rapidly and consequently are nearly independent of the pulse length. Only

for pulse lengths less than the shell diameter is there a likelihood that the maximum-peak-positive velocities will not be obtained.

(2) For very long pulse lengths, the absolute values of the peak positive and negative velocity maxima are identical.

(3) For an intermediate range of pulse lengths ($5 < \beta < 20$ for the range of parameters investigated in this report) it is possible, under certain conditions, for the maximum-peak-negative-velocity response to have a greater absolute value than the maximum-peak-positive response.

(4) Greater absolute values of maximum-peak-negative velocity will occur, however, only when the medium-shell satisfies the conditions required to achieve the underdamped state.

(5) The absolute values of the maxima of both peak positive and negative velocities increase with increasing shell thickness.

(6) Absolute values of the maxima of both peak positive and negative velocities decrease with increasing soil-modulus values.

(7) For equal shell thicknesses, increasing values of soil modulus produce decreasing damping effects and consequently make the possibility of maximum-peak-negative velocity exceeding those of the maximum-peak-positive velocity more likely.

Moreover, as the damping decreases, the frequency of the oscillatory shell motion decreases so that longer pulse lengths are required to obtain the absolute maximum values of the velocity.

4.2.2 Rigid-Body Response

Rigid-body-peak-positive-displacement response to a rectangular-pulse input is shown in Figure 39. Except for very short pulse lengths, the peak-positive response is a linearly increasing function of pulse length. Figure 84(c), a typical rigid-body-motion-time curve, illustrates this type of motion. If the pulse length is sufficiently long for the shell to reach its terminal velocity, further increase in pulse length will merely result in an extension of the linear portion of the displacement-time curve. Therefore, for all cases where the pulse length is of sufficient duration to raise the shell to terminal velocity, the maximum displacement will be found along the linear portion of the curve in Figure 39. When the pulse length is too short for the shell to reach its terminal velocity, the shell motion is taken up completely in the initial acceleration and final deceleration phase. The range of the pulse lengths which are too short to accelerate the shell to terminal velocity is very narrow. The pulse lengths must be less than 2 shell diameters ($\ell = 4$) to qualify for this distinction.

In each case, the terminal velocity which is approached is that of the free-field particle motion due to the passage of the stress wave.

The peak positive and negative velocity response curve for the rectangular-pulse input is given in Figure 67. As might be expected, the curves in Figure 67 are identical to those found for the step pulse. (Compare Figures 25 and 26).

4.2.3 Second-Mode Response

The most striking feature of the second-mode-maximum-displacement response curve, as shown in Figure 45, is the large magnitude of the thick shell-peak-negative-displacement curve. Its absolute magnitude is nearly twice that of the corresponding peak-positive-displacement curve shown in the same figure for the same case. The explanation of the phenomenon can be obtained by considering the long-time-second-mode-response curve to the step pulse shown in Figure 22. These long-time-displacement-time histories for the step pulse indicate that the shell responds very rapidly, initially, attaining what appears to be an initial displacement. Then, in a manner similar to a damped single-degree-of-freedom system subject to an initial displacement, the shell oscillates about its null displacement in a damped manner. If the length of the rectangular pulse is such that in the superposition process the maximum value due to the negative phase is attained just as the positive phase of the motion has reached its first peak-negative response, then the response will be augmented and a response in the negative direction is obtained which is nearly double the peak positive-response value. The greatest absolute value of the peak-negative displacement curves is obtained for the shell thickness $H = .08$ at a pulse length of approximately $\ell = 14$. As can be seen in Figure 22, this pulse length closely corresponds to a half period of the apparent natural frequency of the shell-medium system. Similar values would be obtained for the other thicknesses shown if the curves were carried out to sufficient length.

The remaining portion of the response curves shows that the maximum peak-positive values of the response are reached for very short length pulses, after which the peak-positive response remains constant.

Again, the shell response for both peak positive and negative displacement increases with increasing shell thickness. This appears to be true in general except for some minor adjustments which must be made for certain long pulse lengths where there is a crossover point in the minimum curves (e.g., $\ell = 25$ in Figure 45).

As the soil modulus increases, the peak positive and negative values of the displacement decrease.

Examination of second-mode-velocity response of the shell to a rectangular pulse, as shown in Figure 73, indicates that the maximum-velocity-response curves are very similar in appearance to the maximum-displacement curves. They are not, however, nearly so extreme in the manner in which the maximum values of the peak-negative-response curves exceed the corresponding values of the peak-positive curves. Comparison of the step-pulse-velocity-time curves indicates, however, that a response in the velocity curves very similar to that shown in the maximum-displacement curves is to be expected. That this is actually the case is clearly indicated for the combination of shell thickness $H = .08$ and modulus $B = .4 \times 10^6$ psi, where a distinctly larger absolute magnitude of the peak negative value of the response is obtained compared with the corresponding peak-positive response. The oscillatory nature of the peak-negative-response curve is also apparent in the same figures. For the other thicknesses shown, the period of the oscillation is so much longer and the amplitude of oscillation so much less, that the oscillatory motion of the peak negative curve cannot be shown with the scale of Figure 73.

It should be noted that the same generalizations concerning the influence of shell thickness and soil modulus on the magnitude of the maximum-velocity-response curves made for the maximum-displacement-response curves may be applied here. That is, the peak positive and negative velocities both increase with increasing shell thickness, and decrease with increasing soil modulus. Here again, the analogy may be made between displacement and velocity. However, the rate of decrease with increasing soil modulus is somewhat less in the case of the velocity curves than it is for the case of the displacement curves.

4.2.4 Higher-Mode Response

Curves of the peak positive and negative displacement response for the third and fourth modes are shown in Figures 57 and 59. Where reliable results exist, it appears that the shell displacement response in the third mode is nearly symmetrical in both peak positive and negative response. Moreover, the response in the higher modes for all practical purposes may be considered to end when the front has traversed the shell (compare with Figure 19). The maximum-peak-positive shell response is constant for all wavelengths where $\ell > 2$. Similarly, the maximum value of the peak-negative response is identical with that of the maximum-peak positive response. But, the length of the rectangular pulse required to obtain the maximum-peak-negative response must be twice the value of that required to obtain the maximum-peak-positive-response value, i.e., $\ell > 4$.

For the third mode, the peak positive and negative response seems to increase with increasing shell thickness. Note however, that no results are

shown in the low-modulus soil case for the thickest shell, $H = .08$. This is because convergence problems with the incomplete Bessel functions for this particular combination of parameters caused the computer results for the shell displacement-time response to be considered unreliable. Again, as the soil modulus increases, the peak-positive displacement decreases. As was the case in several other modes, the response appears to be inversely proportional to soil modulus.

In the fourth-mode-displacement response, even greater problems were experienced with the reliability of the numbers obtained for certain cases. However, notice that maximum responses as shown are significantly less than in the third mode. There is a very satisfactory convergence of the maximum response values with increasingly higher modes. It was for this reason that it was felt unnecessary to determine more accurately the remaining cases whose response-time curves were considered unreliable because of difficulties with convergence of the incomplete Bessel function computation routine.

As appears to be the general case for all the bending modes, the magnitude of both peak positive and negative displacements increase with increasing shell thickness. Also, for the one case which can be compared ($H = .01$) the maximum peak positive and negative response appears to be inversely proportional to the soil modulus.

A small blip appears in the peak negative displacement curves for pulse lengths less than 2. For such lengths, it is again possible to achieve a sort of resonant situation in which the pulse length is directly related to the

minimum of an oscillatory condition in the displacement of the fourth mode.
(Compare with Figure 84 (1).)

The third and fourth mode velocities are shown in Figures 80 to 83. Again, due to problems with the incomplete Bessel functions, little can be said concerning the effect of shell thicknesses. The maximum velocities of the shell for all pulse lengths decrease as the soil modulus increases.

4.3 Response to Exponentially Decaying Pulse

Peak-modal-displacement-response curves for the shell-medium interaction with an exponentially decaying pulse are shown in Figures 34, 40, 47, 48, 58 and 60. Peak-modal-velocity curves for this case are shown in Figures 62, 68, 74, 75, and 80 through 83.

Since analytical and experimental results indicated the possibility of a waveform existing with a sharply decaying pressure spike at the leading edge, an exponentially decaying pulse was selected for investigation as one of the shapes approximating this form. In order to investigate the effect on the response of variation of shell thickness, medium modulus, the pulse length, an exponential form was selected which would give the same general waveshape regardless of pulse length of the forcing function. To satisfy this condition, the pulse selected was of the form

$$P = P_0 (1 + e^{-\beta T}) \quad (16)$$

A decay factor of $\beta = 5/l$ guarantees that the tail of the wave will always be within approximately $1/2\%$ of P_0 . A waveshape of this form was selected because it represented the superposition of an exponentially decaying spike on a

rectangular pulse with an initial pressure of twice that of the pure rectangular pulse but decaying to the rectangular pulse pressure at the tail of the pulse.

Although detailed comparison of the influence of the waveshape on response will be considered in a later section of this report, it should be noted here that there is a great deal of similarity between the response curves for the rectangular pressure pulse and the exponentially decaying pulse. For this reason, the discussion of variation in response with variation in parameters will deal only with the influence of pulse length where it produces a significantly different result than that obtained with the rectangular pulse.

In the zeroeth mode, for relatively long pulses, the absolute value of the peak positive and negative displacements decrease with increasing shell thickness. In all other modes where comparison is possible, the absolute value of peak displacements increase with increasing shell thickness. In the first and higher modes, the maximum displacement varies linearly with the logarithm of the shell thickness. In the zeroeth mode, the variation of the response is nearly inversely proportional to the logarithm of the shell thickness.

A general characteristic of the peak-displacement-response curves for the response to an exponentially decaying wave is that the peak positive values do not appear to have a maximum value as a function of pulse length. That is, for all modes, the peak positive displacement values, regardless of shell thickness or medium modulus, appear to be gradually increasing with pulse length. This cannot continue indefinitely since, in the limit of very long pulse lengths, the exponentially decaying pulse approaches the step pulse of strength $2 P_0$. Thus, a limiting factor on the peak positive displacement response of twice

that of the unit-step pulse response will exist for these curves. The pulse lengths for an exponentially decaying wave would have to be quite a bit larger than those for which data were obtained before this limit would be reached.

In the zeroeth mode, changes in the medium modulus do not produce pronounced effects. The phenomenon of the overdamped shell-medium system does not seem to appear in Figure 34. Apparently, the higher pressures of the exponentially decaying wave are sufficient to ensure that the dynamic displacement response of the shell will always exceed the static displacement. However, it may be observed that, for the low-modulus medium, the peak-negative values of the response curves of Figure 34 are considerably less than those of the high-modulus medium. In fact, for the thicker shells, which for the rectangular pulse were found to be overdamped, the peak-negative response is negligible, indicating that these shells return to their equilibrium position after passage of the wave with no oscillatory motion thereafter. For the higher-modulus medium, however, observe that there is a notable value of the peak-negative response for all shell thicknesses, especially the thinner ones.

In the variation of the response with increasing medium modulus for the zeroeth mode, note that the response appears to become more sluggish with increasing modulus. That is, the increase in peak positive displacement requires pulses of greater length in the high-modulus medium than in the low-modulus one to obtain the same displacement values.

In the higher modes, it can be seen that peak-displacement values appear to be inversely proportional to the modulus of the medium. In the second mode, this appears to be true for all shell thicknesses. In the first mode, some

minor variation from inverse proportionality is experienced as shell thickness increases, but for thin shells these minor variations do not exist. In the higher modes, for the cases where comparison is possible, the relationship seems to be approximately valid and gives a fair estimate of the small values of the maximum displacements which would be expected under such conditions.

In the case of the peak-velocity-response curves, it may be observed that increasing the shell thickness for a given medium causes the absolute value of peak positive and negative velocities to increase. This appears to be true of the peak positive and negative velocity in all modes where it is observable. The variation in peak positive velocity as a function of shell thickness is proportional to the logarithm of the shell thickness. Peak-negative velocities are subject to a sort of pseudo-resonance condition where the negative response is strongly augmented at certain pulse lengths.

There is no apparent peak-positive value of the velocity obtained in any mode investigated. All of the velocities increase with increasing pulse length. If the pulse-length curve were extended the peak-positive velocity curves would approach the peak-positive velocity associated with a step pulse of twice the strength. But for the step pulse, doubling the strength simply doubles the values of the displacements and velocities obtained in the response. Hence, in the limit of long pulse lengths, the peak-positive velocities of the shell obtained with the exponentially decaying pulse must approach a value equal to twice that obtained for the step pulse.

It should also be noted that increasing the value of the soil modulus causes a decrease in the shell velocities. In the first and second modes, the

peak positive and negative velocities are inversely proportional to the modulus of the medium.

4.4 Summary of Shell Response to Step, Rectangular and Exponentially-Decaying Pulses

Results discussed in preceding subsections of Section 4 are summarized in this section. Note that displacements and velocities are compared in this subsection, whereas most of the preceding discussion is based on the comparison of the nondimensional quantities plotted in the figures at the end of Section 4.

4.4.1 Zeroeth Mode

Peak positive and negative displacements decrease with increasing shell thicknesses. The displacement-time history has the appearance of an under-critically-damped spring-mass system for thin shells and high modulus soils. Motions become more sluggish, resembling an over-critically-damped spring-mass system for thick shells and low modulus soils.

4.4.2 First Mode (Rigid Body Displacement)

The shell rapidly accelerates to the particle velocity associated with the stress wave in the free field. Total displacement is substantially the same as the free field.

4.4.3 Second and Higher Modes (Bending Modes)

Peak displacement is greatest for the lowest modulus soils. Peak displacement of the second mode is practically independent of shell thickness. Displacement decreases rapidly with increasing modal number.

4.5 General Response to Change in Shell and Medium Properties for Other Waveshapes

There is little further to be gained by separate analysis of the influence of changes in shell and medium parameters on the maximum shell response for the remaining waveshapes. Examination of the response curves will show that a pattern has been established which can be generalized for all cases.

In general, the zeroeth-mode peak positive and negative response is characterized by a decrease in absolute value of the displacement with increasing shell thickness for the long pulse lengths. For short lengths, a transition point occurs and the opposite effect may be observed with increasing shell thickness producing increased peak-positive responses. The most marked effect which change of medium modulus has on zeroeth-mode response is the change in the position of the transition point in displacement response with shell thickness. For the low-modulus medium the transition point occurs at pulse lengths of approximately $\ell = 5$. For the high-modulus medium, the shell response appears to be more sluggish and the transition occurs at values of the pulse length of about $\ell = 10$.

Another notable effect of variation in the medium modulus is the characteristically overdamped response for the low-modulus medium and the thicker shells. Only a relatively minor variation occurs in the actual value of the peak positive and negative zeroeth-mode displacements with change in soil modulus when compared with the effect which this parameter has on displacement in other modes. It should also be noted that for pulse shapes (which have only a positive phase as opposed to waveshapes which have both positive and negative phases), the peak-negative response for the shell experiences no transition point in the effect

of shell thickness as do the peak positive responses. However, when waveshapes such as the sine or modified sine are used, the zeroeth-mode peak negative responses are nearly identical to those of the peak-positive responses.

The rigid-body-positive response is basically identical in form for all waveshapes. In general, the shell response increases linearly in magnitude with increasing wave length. Shell response may be considered, for all practical purposes, as varying inversely with modulus of the medium.

The second mode is characterized more by values of the peak-negative response than that of the peak positive. The absolute values of both peak-positive and peak-negative response increases with increasing shell thickness. As with the first mode, both values appear to be inversely proportional to the modulus of the medium. The effect of changes in wavelength upon the response can most properly be discussed later as part of the consideration of the effect of waveform on shell response.

Where observations are possible with the higher modes ($n = 3$ and 4), it appears that absolute values of the peak-positive and peak-negative displacements increase with increasing shell thickness. Again, the response of the shell in the third mode seems to be inversely proportional to the soil modulus.

As far as modal velocities are concerned, the absolute values of the peak-positive and peak-negative responses are seen to increase with increasing shell thickness in all modes. Although they also appear to decrease with increasing soil modulus, an inverse proportionality relationship with soil modulus again appears to hold reliably only in the first and second modes. Some indication exists that the relationship may hold for the higher modes as well, but it

cannot be completely verified in all cases and existing data are rather slim to give a definite answer to this question.

4.6 Influence of Variations in Waveform on Response for Given Medium and Shell Properties

In considering the influence of variations in waveform on shell response, the exponentially decaying pulse must be considered as a special case. Peak pressures associated with the exponentially decaying pulse were permitted to vary. Thus, it is not possible to compare directly the numerical values of the displacements obtained with the exponentially decaying pulse with those obtained with other shapes where peak pressures were uniformly normalized. Therefore, the exponentially decaying pulse will be discussed separately following the general comparison of the other waveshapes. The general waveshape comparison will be conducted by consideration of the response in the several separate modes individually. Wide variations in peak-response curves make it impossible to generalize a single description of waveshape effects which would satisfy the conditions in all modes. In the following modal analysis, the influence of waveshape on displacement and velocity will also be considered separately.

4.6.1 Zeroeth-Mode Response

Zeroeth mode response to variation in pulse and waveshape can best be analyzed by dividing the shape into two categories; those with positive phases only (pulses), and those with both positive and negative phases (waves). The first group includes the rectangular pulse, the half-sine, and the haversine. The rectangular-pulse-positive-and negative-response curves represent upper and lower bounds for all the pulses with the exception of the exponentially,

decaying pulse. In all these cases, maximum shell response attains or is slightly greater than the static-displacement response. In the transition from rectangular to half-sine pulse, a decrease in the maximum response of the shell is experienced which is less than 5% of the rectangular-pulse maximum displacement. The response, however, is more sluggish in the half-sine case, requiring somewhat longer pulse lengths to achieve the maximum-response values. In going from half-sine to haversine shape, there is a negligible change in appearance of the zeroeth-mode-peak-positive-displacement-response curves.

The influence of shape on the zeroeth-mode velocities is more apparent than it is on displacements, but many of the same conclusions are applicable. The rectangular-pulse-peak-response curves represent an upper bound for the maximum velocity of all the pulses. In fact, the rectangular-pulse-peak-response curves very nearly bound cases of both pulses and waves.

In the transition from rectangular to half-sine pulse input, the half-sine-peak-positive-velocity responses approach those of the rectangular pulse only for very short pulse lengths. The influence of pulse length on peak-positive-and negative-velocity response for the half-sine shape is very pronounced.

As the wavelength increases, the peak-positive-and peak-negative-velocity responses decrease rapidly in absolute magnitude. This is readily explainable in that at very short pulse lengths, a half-sine pulse of unit amplitude and rectangular pulse of unit amplitude have practically identical impulses as well as physical appearance. As the length of the half-sine pulse increases though, the relative impulse which it provides when compared with the rectangular pulse decreases sharply. This influence is more noticeable for the velocities of the

shell than for the displacements, since displacements seem to be relatively independent of pulse length and shape in zeroeth mode. At least this displacement independence appears to hold for the large pulse lengths where the velocity is significantly affected. For lengths greater than $\ell = 20$, the thick shell ($H = .08$) velocities are less than $1/6$ their value in the response to a rectangular pulse. At large lengths for the half-sine pulse, the velocities become relatively independent of thickness approaching a constant value for both peak positive and negative velocity curves, regardless of soil modulus. This constant value is approximately 0.2.

Little change in peak velocities is attained in going from the sharp-edged half-sine pulse to the haversine, with its more gradual change in derivatives. In fact, the absolute value of the peak positive and negative velocities is slightly greater for the haversine shape than the half-sine.

In transforming from the half-sine and haversine pulse shapes to the sine and modified sine waves, the peak-positive values of the velocity are almost unchanged. The peak-negative values of the velocity for small wavelengths, however, are nearly doubled in absolute magnitude. For the sine-wave shapes, the maximum peak-negative velocities are nearly 50% greater than the maximum-peak-positive velocities at the same wavelengths. This large variation in zeroeth-mode velocity as a result of waveshape is only true for very short wavelengths. For wavelengths for $\ell > 5$ the half-sine and sine curves are within 6% of one another for the low modulus medium. However, a rather wide variation still exists at these wavelengths for the high-modulus medium and continues to be larger than that for the low-modulus medium until a wavelength

of about $\ell = 10$ is reached. For longer wavelengths, the response for absolute values of both peak positive and negative velocities again appears to approach a constant value of 0.20 which is independent of wavelength, soil modulus, and shell thickness. The variation in velocity obtained in going from the sharp-edged sine-wave shape to the modified sine is negligible as may be seen in Figure 66.

4.6.2 Rigid-Body Response

Although the basic shape of the rigid-body-peak-displacement response curves is unchanged with variation of waveshape, the magnitude and the slope of the linear portion of the curve is strongly influenced by waveshape. One observes that in going from the rectangular pulse to the half-sine pulse, the peak response is reduced by approximately 40%. In reducing the accelerative forces by smoothing the pulse shape from half sine to haversine, the peak displacements are reduced even more. The peak response for the haversine is approximately 75% that of half sine.

The half-sine pulse and the sine wave, on the other hand, have essentially identical peak-positive-displacement values. The reduction in maximum displacements in going from the sine to the modified sine is not as marked as the corresponding transition from half sine to haversine. Reductions of approximately 10-15% are obtained in this transition.

In the rigid-body-peak-velocity-response curves, the rectangular pulse velocity curves represent the limiting values for all other cases. Velocities equal to rectangular-pulse velocities are obtained for half-sine pulses of sufficiently long pulse lengths. For shorter lengths however, the velocity

response is more sluggish and peak-positive velocities remain behind the rectangular-pulse velocities by as much as 50% at $\ell = 2$. Nearly equal values are obtained for lengths of $\ell \geq 10$.

The velocity response to the haversine is essentially identical to the rectangular-pulse velocity for wavelengths $\ell \geq 10$. For shorter wavelengths however, the haversine velocities are found to be even less than the half-sine velocities by as much as 20%. These values are again obtained at wavelengths of approximately $\ell = 2$.

Response curves for the sine and modified-sine waves are essentially identical in form to those of the half-sine and haversine pulses, respectively, with the exception that the sine and modified sine have a set of minimum velocity curves which are essentially mirror images of the maximum-velocity curves for the same material and medium properties.

4.6.3 Second Mode Response

The peak response curves of the second-mode displacement are strongly dependent upon waveshape and shell thickness. Because there is a wide variation in peak response under the influence of different waveshapes and shell and medium properties, it is difficult to compare the response in general terms.

The peak-displacement-response curves for the sine and modified sine waveshapes are particularly complex in interrelationship of the parameters. But it is for these waveshapes that the maximum values of the peak-displacement response are obtained. Figures 53 through 56 present the peak-response curves for the sine and modified-sine waveshapes. Maximum-response values are obtained

for the low-modulus soil from a bulbous response curve shown in Figure 53. The maximum value of the response shown for the peak-positive displacement at $\ell = 16$ is the largest value of the response obtainable regardless of wavelength. The peak-positive-response curve for larger wavelengths than those shown will follow a series of humps of decaying amplitude. In Figure 53, the maximum-peak-positive response is shown to have a value of approximately 12. This is about twice the value of the maximum-peak-positive response for the rectangular pulse in the second mode, and approximately 30% greater than the maximum-peak-negative-response value for the rectangular pulse. The maximum value of the peak-negative response for the sine and modified-sine wave is also very large with a maximum value larger than either the maximum peak positive or negative response of the rectangular pulse.

Peak response to the sine and modified-sine wave is much larger than that due to other waveshapes. Peak-response values for all other shapes may be bounded by the response to the rectangular pulse. In the case of the response to the half-sine and haversine pulses, for relatively short wavelengths ($\ell \leq 5$) the response curves follow closely those of the rectangular pulse. At longer pulse lengths, the peak displacement responses, both positive and negative, decrease rapidly to values much below the rectangular-pulse values.

For the peak-velocity-response curves, the second-mode response is much more well behaved than was the case with the displacements. For the peak-velocity-response curves, except for very small values of ℓ , maximum-response values for the rectangular pulse exceed the response values of all other wave and pulse shapes. In general, the peak positive and negative response curves

are nearly symmetric. However, for the case of thick shells and the low-modulus medium, the peak-negative-velocity response curves exceed the peak-positive values for nearly all shapes. In particular, for the sine and modified-sine shapes, the maximum peak-negative-velocity response (at $\ell = 1.5$) can be seen to be slightly greater than maximum peak negative response of the rectangular pulse. For these short lengths, the maximum value of the sine and modified sine are almost the same and exceed the maximum response of the rectangular pulse by approximately 30%. As the pulse lengths increase, $\ell > 2$, the peak response, both positive and negative, for all shapes other than rectangular pulse, decreases very rapidly. Thus, in the case of the second-mode velocities, the assumption that the incoming wave is rectangular leads to maximum response values.

4.6.4 Higher-Mode Response

Higher-mode displacement response is shown as a function of waveshape in Figures 57 through 60. In the range of $0 < \ell < 1$, the displacement has an extremely rapid increase with ℓ in its peak-positive values. For all greater lengths, displacement remains constant. The curves for peak negative velocity for the third-mode response to the rectangular pulse are quite unusual since they are practically mirror images of the maximum displacement curves.

The effect of changes in waveshape on the displacement is shown graphically for the thickness $H = .01$ in Figure 58. At a glance, one can observe that the peak-positive-displacement response for half sine, sine, haversine, and modified sine are practically identical. The peak positive values associated with these curves are 12% to 15% lower than the rectangular-pulse value. Values for all

shapes except the rectangular pulse are recorded only for $0 \leq l \leq 5$. It can be seen however that for all waveshapes the maximum values decrease sharply for $l \geq 2$. Since the waves decay rapidly, it was not felt necessary to obtain data beyond the limits shown.

Similar results can be seen for the peak-negative-displacement portion of the response curves with only two basic changes. First, the sine and modified-sine peak-negative displacements exceed all others for the third mode. Their maximum values of displacement are nearly 40% larger than the largest peak-rectangular-pulse displacements.

The unique form of the rectangular-pulse displacement in the fourth mode (see Figure 84) produces some unusual maximum-displacement curves. As indicated in Figure 59, the rectangular-pulse-peak-displacement curves have their absolute maxima on the negative side of the curve for very small values of the pulse length, $.5 \leq l \leq 2$. For these short lengths, values of the peak displacement approximately 25% to 35% greater than the long-pulse-length-peak-displacement values may be obtained. For all lengths greater than $l > 2$, the maximum displacements become constant and are of equal absolute value for both peak-positive and peak-negative-response curves.

In Figure 60, the effect of alteration of waveform can be seen for the thin-shell case. It can be seen that maximum values of peak displacement are obtained at very short wavelengths. The amplitudes of peak-positive and peak-negative response for the half sine and haversine are sharply reduced and fall below the long-pulse-length values of the rectangular pulse. For long pulse lengths, it appears that half-sine and haversine fourth-mode influence would

soon become negligible. However, for the sine and modified-sine response curves, the short-pulse-length maximum values exceed slightly (by only about 10%) those of the rectangular pulse. Again, for long waves, the sine and modified-sine peak-displacement response values decrease rapidly so that at $\ell = 5$, their value is no greater than that of the half-sine and haversine pulses.

Maximum higher-mode velocity profiles for various waveshapes are shown in Figures 80 through 83. Following the pattern of the third and fourth-mode displacements, the maximum values of velocity are those associated with peak-negative velocities and short pulse lengths. Short pulse length peak-negative velocities as much as 85% greater than the long pulse length rectangular-pulse-peak positive velocities are obtained for the rectangular pulse and sine and modified-sine waves. In the case of all waves and pulses except the rectangular and exponential pulses, the velocity amplitude decreases rapidly toward what appears to be negligible values for long wavelengths.

The same general remarks are true about fourth-mode velocity response. Maximum peak-positive velocities are obtained at very short wavelengths, $\ell \leq 2$. At these wavelengths, the sine and modified-sine have peak positive velocities approximately 85% greater than the long rectangular-pulse velocity. But as was true with the third mode, the responses decay rapidly with increasing pulse lengths for all shapes other than the rectangular and exponential pulses. So that at wavelengths greater than $\ell = 5$, the fourth mode velocity response to any waveshape other than these becomes negligible.

4.6.5 Exponentially Decaying Pulse

The results of more extensive investigation of the effect of decay rate and peak-pressure value on the response to the exponentially decaying pulse are shown in Figures 85 and 86. In Figure 85, the effect of varying the decay rate of the basic pulse shape on the zeroeth-mode response is shown. For this study, the parameters chosen were $H = .01$, $B = .4 \times 10^6$ psi, $\ell = 5$. For very small values of β , the displacement approaches a value which would be somewhat greater than 2. This value is the anticipated $2 P_o$ rectangular-wave-response limit. As β increases, the maximum displacement decreases very rapidly. In the limiting case of very large β , the maximum displacement is 1.1, which corresponds with the value for the rectangular pulse of strength P_o . For all values of the decay rate greater than 1.5, the maximum displacement for the exponentially decaying pulse is less than 5% greater than the rectangular-pulse displacement of strength P_o . For decay rates greater than $\beta = 2$, the difference in response is negligible. Therefore, as the spike becomes only moderately sharp, its influence on the displacement response is greatly reduced.

In Figure 86, the results of an investigation to determine the effect of varying the peak value of the pressure while maintaining the same decay rate for two given pulse lengths ($\ell = 5, 10$) are shown. The pressure-time relationship for this case is defined by

$$P = P_o + (P_i - P_o) e^{-\beta T} \quad (17)$$

Although a significant increase in the maximum displacement response may be observed as the peak pressure increases, particularly as the pulse length

increases, it is important to note that for neither of the two pulse lengths does the maximum response increase as rapidly as the peak pressure. Although the slope of the curve appears to be increasing as the peak pressure advances, the effect of a mildly sharper spike would greatly reduce the effect of the increased pressure.

In general, it may be concluded that the superposed spike may be ignored if the decay rate is large. For spikes in which the decay rate is not large (or for large pulse lengths) the effect on the maximum displacement may not be negligible. However, the maximum displacement is bounded by the rectangular-pulse displacement at the magnitude of the peak pressure of the spike and an exponential fit for the response between upper bound and established values would appear to give a good estimate of unknown maximum-displacement values.

In the case of the peak-velocity-response curves, the exponentially decaying pulse leads to the same general results as for the displacement. That is, the response lies somewhere between the response to a rectangular pulse of strength P_0 and one of strength $2 P_0$. The exact value of the peak velocity response depends upon the length of the pulse. If the decay parameters were varied, one would anticipate that the same results would be obtained for the effect of variation in decay parameters and peak-pressure or velocity response as were obtained for the peak displacement curve, although no data were generated to validate the theory. That is, for sharply decaying exponential pulses, the velocity would approach that of the rectangular pulse of strength P_0 . On the other hand, increasing the peak pressure while maintaining the same decay rate would gradually increase shell velocity. As with the displacements, it is

possible that the superposition of a decaying spiked pulse may significantly alter maximum-velocity response. In general, it may be anticipated that for a sharply decaying spike, regardless of peak pressure, the effect of the spike can be ignored. If the decay rate is more gradual, or the wavelength very long, then the influence will be felt. Its effect may be estimated by using the limiting values corresponding to the maximum velocities of rectangular pulses having maximum and minimum pressure values of the pulse and exponentially interpolating for peak responses between these values as function of pulse length and decay parameters.

4.7 Ranking of Parameters

To correctly rank the site, weapon, and structure-medium interaction parameters which influence structural interior motion in the order of their physical importance presents a difficult problem. The difficulty is caused primarily by the nature of the modal analysis conducted for this presentation. When the modal results for dynamic displacements and velocities of the shell are considered individually, it can be seen that the importance of the parameters may be significantly different in one mode than in another. To help resolve this problem, the modal responses have been ranked in the "order of their physical importance". Since the response amplitudes in certain modes are much greater than they are in others, this knowledge of the maximum-response amplitudes in various modes is used to weight the parameter rankings within each mode.

The maximum displacement and velocity responses to a rectangular pulse, for various values of B and H, are shown in the table which follows.

MAXIMUM DISPLACEMENT AND VELOCITY RESPONSES FOR VARIOUS MODES

Mode Number	0	1	2	3	4
Maximum Displacement	1.35	-*	9.0	2.1	.88
Maximum Velocity	1.2	7.7	5.5	2.9	2.1

This table illustrates that, in terms of physical importance, parameters affecting the displacement must be heavily weighed by the first or rigid body mode of motion. The velocity response, on the other hand, is influenced to relatively the same extent by all modes. Since this is the case, and since the relative importance to the design of displacement vs. velocity depends on the specific circumstances of the design problem, ranking of parameters for the displacement and velocity will be presented separately. The ranking will consider the following parameters as controlling the structural response: the weapon parameters of peak pressure, wave shape and wavelength; the site parameter of the soil modulus; and the structure-medium interaction parameters of the shell thickness and the density ratio of shell to medium.

4.7.1 Ranking of Parameters Affecting Displacements

In ranking the displacement-response parameters, it is immediately evident that the parameter of greatest importance must be the peak pressure associated with the incoming wave. The response in all modes is directly proportional to this peak pressure.

Because of its pronounced effect on displacement in the first mode (although not as universally important in all modes of displacement response)

*This value is directly proportional to the pulse length.

the pulse length of the incoming wave must be considered the second most important parameter. In the first mode, the displacement response of the shell has been shown to be directly proportional to the length of the incoming pressure pulse. In the second mode, the pulse length is one of the parameters of lesser importance. In the zeroeth mode, the effect of pulse length on response is similarly of small importance, since the displacement is nearly constant over a wide range of pulse lengths in this mode. However, the pulse-length influence may be very important in the remaining modes, since large variations in the displacement response take place with changes in pulse length. It is the strong influence of the pulse length on the first mode, however, which almost alone causes it to be second place among the parameters affecting displacement.

In third place, in the order of physical importance of the parameters affecting the displacement of the shell, is the shell thickness. The shell thickness has a very pronounced effect on the second and higher modes.

Fourth in the order of importance of parameters affecting shell displacement is the soil modulus. In the all-important first mode, the response is inversely proportional to the soil modulus. For the cases of thin and intermediate shell thickness in the second mode, this relationship appears to be true also. In the thick-shell case, the shell response is so intimately connected with the wavelength and waveform that it is difficult to separate the effect of the soil modulus from these other parameters. But, it is clear that the soil modulus is important here also, as reductions in response of nearly 95% of the maximum shell responses which appear to be connected with the

variation of the soil modulus are observable. The range of the soil modulus of from $.4 \times 10^6$ psi to 2×10^6 psi, includes a rather wide range of soil and rock varieties and causes a reasonably large variation in displacement throughout the material presented in this study. It should also be pointed out that the higher mode displacement response appears to be related to the soil modulus through an inverse proportionality relationship. Although this cannot be substantiated in all cases for the higher modes, it appears to hold well for relatively-long-pulse-length cases. Only in the zeroeth mode does the inverse proportionality to soil modulus appear to break down. However, in this mode, variations in response of up to 22.5% of the maximum values may be directly attributed to the soil modulus.

The fifth parameter, in order of its physical importance, is the waveshape. Although relatively low in the parametric standings, the influence of the waveshape on the displacement is still significant. In the first mode, variations in waveshape produce reductions in response of from 40% to 53% of maximum response values. In the second mode, the effect is even more pronounced. Reductions of up to 90% of maximum response are recognizable simply as a result of variation of the shape. In the higher modes and the zeroeth mode, the influence of waveshape does not appear to be of such importance. Reductions of displacements in these modes range only from 35% to 50% of maximum values.

The sixth and least important parameter in shell displacement is the density ratio.

In summary, the parameters affecting displacement of the shell, in order of their importance, are: (1) peak overpressure, (2) length of the pressure pulse, (3) shell thickness, (4) soil modulus, (5) the shape of the incoming pressure pulse, and (6) the density ratio of the shell to medium.

4.7.2 Ranking of Parameters Affecting Velocities

Applying similar reasoning to the problems of the velocity response of the shell, the most important single factor affecting the velocity is the peak pressure. As in the case of the displacement response, the velocity response is directly proportional to the peak pressure of the incoming pulse.

Second in order of importance to the velocity response, is the shell thickness parameter. In the second mode, the velocity response appears to be nearly directly proportional to the shell thickness. Except for a few isolated cases, this proportionality seems to hold true. Even where it does not appear to fit exactly, i.e., the sine-wave thick-shelled case and the modified-sine-wave high-modulus case, it gives a very good approximation of the velocity response. In the zeroeth mode, the velocity shows a 65% variation between the maximum and minimum response as a function of shell thickness. In the higher modes, insufficient data preclude specifying the exact relationship between velocity and shell thickness, but from the remaining modes, this parameter can be an important factor.

The third factor of influence to the velocity response is the soil modulus. In the first and all higher modes, it has been shown that the velocity is inversely proportional to the soil modulus. Variations in response of up to 80% of the maximum velocity response in each mode is caused by the soil modulus.

In the first mode, the variation is limited to a reduction of 50% below the maximum response values.

Ranked fourth in the velocity parameters, is the length of the incoming pressure pulse. The lowering in importance of this parameter results from its relative unimportance in the first and second-mode velocity response. In the first-mode response, the velocity is essentially independent of pulse length for relatively long pulse lengths. In the second mode, a reduction in the maximum response values of from 35% to 50% results from the influence of pulse length, in a relatively short wavelength range, $1 \leq l \leq 5$. In the higher modes and the zeroeth mode, this factor pays a more important role. The velocity is reduced by factors of from 80% to 90% of the maximum velocity response in these modes. However, the influence of the zeroeth and higher modes on the physical importance of the parameters is insufficient to increase the importance of the role of the pulse length in determining velocity response and, therefore, it must occupy the fourth position in the relative ranking.

The fifth position is occupied by the shape of the incoming wave. Examination of the effect of changing the waveshape through the rather wide variety of shapes examined for this study indicated that this parameter was of relatively minor importance to the response of the shell. In the first and second modes, reductions in maximum velocities of no more than 23-33% were observed to be caused by variations in waveshape. In the zeroeth mode, an even narrower band of velocity reduction was noted, ranging from 15% to 17%. In the higher modes, the effect was somewhat more pronounced, with reductions of from 10% to 55% of maximum velocities noted.

Once again, the least important parameter was the density ratio of the shell to the medium. The density ratio variation of 25% produced a resulting variation in velocity response of only 5%. This parameter, although difficult to separate from the soil modulus in its effect on shell response, seems to cause very negligible changes in either the displacement or velocity response.

In summarizing the effects of the site, weapon, and structure-medium parameters on the velocity response, they may be ranked as: (1) peak pressure, (2) shell thickness, (3) soil modulus, (4) wavelength, (5) shape of the incoming pressure pulse, and (6) the density ratio of shell to medium.

It is interesting to note that there are several similarities between the rankings of the displacements and velocity parameters. In first place, for both cases the position of the peak pressure is insured by its direct proportionality to both displacement and velocity. In fifth and sixth places are found the waveshape of the incoming pulse and the density ratio of the shell for both cases. It may be somewhat surprising to find that the shape of the incoming pressure pulse should be one of the parameters with the least importance in the response. However, that this should be the case is gratifying, since it simplifies the problem of estimating the effect of unforeseen changes in the waveform on the response of the shell.

4.8 Influence of Deviations in Parametric Values on Shell Response

It can clearly be seen that because of the direct relationship between peak pressure and shell displacement or velocity response, a given deviation from the anticipated pressure will change the value of the particular response in the same proportion. This will be true in all cases except where the input

waveshape is in the form of an exponentially decaying pulse. Under these conditions, the percentage deviation in the response will be somewhat less than the percentage deviation in the pressure, whatever the values of the decay factor and wavelength associated with the decaying exponential are. (Compare Figures 85 and 86.)

From the parameter ranking, it can be seen that even if the soil density is known only within broad limits, or can be estimated only, any deviation from an assumed average value would appear to have negligible influence on the shell response. Thus, its effect can be safely ignored.

Similarly, it is quite probable that the exact form of the incoming wave will not be known. Therefore, it is encouraging to note that variations from the rectangular pulse response to practically any other form of wave at the same pressure result in variation in displacement response no greater than approximately 50%. For all practical purposes, the variations in velocity resulting from a wrong choice of waveshape will be between 25% and 30%. If, on the other hand, the actual waveshape is close to the design waveshapes, then the deviation in response will be even less than the value indicated.

With regard to deviations from the assumed value of the soil modulus, or alternatively, if the modulus is only known to within a given accuracy, then it can be seen from the response characteristics of the shell to the soil modulus that a deviation ΔB would result in a change in the response given by the factor - $\frac{\Delta B}{B}$.

Of all the parameters mentioned here, the shell thickness is the only parameter which would be completely within the control of the designer and

builder of the protective structure. However, if one considers an unforeseen perturbation in shell thickness, it can be seen from the results of the studies performed here that such a perturbation will result in a proportional change in displacement and velocity. Thus, if the perturbation is small, its effect is negligible.

Similarly, if the weapon detonation produces a pulse length which deviates from the estimated value used in the design of the shock isolation system, the displacement response will be changed proportionately. On the other hand, as can be seen from velocity ranking parametric study and inspection of the curves, it is very likely that change in pulse length will not alter the velocity of the shell or, at most, cause some slight reduction in its value.

These parameters, as listed and discussed above, for all practical purposes, may be considered as independent variables in their effect upon shell response. Thus, it is felt that they may be considered to be independent in application, and their totality of effect obtained through superposition of the estimated variation for each perturbing factor alone.

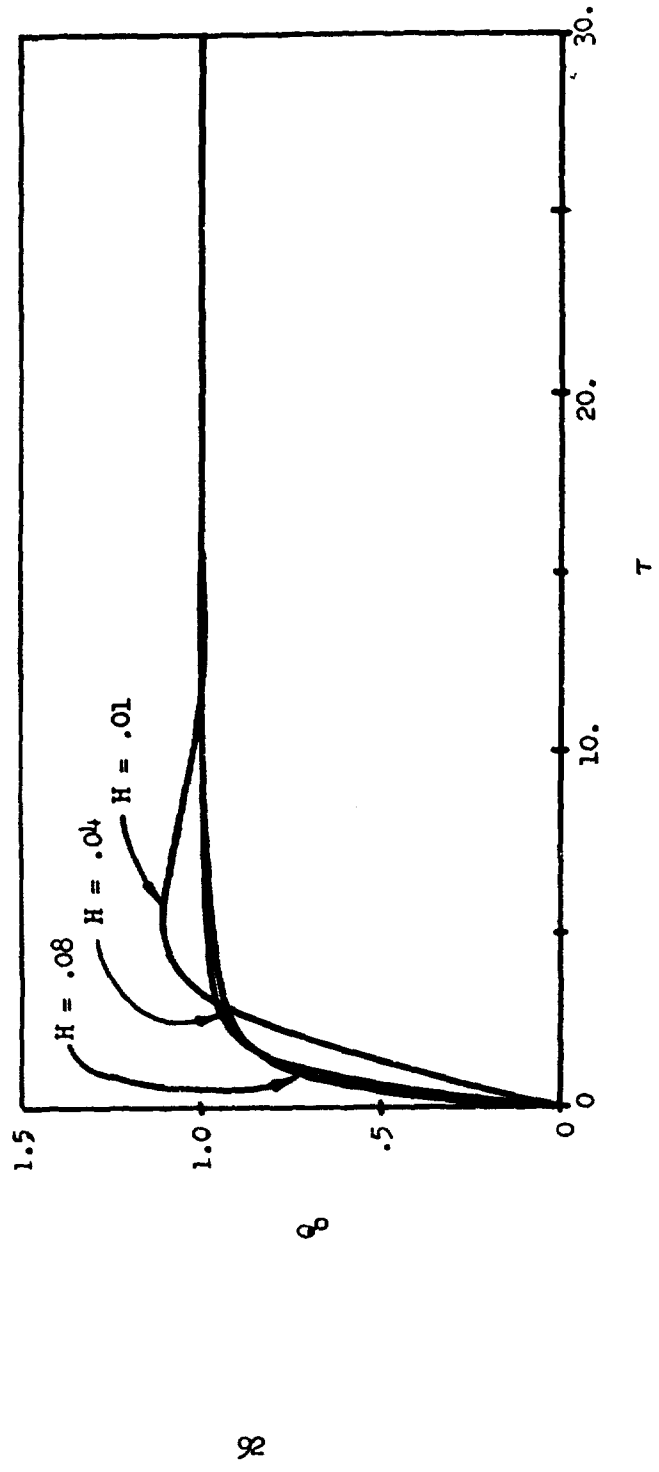


Figure 12 Q_0 VS. T FOR VARIOUS VALUES OF H
 $B = .4 \times 10^6$

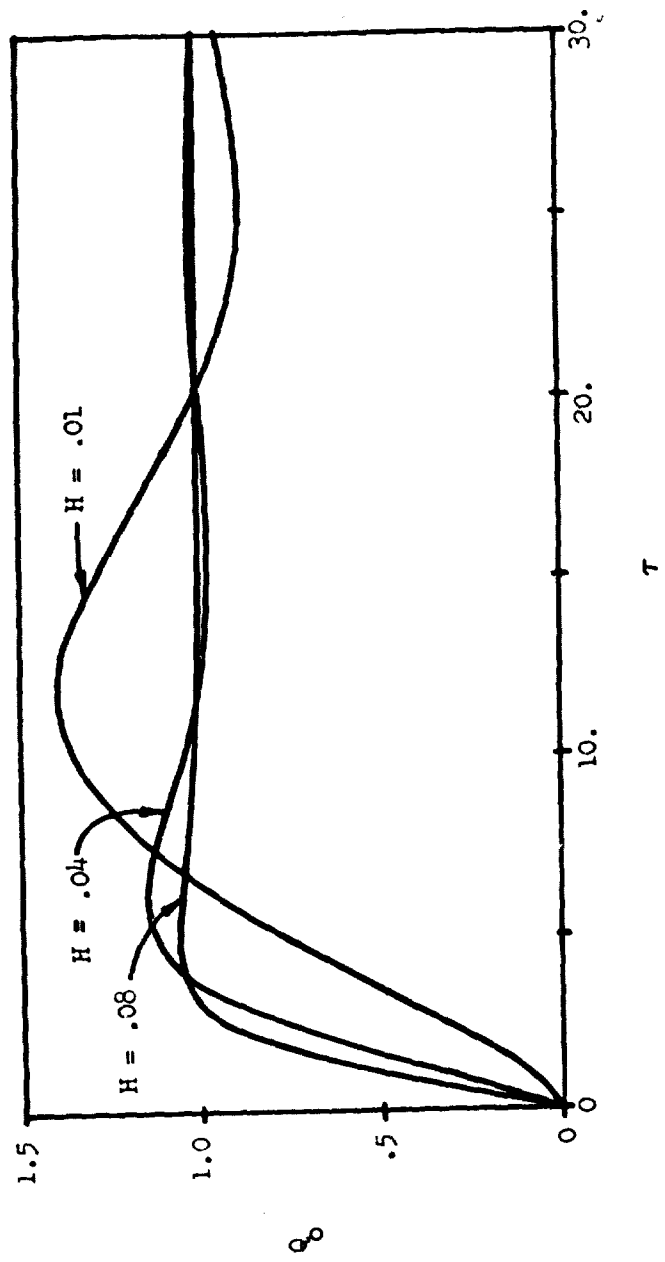


Figure 13 Q_0 VS. τ FOR VARIOUS VALUES OF H
 $B = 2.0 \times 10^6$

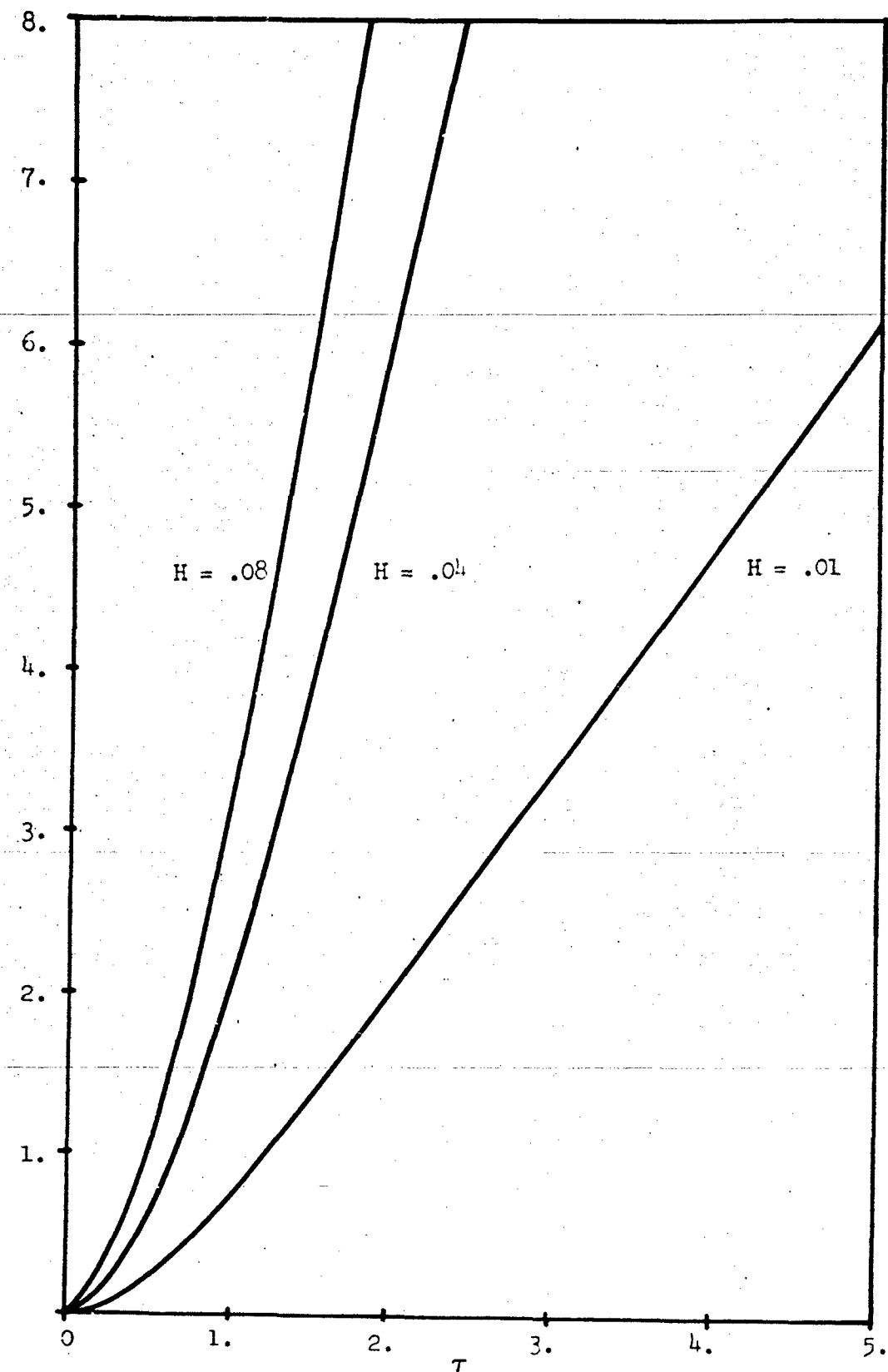


Figure 14 Q VS. τ FCR VARIOUS VALUES OF H
 $B = .4 \times 10^6$, $\mu = 4$

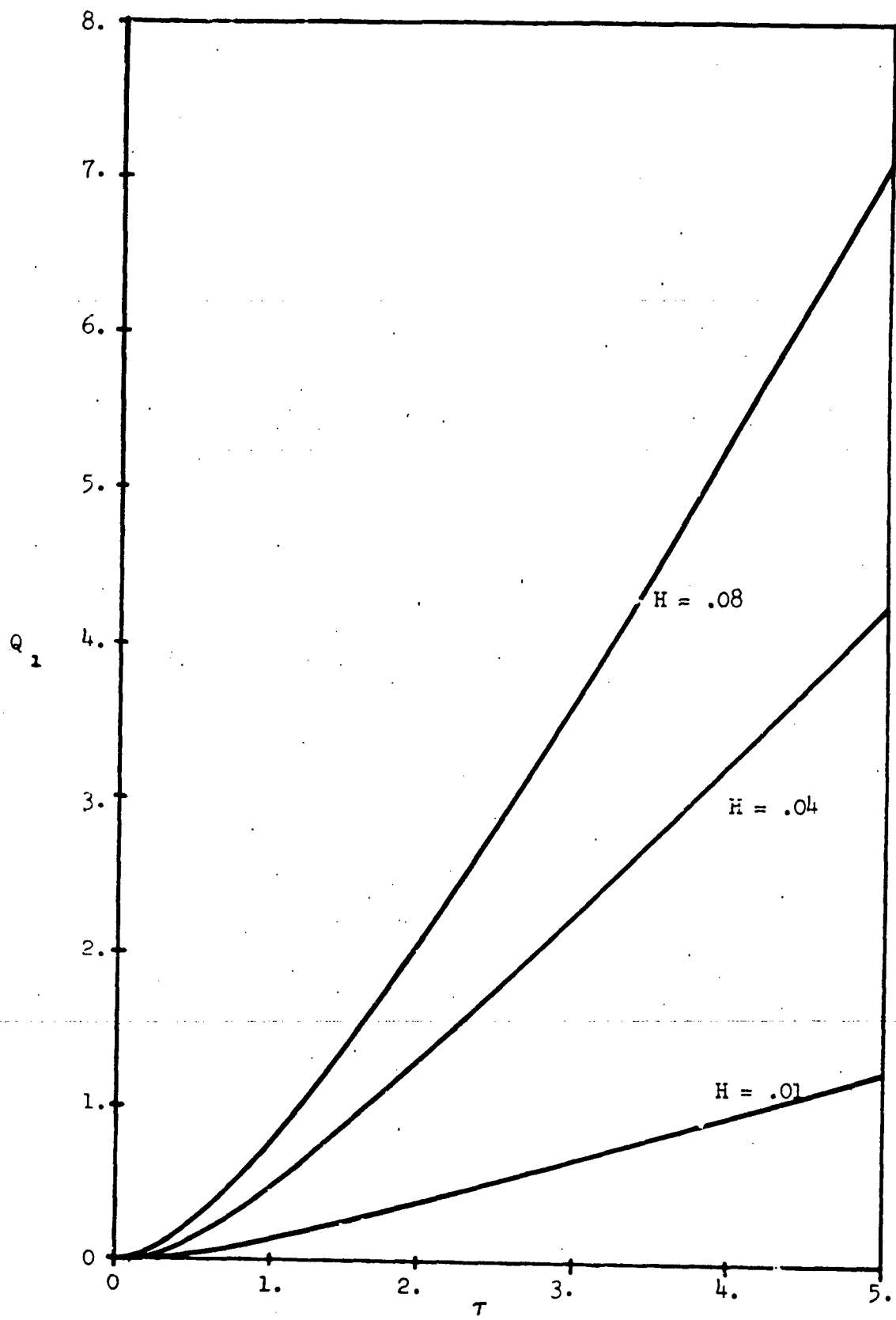


Figure 15 Q_1 VS. τ FOR VARIOUS VALUES OF H
 $B = 2.0 \times 10^6, \mu = .3$

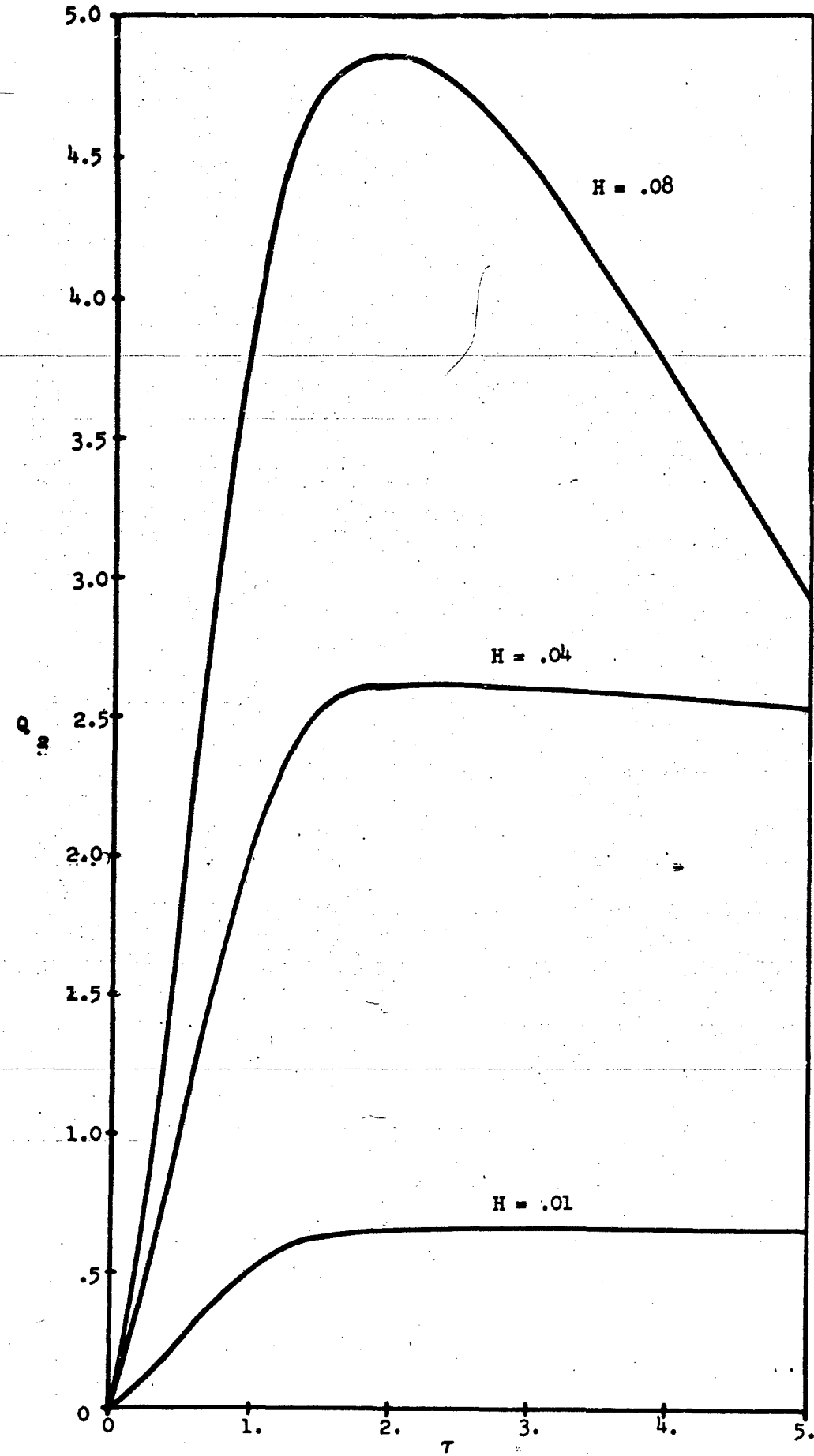


Figure 16 Q_2 VS. τ FOR VARIOUS VALUES OF H
 $B = .4 \times 10^6$ 96

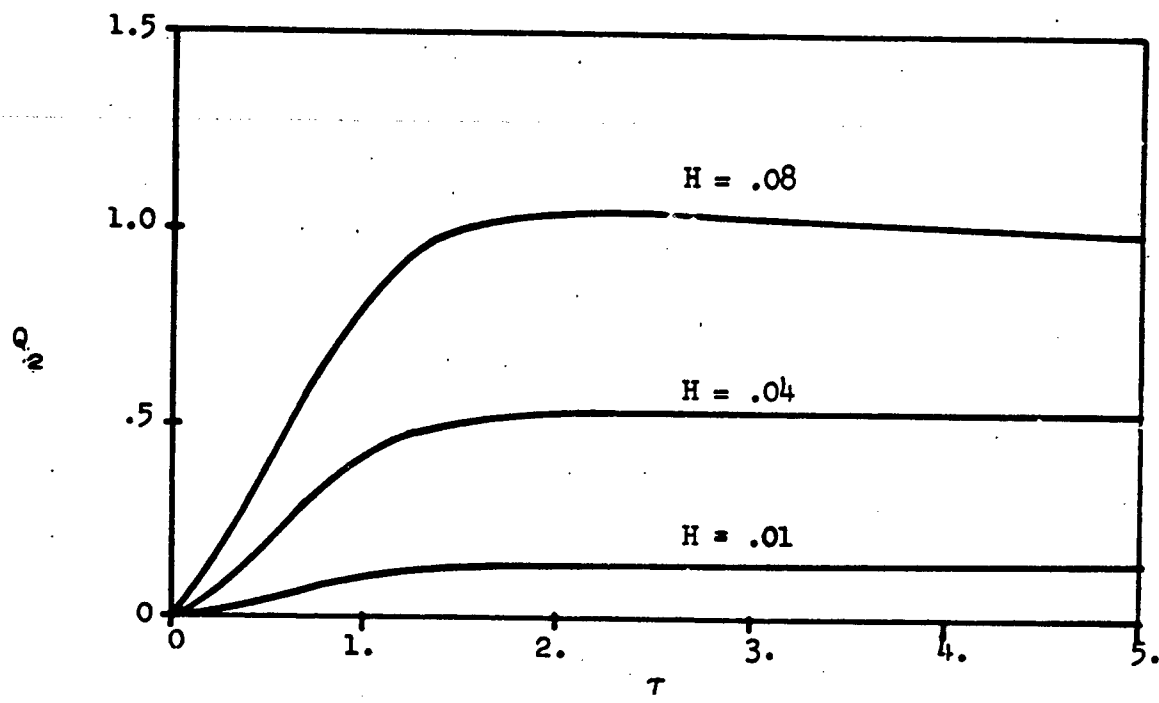


Figure 17 Q VS. τ FOR VARIOUS VALUES OF H
 $B^2 = 2.0 \times 10^6$

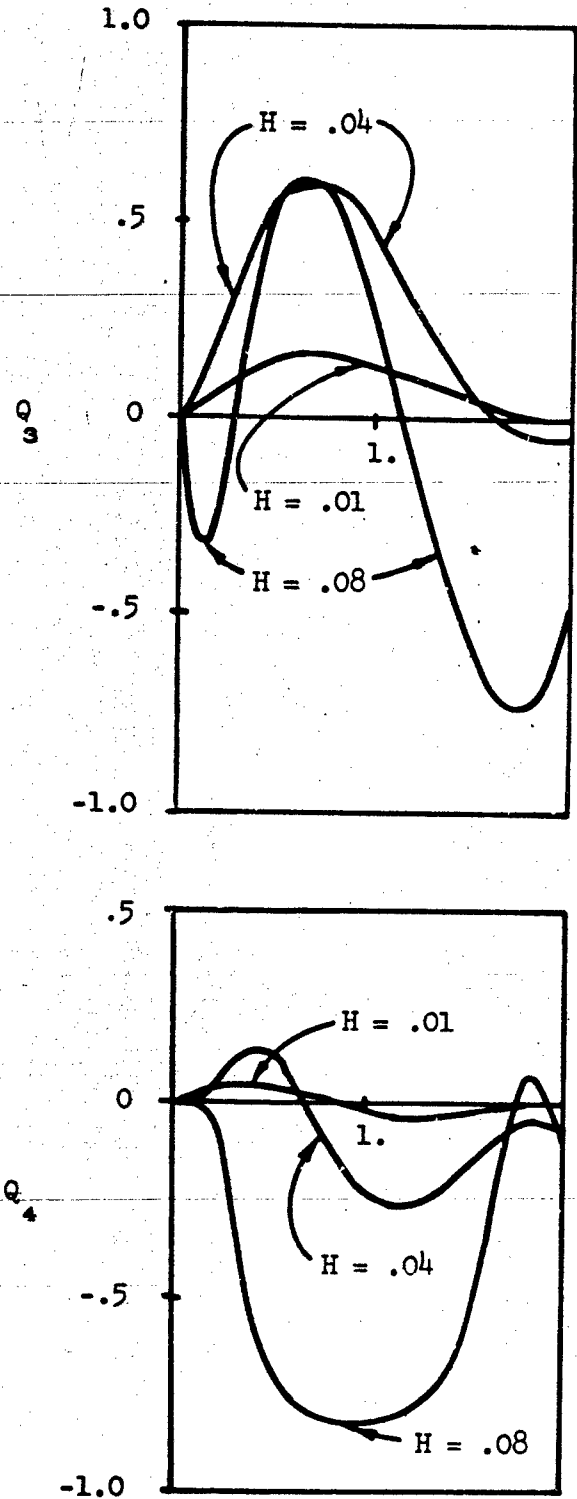


Figure 18 Q_3 AND Q_4 VS. T FOR VARIOUS VALUES OF H
 $B = .4 \times 10^6$

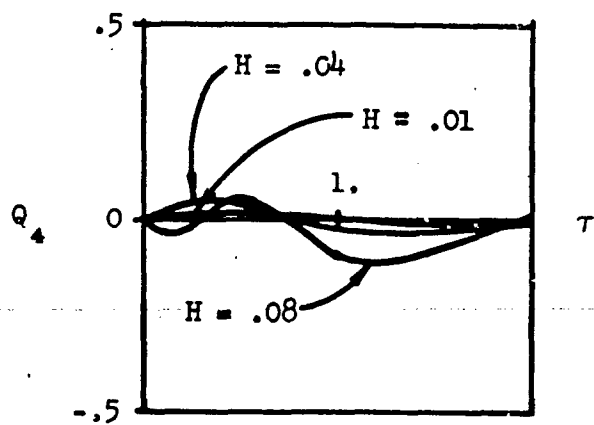
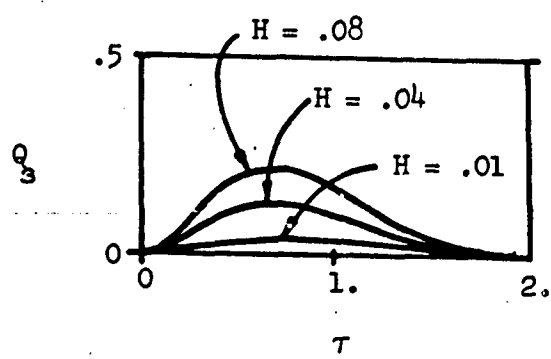


Figure 19 Q_3 AND Q_4 VS. τ FOR VARIOUS VALUES OF H
 $B = 2.0 \times 10^6$

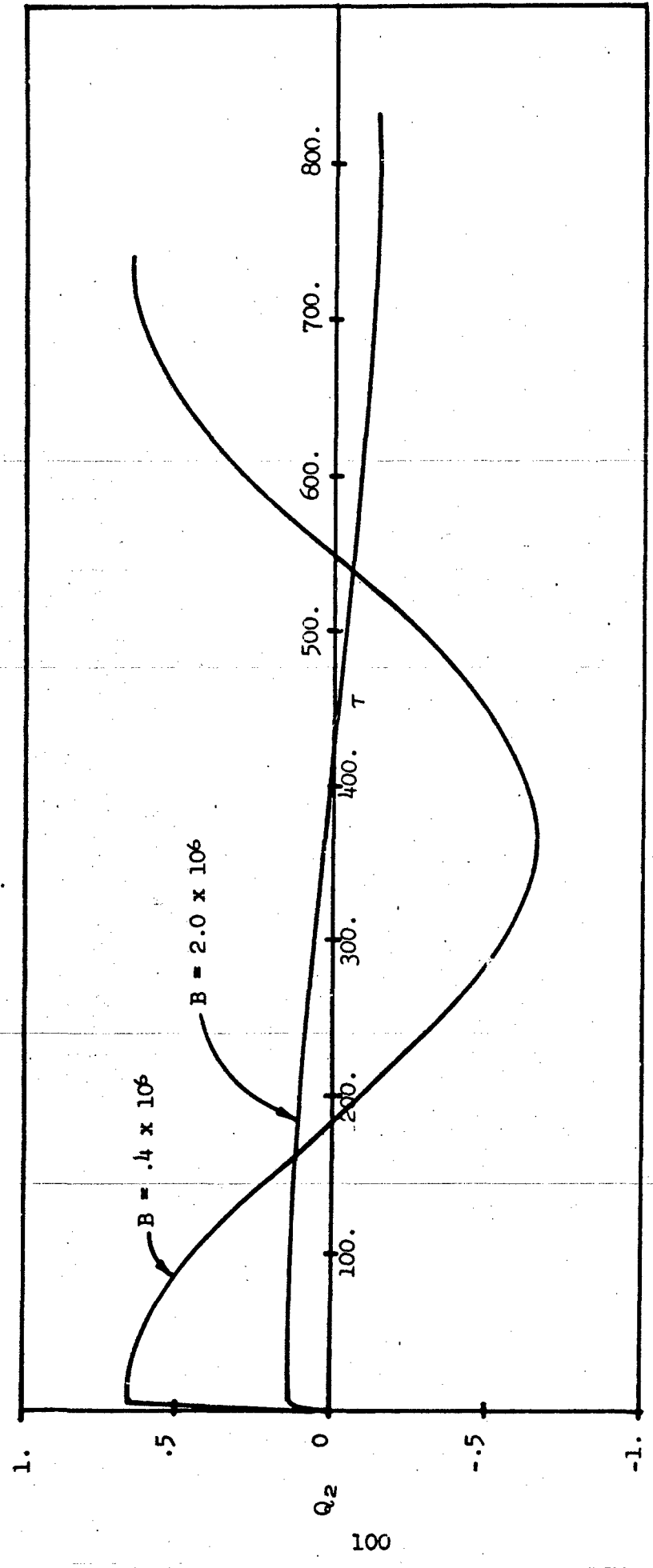


Figure 20 Q_2 VS. τ FOR LONG TIMES, $H = .01$

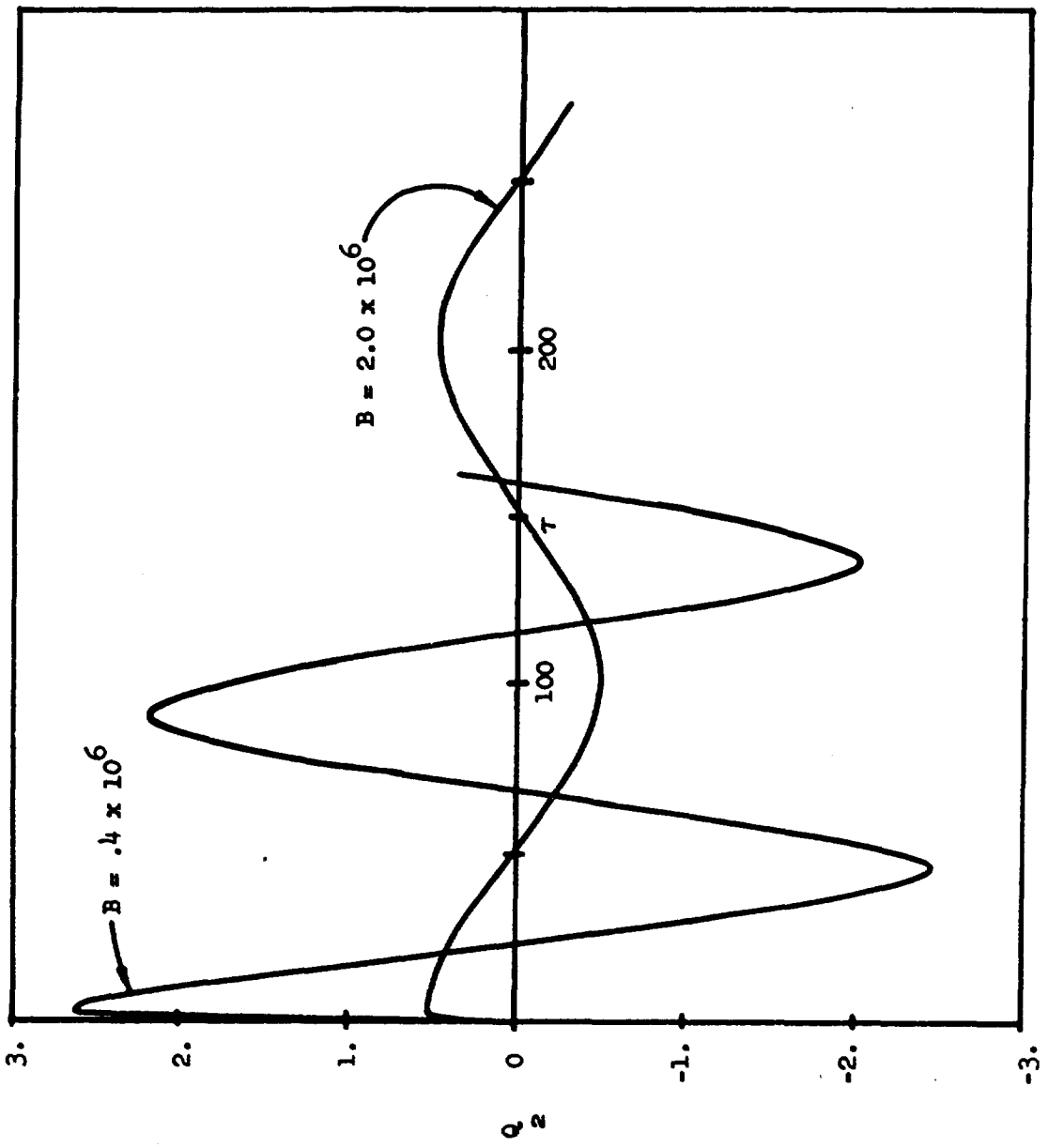


Figure 21 Q_2 VS. τ FOR LONG TIMES, $H = .04$

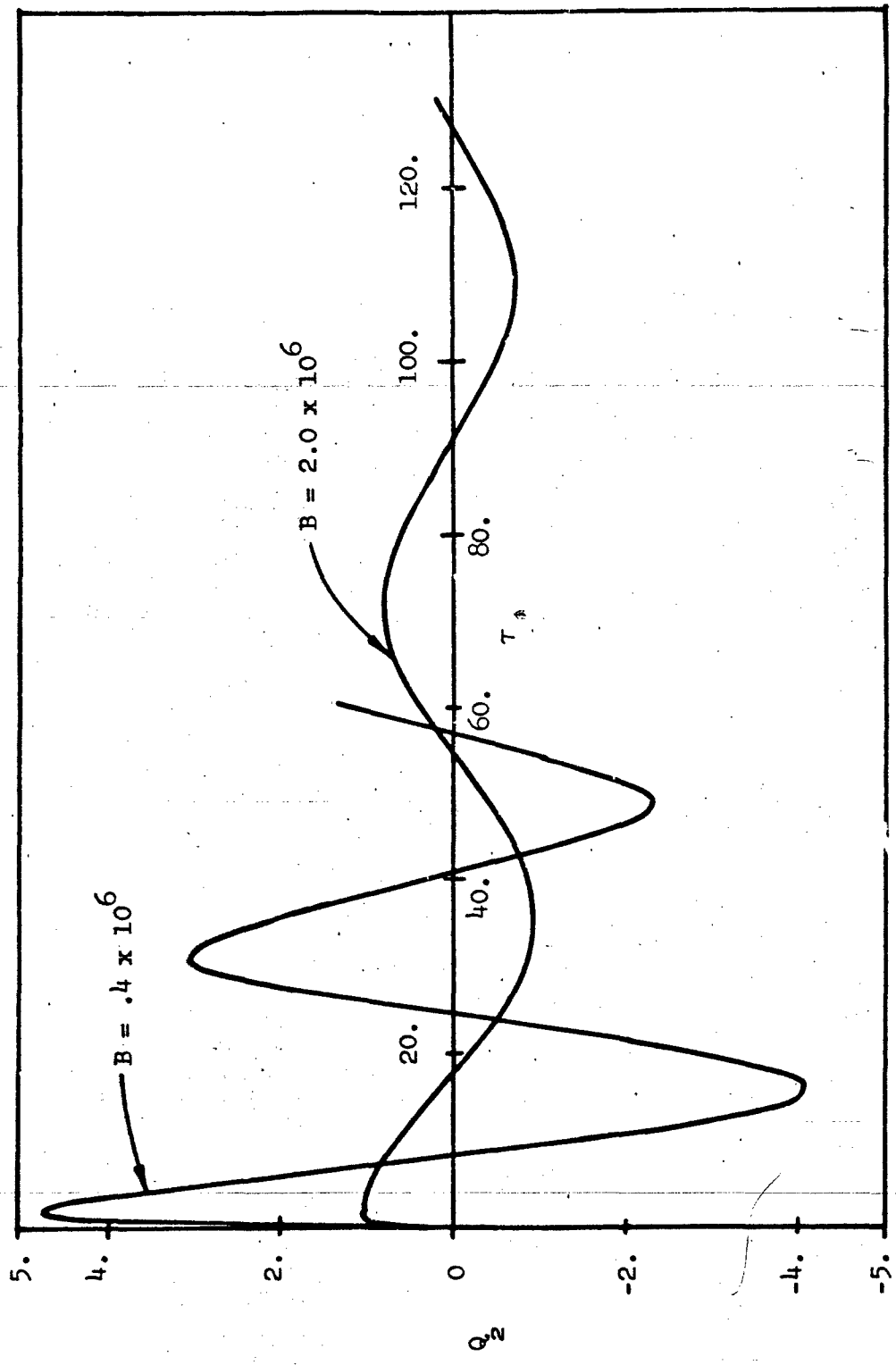


Figure 22. Q_2 VS. T FOR LONG TIMES, $H = .08$

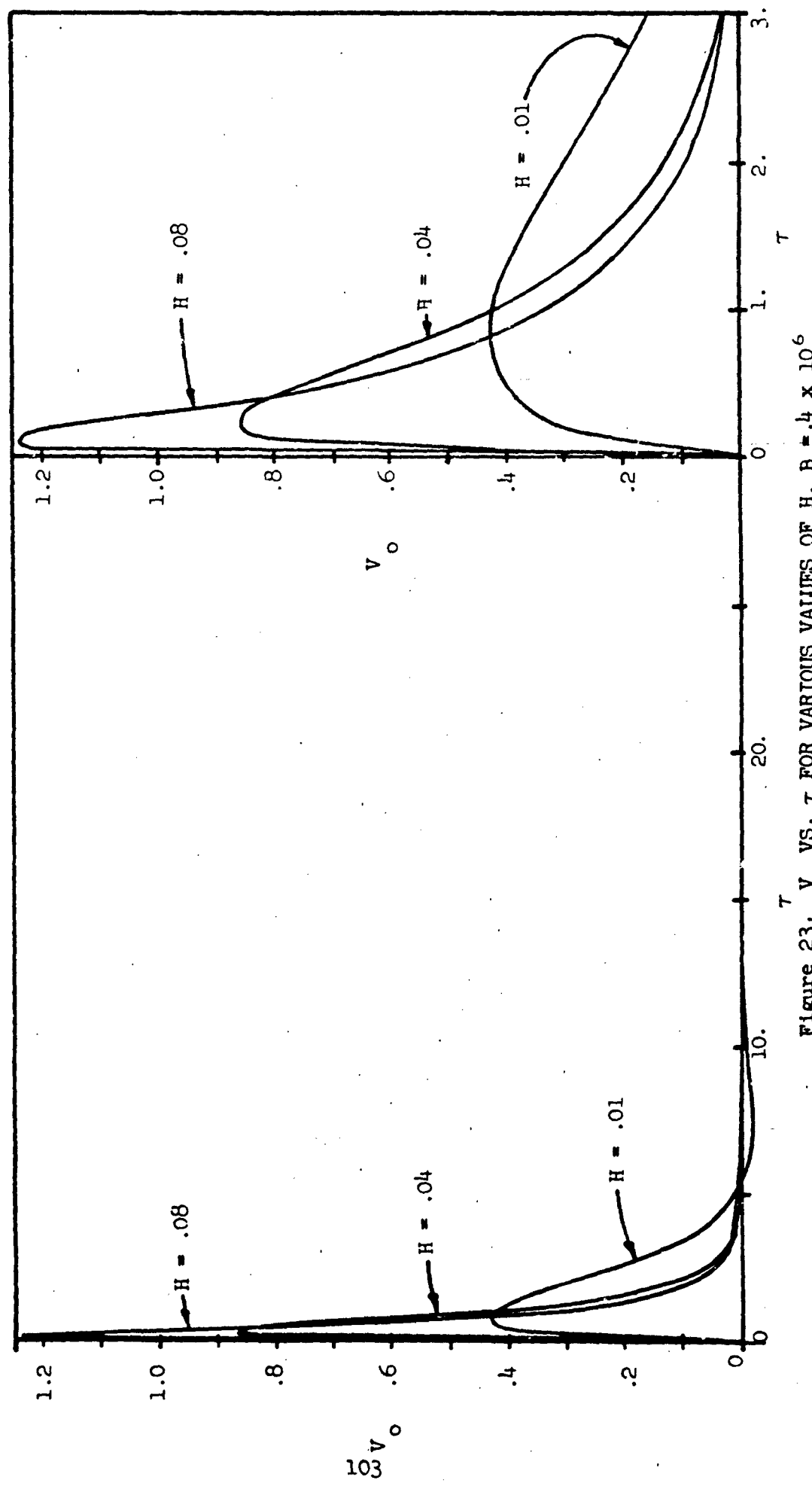


Figure 23. V_0 VS. τ FOR VARIOUS VALUES OF H , $B = .4 \times 10^6$

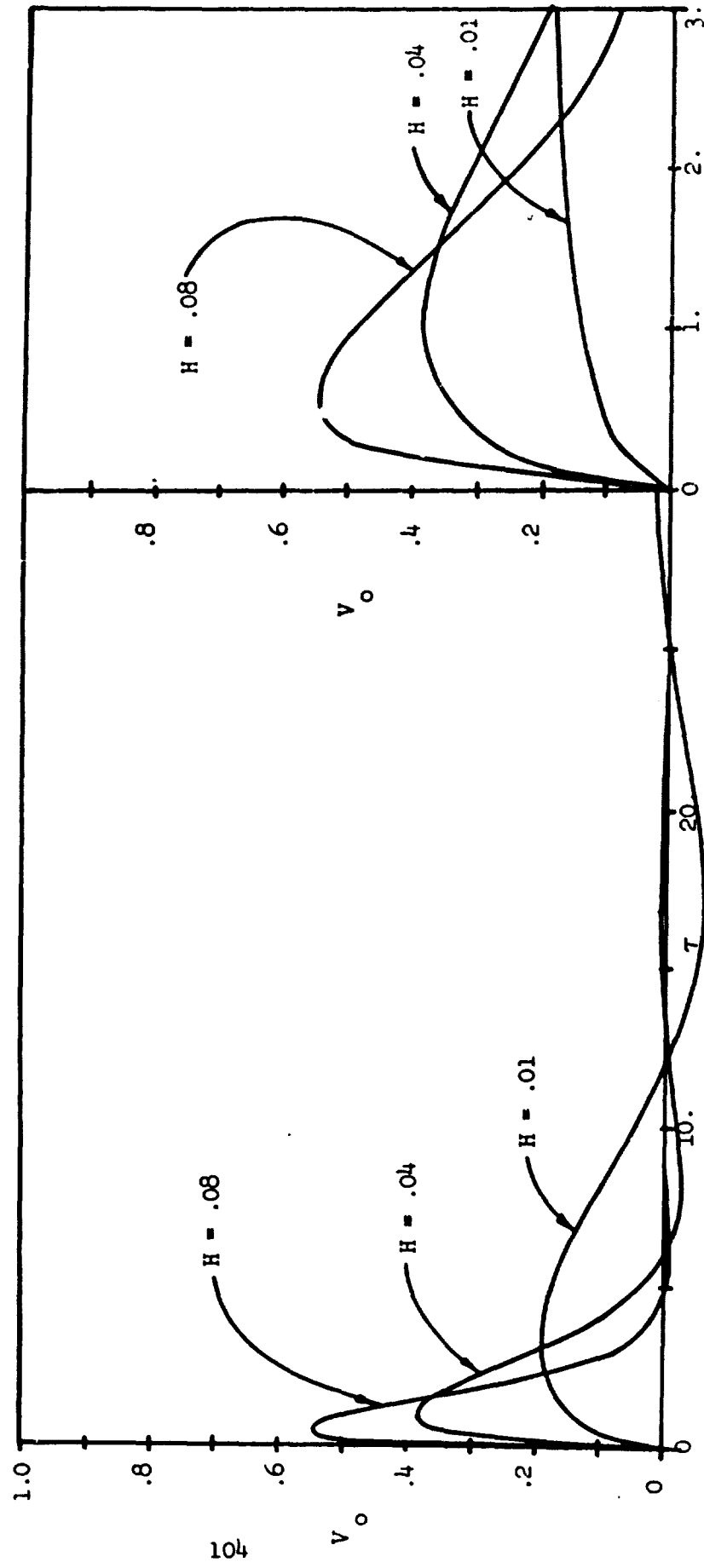


Figure 24. V_0 VS τ FOR VARIOUS VALUES OF H , $B = 2.0 \times 10^6$

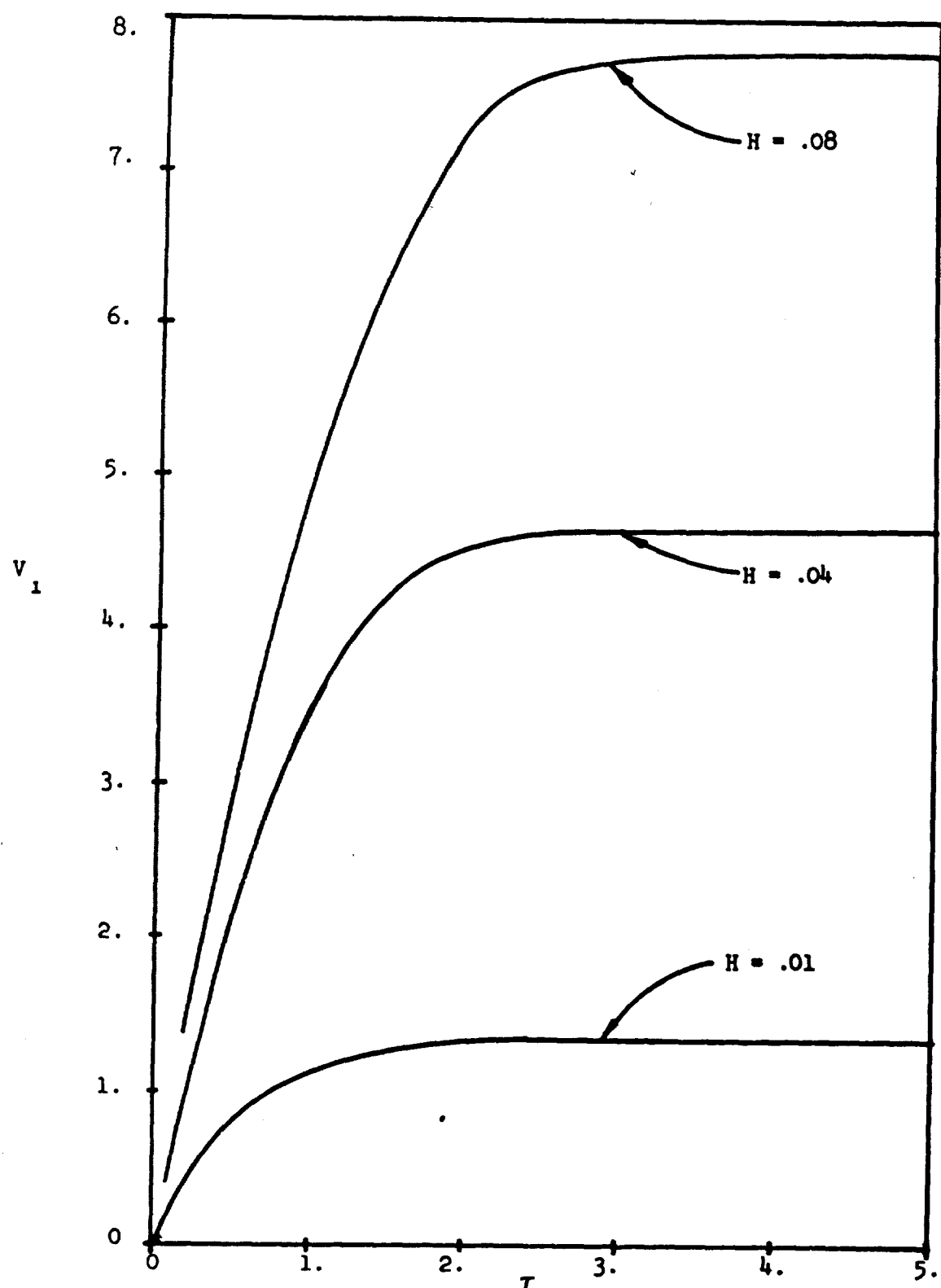


Figure 25 V_1 VS τ FOR VARIOUS VALUES OF H

$B = .4 \times 10^6$, $\mu = 4$

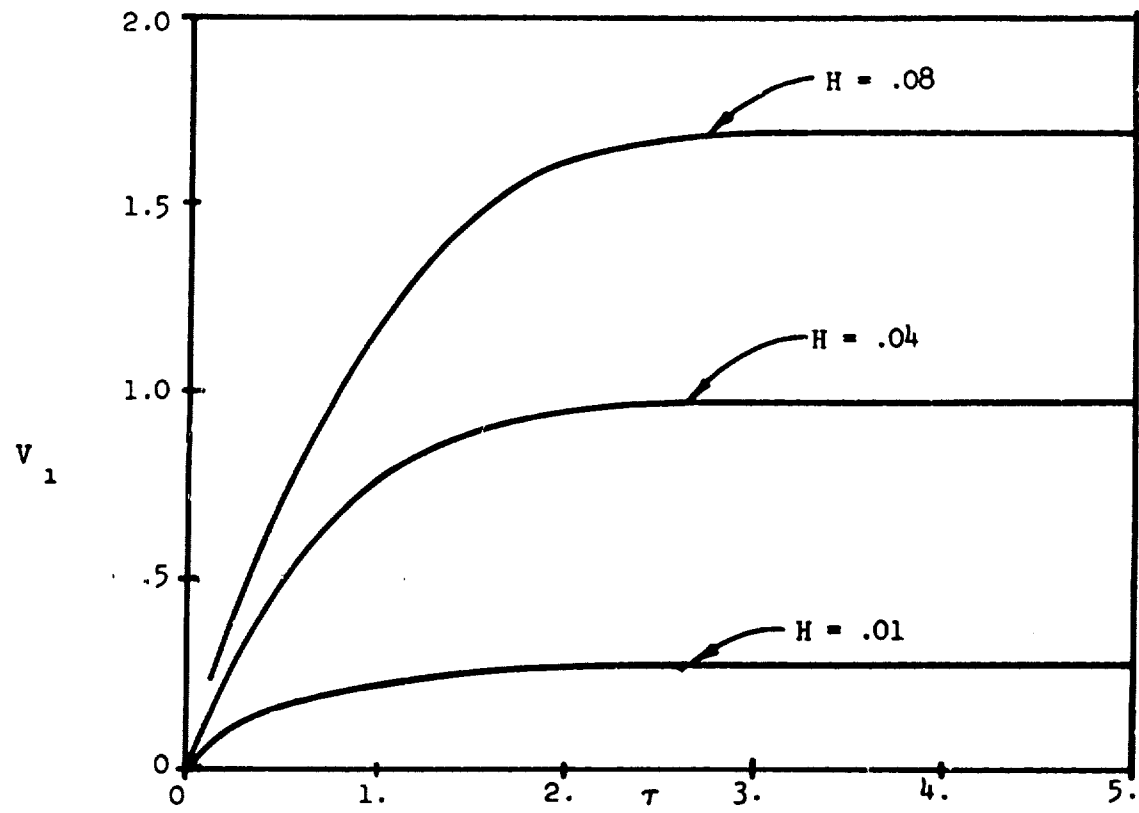


Figure 26 V_1 VS τ FOR VARIOUS VALUES OF H

$B = 2.0 \times 10^6$, $\mu = 3$

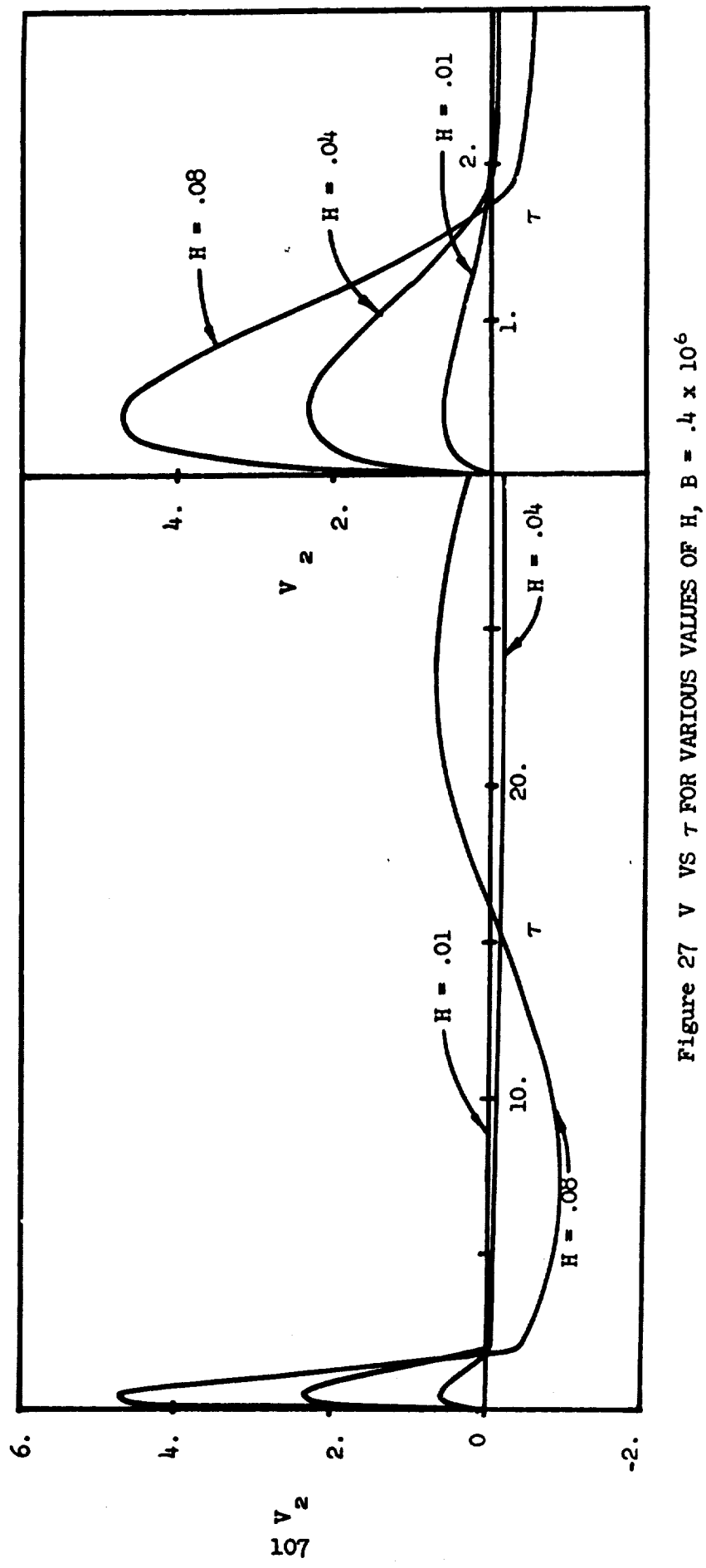


Figure 27 V_2 VS τ FOR VARIOUS VALUES OF H , $B = .4 \times 10^6$

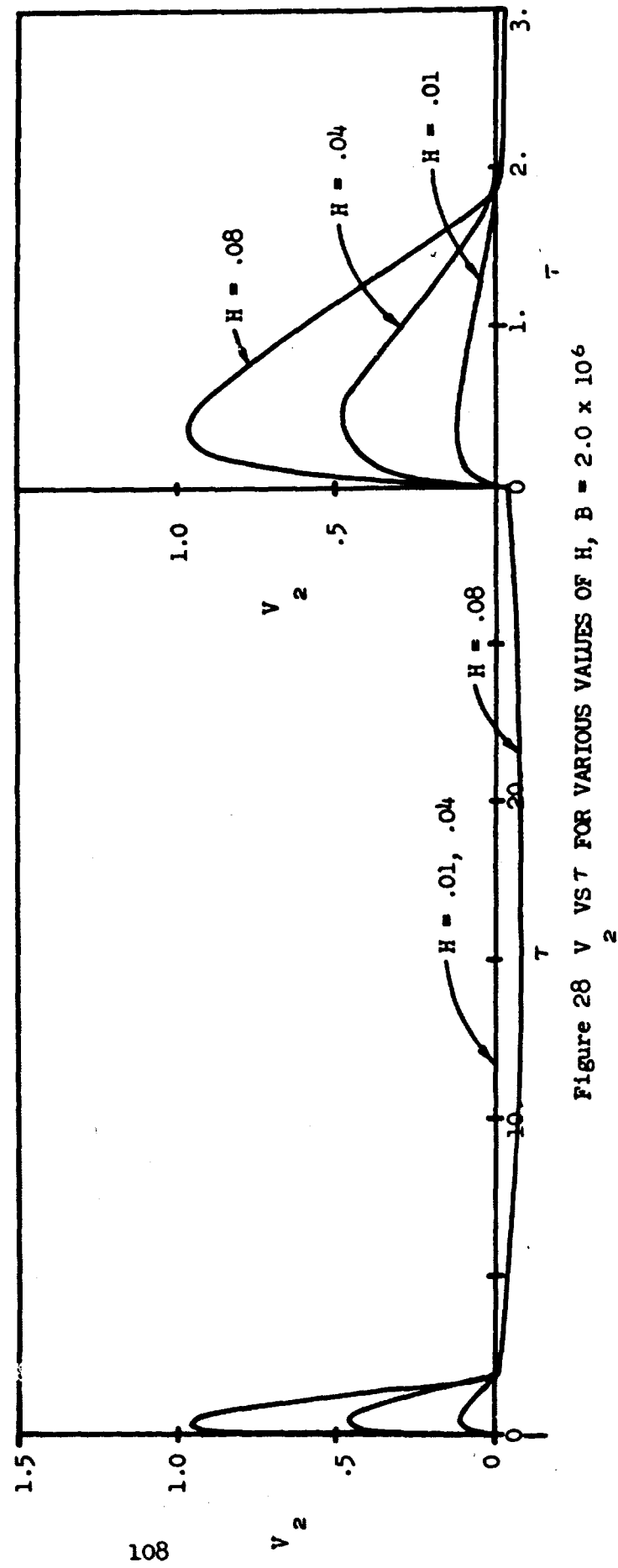


Figure 28 V_2 VS T FOR VARIOUS VALUES OF H , $B = 2.0 \times 10^6$

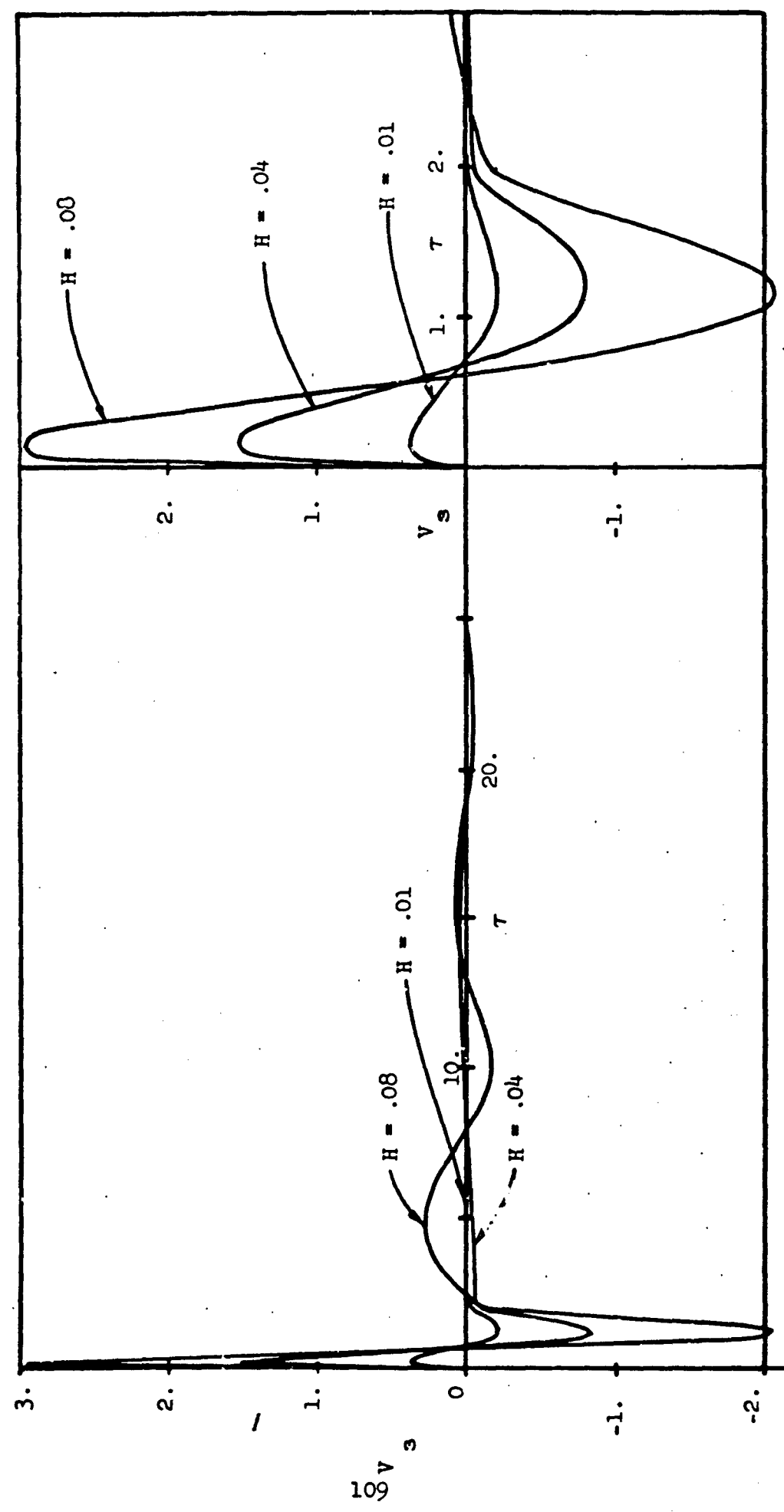


Figure 29 V_3 VS τ FOR VARIOUS VALUES OF H , $B = .4 \times 10^6$

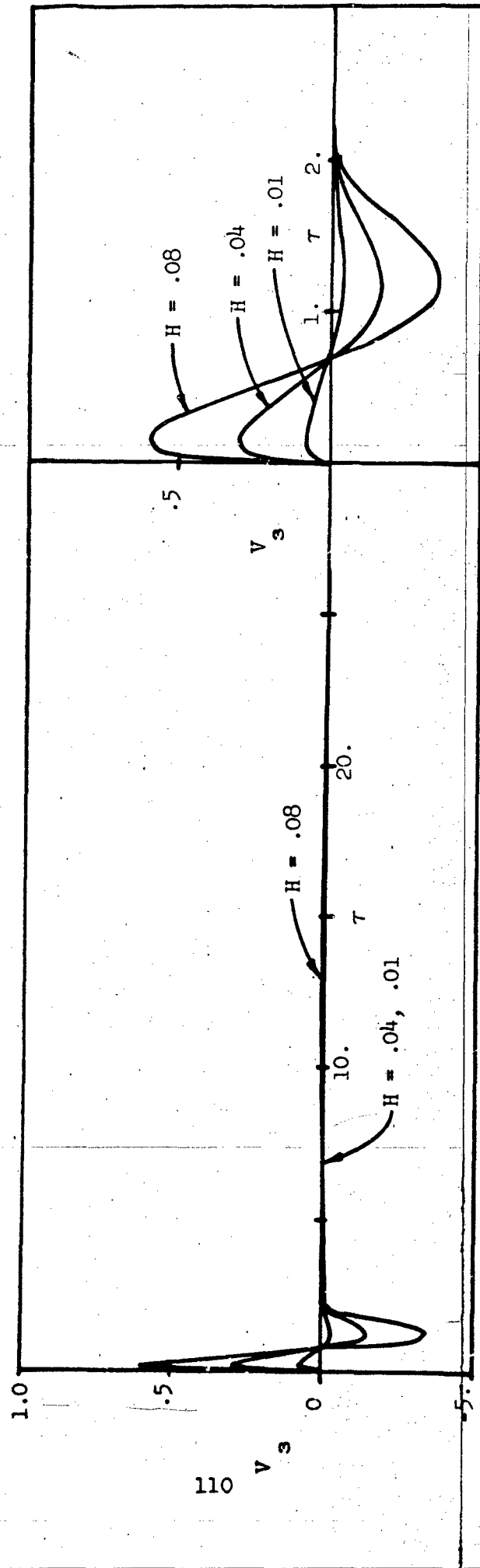


Figure 30 V_3 VS τ FOR VARIOUS VALUES OF H , $B = 2.0 \times 10^6$

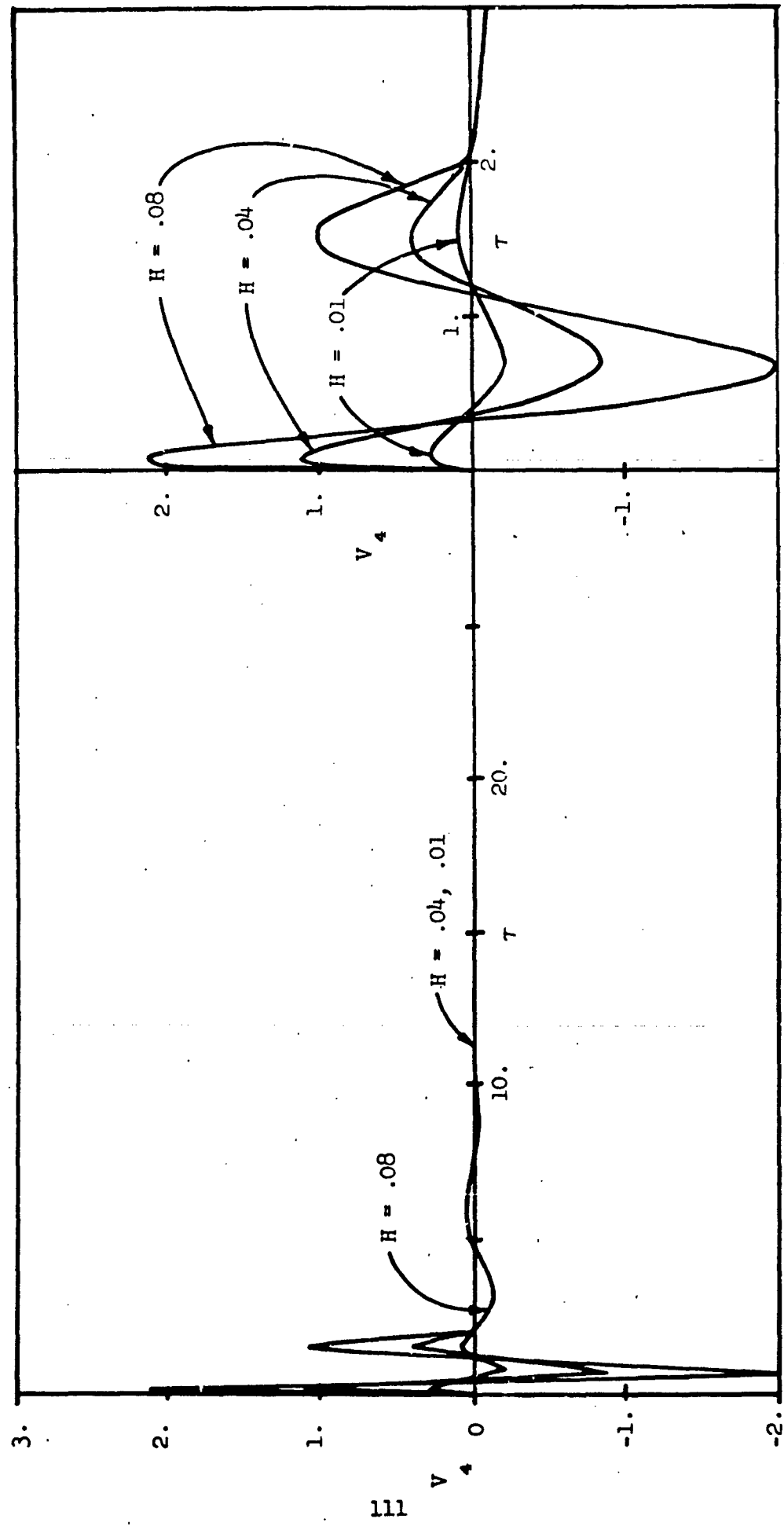


Figure 31 V_4 vs τ for various values of H , $B = .4 \times 10^6$

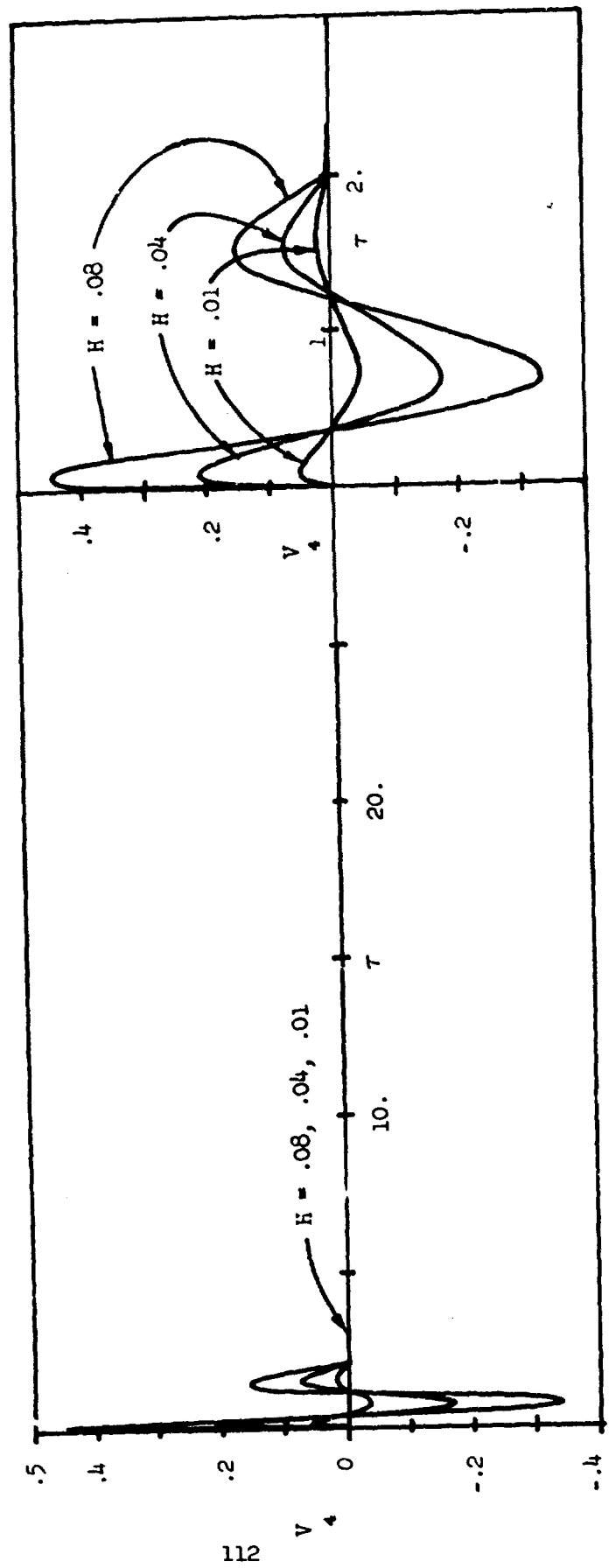


Figure 32 V VS T FOR VARIOUS VALUES OF H , $B = 2.0 \times 10^6$

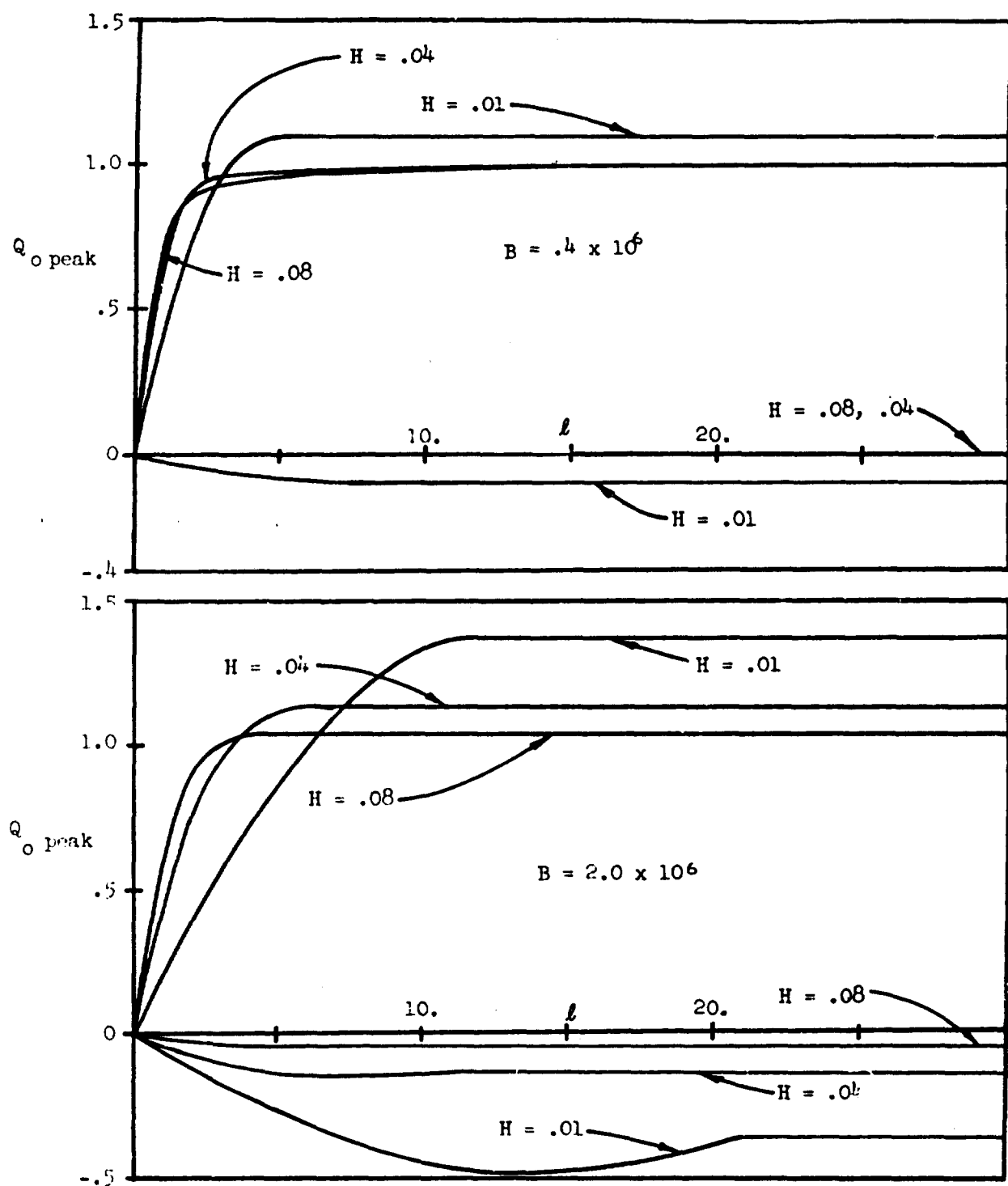


Figure 33 $Q_0 \text{ peak}$ VS. ℓ FOR A RECTANGULAR PULSE AT VARIOUS VALUES OF H

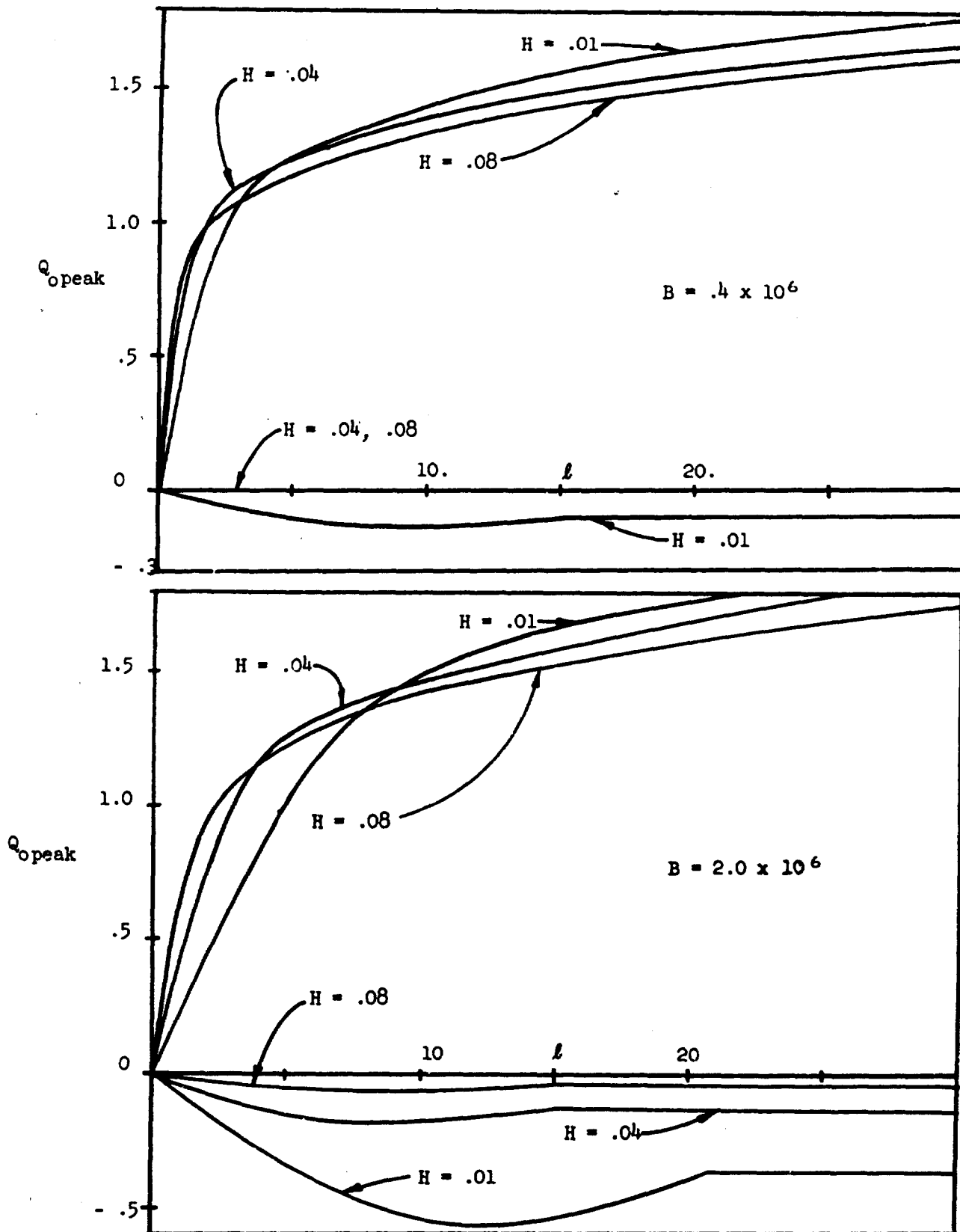


Figure 34 Q_0 peak VS. ℓ FOR AN EXPONENTIALLY DECAYING PULSE
AT VARIOUS VALUES OF H .

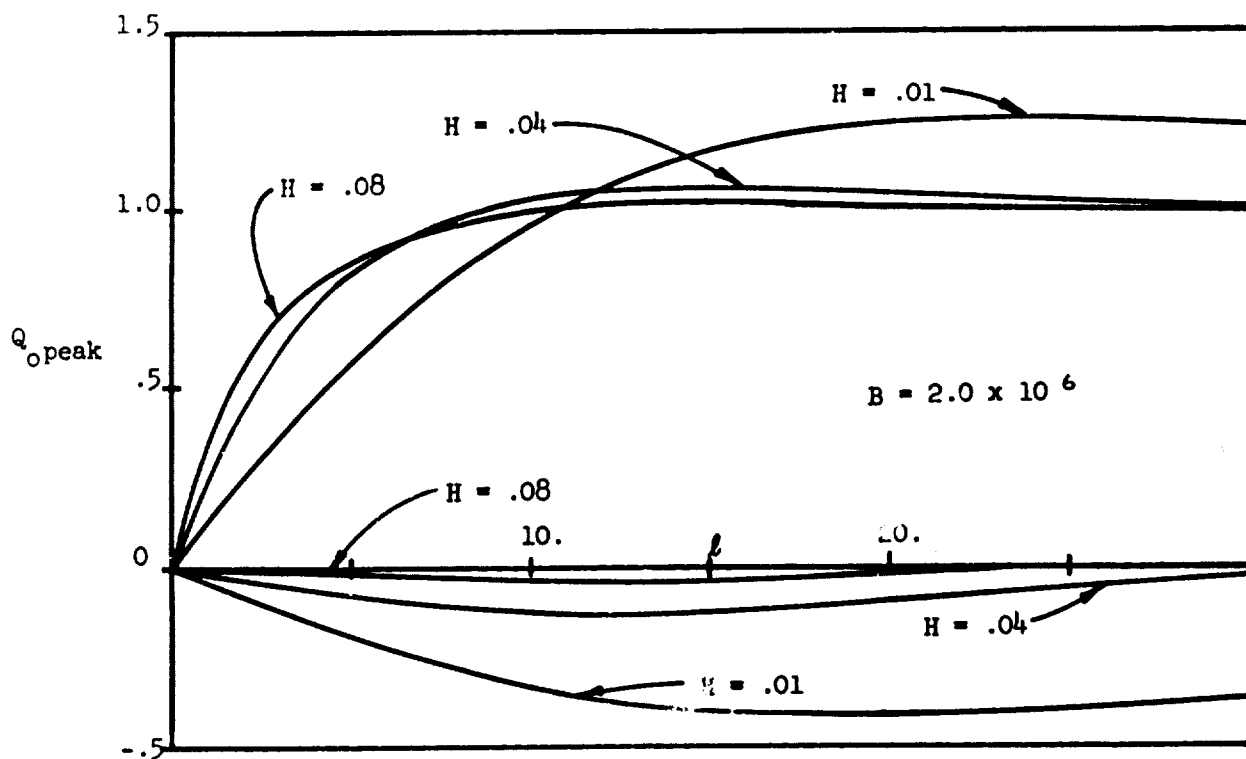
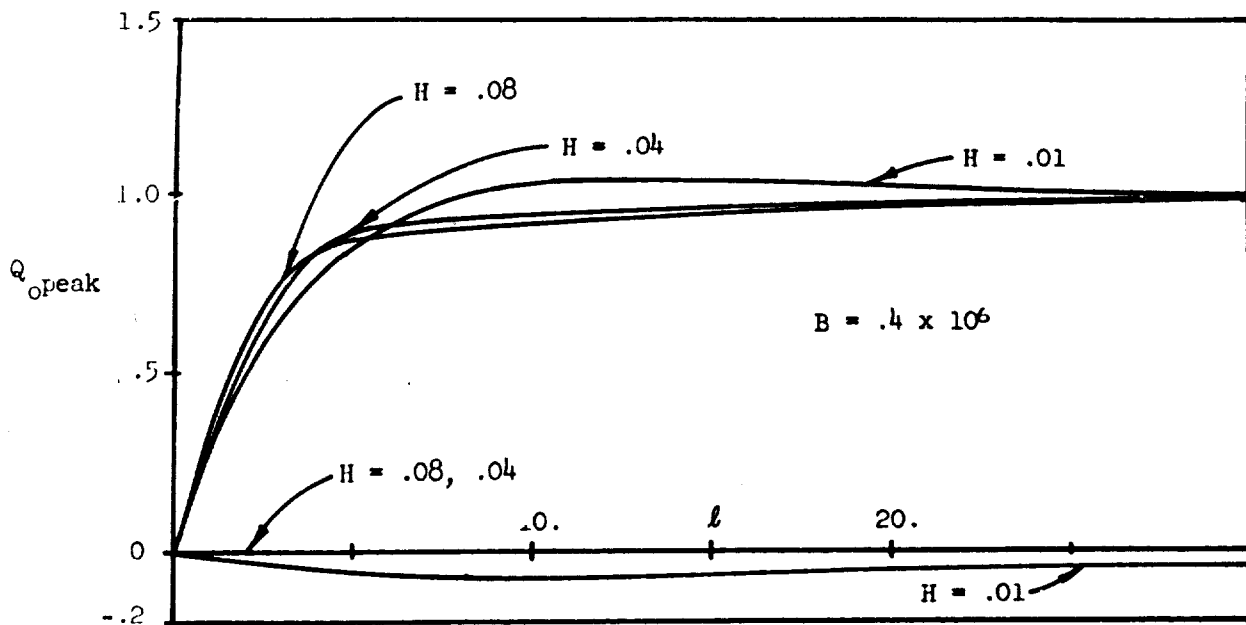


Figure 35 $Q_{0\text{peak}}$ VS. l FOR A HALF SINE PULSE AT VARIOUS VALUES OF H .

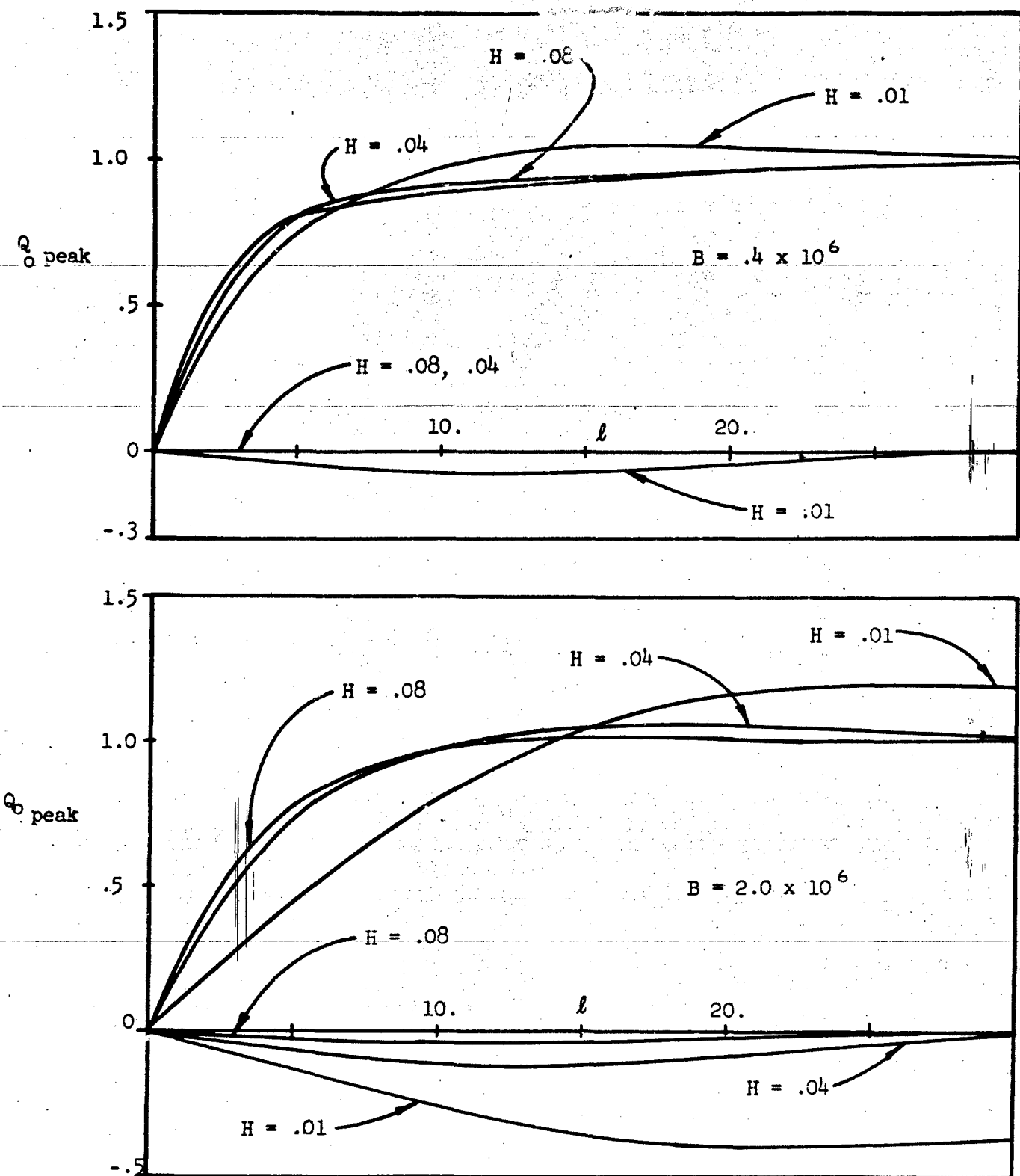


Figure 36 $Q_0 \text{ peak}$ VS. l FOR A HAVERSINE PULSE AT VARIOUS VALUES OF H .

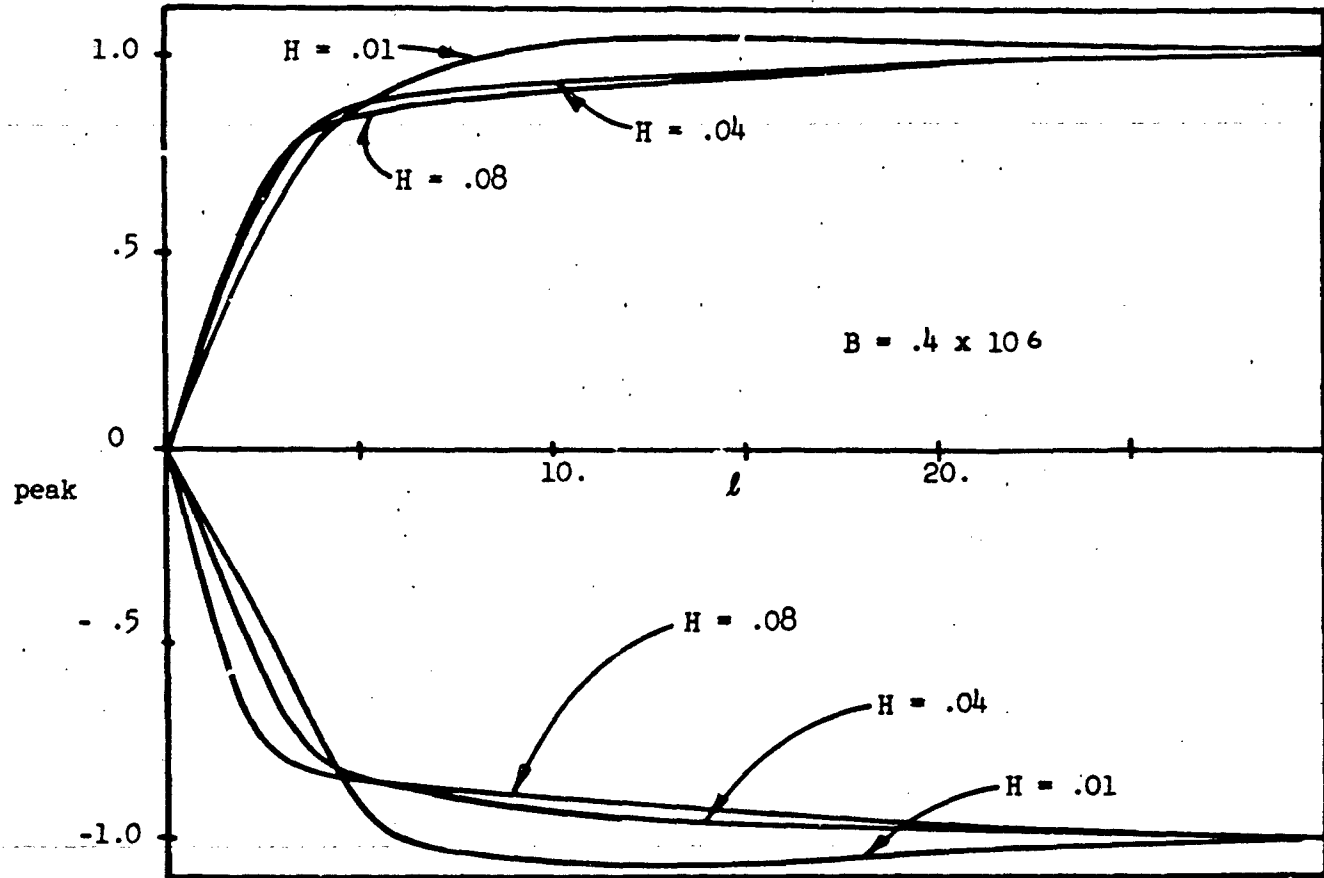


Figure 37a Q_o peak VS. l FOR A SINE WAVE AT VARIOUS VALUES OF H .

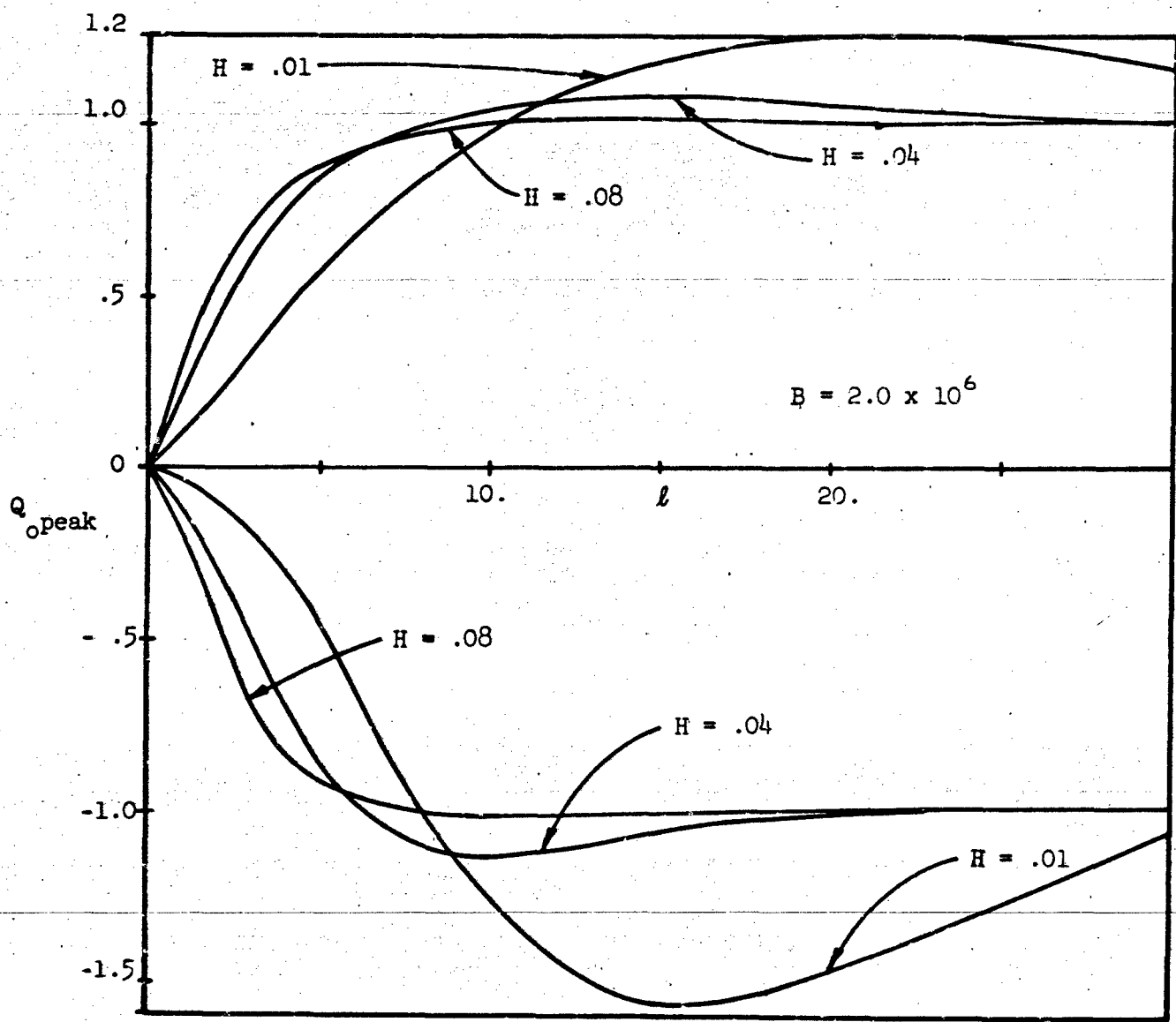


Figure 37b Q_0 peak VS. ℓ FOR A SINE WAVE AT VARIOUS VALUES OF H .

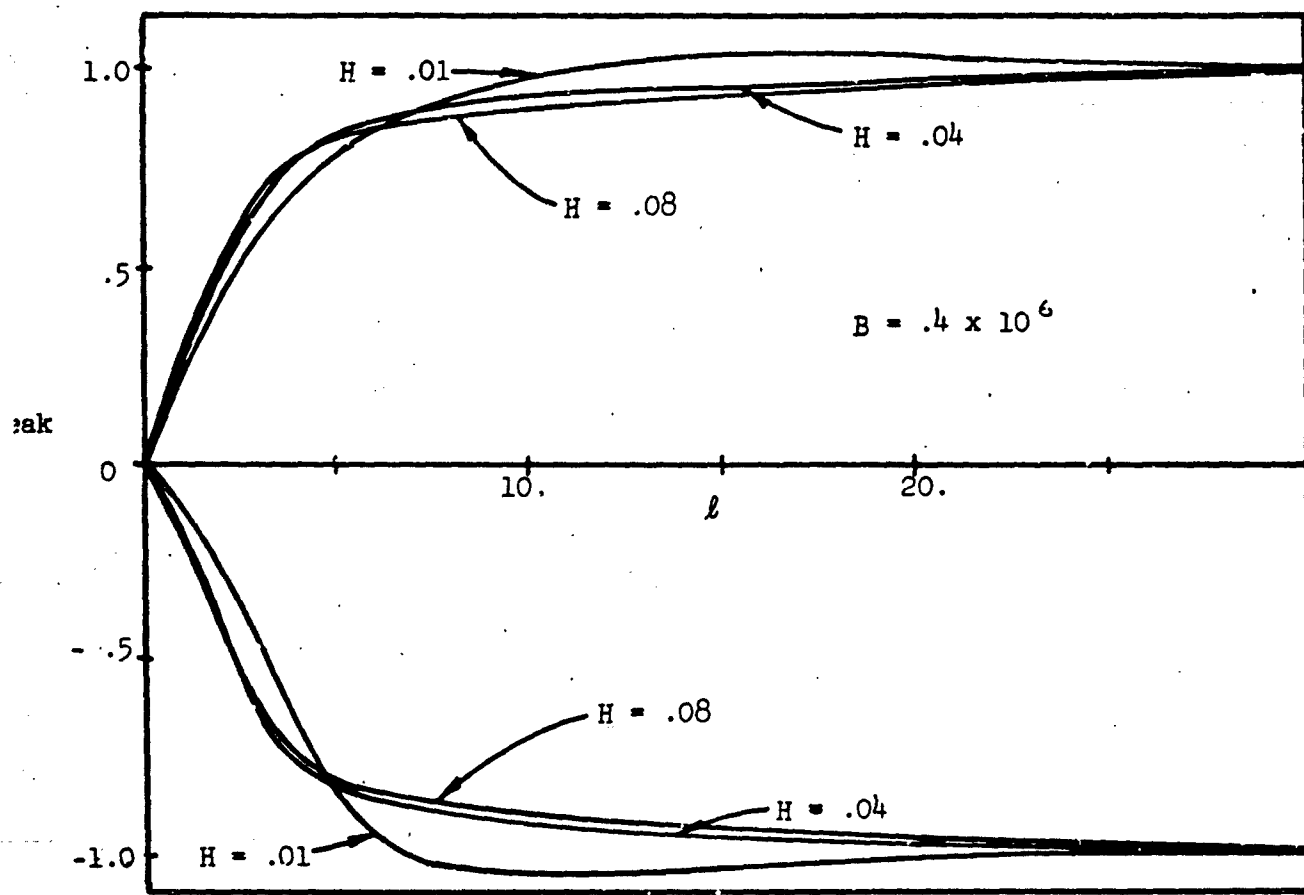


Figure 38a Q_0 peak VS. l FOR A MODIFIED SINE WAVE AT VARIOUS VALUES OF H .

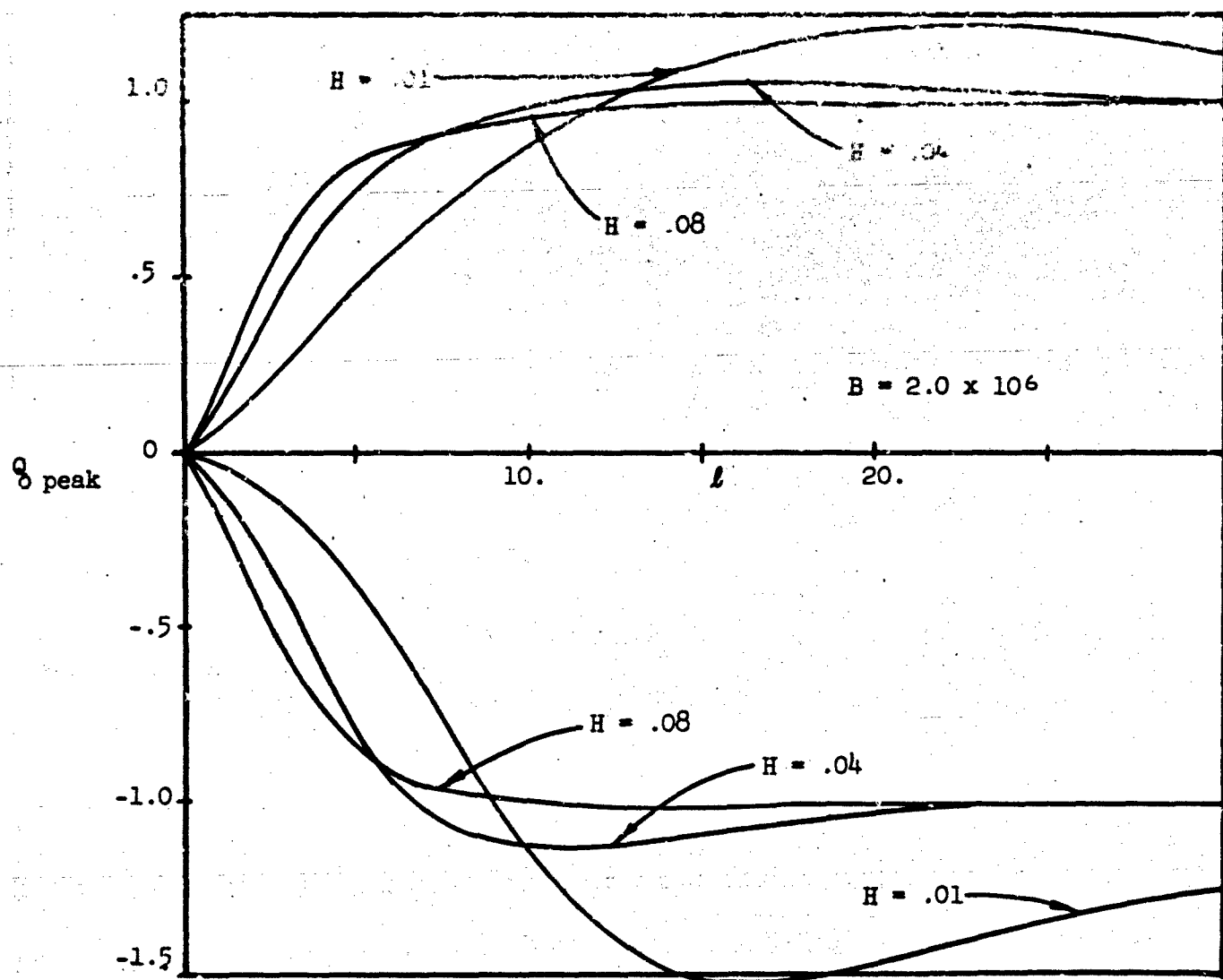


Figure 38b. Q_0 peak VS. t FOR A MODIFIED SINE WAVE AT VARIOUS VALUES OF H .

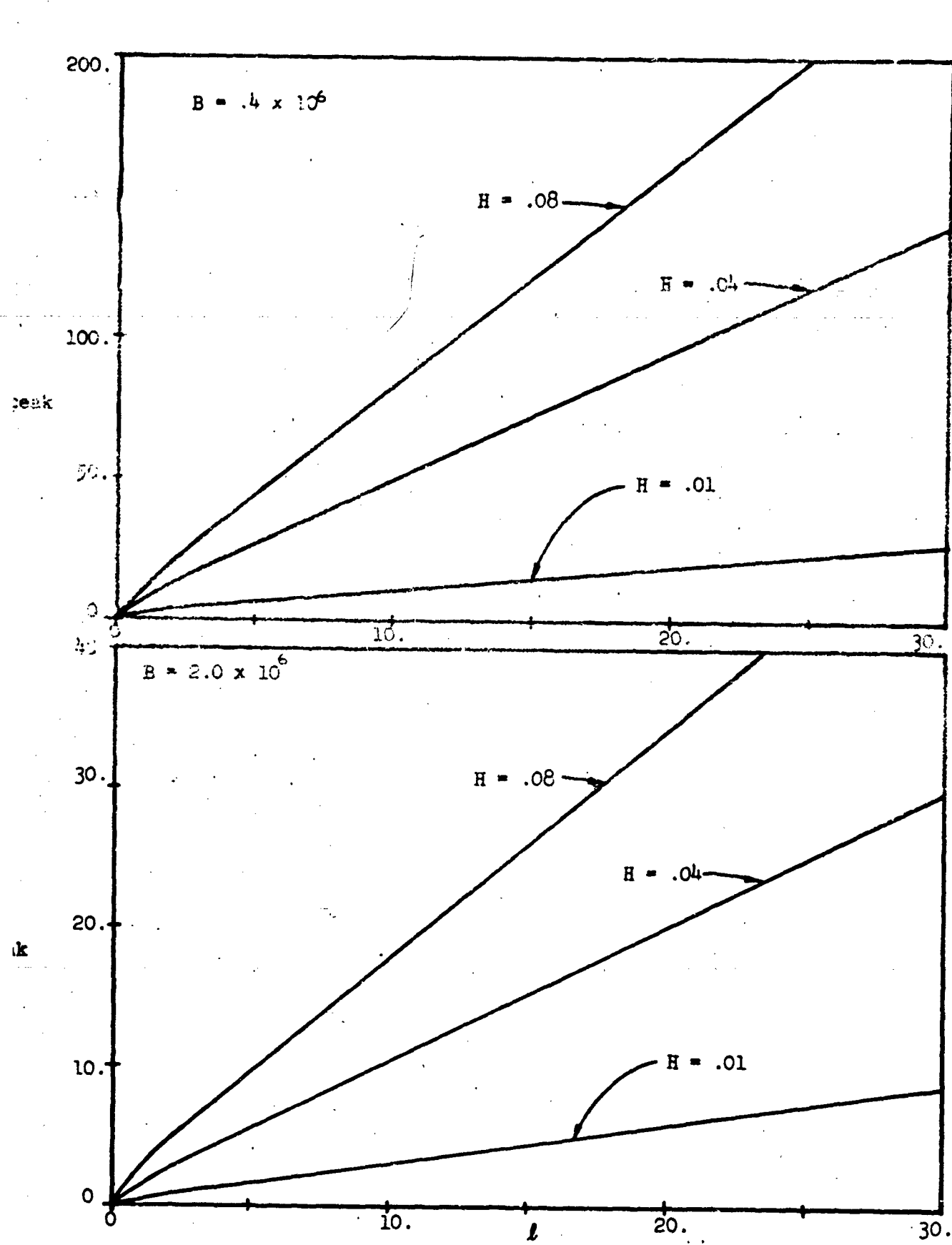


Figure 39 $Q_{1\text{peak}}$ VS. t FOR A RECTANGULAR PULSE
AT VARIOUS VALUES OF H .

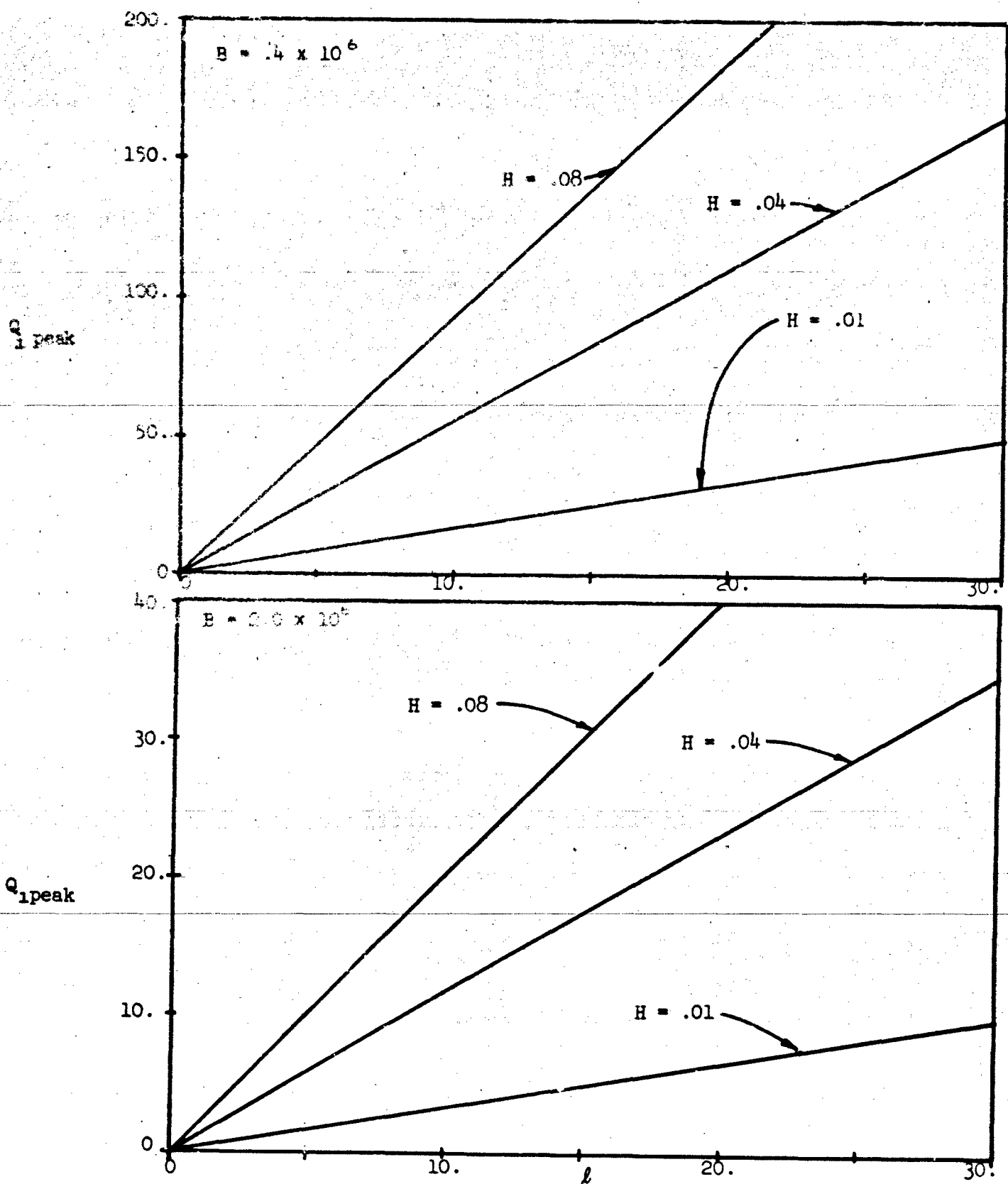


Figure 40 $Q_{1\text{peak}}$ VS. ℓ FOR AN EXPONENTIALLY DECAYING PULSE AT VARIOUS VALUES OF H .

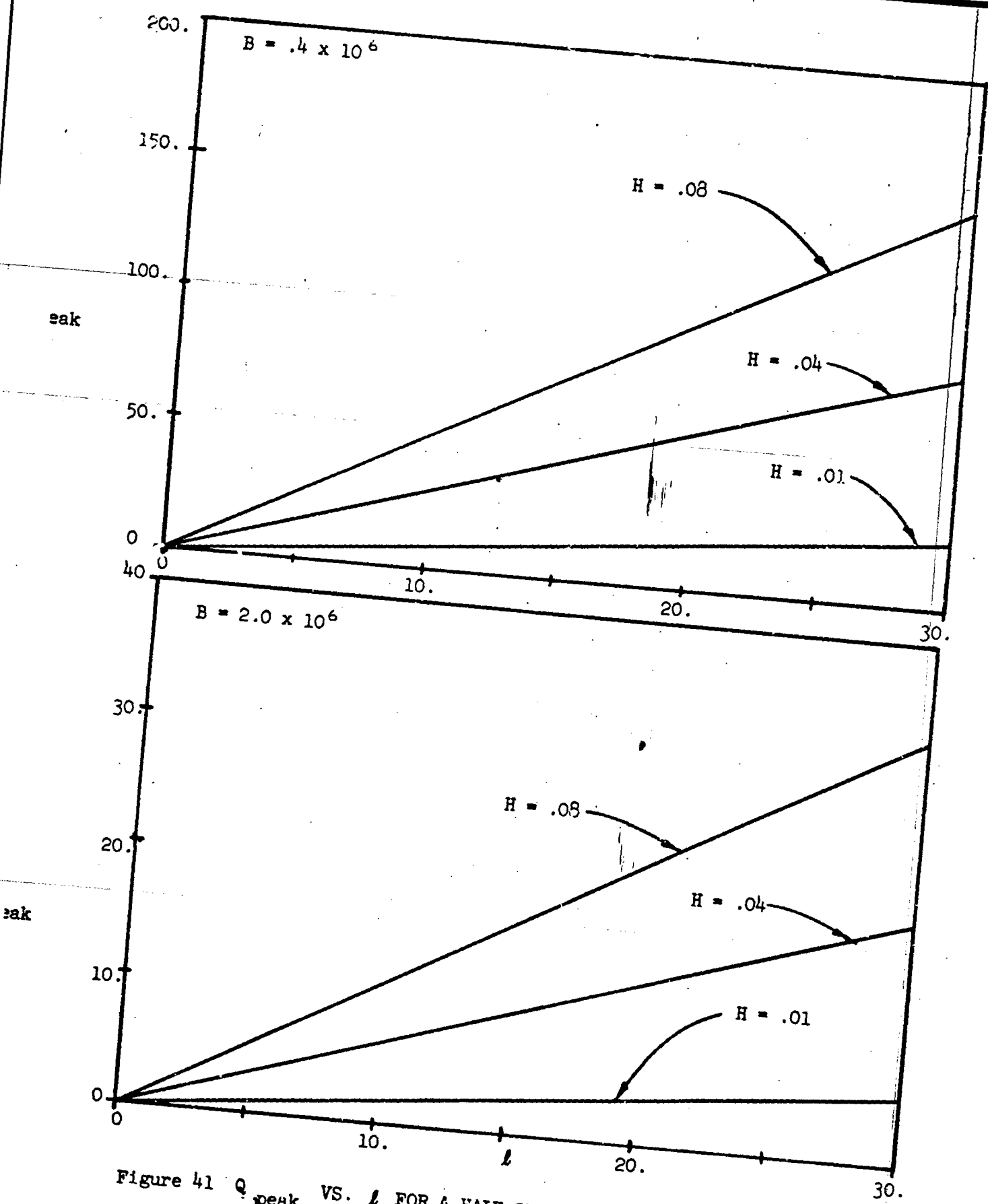


Figure 41 Q_{peak} VS. l FOR A HALF-SINE PULSE AT VARIOUS
VALUES OF H .

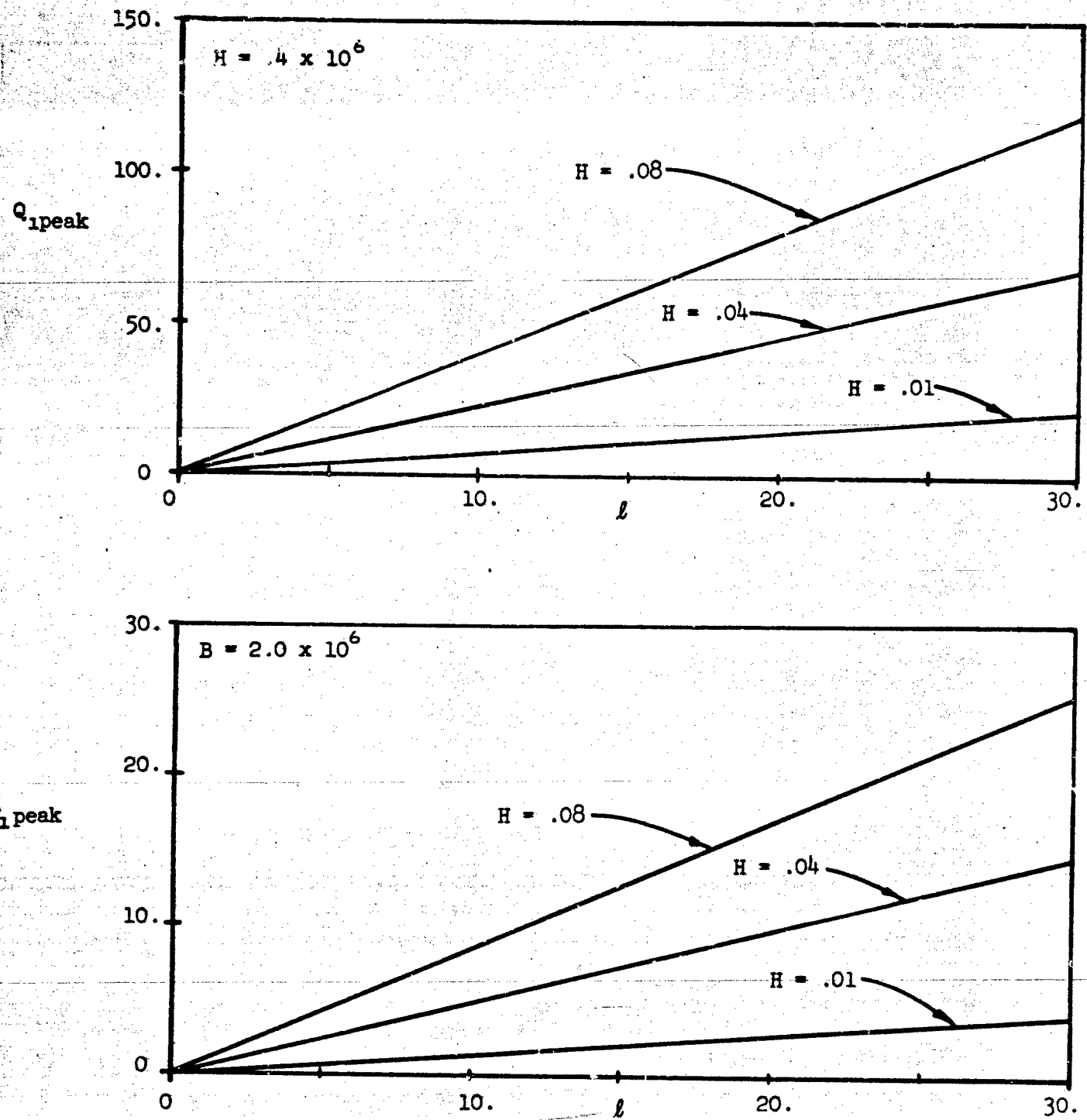


Figure 42 $Q_{i\text{peak}}$ VS. l FOR A HAVERSINE PULSE AT VARIOUS VALUES OF H .

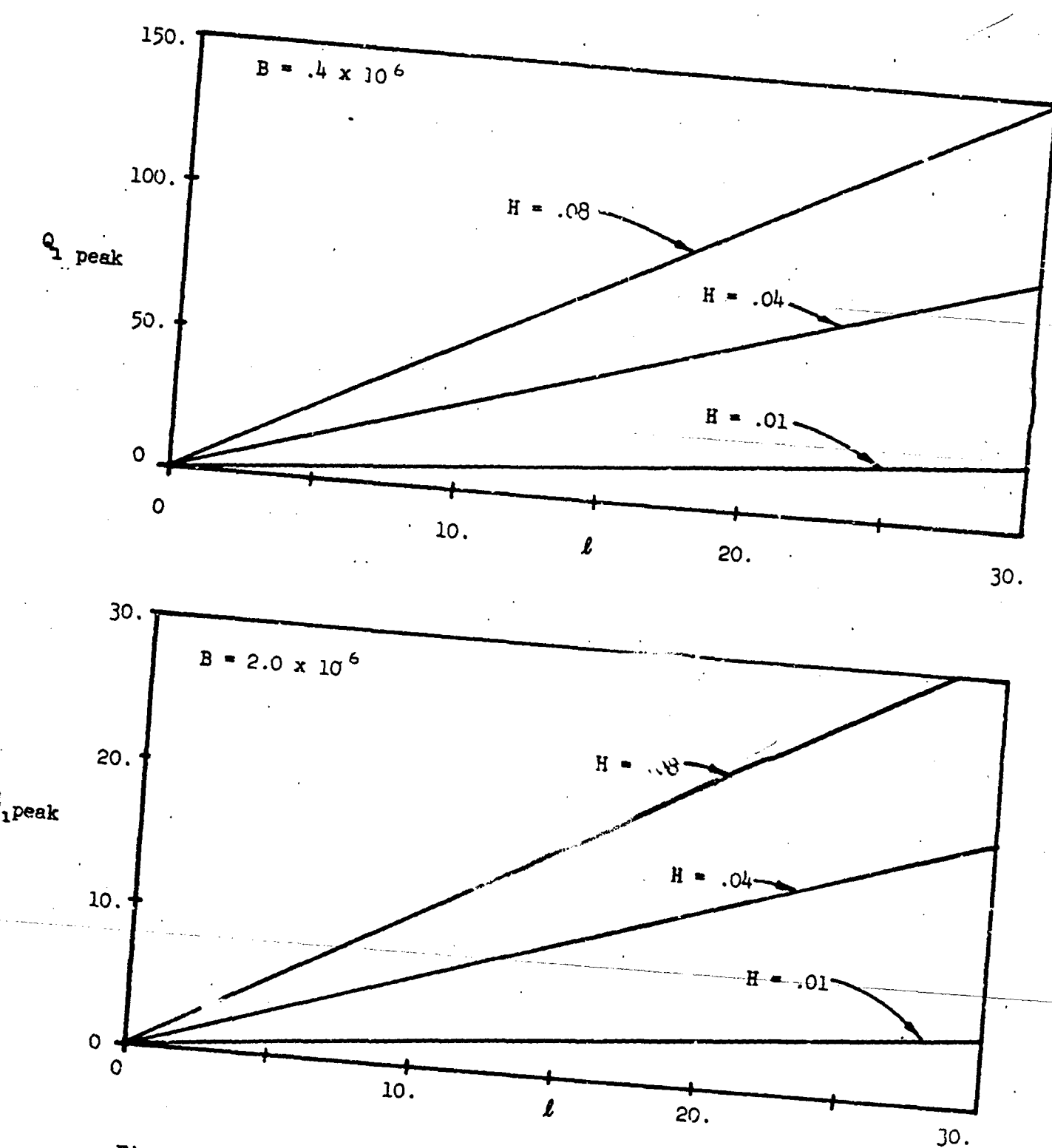


Figure 43 $Q_1 \text{ peak}$ VS. l FOR A SINE WAVE AT VARIOUS VALUES OF H .

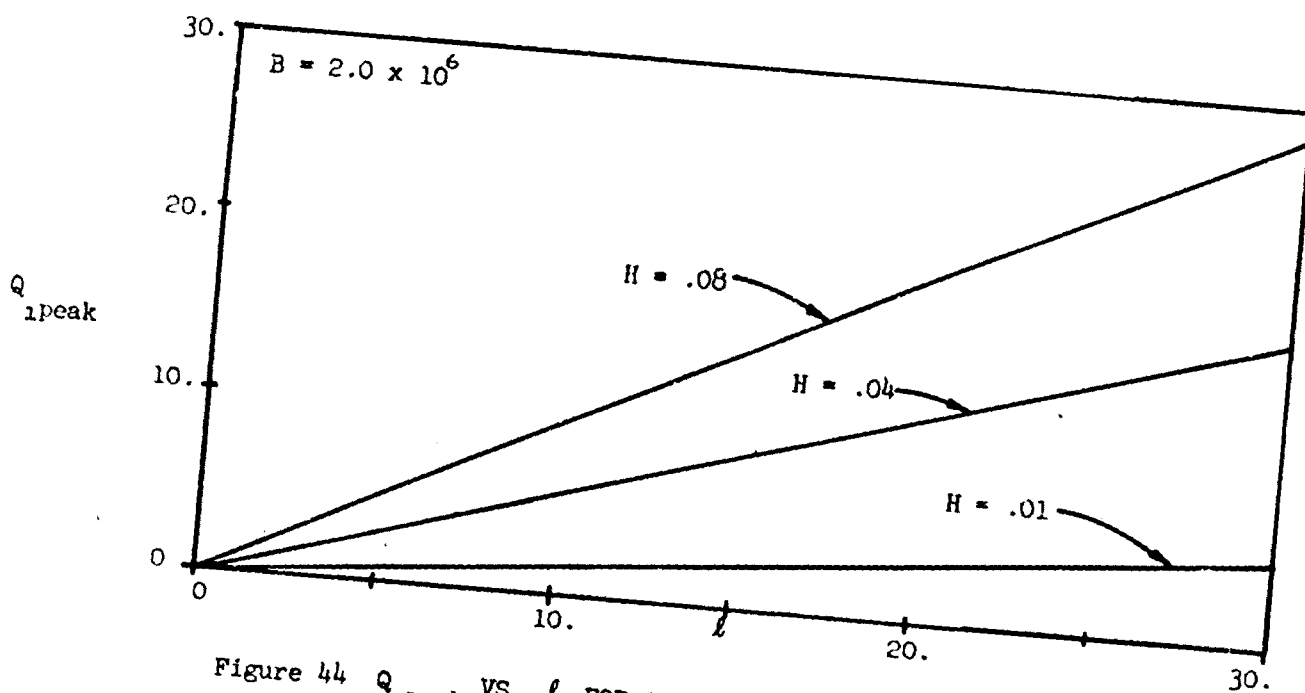
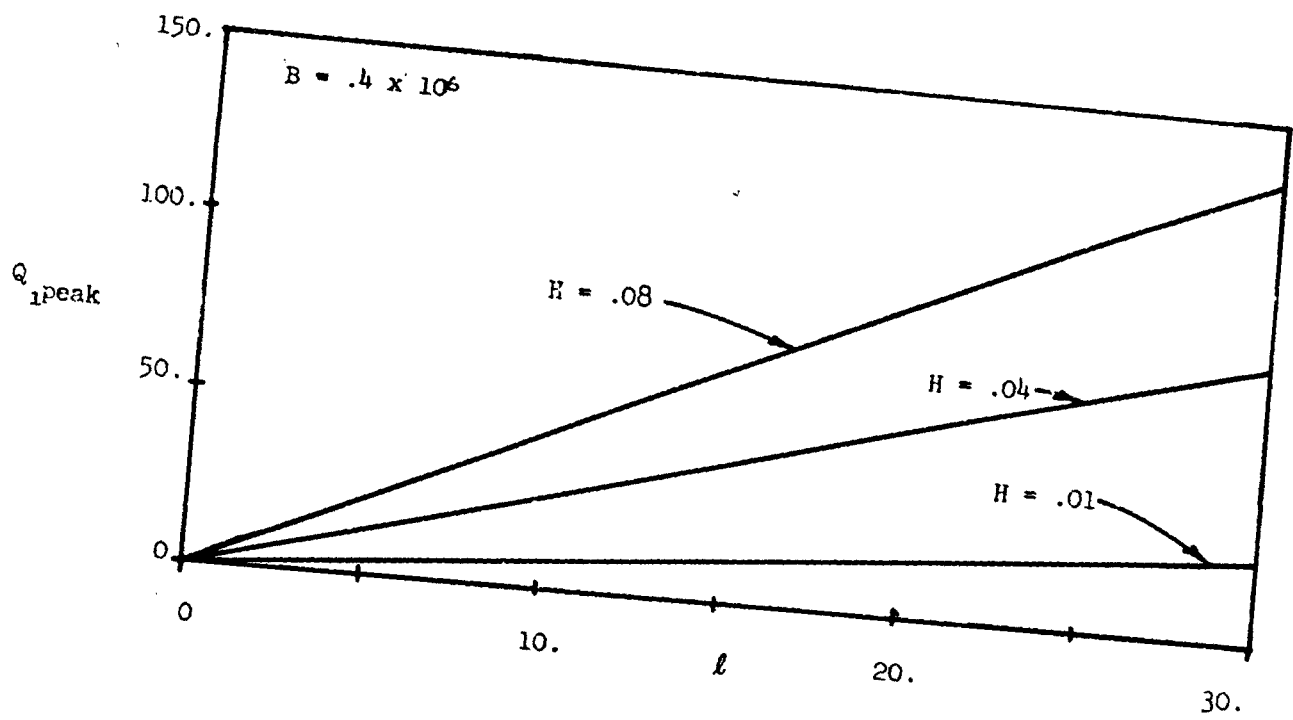


Figure 44 $Q_{1\text{peak}}$ VS. ℓ FOR A MODIFIED SINE WAVE AT VARIOUS
VALUES OF H .

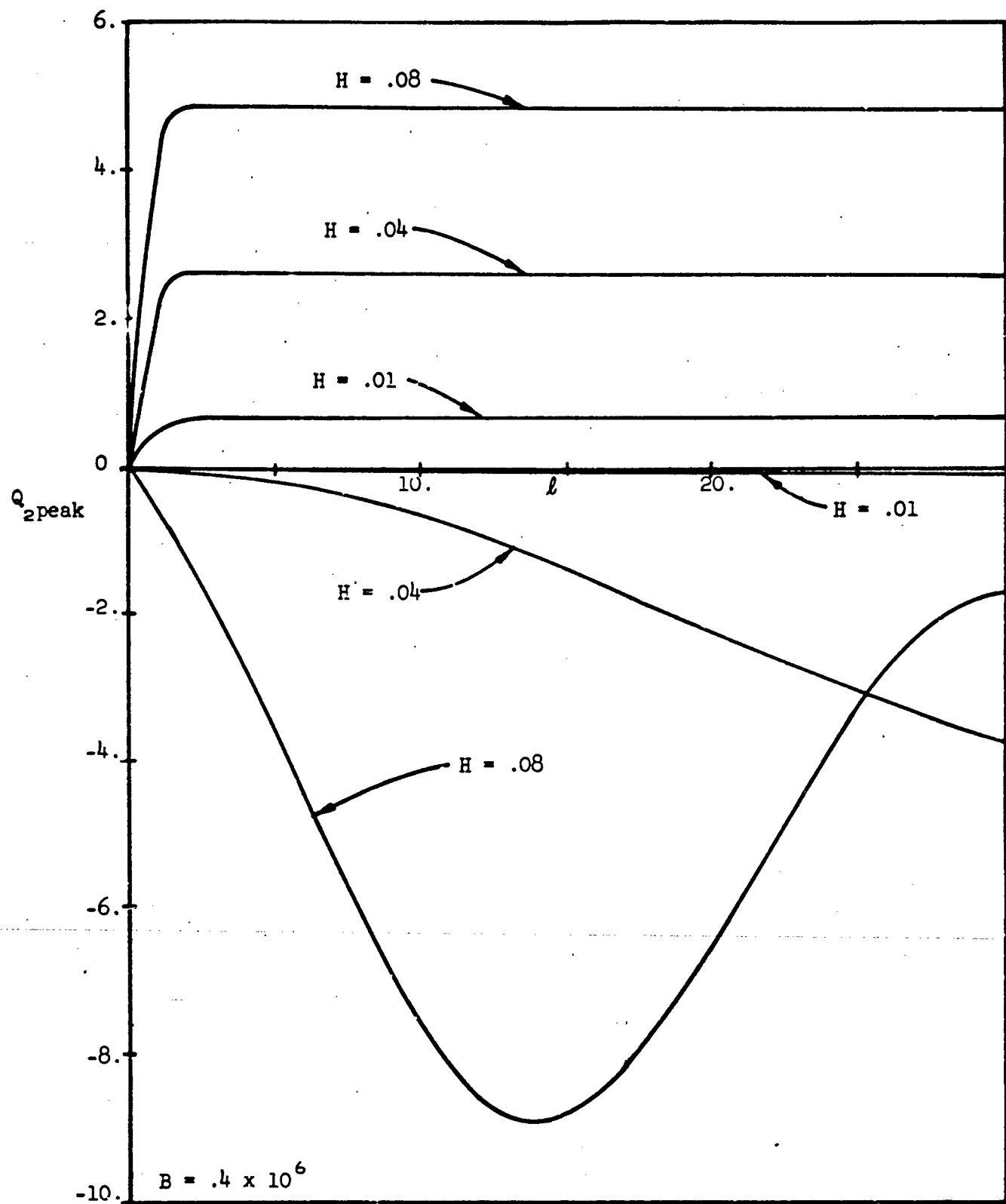


Figure 45 $Q_{2\text{peak}}$ VS. l FOR A RECTANGULAR PULSE AT VARIOUS VALUES OF H .

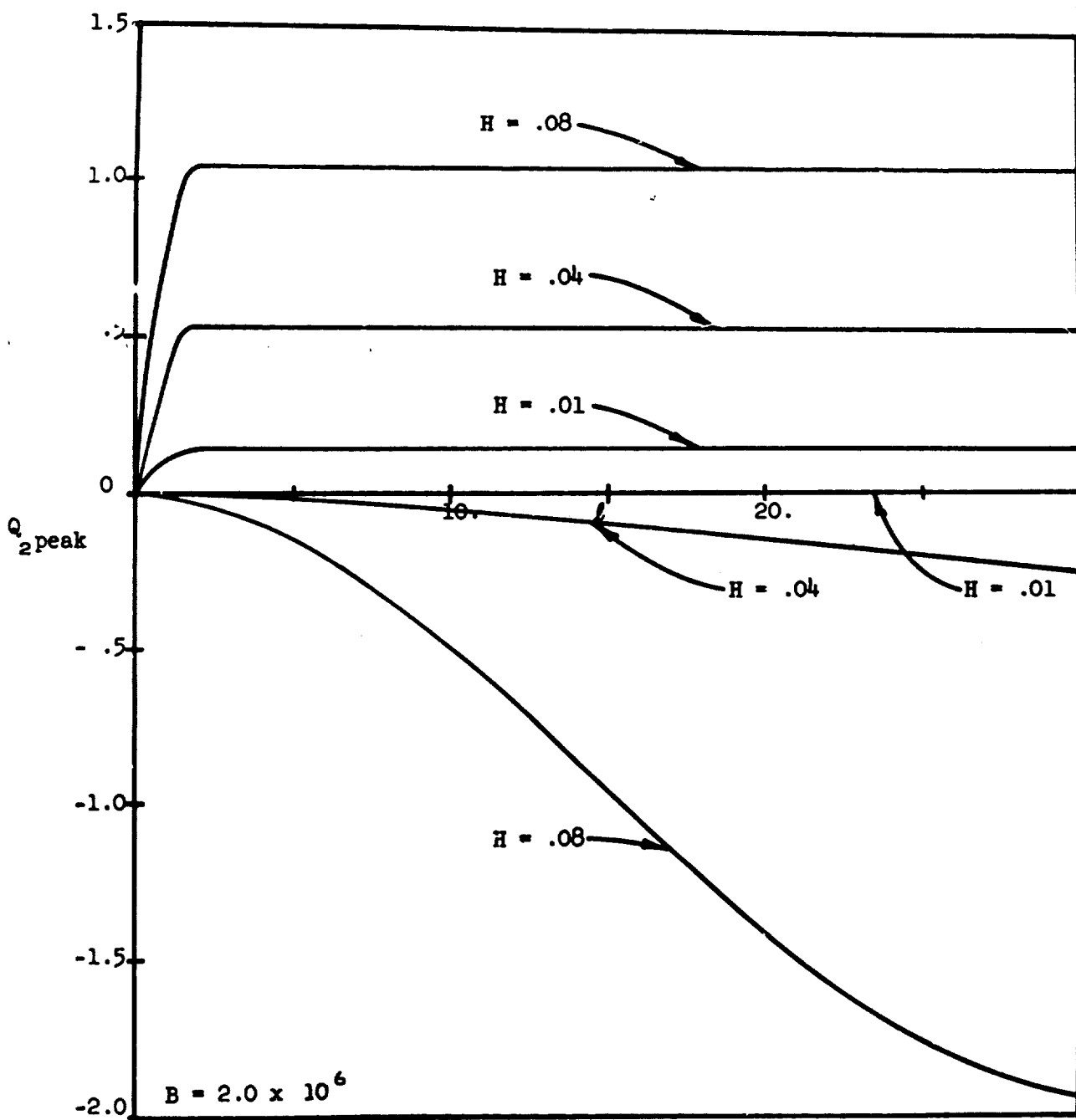


Figure 46 Q_2 peak VS. t FOR A RECTANGULAR PULSE AT VARIOUS VALUES OF H .

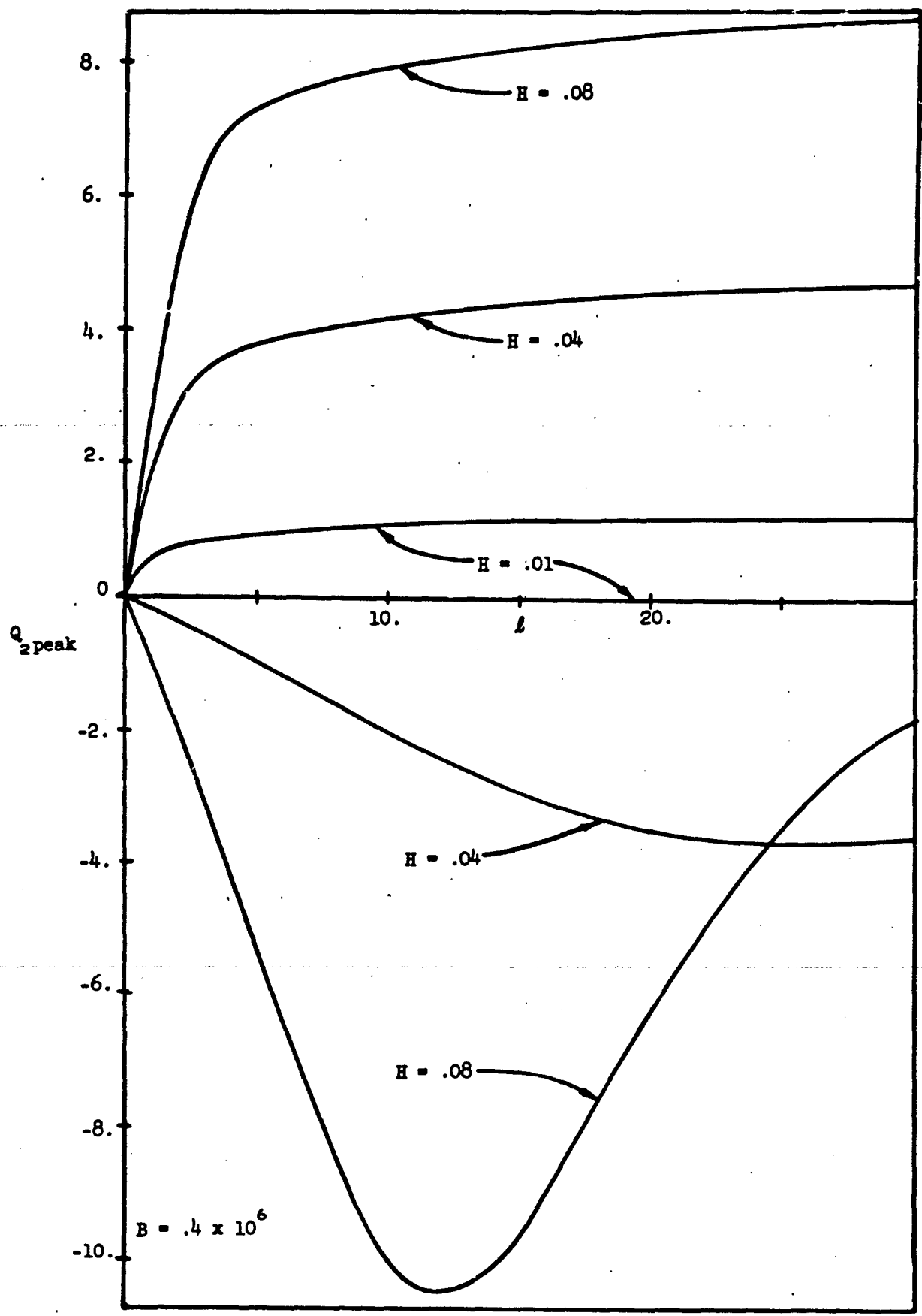


Figure 47 $Q_2\text{peak}$ VS. t FOR AN EXPONENTIALLY DECAYING PULSE AT VARIOUS VALUES OF H .

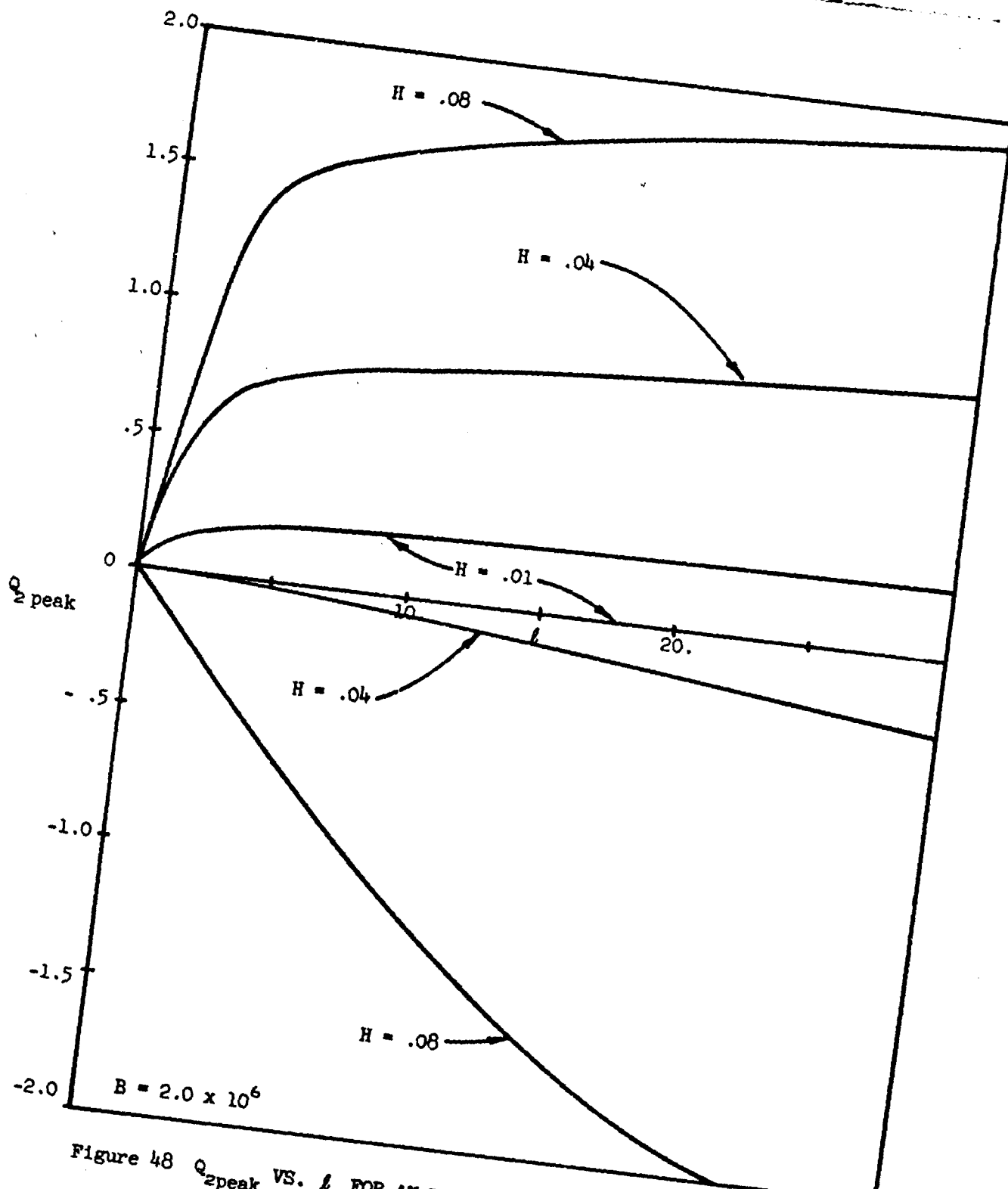


Figure 48 Q_2 peak VS. l FOR AN EXPONENTIALLY DECAYING PULSE AT
VARIOUS VALUES OF H .

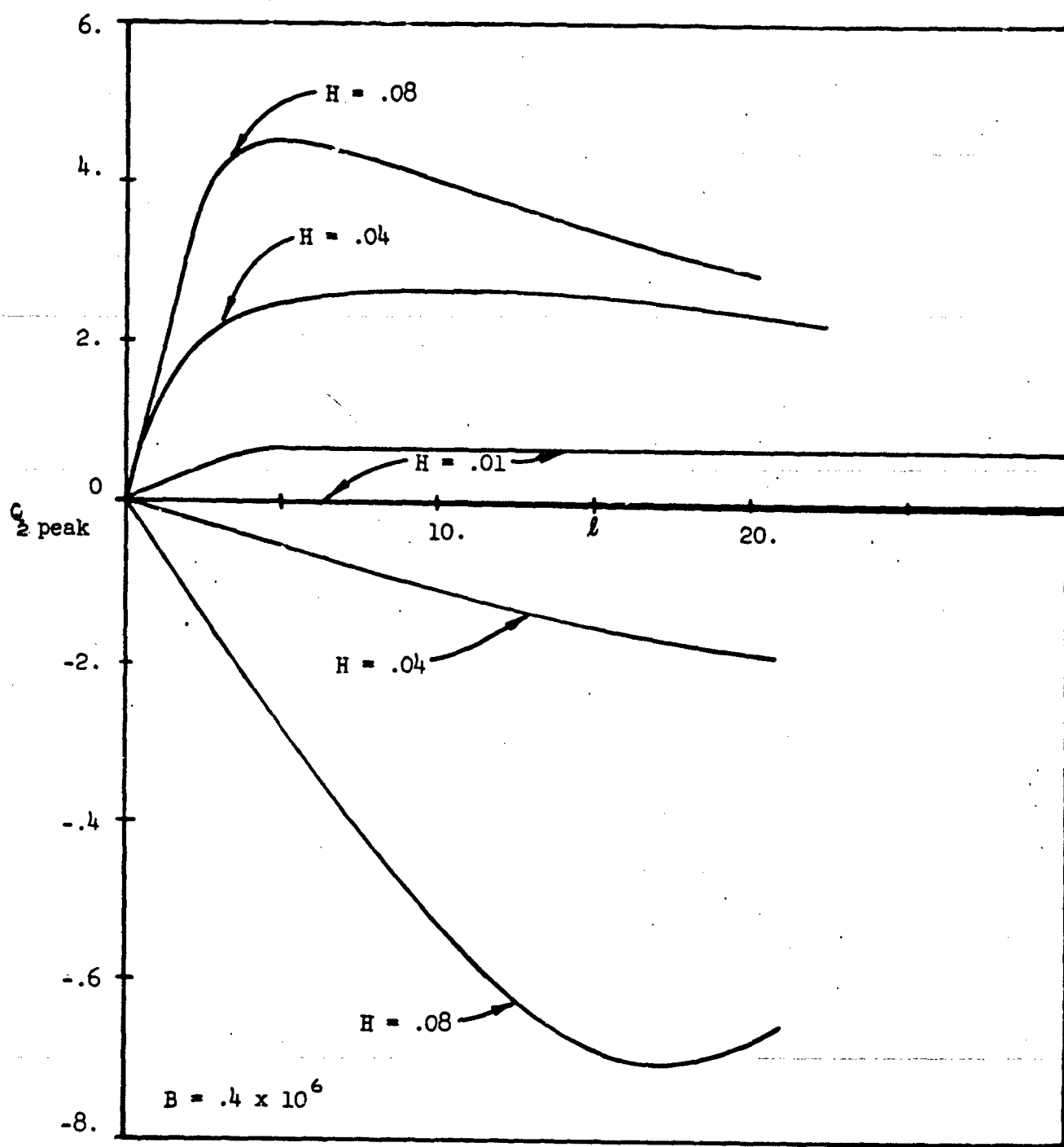


Figure 49 $Q_{\frac{1}{2}} \text{ peak}$ VS. t FOR A HALF SINE PULSE AT VARIOUS VALUES OF H .

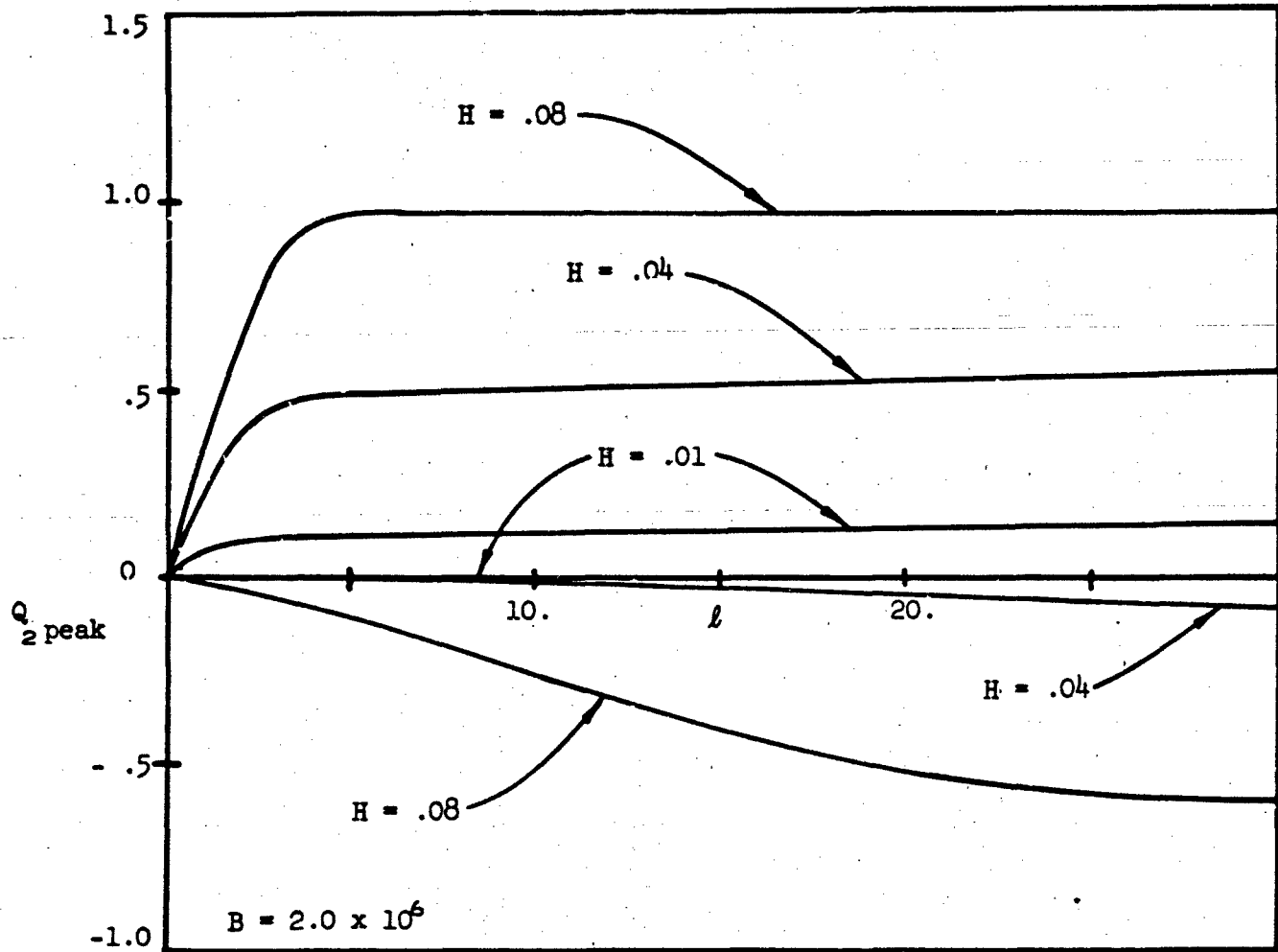


Figure 50 Q_2 peak VS. l FOR A HALF SINE PULSE AT VARIOUS VALUES OF H .

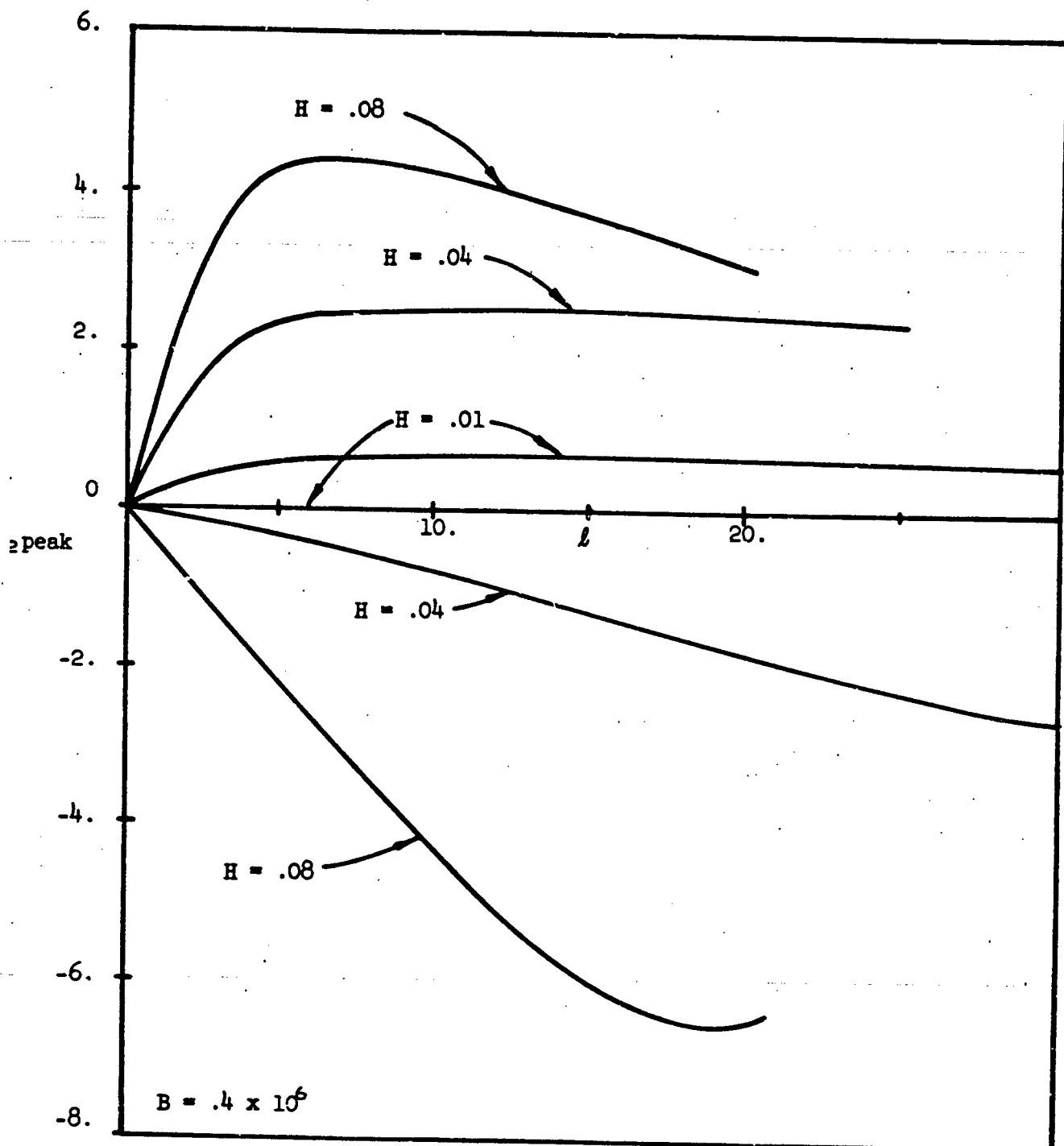


Figure 51 Q_2 peak VS. l FOR A HAVERSINE PULSE AT VARIOUS VALUES OF H .

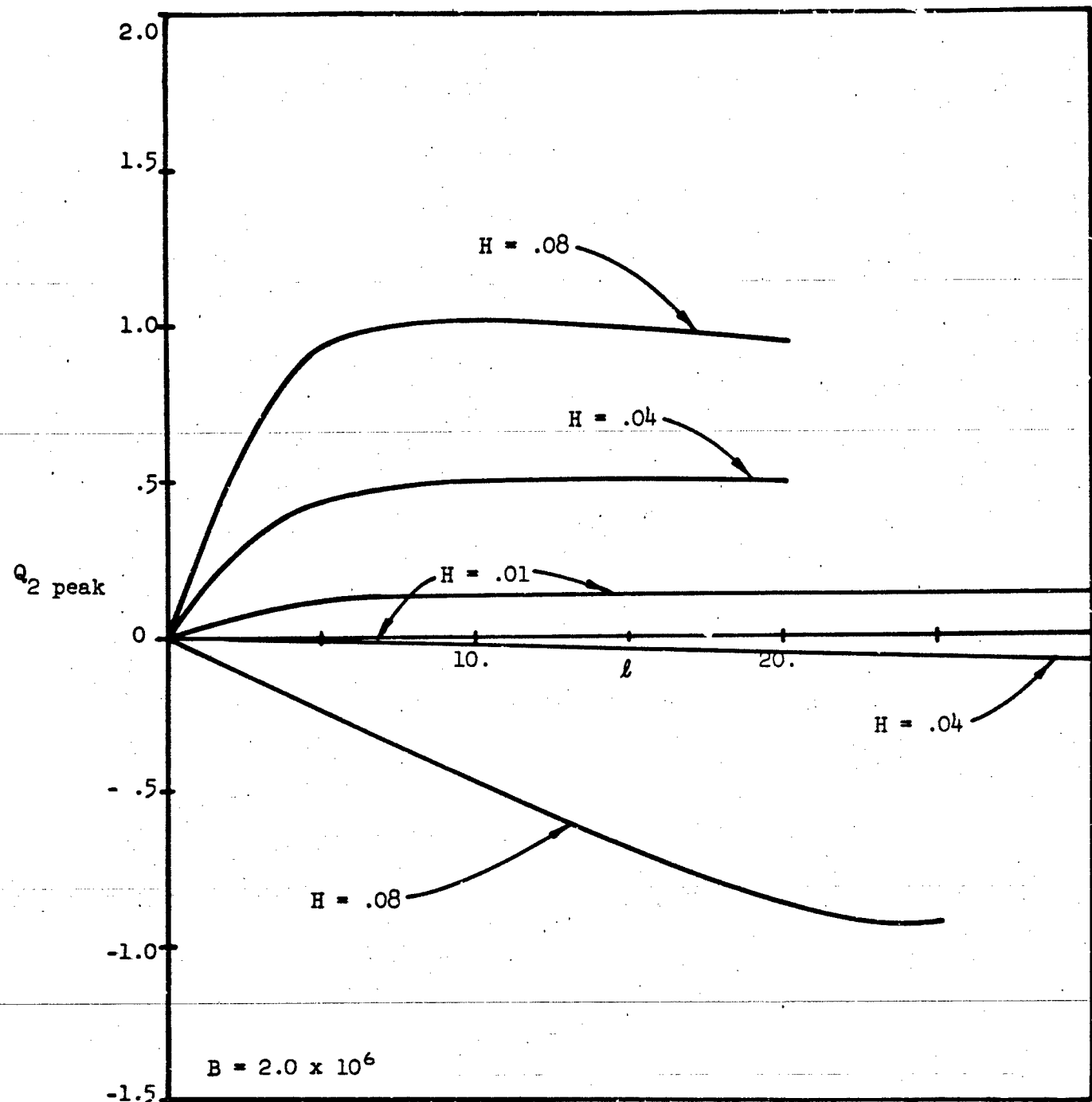


Figure 52 Q_2 peak VS. ℓ FOR A HAVERSINE PULSE AT VARIOUS VALUES OF H .

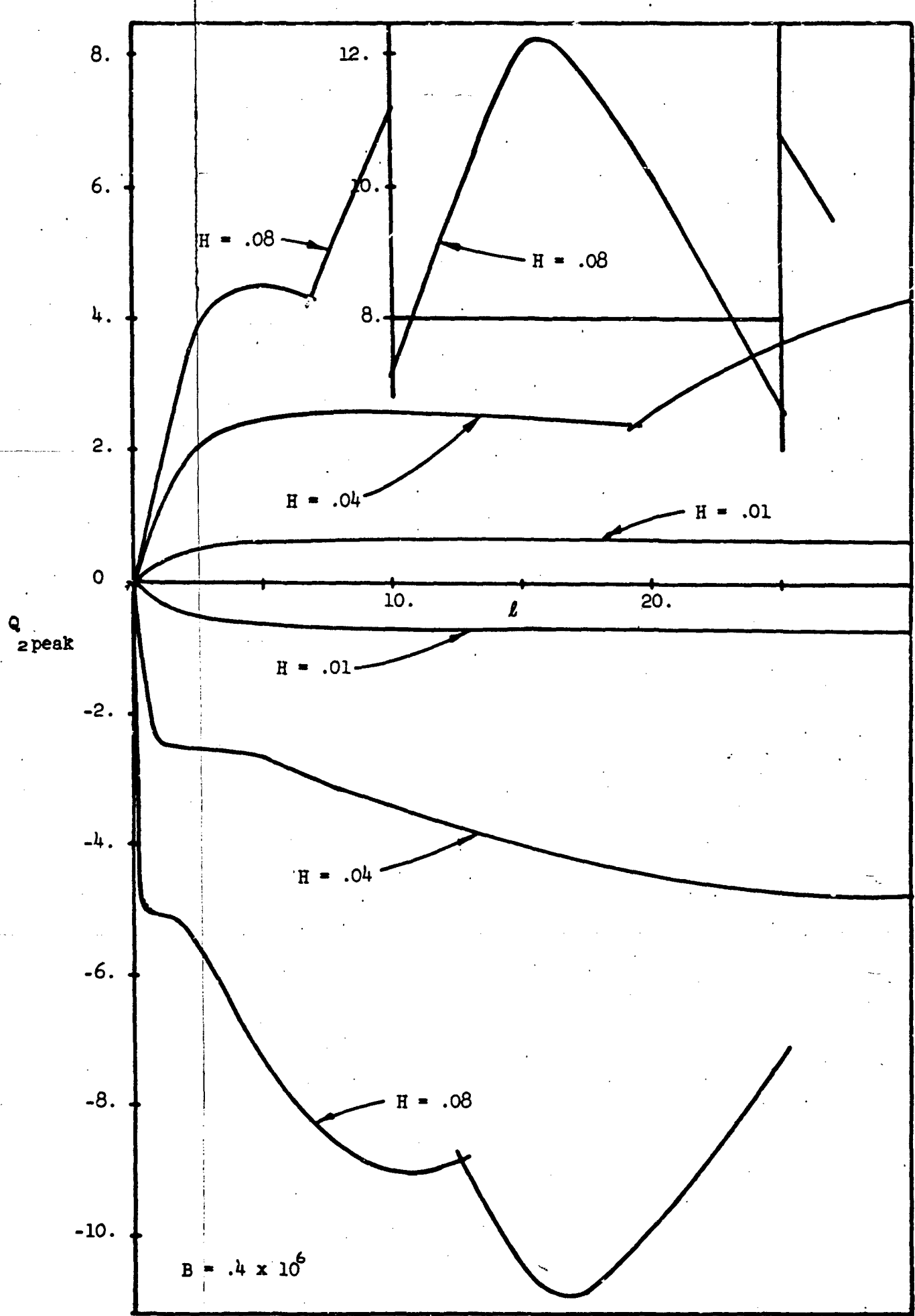


Figure 53 $Q_{2\text{peak}}$ VS. l FOR A SINE WAVE AT VARIOUS VALUES OF H .

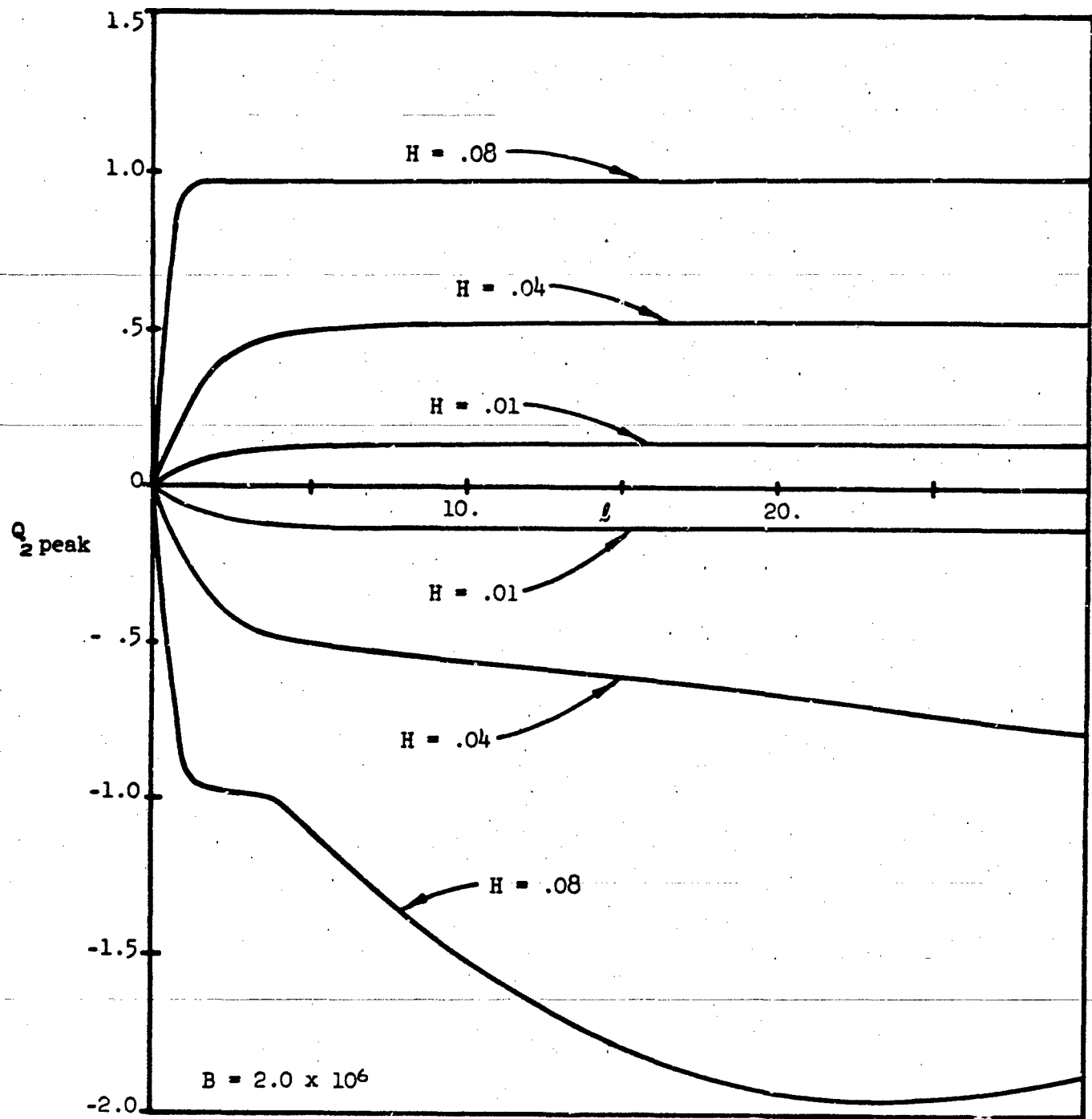


Figure 54 Q_2 peak VS. ℓ FOR SINE WAVE AT VARIOUS VALUES OF H .

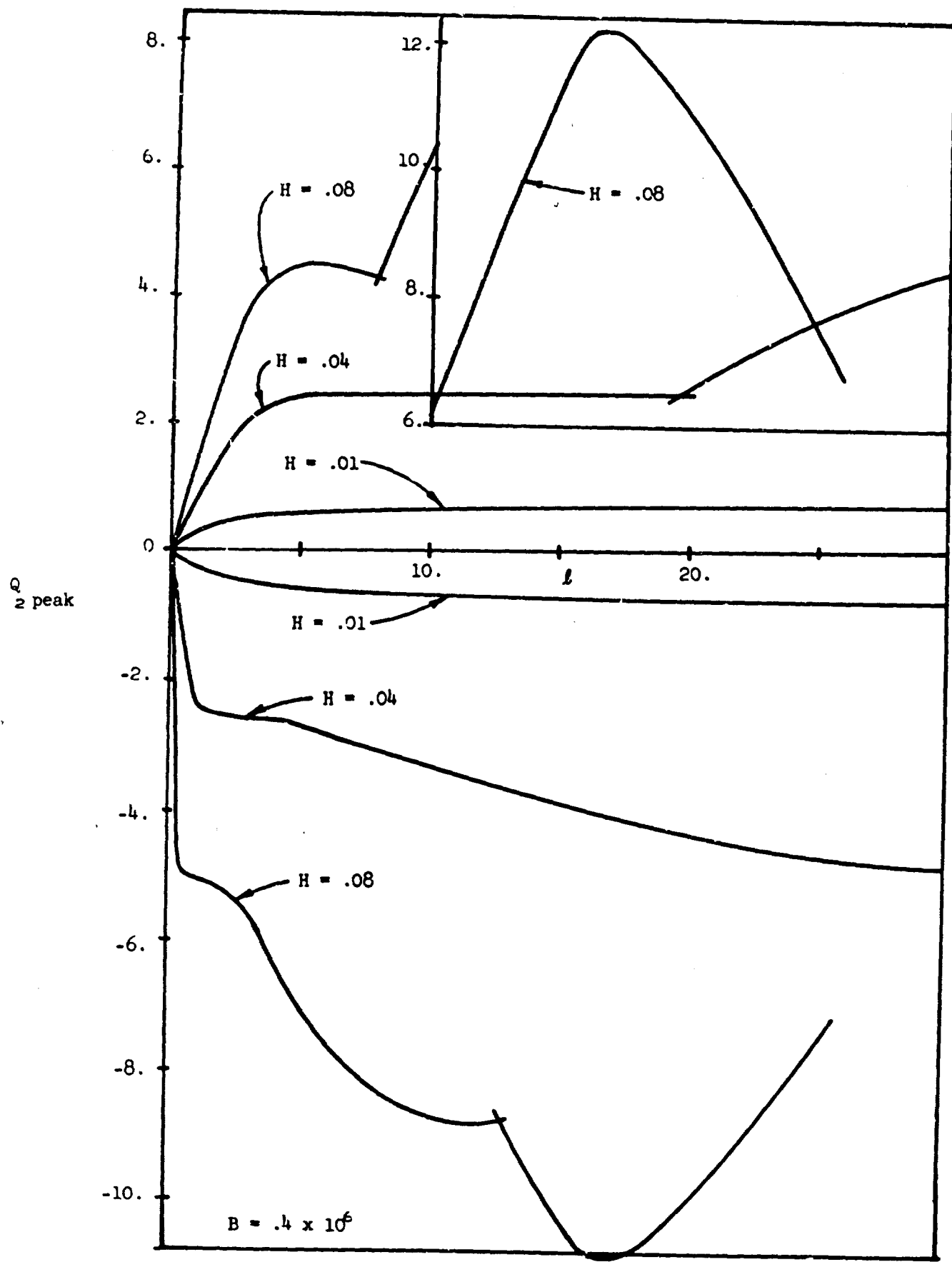


Figure 55 $Q_{2\text{peak}}$ VS. l FOR A MODIFIED SINE WAVE AT VARIOUS VALUE OF H .

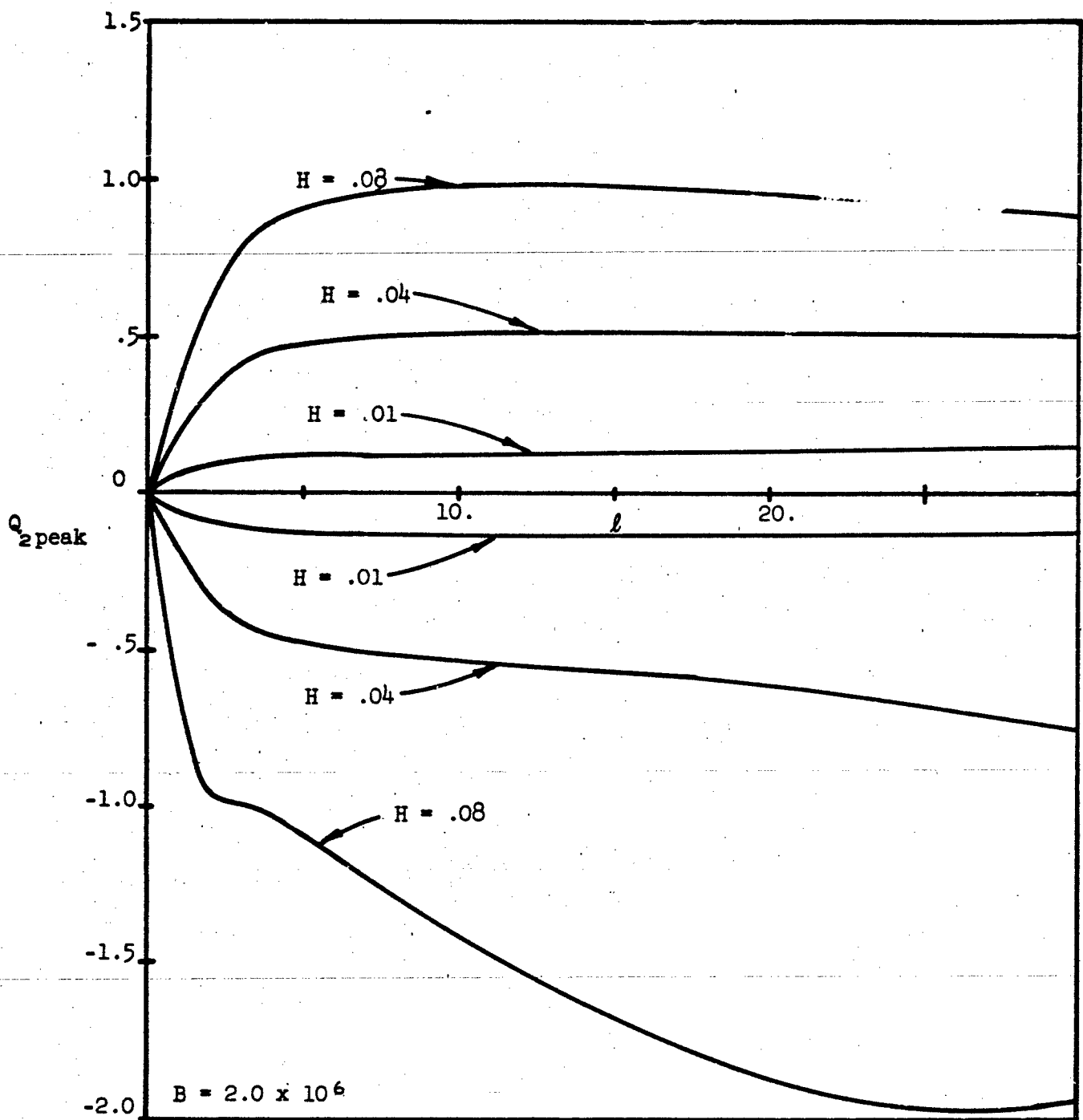


Figure 56 $Q_{2\text{peak}}$ VS. ℓ FOR A MODIFIED SINE WAVE AT VARIOUS VALUES OF H

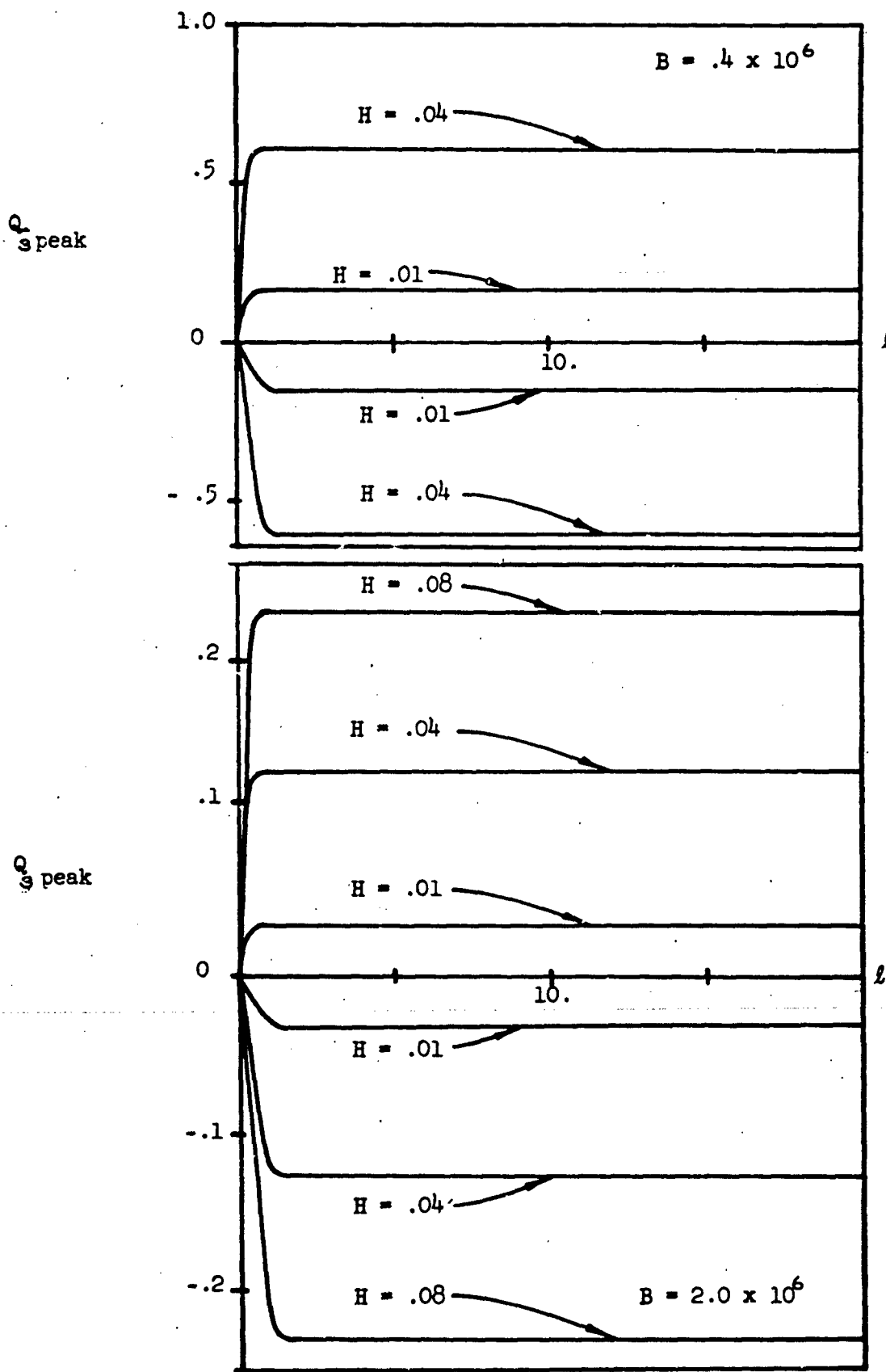


Figure 57 Q_{speak} VS. l FOR A RECTANGULAR PULSE AT VARIOUS VALUES OF H .

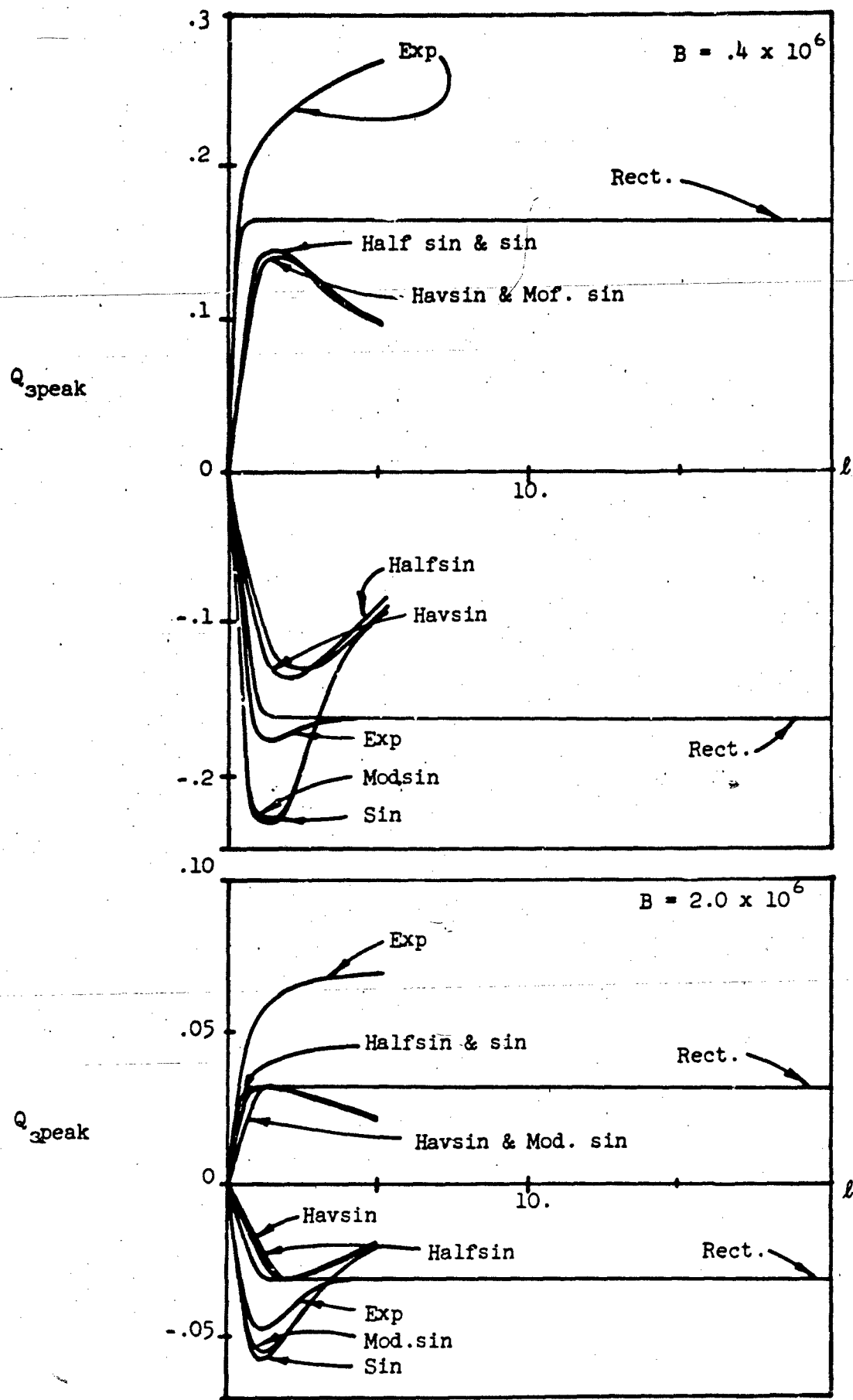


Figure 58 Q_{peak} VS. l FOR VARIOUS FORCING FUNCTION $H = .01$

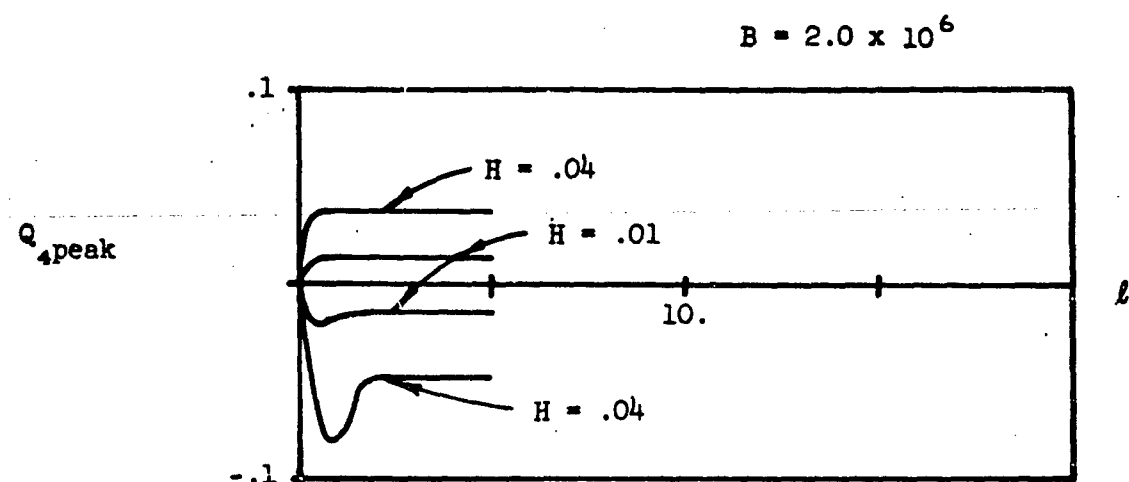
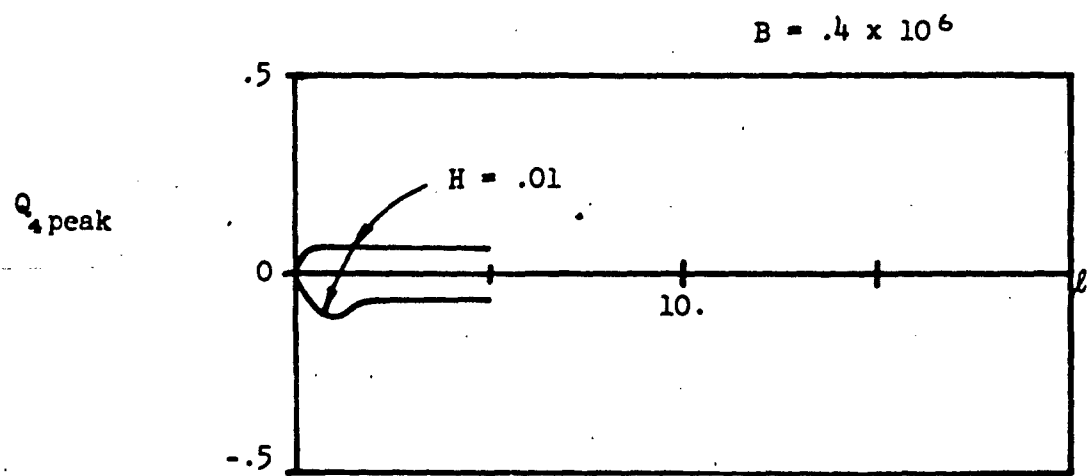
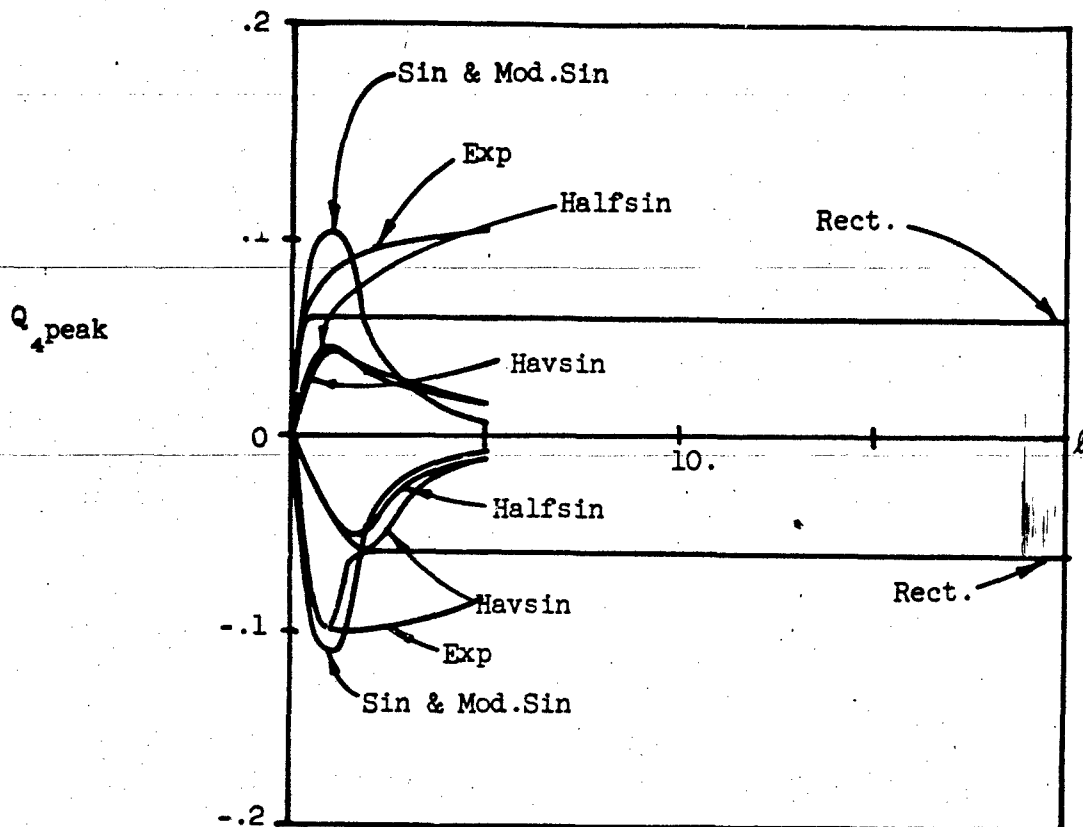


Figure 59 $Q_4 \text{ peak}$ VS. l FOR A RECTANGULAR PULSE AT VARIOUS VALUES OF H .

$$B = .4 \times 10^6$$



$$B = 2.0 \times 10^6$$

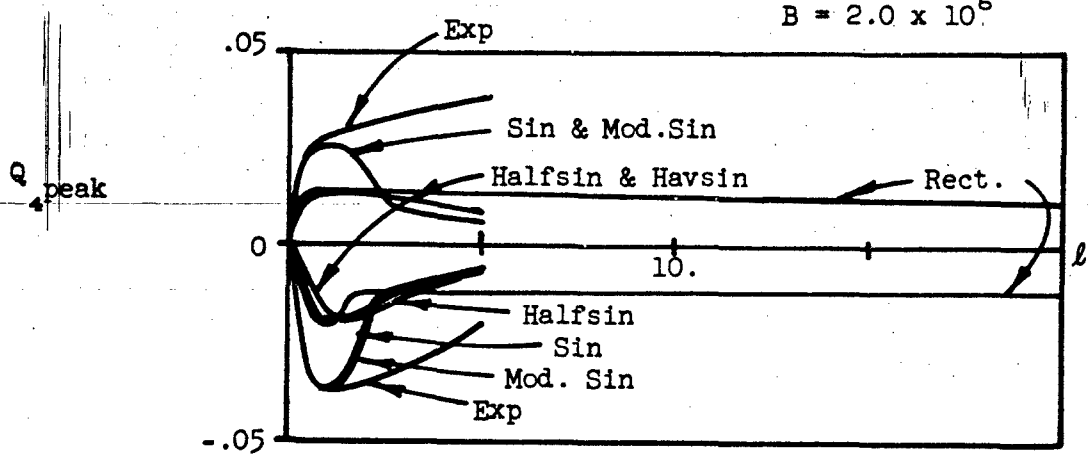


Figure 60 Q_4 peak VS. l FOR VARIOUS FORCING FUNCTIONS $H = .01$

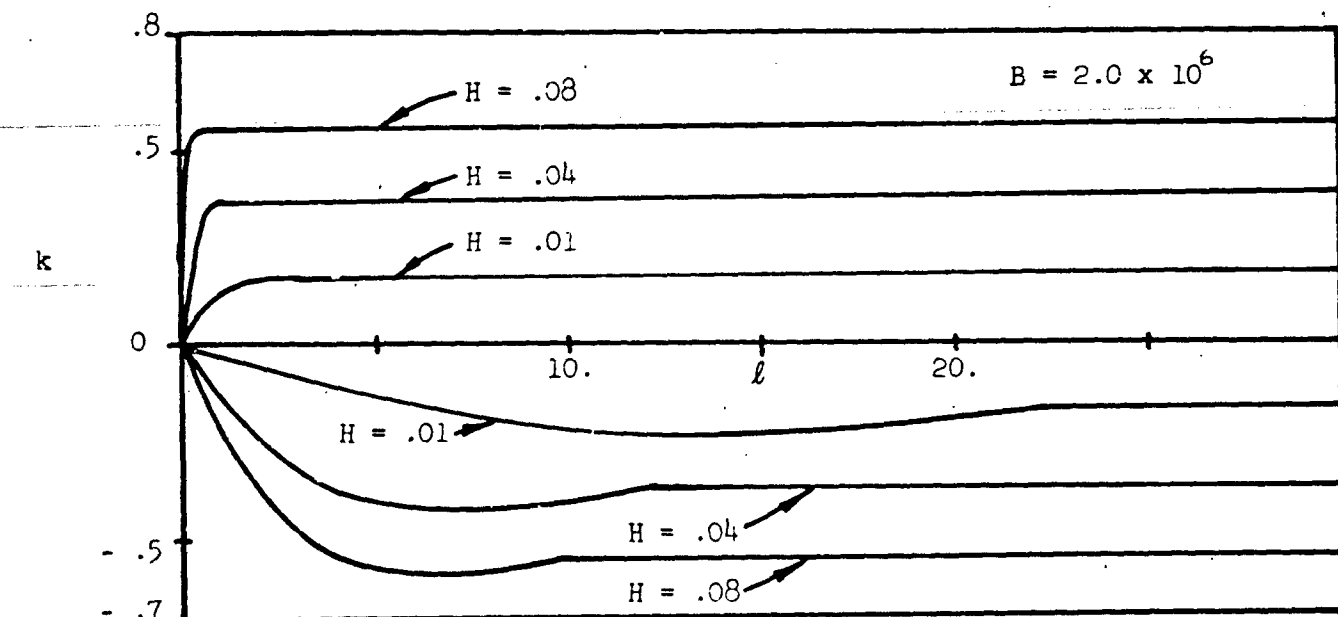
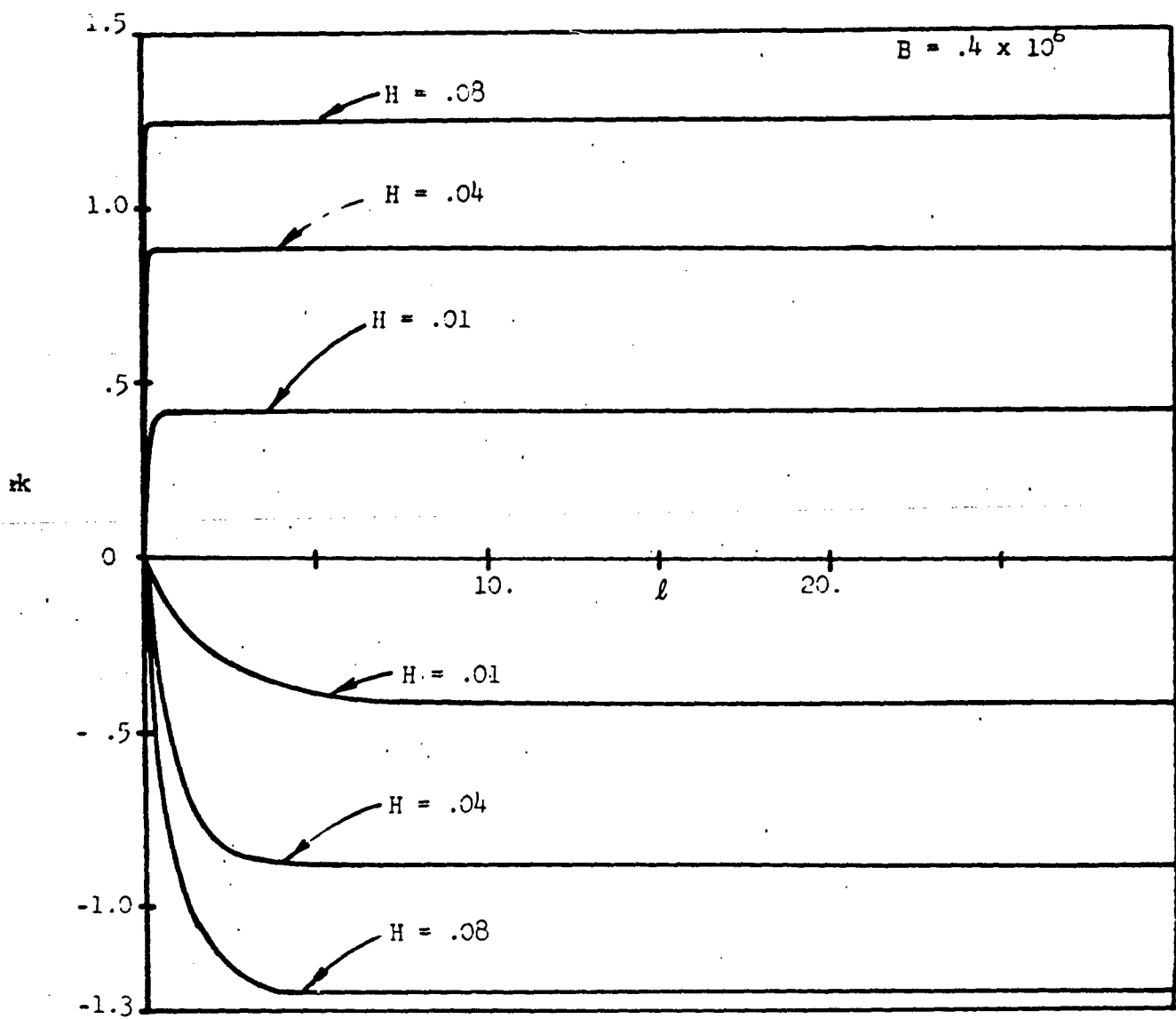


Figure 61 v_{peak} VS. ℓ FOR A RECTANGULAR PULSE AT VARIOUS VALUES OF H .

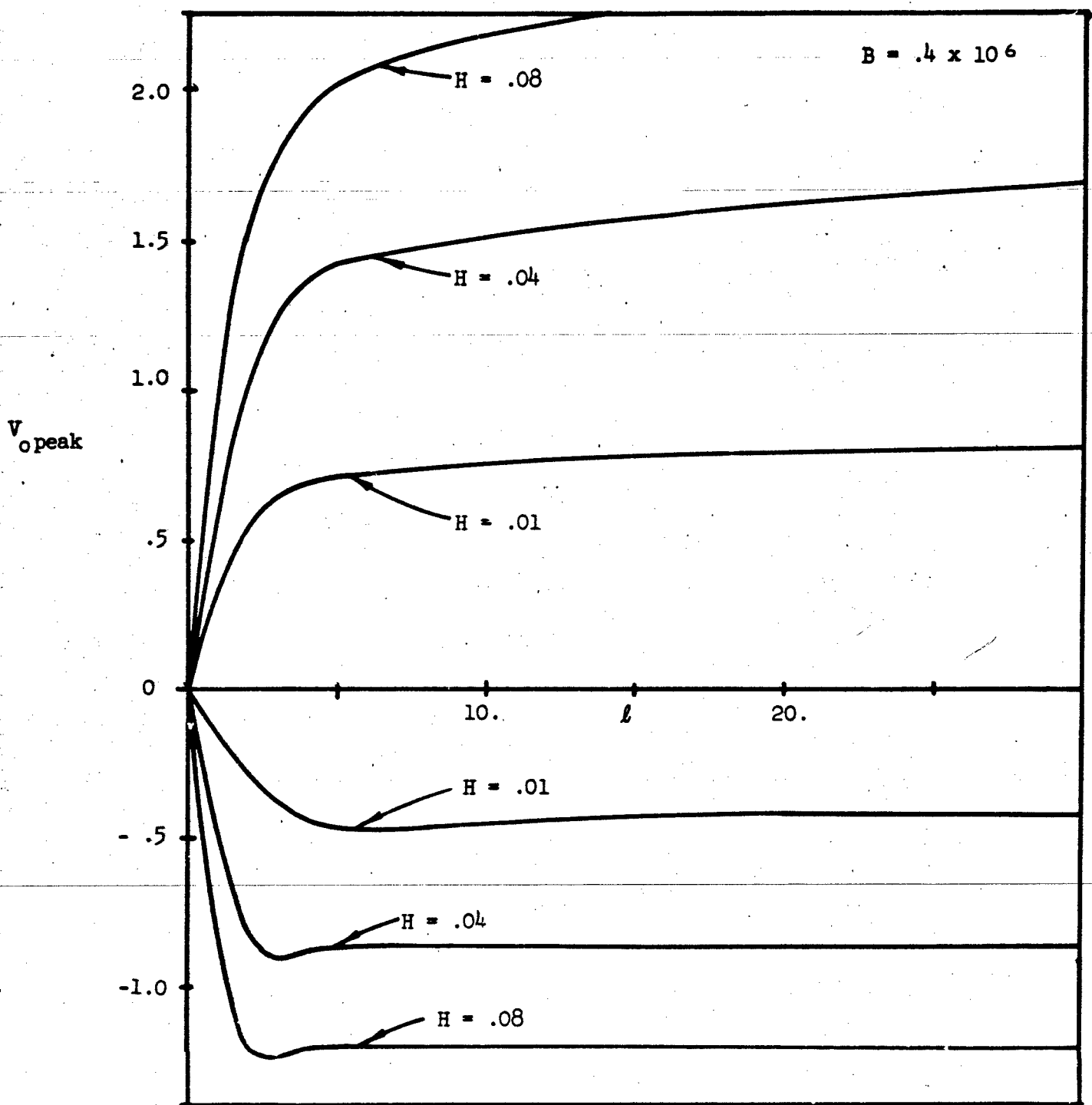


Figure 62a $V_o \text{ peak}$ VS. l FOR AN EXPONENTIALLY DECAYING PULSE AT VARIOUS VALUES OF H .

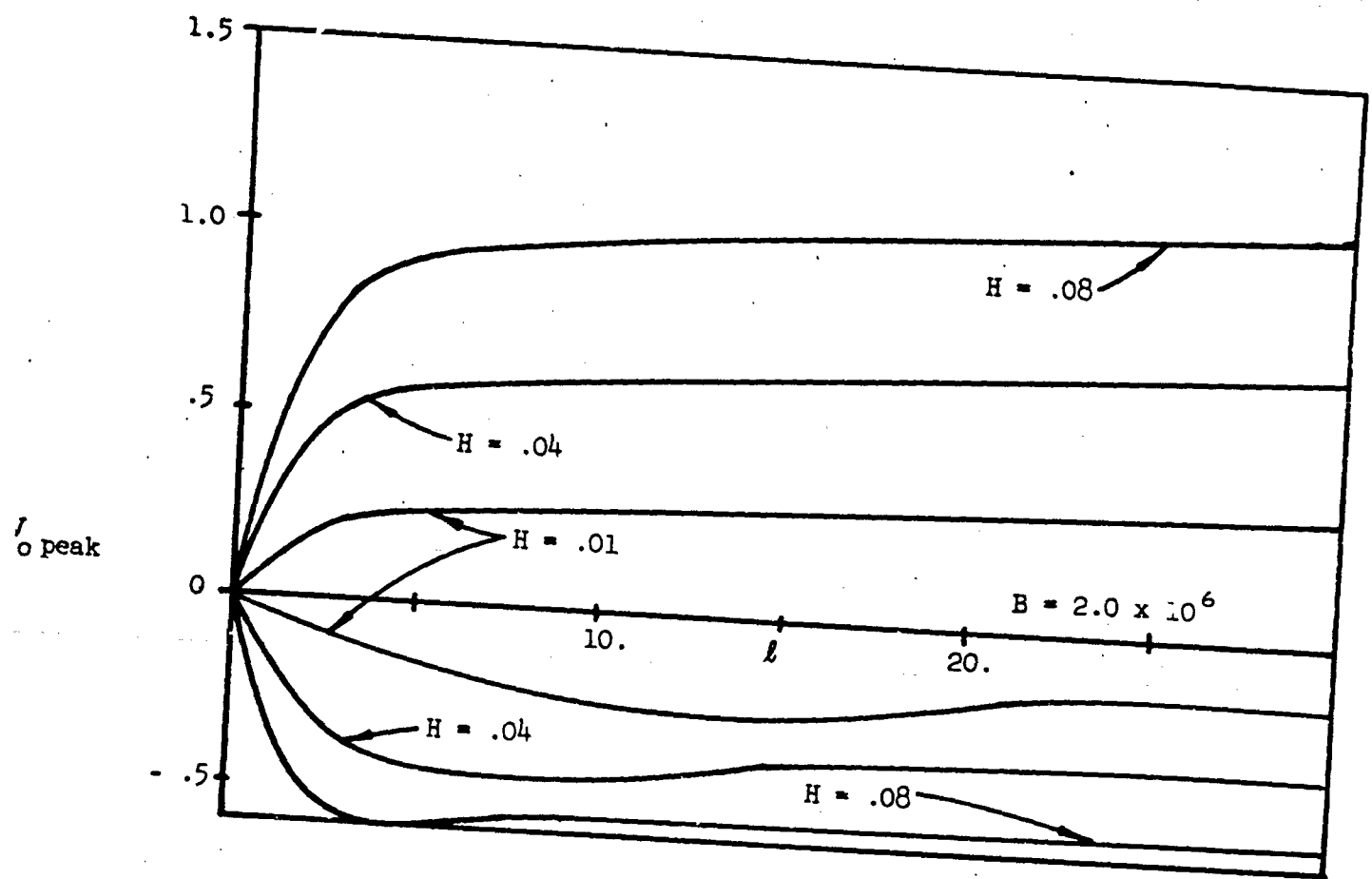


Figure 62b V_0 peak vs. ℓ FOR AN EXPONENTIALLY DECAYING PULSE AT VARIOUS VOLUMES OF H .

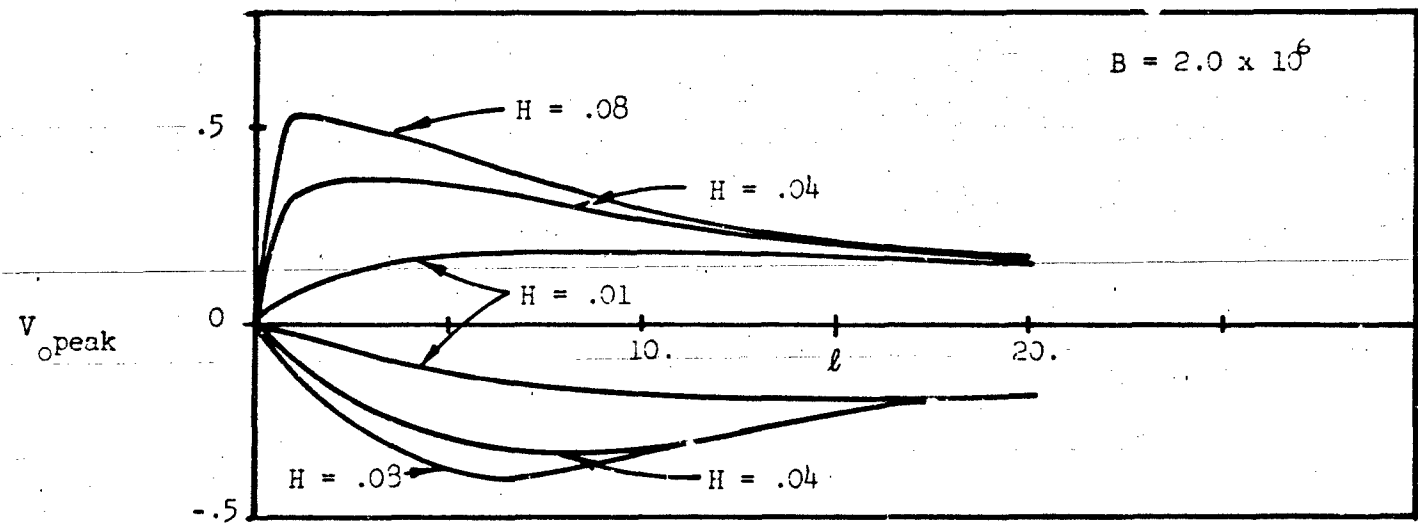
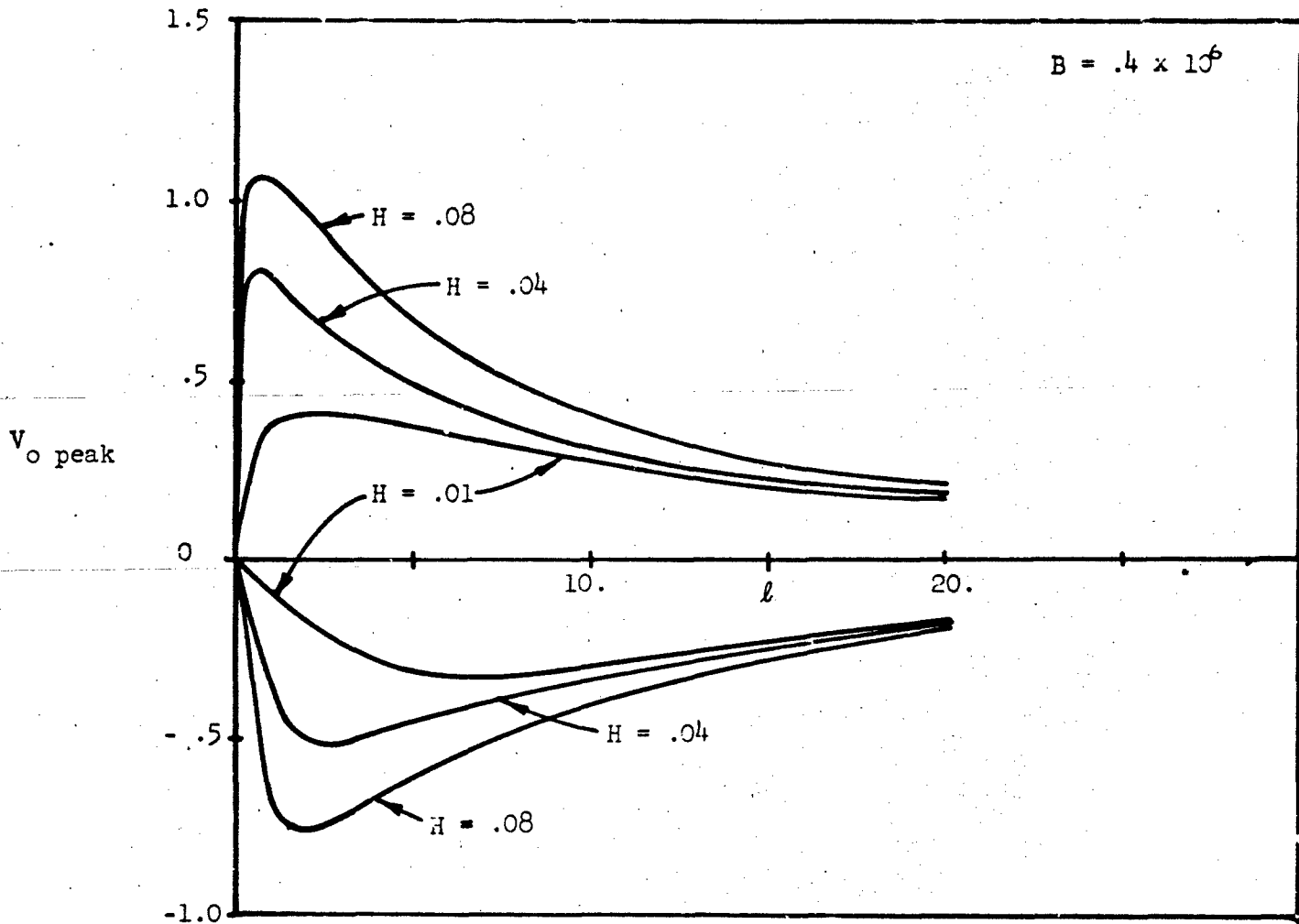


Figure 63 V_o peak VS. l FOR A HALF SINE PULSE AT VARIOUS VALUES OF H .

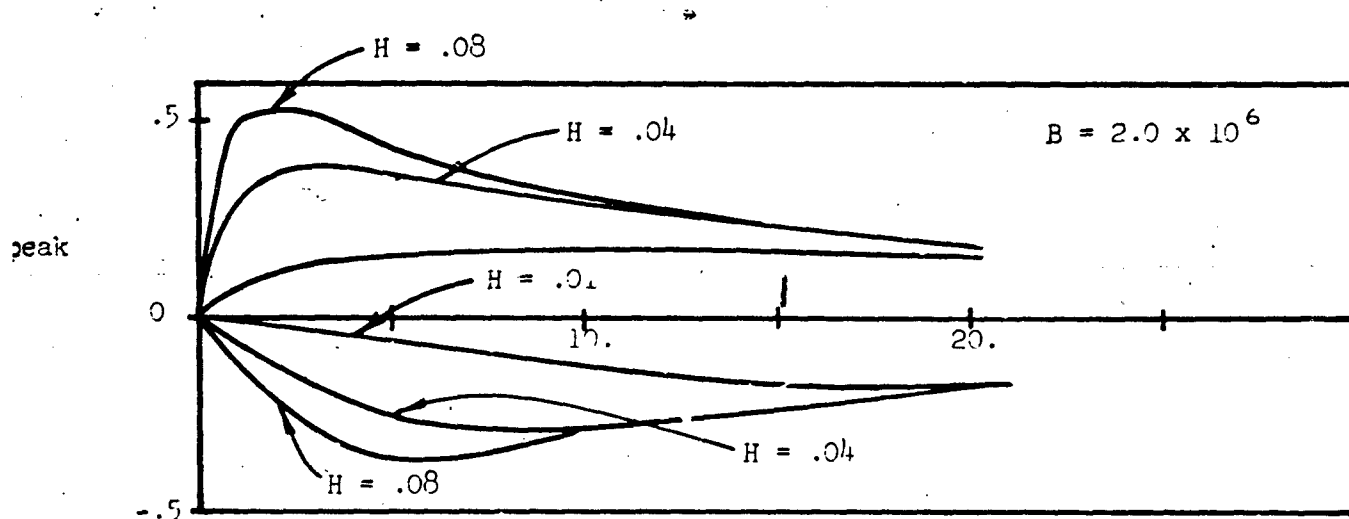
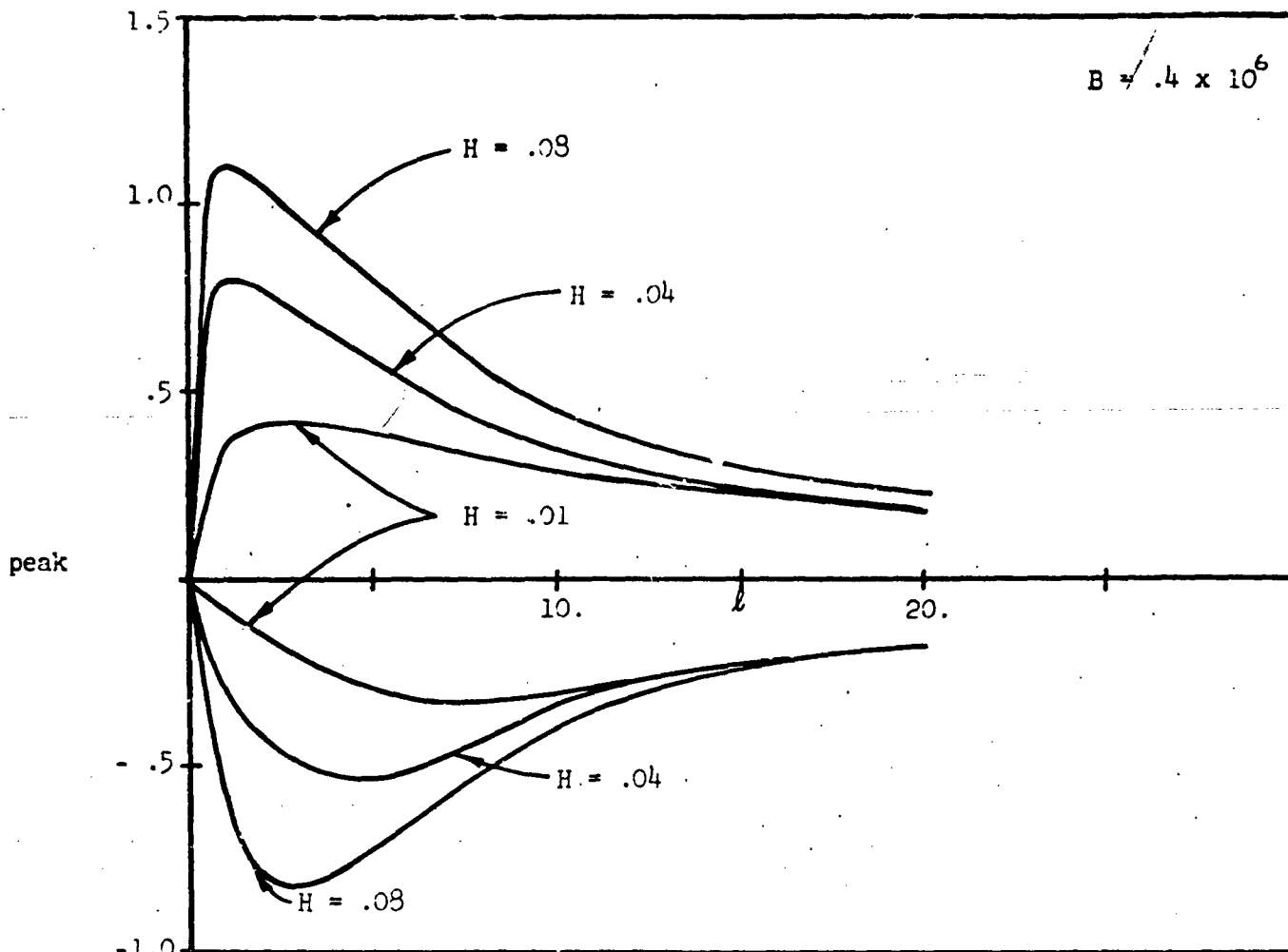


Figure 64 V_o peak VS. l FOR A HAVERSINE PULSE AT VARIOUS VALUES OF H .

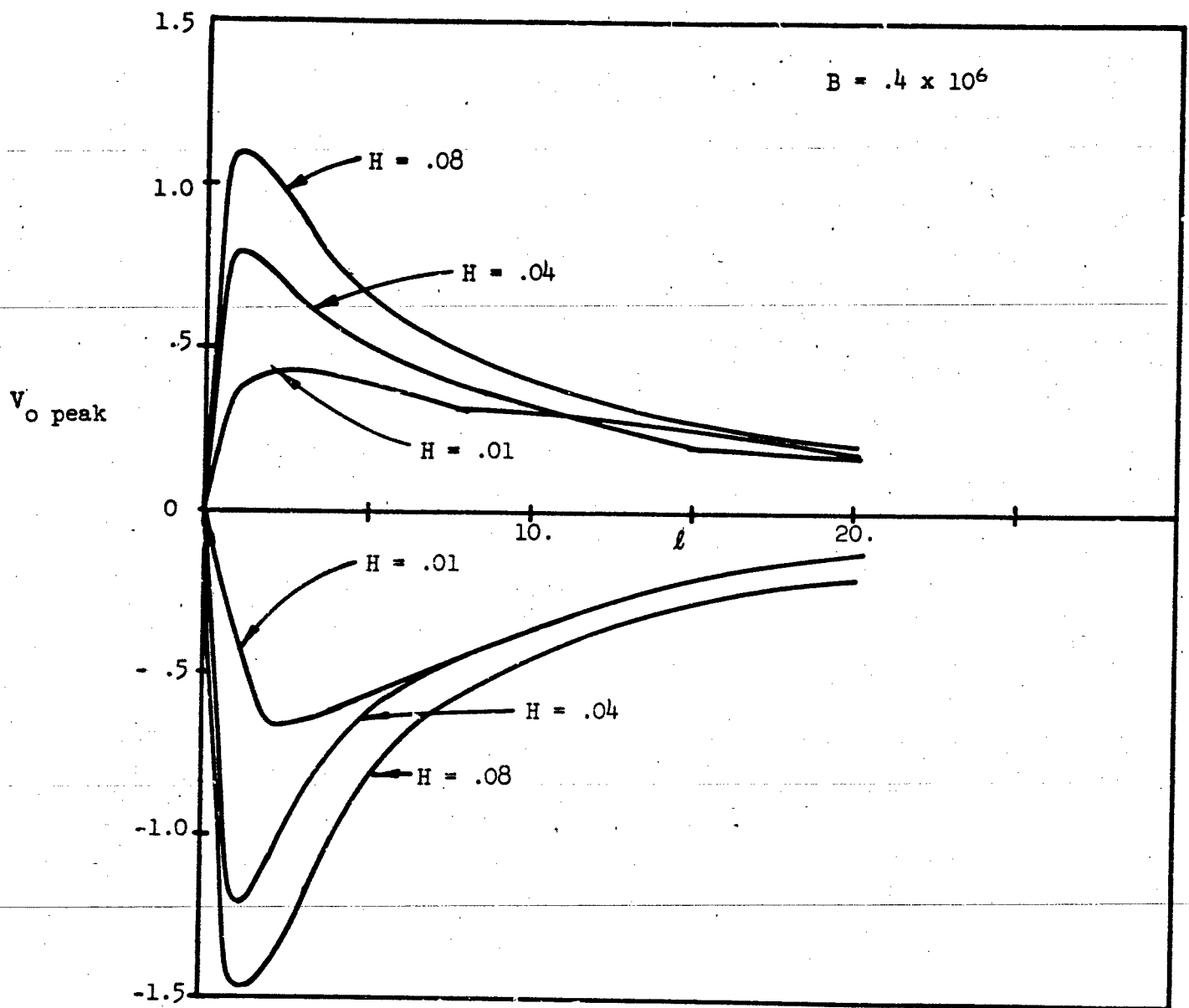


Figure 65a V_o peak VS. ℓ FOR A SINE WAVE AT VARIOUS VALUES OF H .

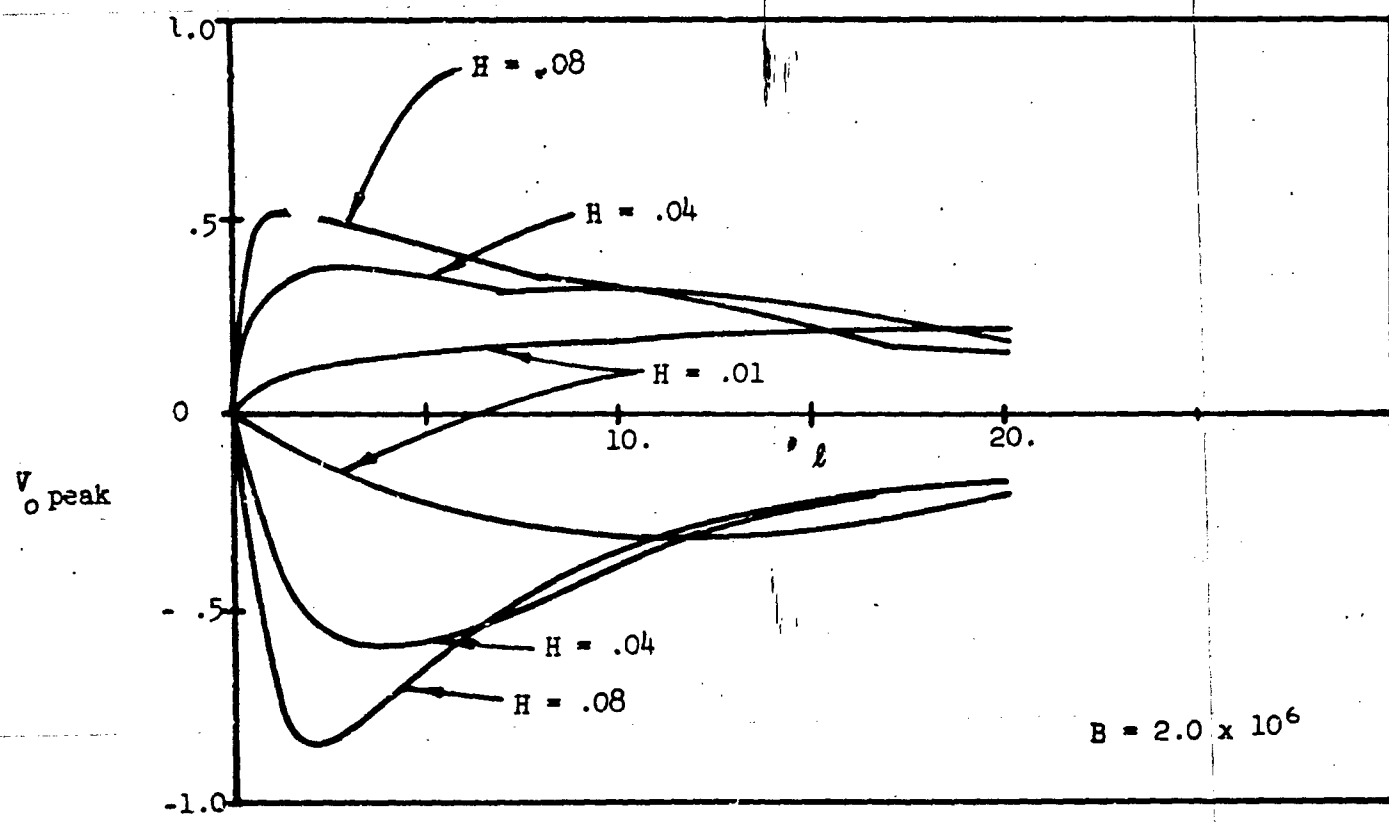


Figure 65b V_o peak VS. ℓ FOR A SINE WAVE AT VARIOUS VALUES OF H .

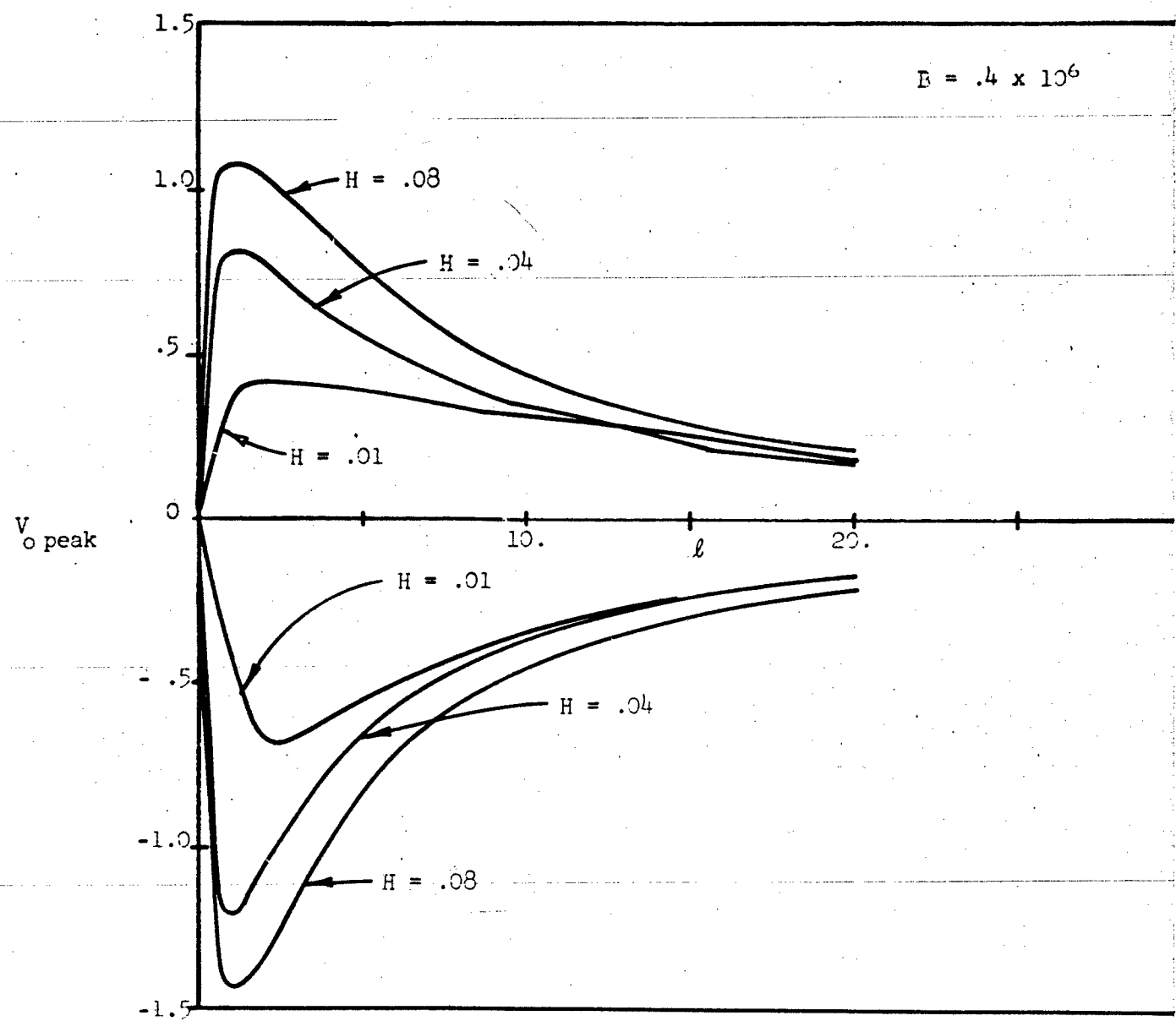


Figure 66a V_o peak VS. ℓ FOR A MODIFIED SINE WAVE AT VARICUS VALUES OF H .

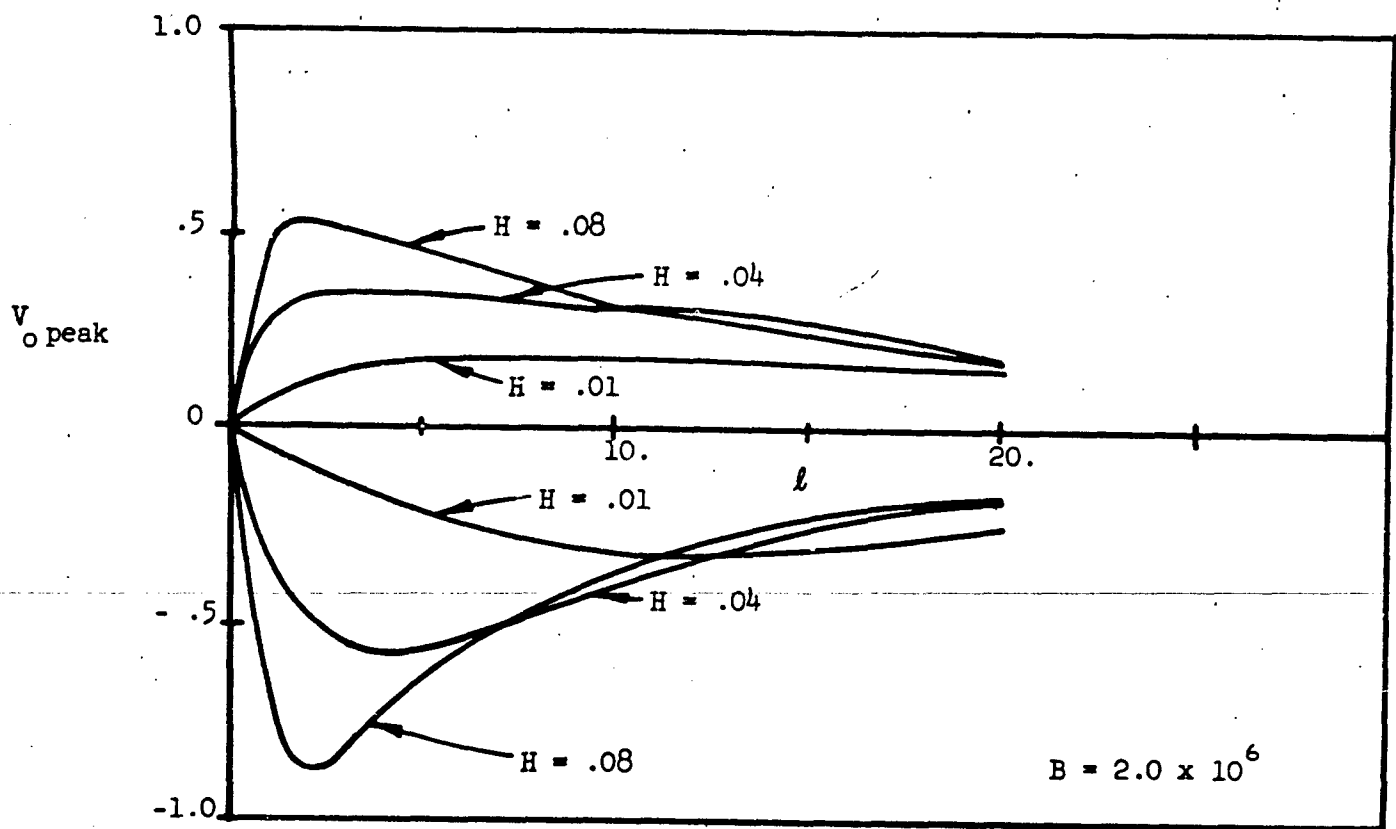


Figure 66b V_o peak VS. l FOR A MODIFIED SINE WAVE AT VARIOUS VALUES OF H .

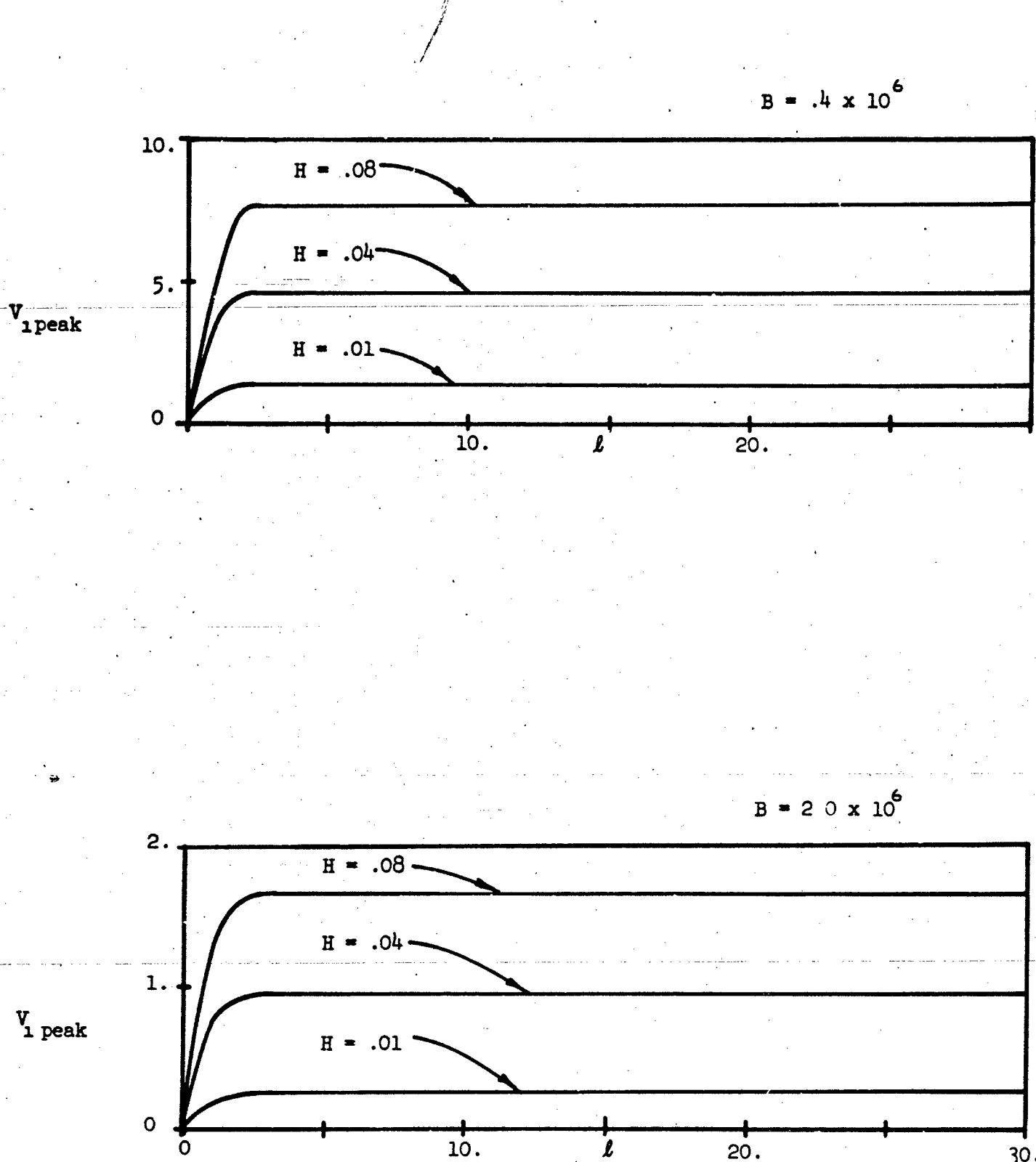


Figure 67 $V_{1\text{ peak}}$ VS. l FOR A RECTANGULAR PULSE AT VARIOUS VALUES OF H .

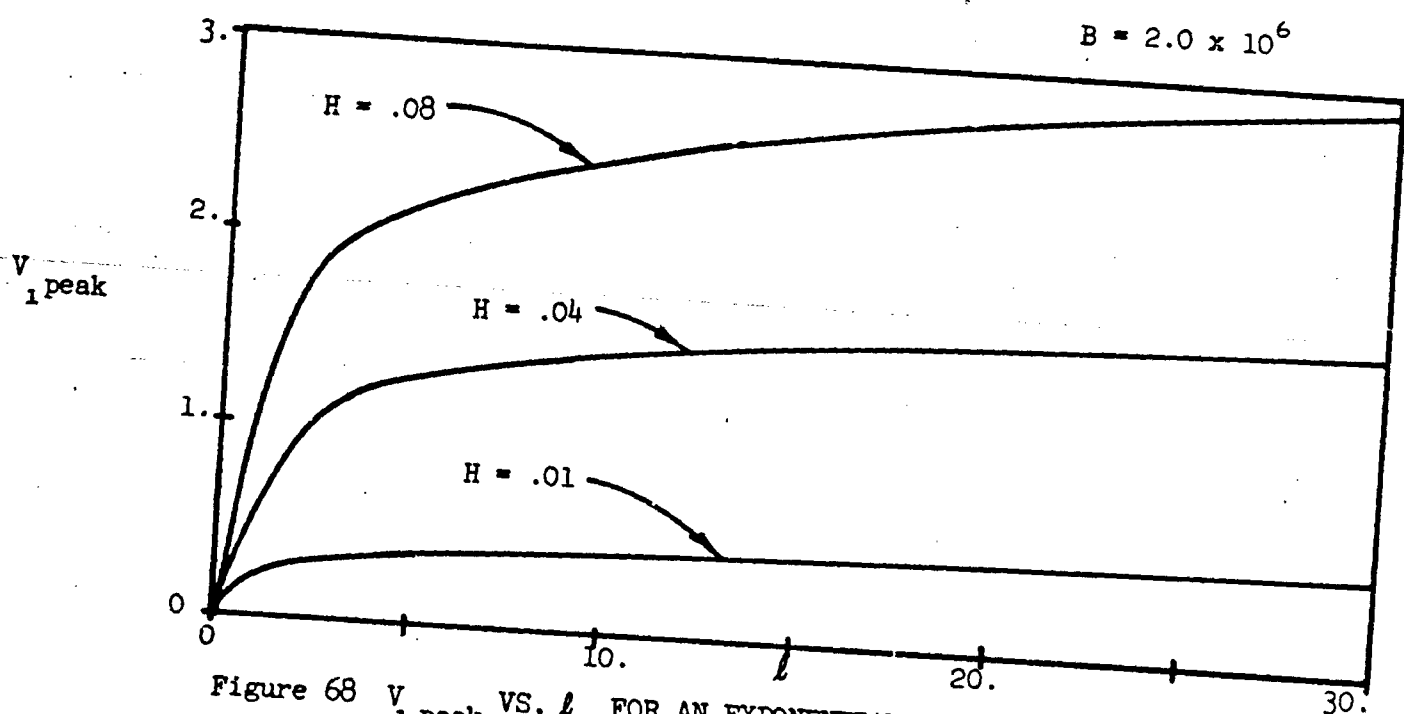
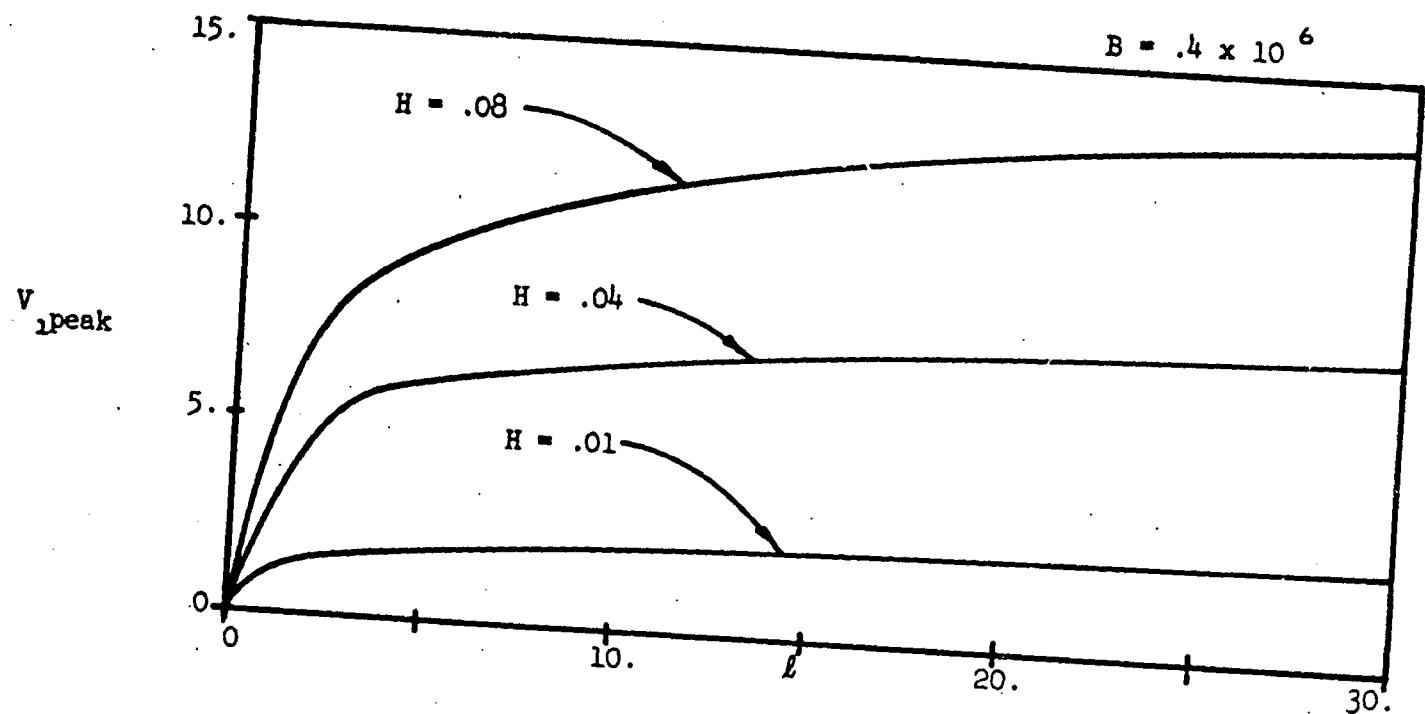
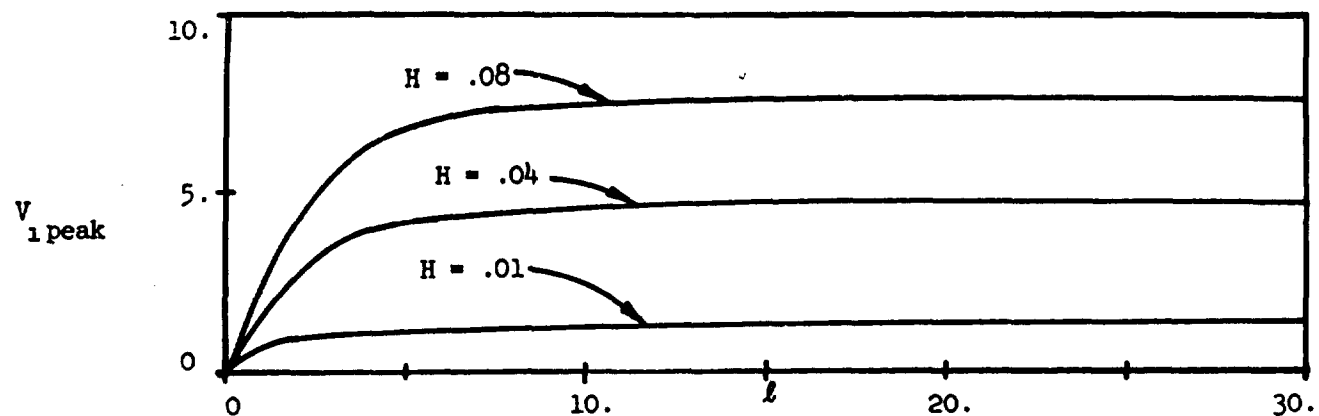


Figure 68 $V_{1\text{ peak}}$ VS. l FOR AN EXPONENTIALLY DECAYING PULSE AT
VARIOUS VALUES OF H .

$$B = .4 \times 10^6$$



$$B = 2.0 \times 10^6$$

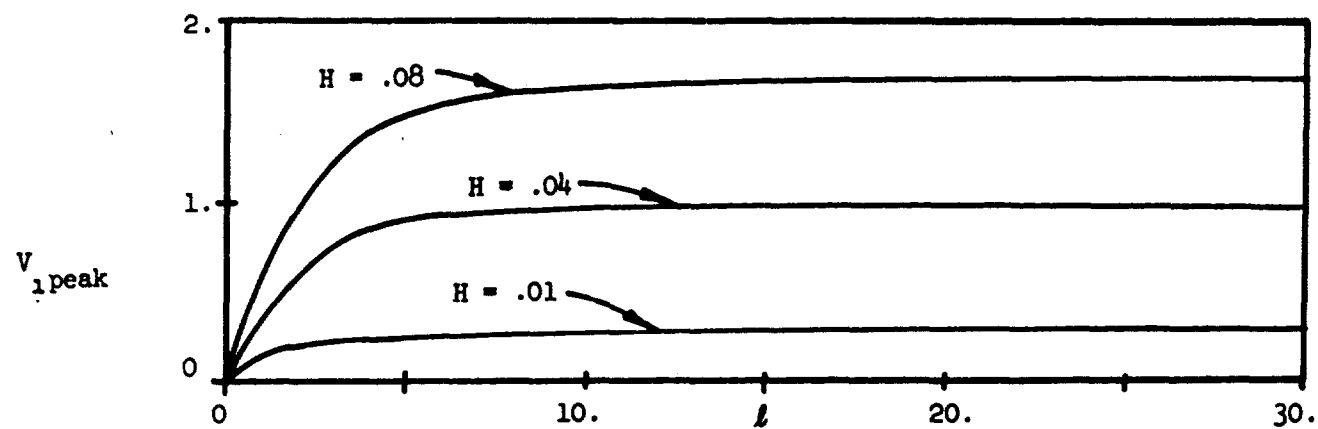


Figure 69 $V_{1\text{ peak}}$ VS. t FOR A HALF SINE PULSE AT VARIOUS VALUES OF H .

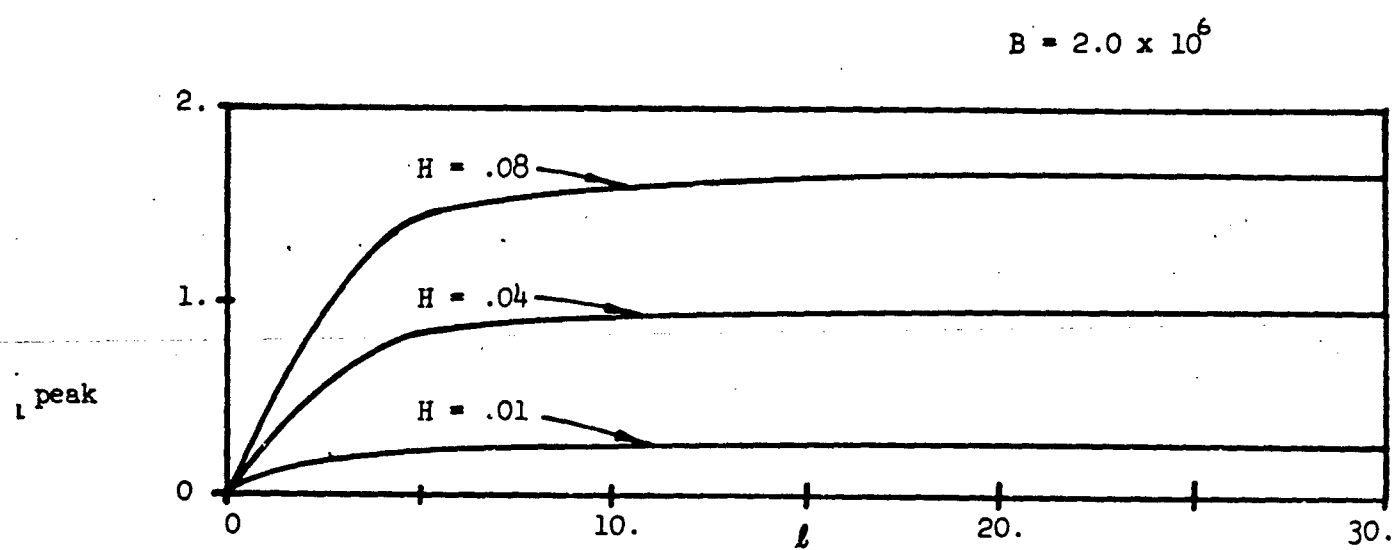
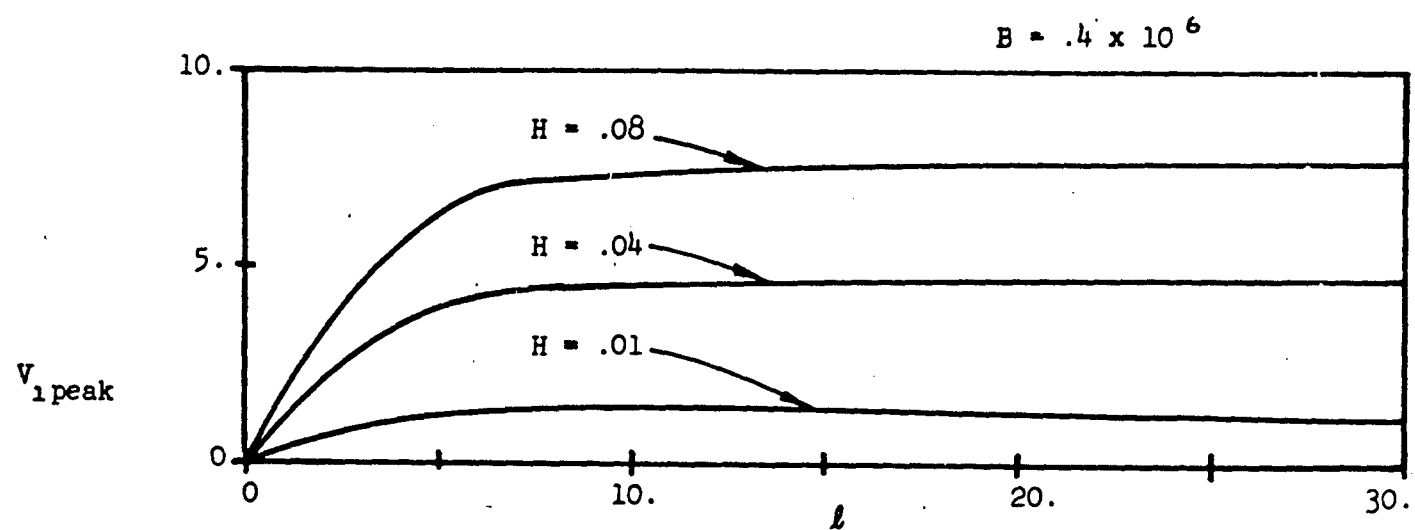


Figure 70 $V_1 \text{ peak}$ VS. l FOR A HAVERSINE PULSE AT VARIOUS VALUES OF H .

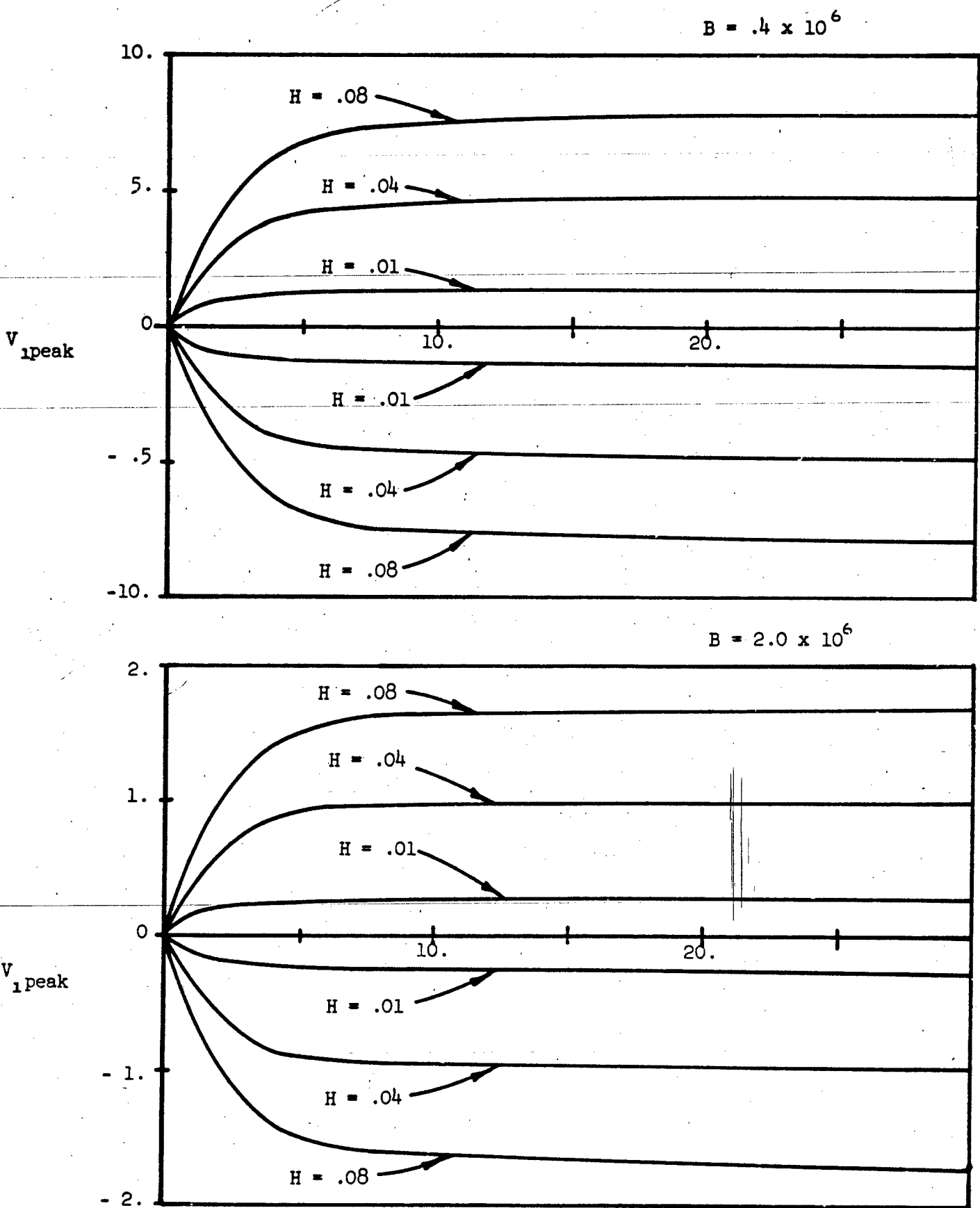


Figure 71 V_{1peak} VS. ℓ FOR A SINE WAVE AT VARIOUS VALUES OF H .

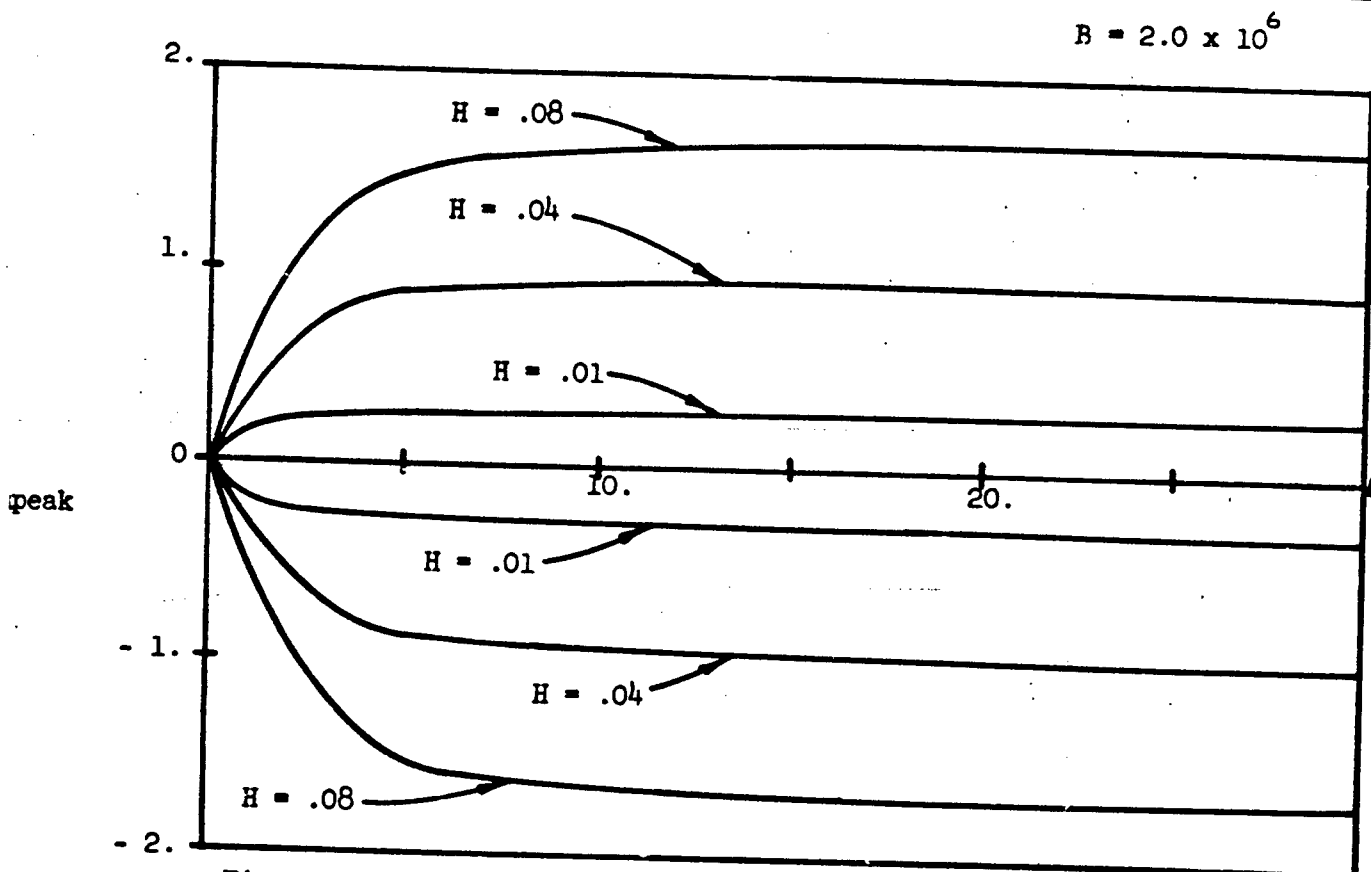
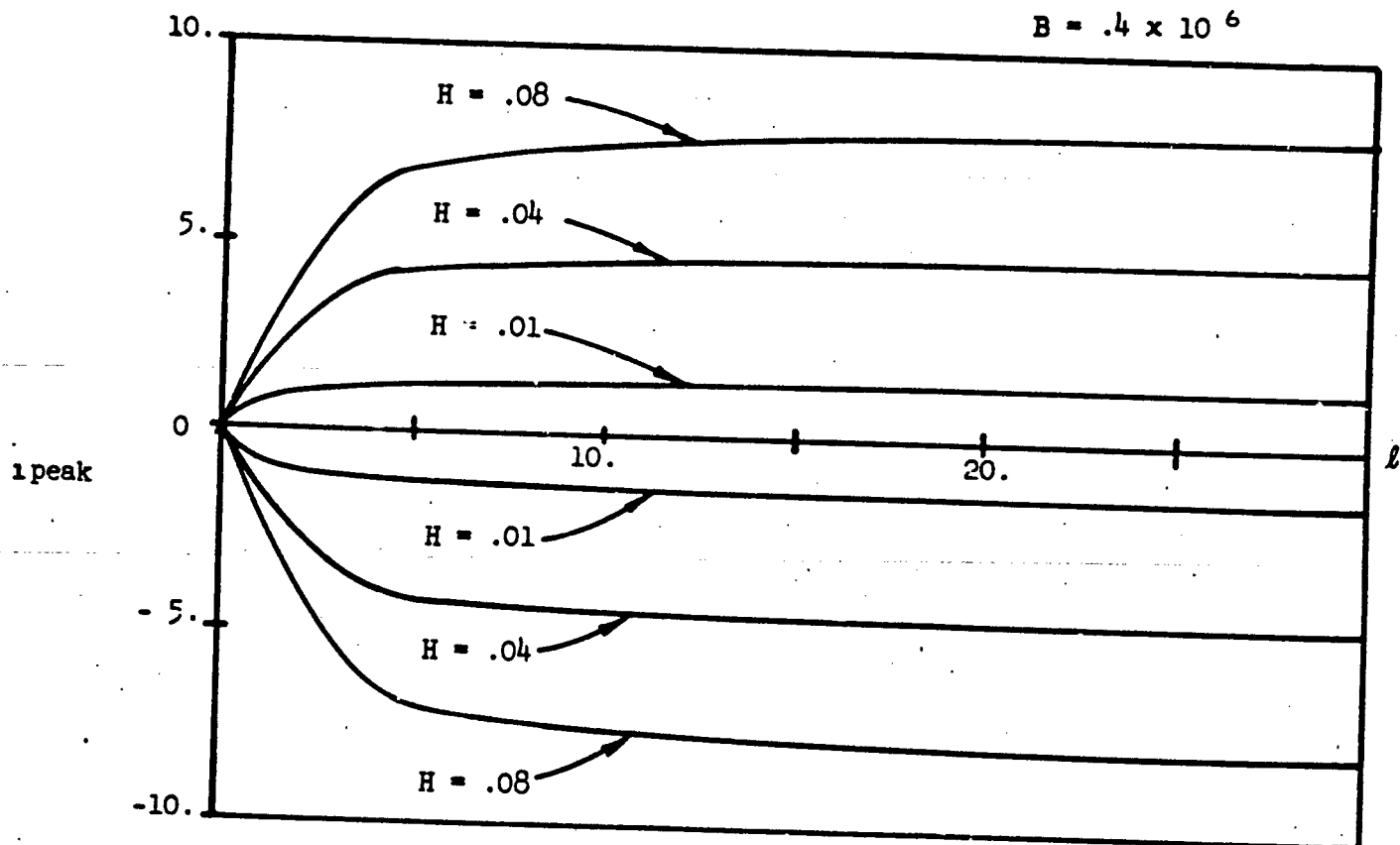


Figure 72 V_{1peak} VS. l FOR A MODIFIED SINE WAVE AT VARIOUS VALUES OF H .

$$B = .4 \times 10^6$$

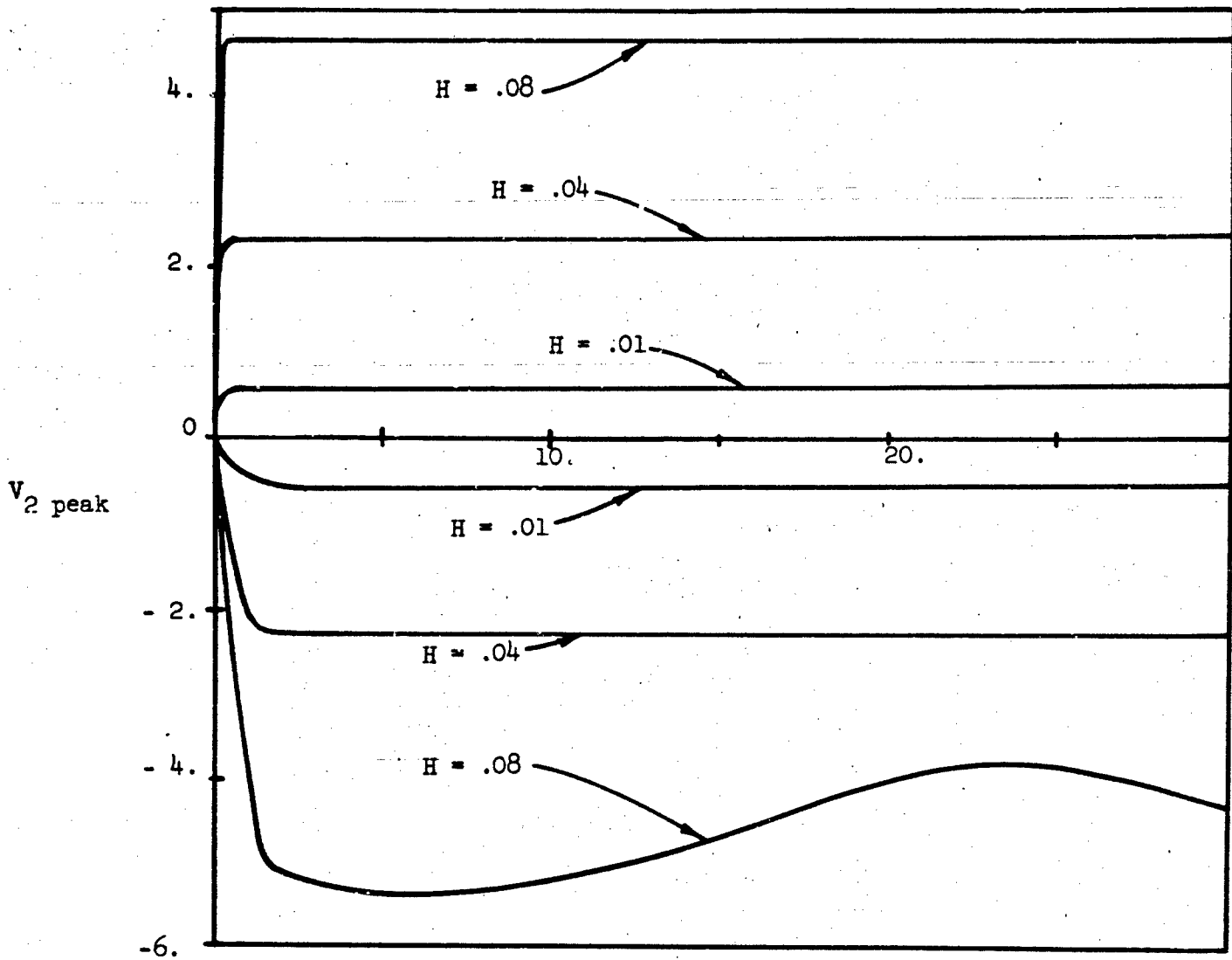


Figure 73a V_2 peak VS. l FOR A RECTANGULAR PULSE AT VARIOUS VALUES OF H .

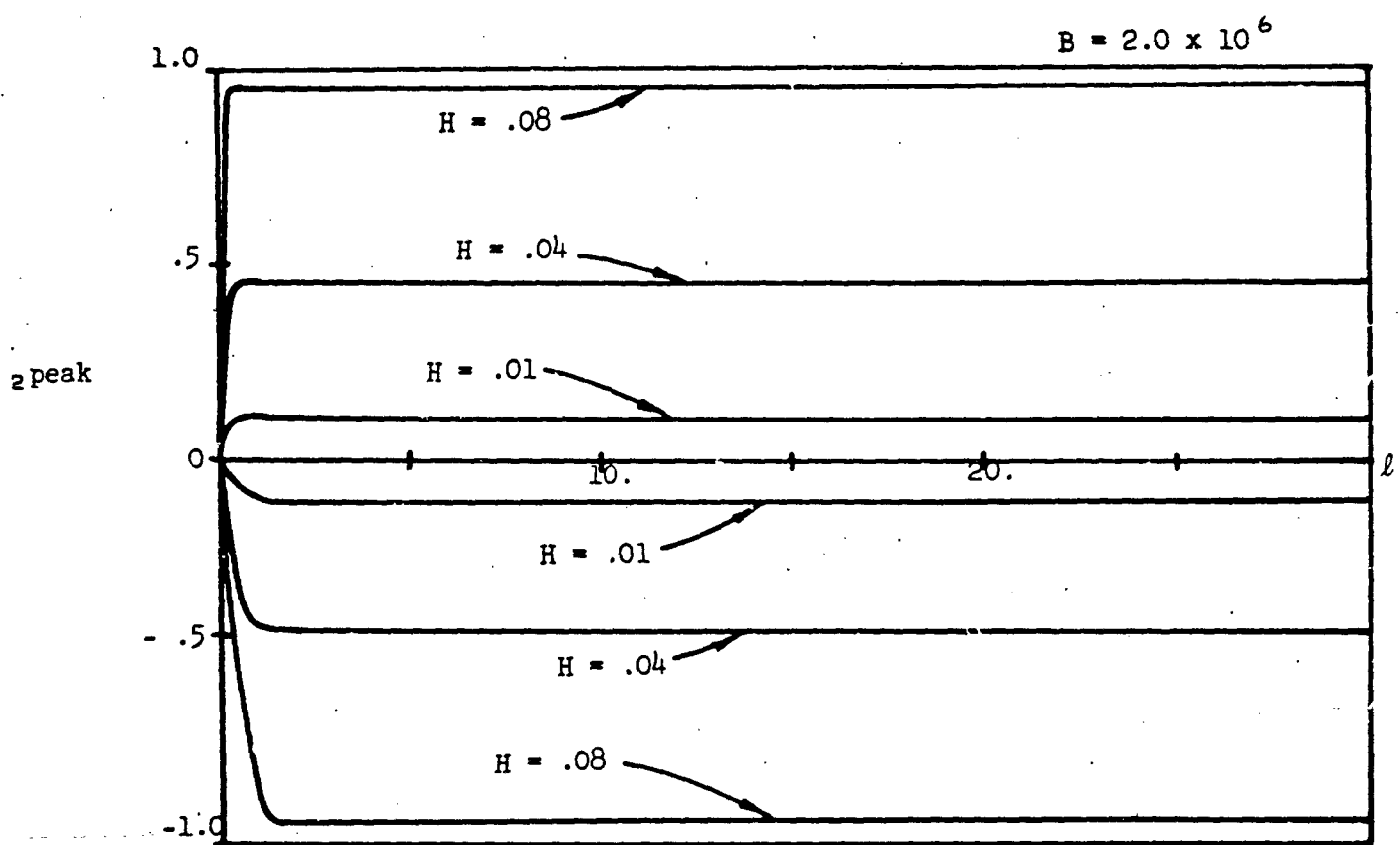


Figure 73b $V_{2 \text{ peak}}$ VS. l FOR A RECTANGULAR PULSE AT VARIOUS VALUES OF H .

$B = .4 \times 10^6$

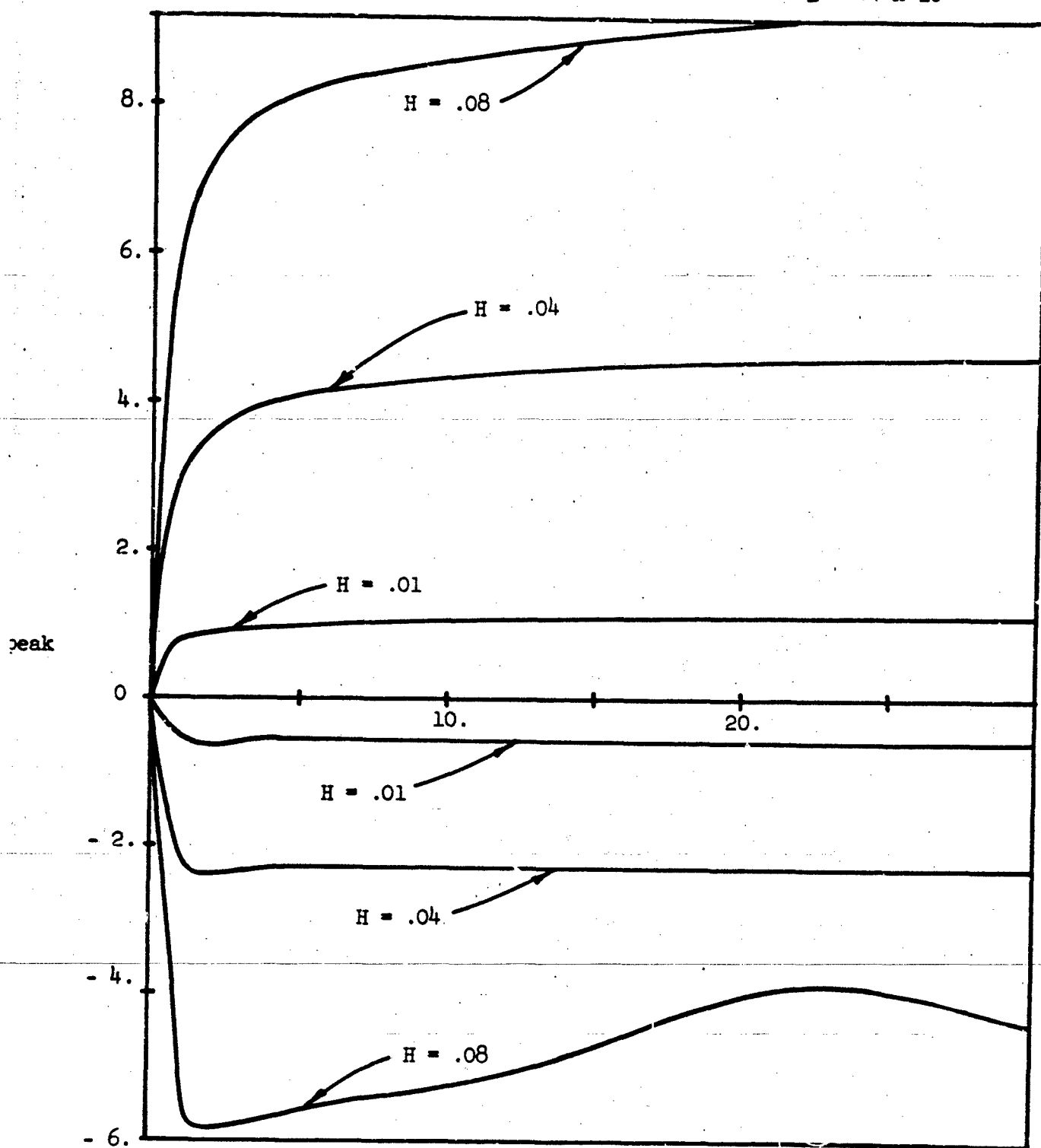


Figure 74 $V_{2\text{peak}}$ VS. ℓ FOR AN EXPONENTIALLY DECAYING PULSE AT
VARIOUS VALUES OF H .

$B = 2.0 \times 10^6$

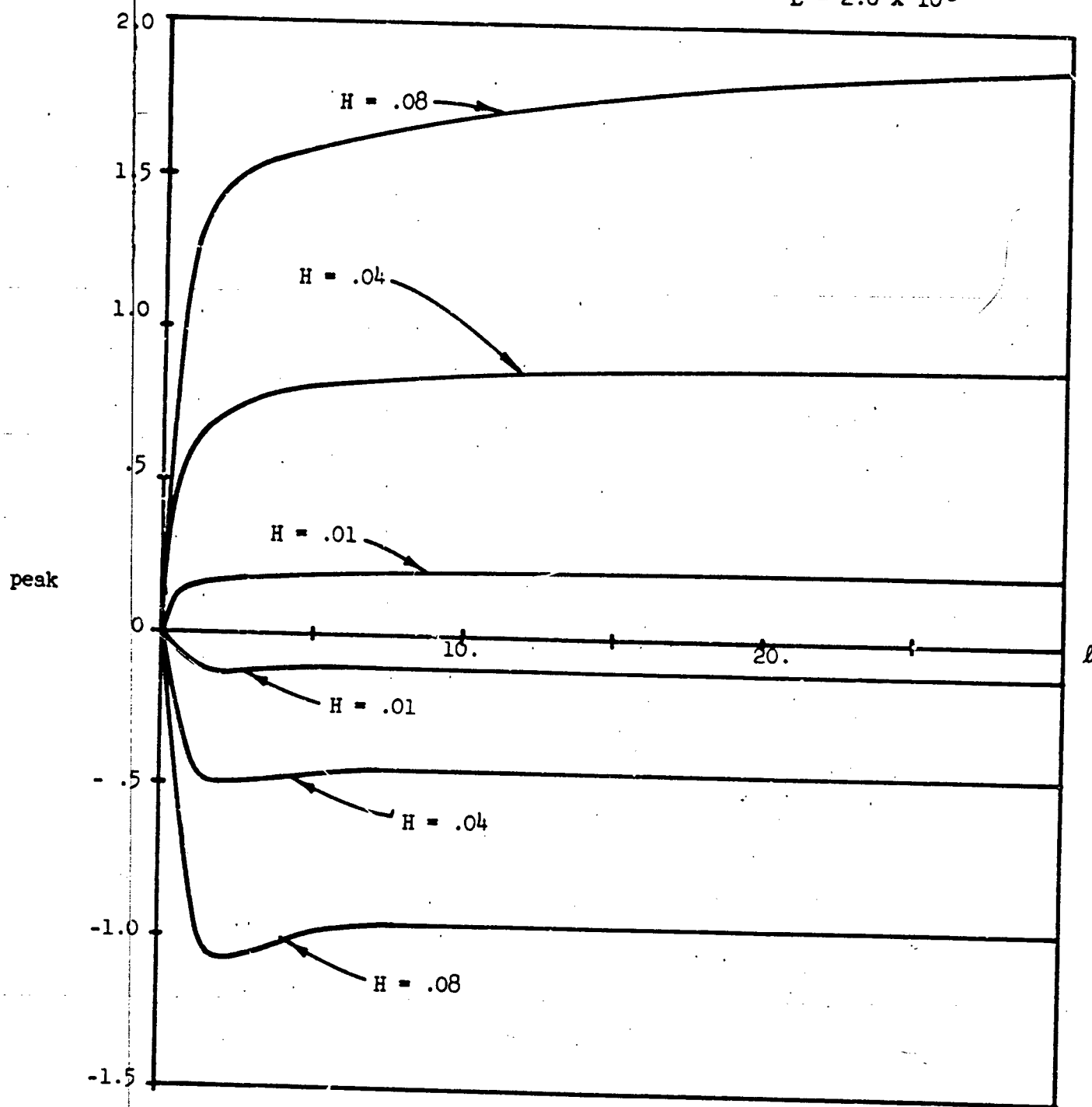
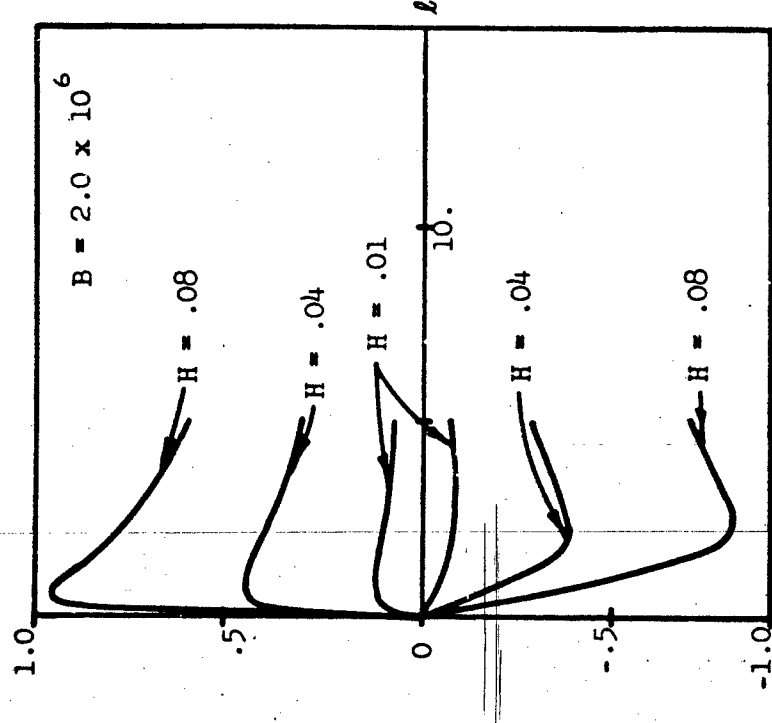
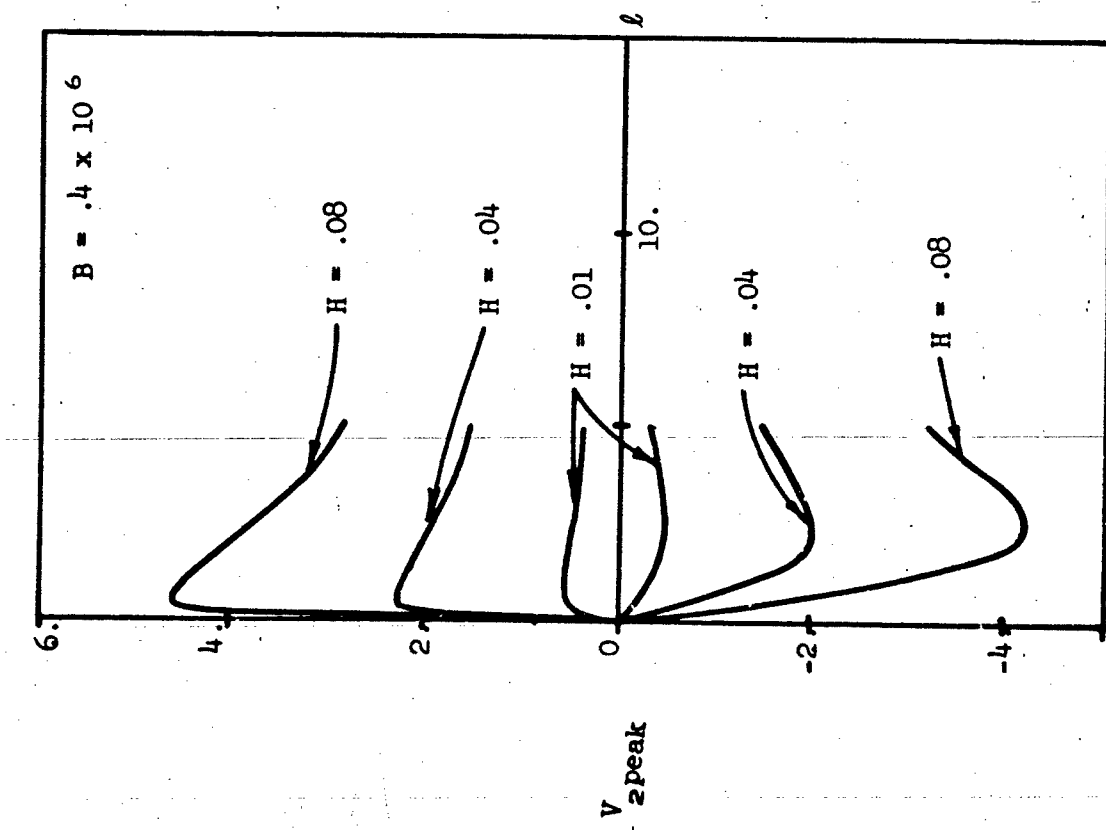


Figure 75 V_{peak} VS. l FOR AN EXPONENTIALLY DECAYING PULSE AT VARIOUS VALUES OF H .

Figure 76 V_2 peak VS. I FOR A HALF SINE PULSE AT VARIOUS VALUES OF H .



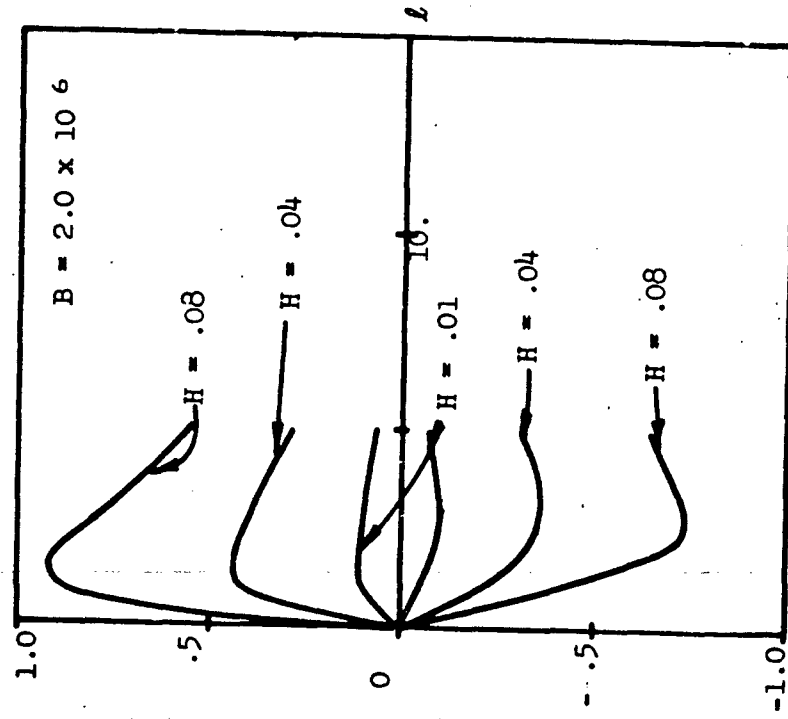
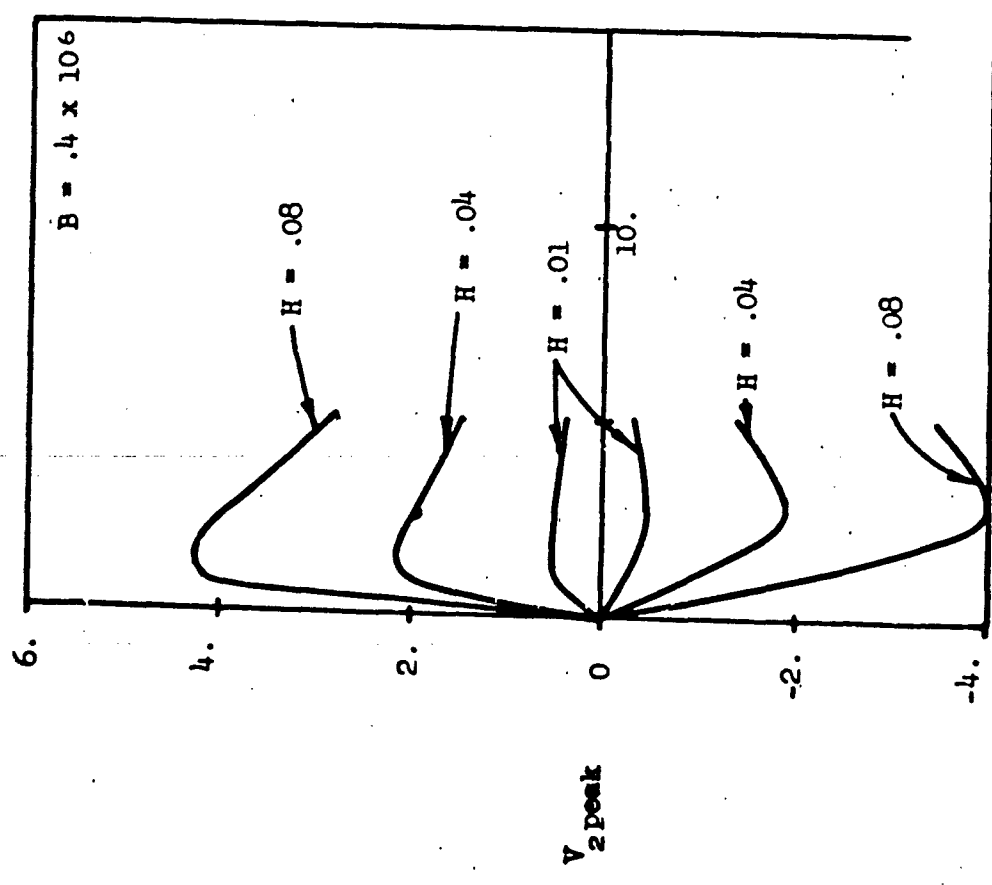
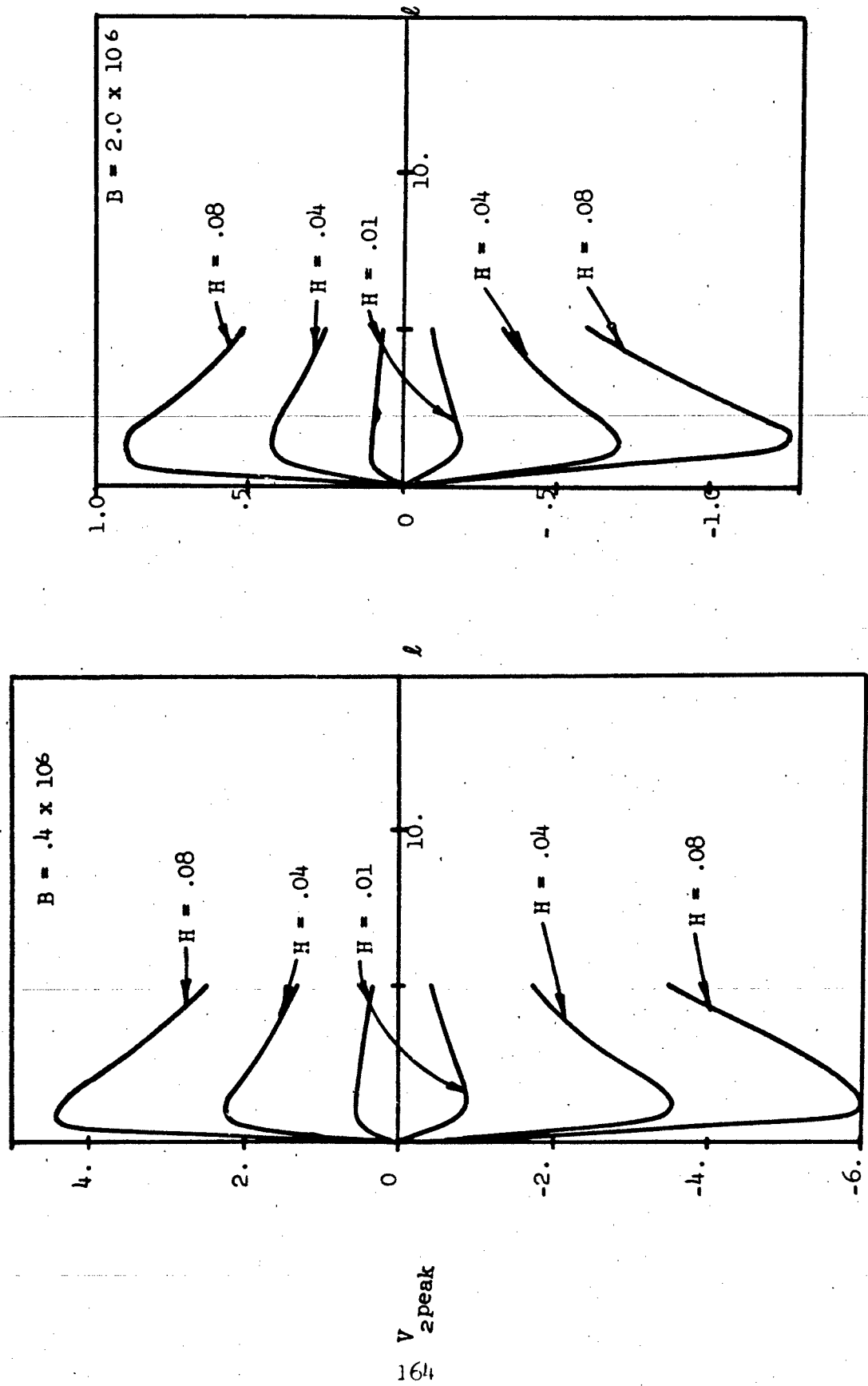


Figure 77 $V_2 \text{ peak}$ VS. t FOR A HAVERSINE PULSE AT VARIOUS VALUES OF H .

Figure 78 V_2 VS. t FOR A STNEMAVE AT VARIOUS VALUES OF H .



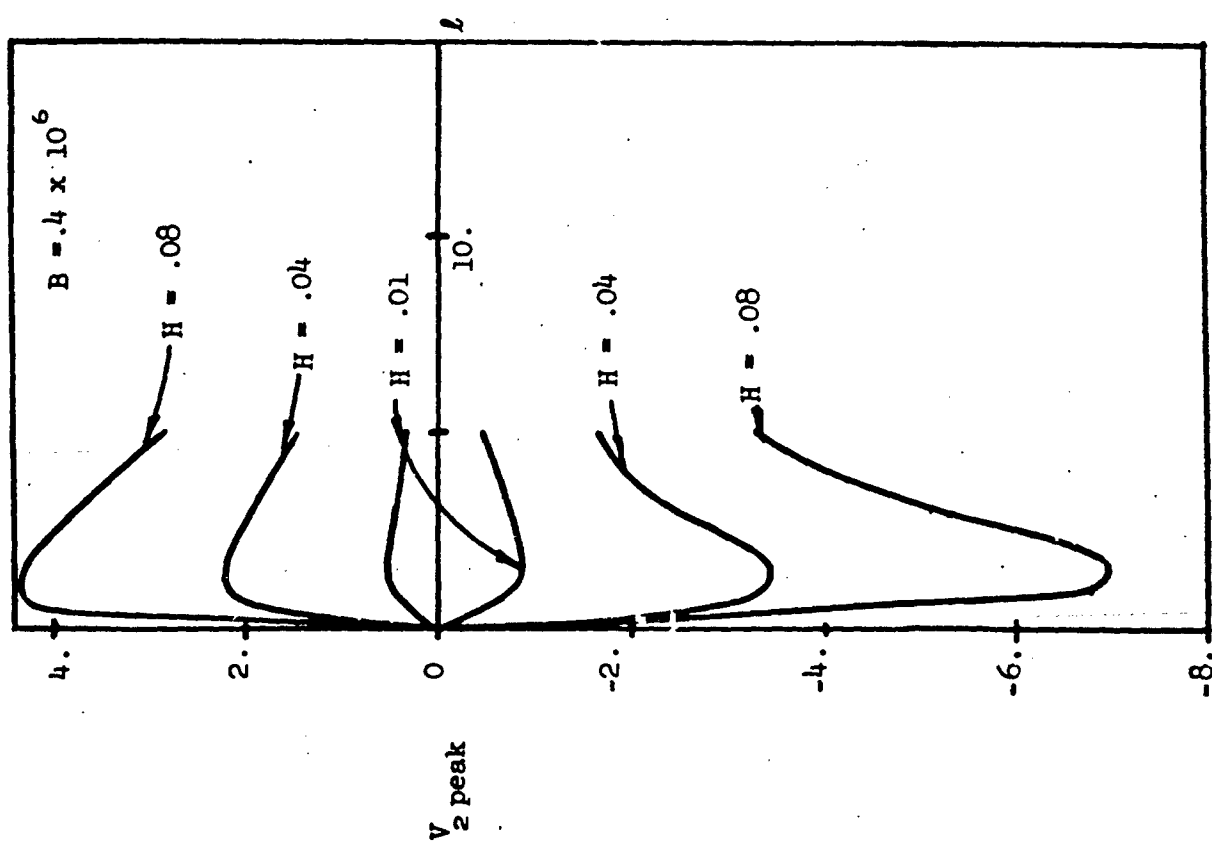
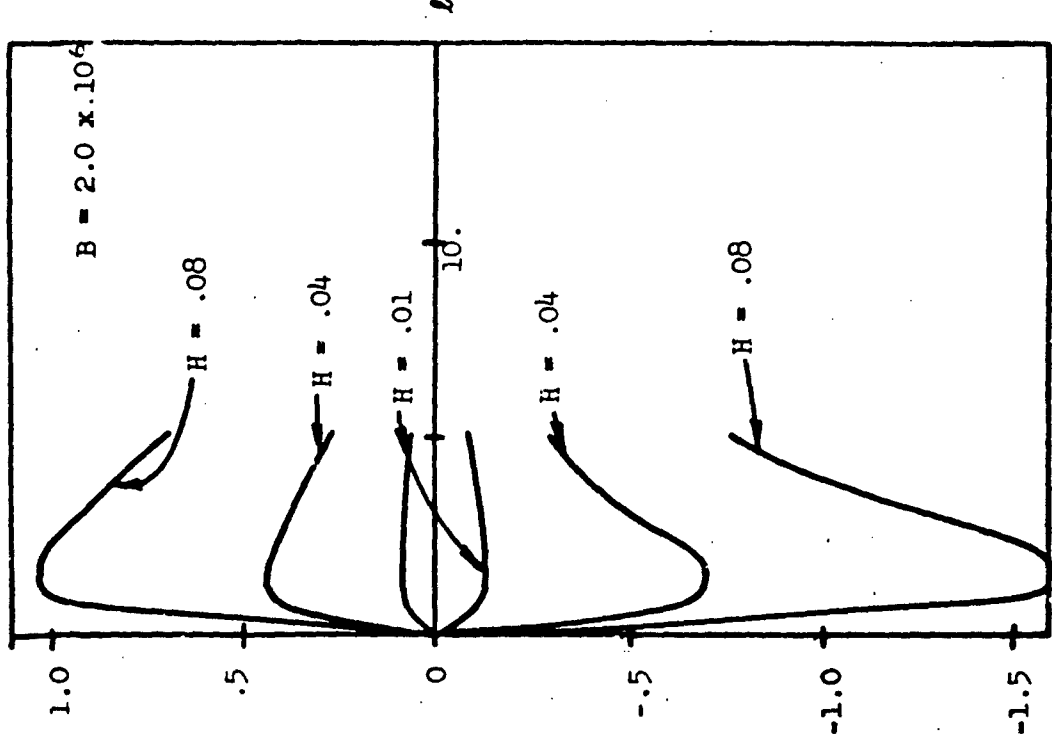


Figure 79. V_2 peak vs. l for a modified sine wave at various values of H .

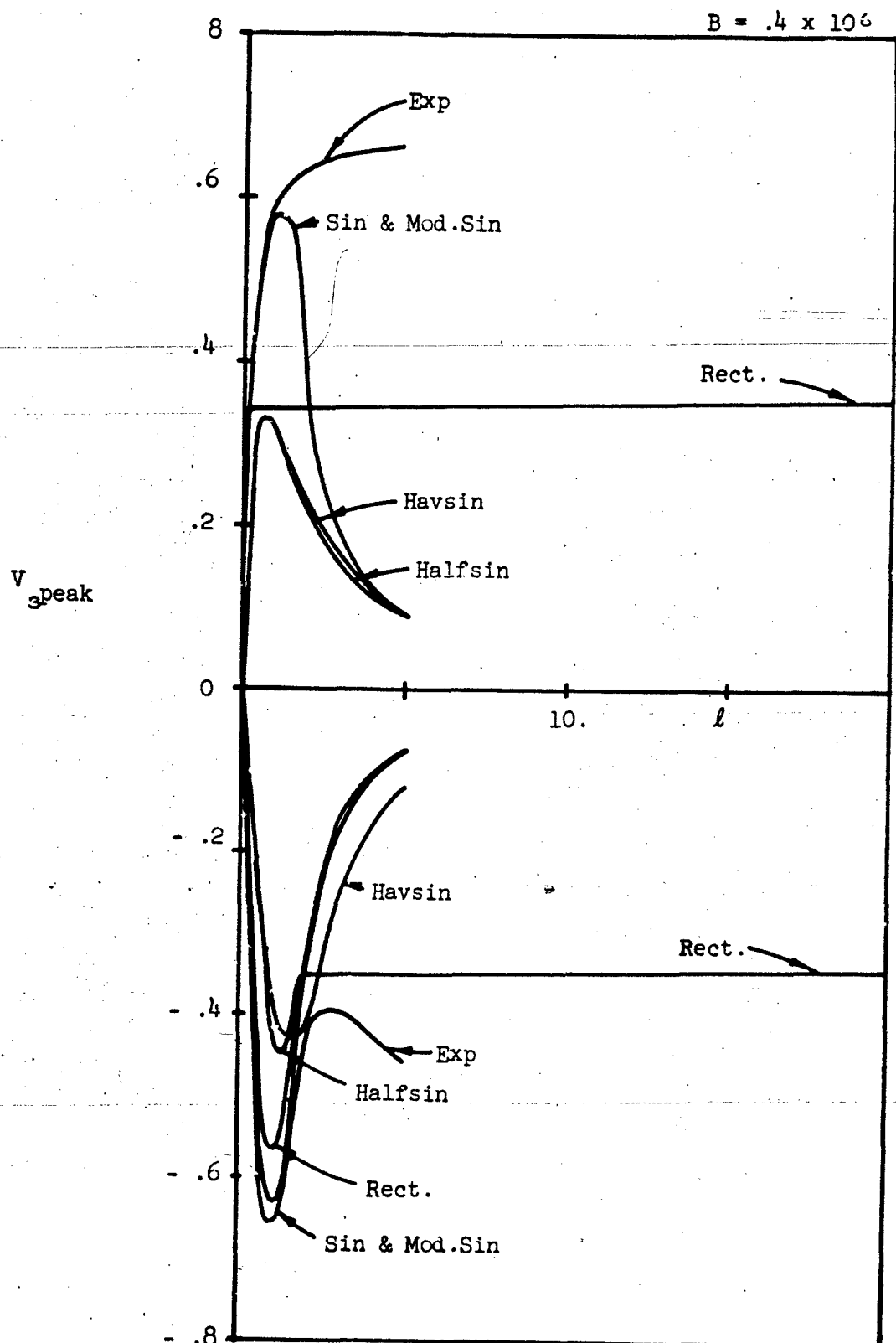


Figure 80 V_{speak} VS. l FOR VARIOUS FORCING FUNCTION $H = .01$

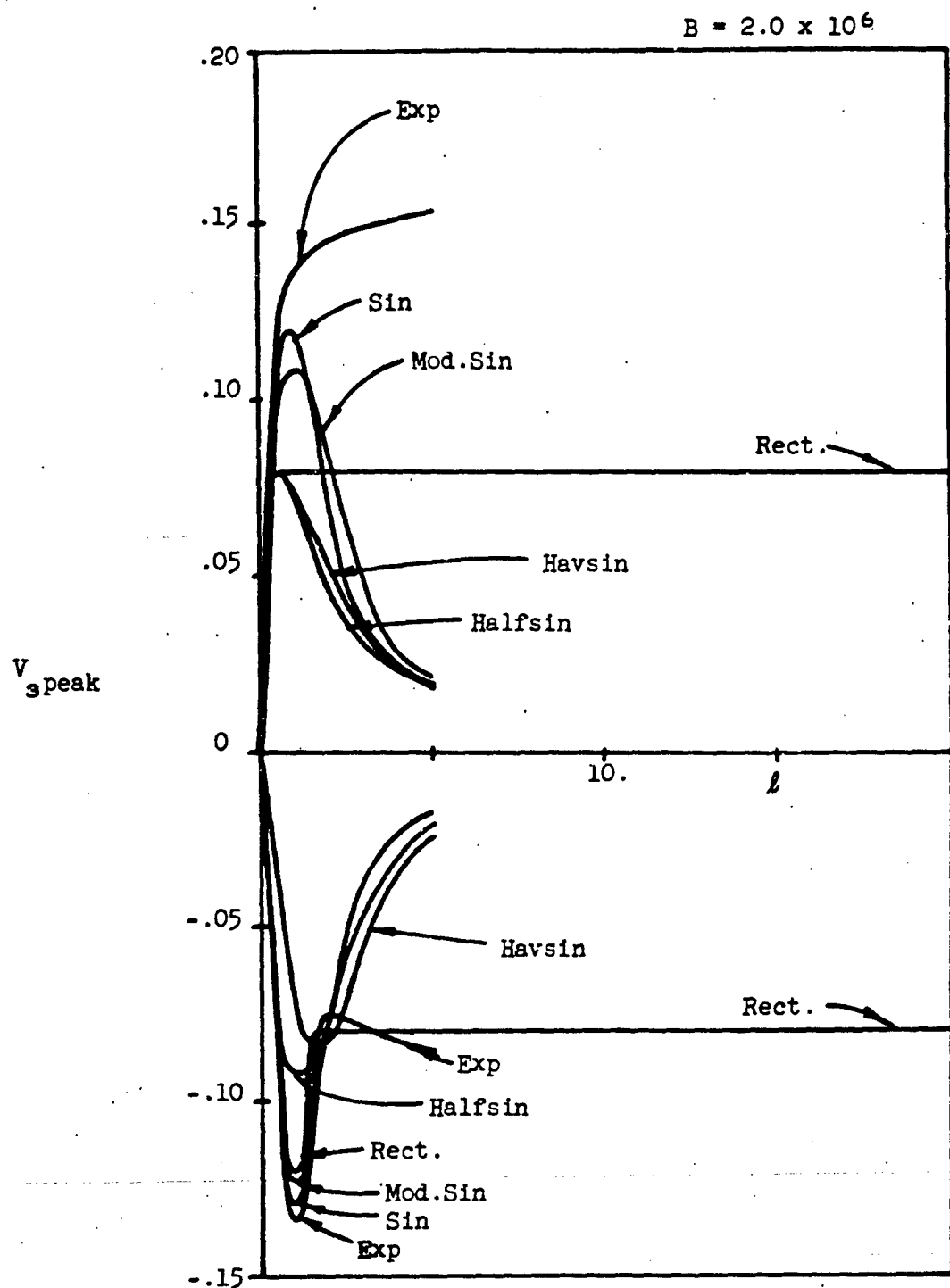


Figure 81 V_{speak} VS. l FOR VARIOUS FORCING FUNCTIONS $H = .01$

$$B = .4 \times 10^6$$

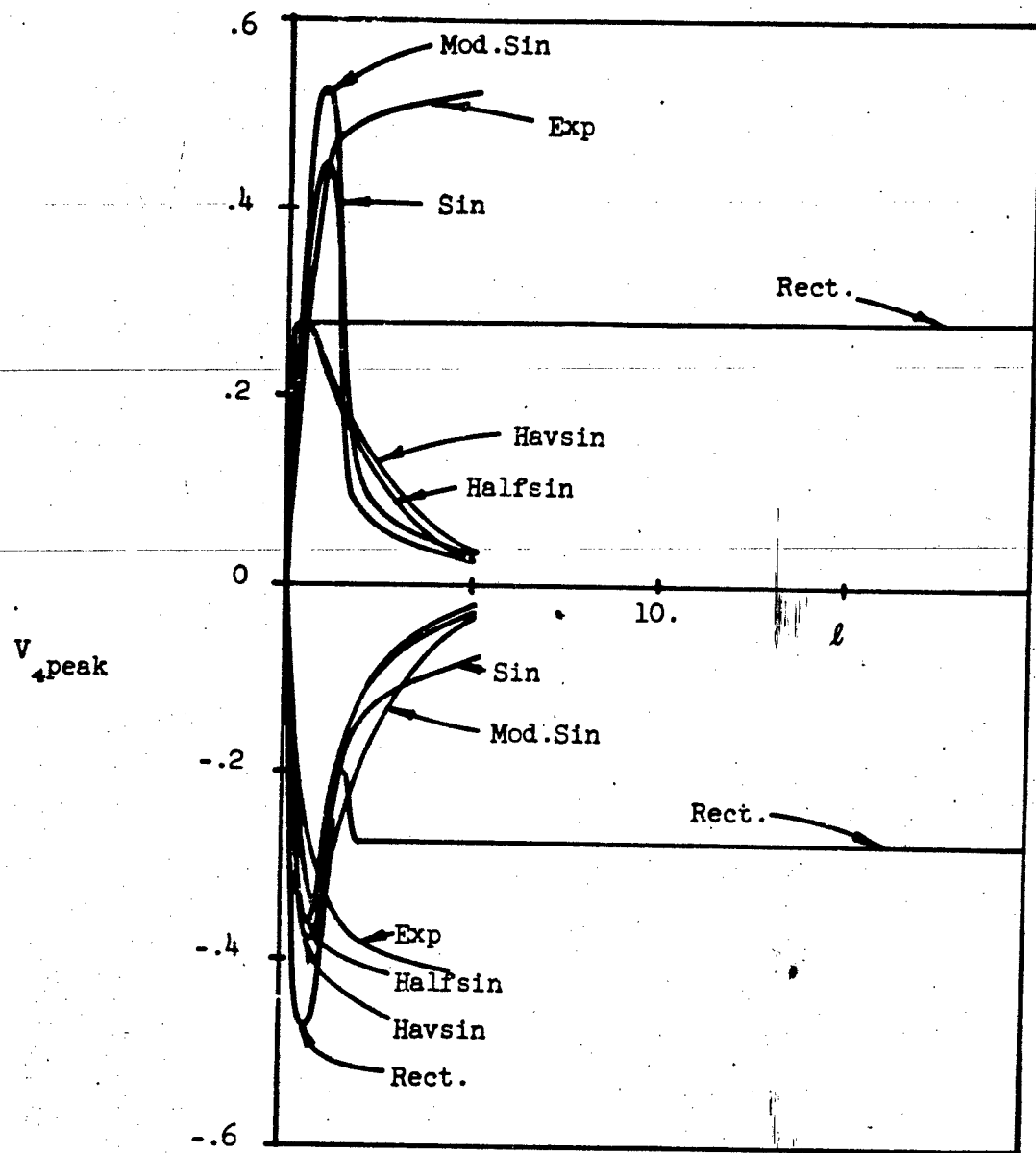


Figure 82 V_{4peak} VS. l FOR VARIOUS FORCING FUNCTIONS $H = .01$

$$B = 2.0 \times 10^6$$

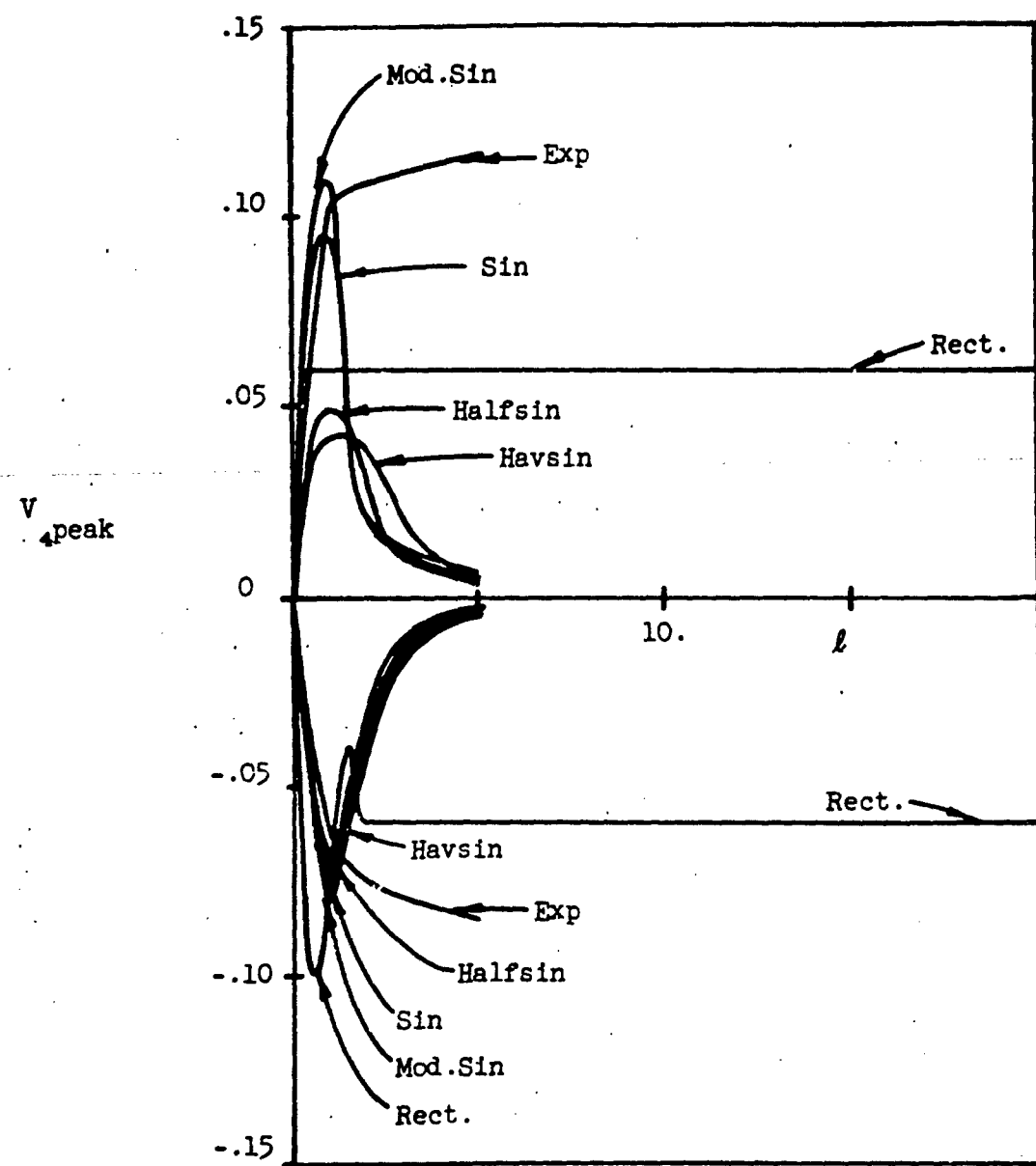


Figure 83 V_{peak} VS. l FOR VARIOUS FORCING FUNCTIONS $H = .01$

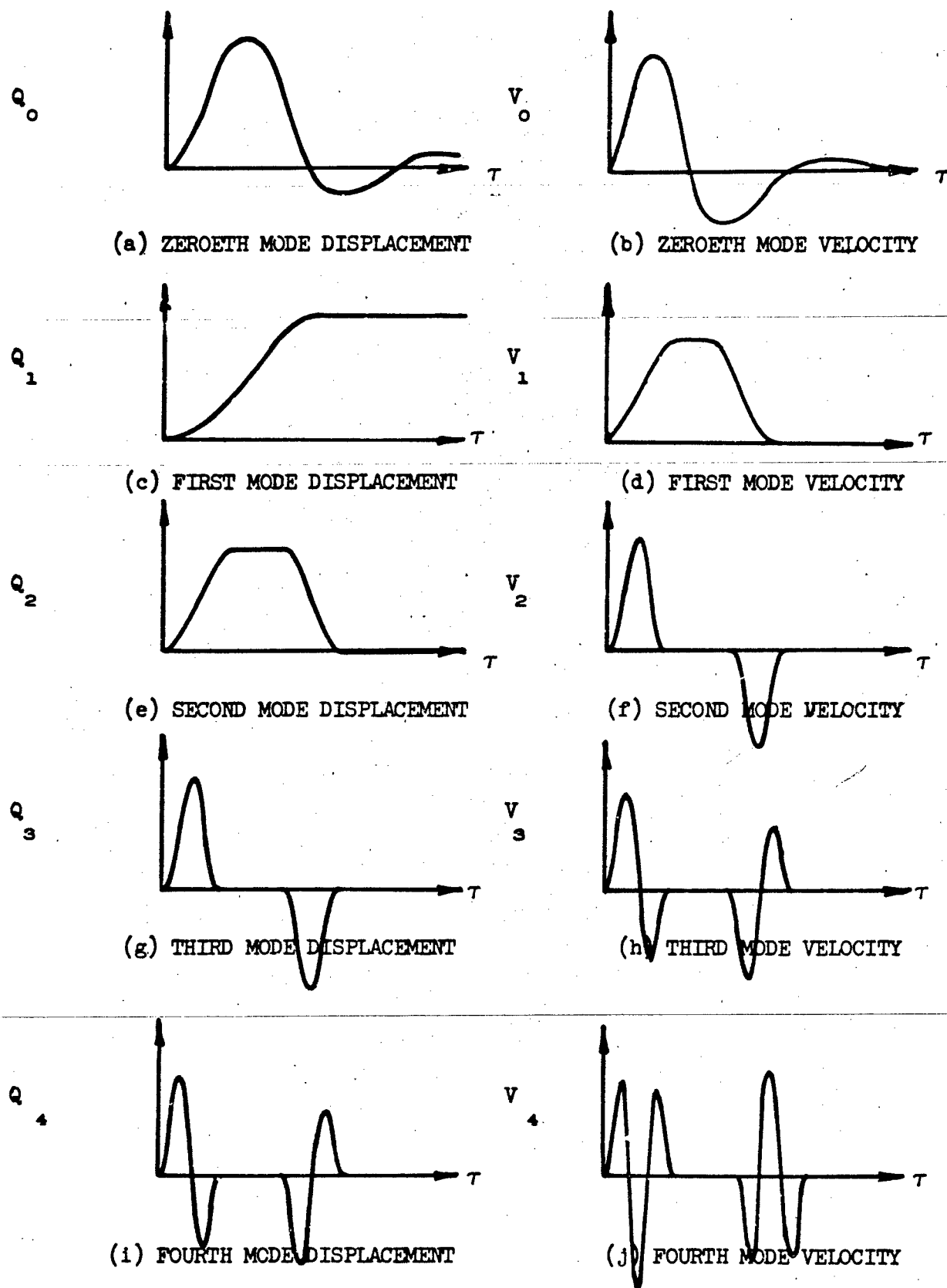


Figure 84 TYPICAL MODAL SHELL RESPONSE TO A RECTANGULAR PULSE

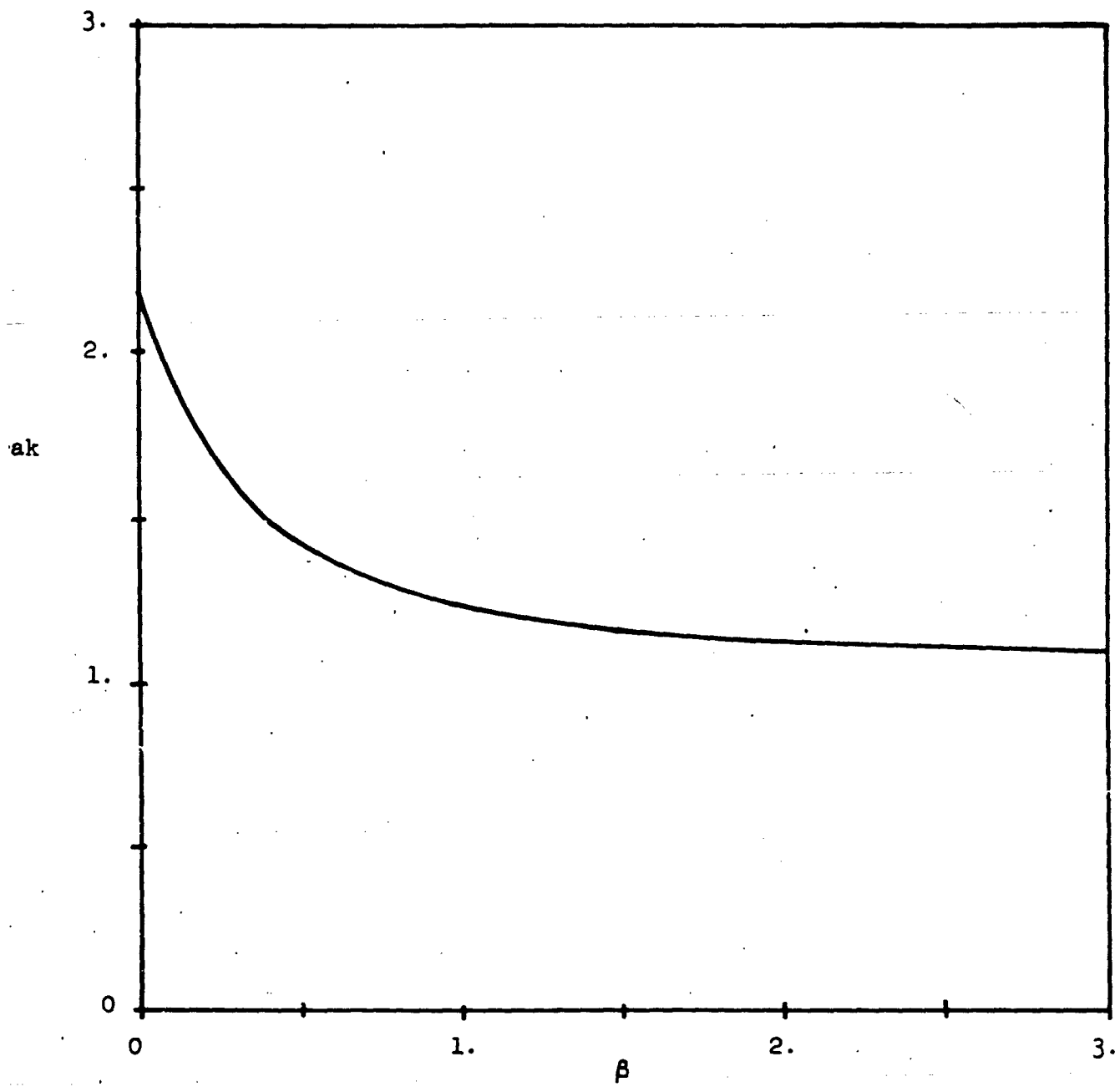


Figure 85 Q_0 peak VS. β FOR EXPONENTIALLY DECAYING PULSE;

$$P = P_0 (1 + e^{-\beta T}) \quad B = .4 \times 10^6, \quad H = .01$$

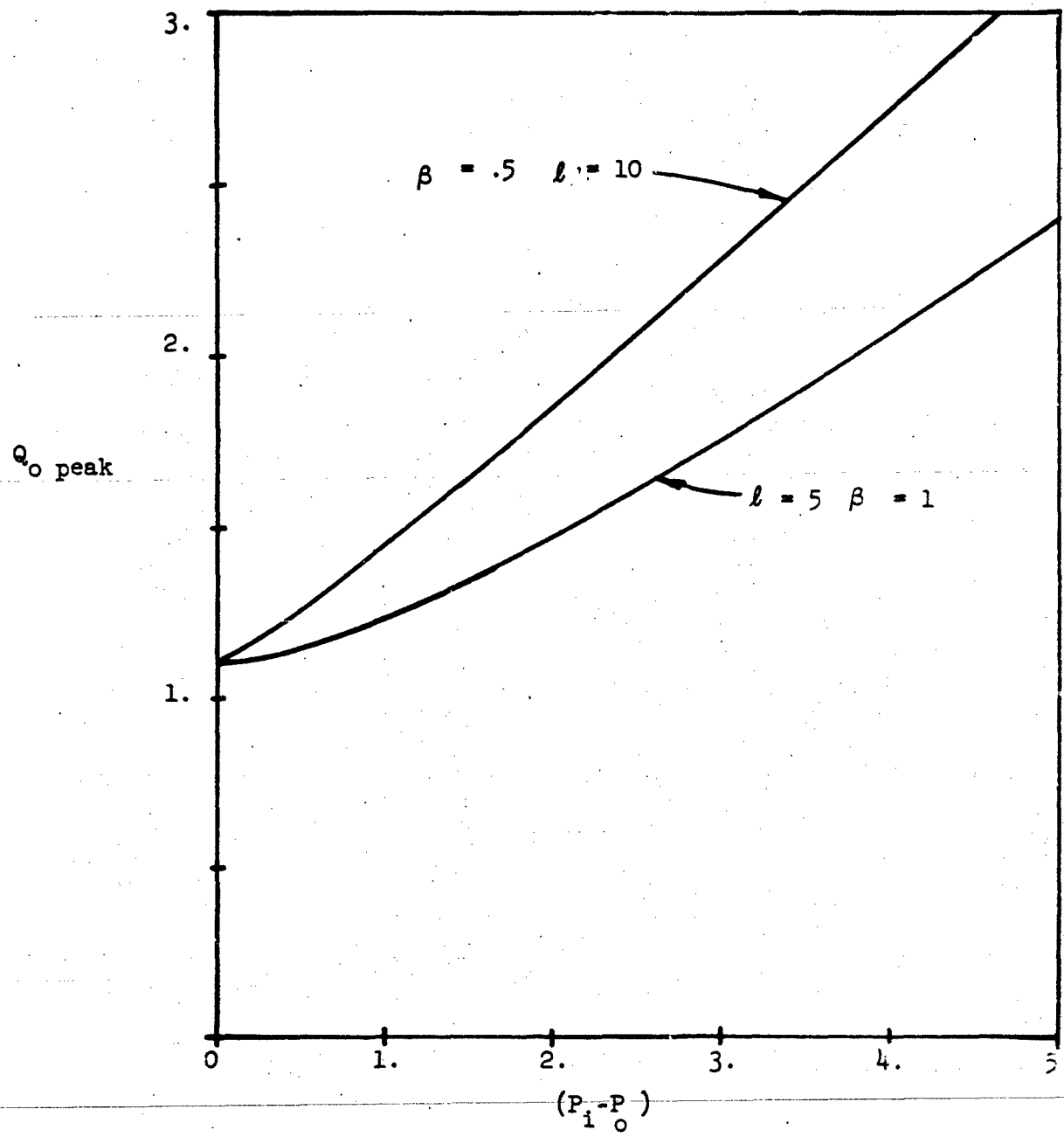


Figure 86 $Q_0 \text{ peak}$ VS. ($P_i - P_o$) FOR AN EXPONENTIALLY DECAYING PULSE; $P = P_o + (P_i - P_o) e^{-\beta T}$, $B = 4 \times 10^6$, $H = .01$

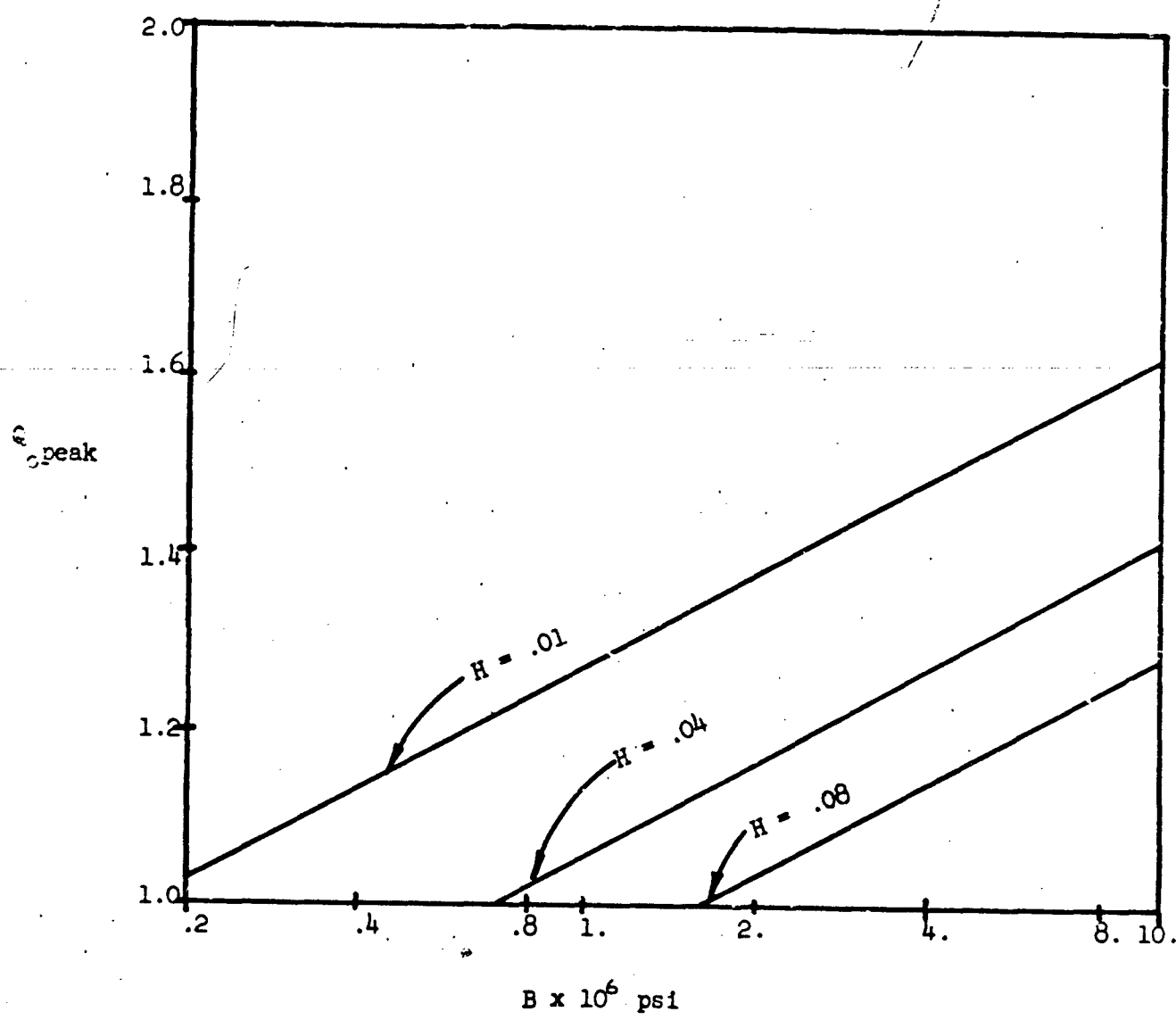


Figure 87 $Q_{0\text{peak}}$ VS. B FOR A STEP PULSE AT VARIOUS VALUES OF H .

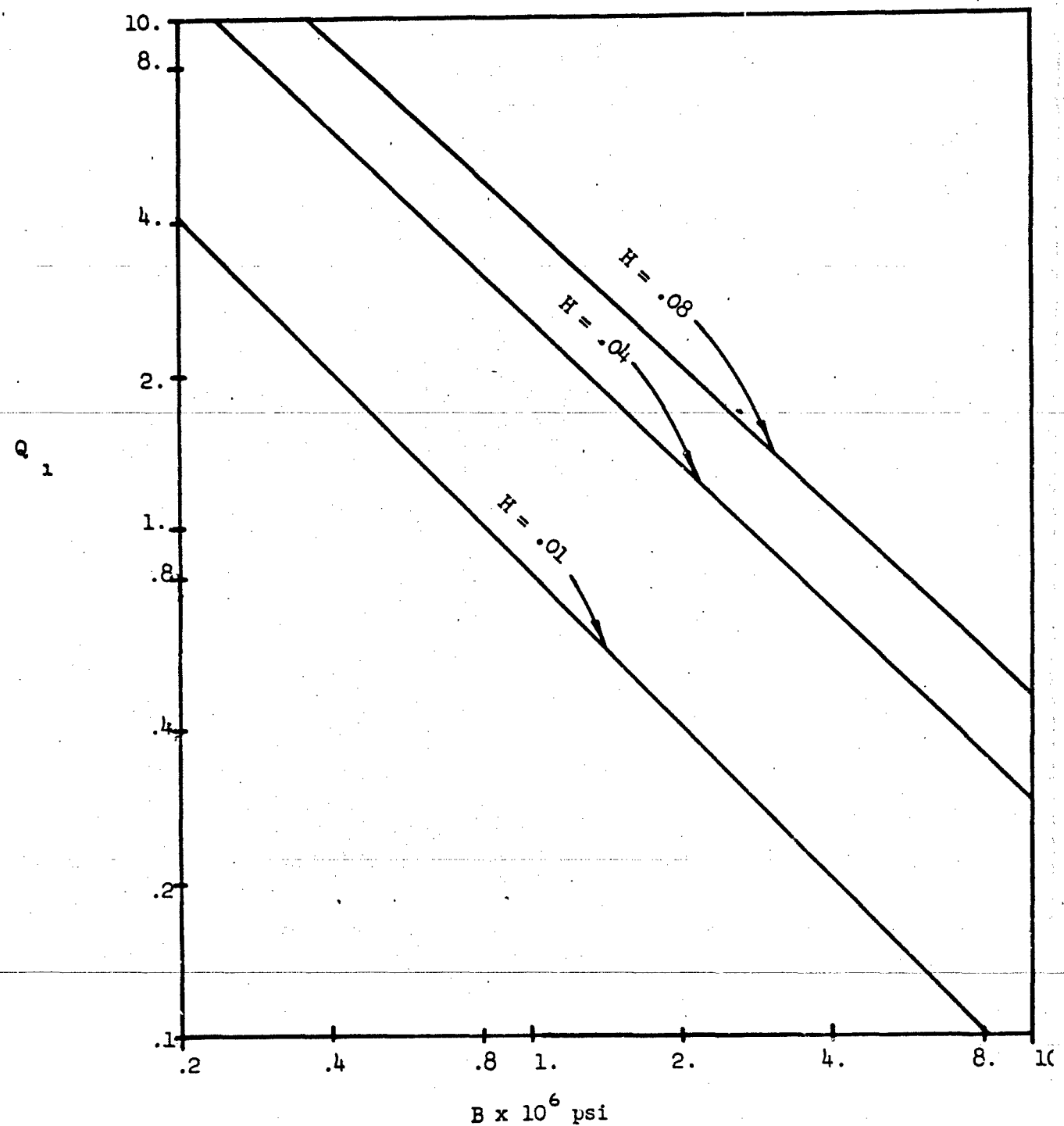


Figure 88 Q VS. B AT $\tau = 2$. FOR A STEP PULSE AT VARIOUS
VALUES OF H .

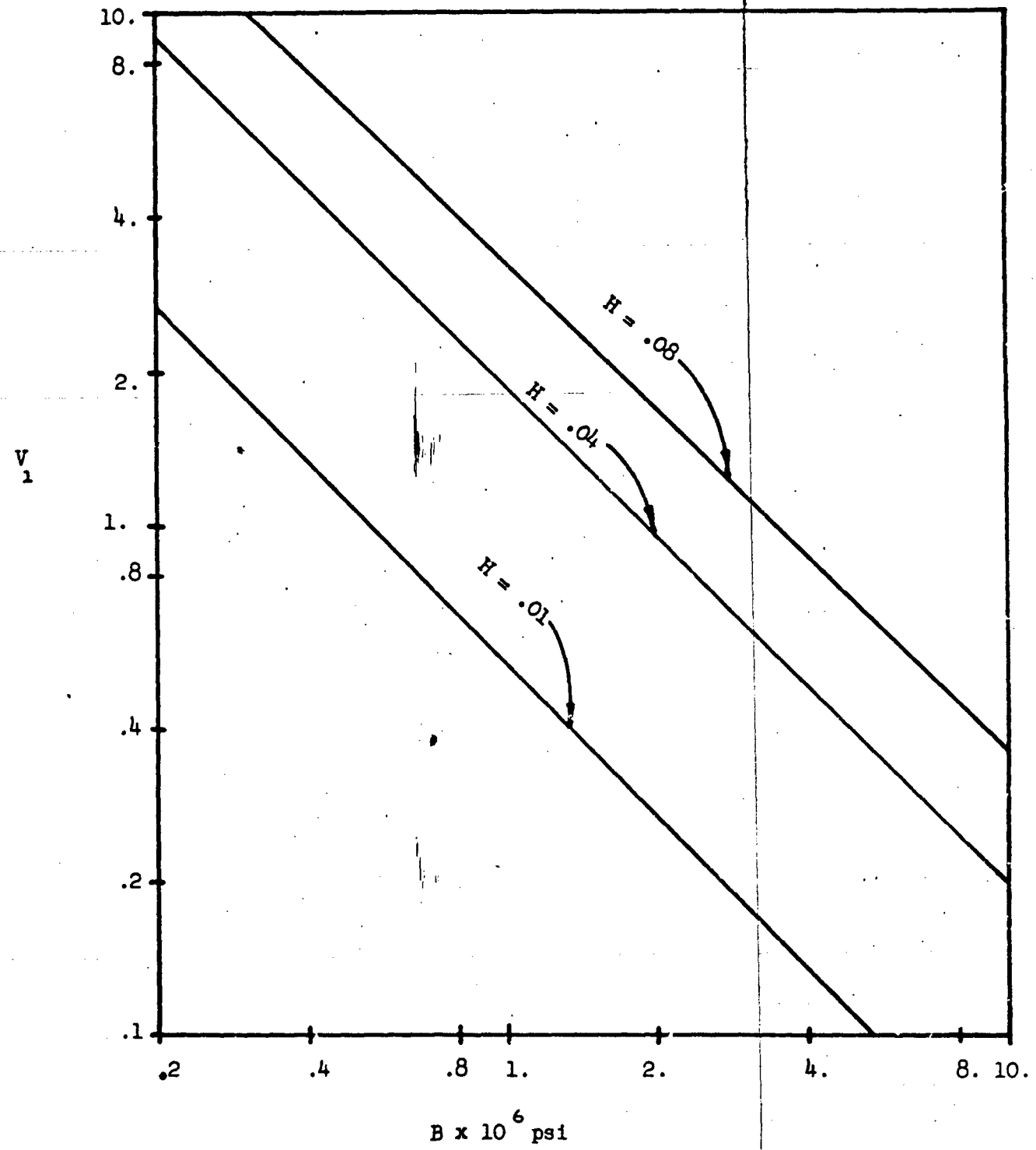


Figure 69 V_1 VS. B AT TERMINAL VELOCITY FOR A STEP PULSE AT
VARIOUS VALUES OF H .

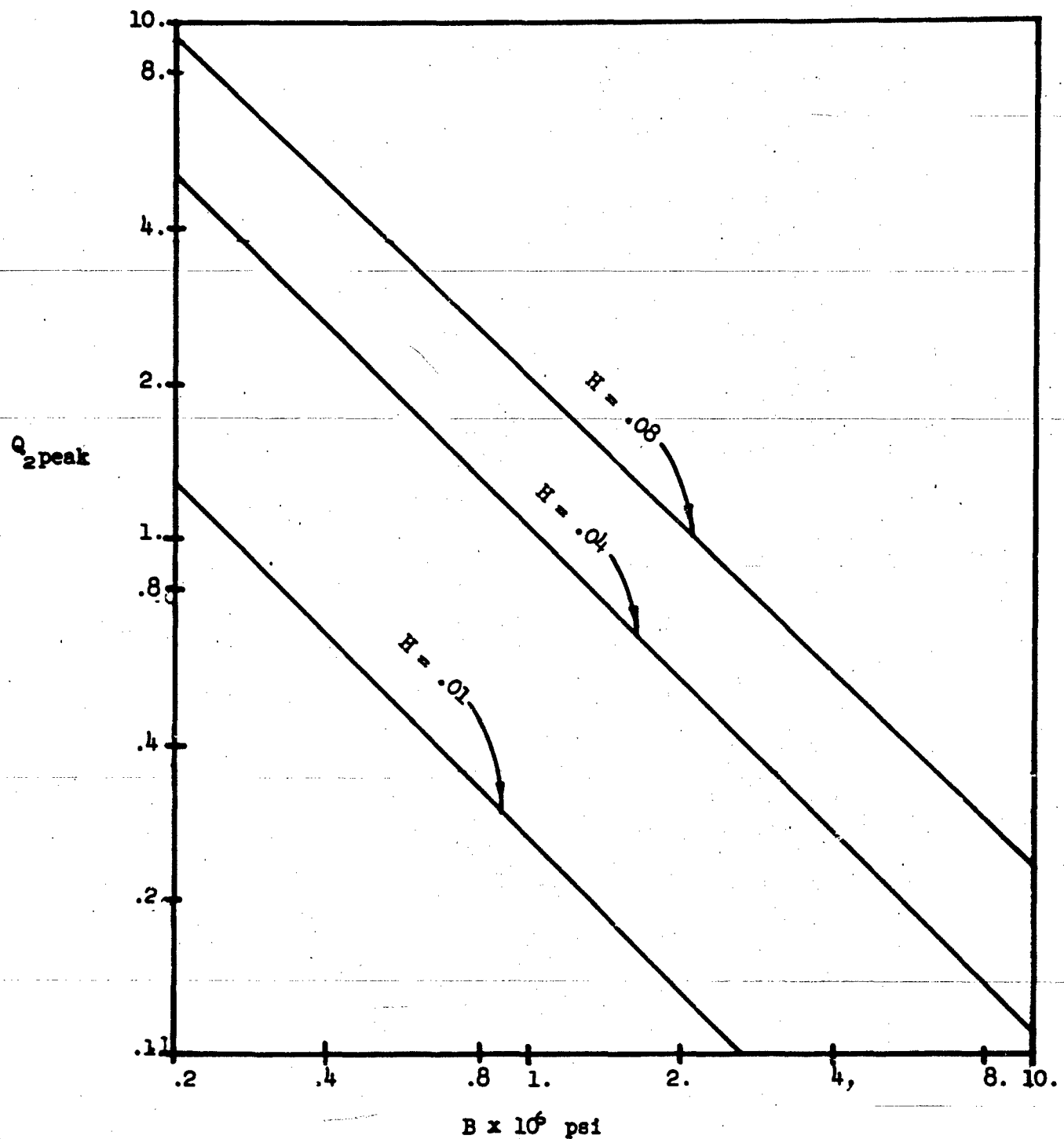


Figure 90 $Q_{2\text{peak}}$ VS. B FOR A STEP PULSE AT VARIOUS VALUES OF H .

SECTION 5

DESIGN METHODS FOR ESTIMATING STRUCTURE MOTION IN DIRECTLY-TRANSMITTED REGION

The results of the analysis of the shell-medium interaction can now be used to develop design methods for estimating interior motion of protective structures subjected to direct ground shock from a nuclear detonation.

Inasmuch as it is not within the scope of this report to determine the relative importance of the displacement and velocity responses to the designer of the shock-isolation equipment (since such relative importance depends very strongly on particular circumstances), the procedure presented here will be directed to developing design methods for estimating both responses.

5.1 Selection of Pulse Shape

The underlying principle guiding the approach towards the development of design methods has been the realization that the biggest unknowns in the whole problem are the characteristics of the pressure pulse engulfing the structure. The results of the ground-motion studies reported in Section 2 are, at best, reasonable estimates of the strength and shape of the pressure pulse. Since only scant experimental data are available to verify the theoretical results, the approach to the estimation of the structural motion must, of necessity, be on the conservative side. Of all the pressure-pulse shapes considered in this report (which represent a large number of possible attenuated-pulse shapes), the one which yields the maximum structural response, and thus the most stringent requirements on the isolation system, must be chosen as representative of the actual pulse impinging upon the buried structure.

The results indicate that the pulse shape so chosen is the long-pulse-length rectangular pulse. In addition, it happens that the theoretical results of Section 2 predict such a pulse shape, at least initially, and this tends to lend credence to the choice. The results of Section 2 may be used to estimate the length of the pulse as well as its strength for any given structural location with respect to the point of detonation.

The degree of conservatism involved in this choice is reasonable since none of the other pulse shapes yields a radically different structural response. The shell response to all pulse shapes is of the same order of magnitude and the rectangular pulse shape represents an upper limit to the responses. All these reasons lead to the conclusion that in spite of the apparent conservatism, this choice represents a rational and economical approach to the shock-isolation problem.

5.2 Parametric Values

Since the level of pulse pressures considered in this study points to the choice of steel as the structural material, it seems that the only parameter controlled by the designer is the shell thickness ratio. All other parameters affecting the response (the density ratio of shell to medium, the medium modulus, and the pressure level) are determined by the geographical location of the structure and its range from the blast.

However, since the design of the structure will, in all probability, be dictated by strength and stability considerations, rather than by interior motion considerations, the designer of the shock-isolation system for interior

equipment will be presented with specific values for the medium and pressure-pulse parameters and a given shell thickness as well. Therefore, it is clear that the problem is not how to design the primary structure to minimize deleterious dynamic effects on interior equipment, but rather, given the values of the various parameters governing the response, how to best estimate the resultant structure motion so as to determine isolation requirements. To this end, the results of the analysis presented in the previous sections are directly applicable.

In the ensuing discussion, therefore, it is tacitly assumed that the values of the various governing parameters are given a priori within certain confidence limits.

5.3 Estimation of Response

A basic conclusion which emerged from the analysis of the shell-medium system is that, although the total shell displacement is not very different from the medium displacement, the interior shell velocity may be substantially different from the medium particle velocity. Thus, it is erroneous to use the medium motion as a direct input in the shock-isolation design in those cases where velocity (and acceleration) is of importance.

The total displacement and velocity response at any location on the circumference of the shell is made up of the contributions of all the modes. For certain applications to shock isolation, it may be convenient to distinguish between the rigid-body motion ($n = 1$) on one hand, and the elastic motion of the shell ($n = 0, 2, 3, 4$) on the other. As the name implies, the rigid-body motion of the structure denotes the translation of the structure as

a whole with respect to the surrounding medium, whereas the motion in all other modes is of the nature of deformation of the shell skin from its undeformed position. Thus, in the former case there is no change in the relative position of points within the shell, while in the latter case these changes are the essence of the motion. This distinction is relevant only to those cases where the relative motion of points within the structure is of importance.

In general, however, the total response at any point is considered in the design of the shock-isolation equipment. Therefore, one must superimpose the contribution of all modes. Since the reliability of the phase differences among the modes given in the results cannot be considered infallible, and since the contribution of each mode to the total motion at any point depends on the particular azimuthal location of the point within the structure, a reasonable estimate of the total maximum expected response is given by the root-mean-square of the maxima of all modes. The numerical results of Section 4 provide the necessary information for this purpose. Results for other values of the parameters may be obtained either directly from the curves by interpolation or by using Figures 87 through 90 or by using the computer program given in Appendix A to generate additional numerical results.

Besides maximum values, knowledge of the actual displacement and velocity pulse shape transmitted by the structure to its interior is also of direct importance. It is evident from the time histories of the structural response presented in Section 4 that the shape of the displacement or velocity pulse

transmitted by the structure, when subjected to the assumed input pressure pulse, is far from being standard. Rather, it is strongly dependent on the combination of the various parameters. The parametric ranking given in Section 4 should provide a guide-line to the evaluation of the effects of each parameter. In any event, it will be necessary to determine the motion history either from the results given in this report or by using the appended computer program. Thus, the combination of knowledge of the response maxima and its history would provide the necessary inputs towards the shock-isolation-system design.

5.4 Numerical Examples

To illustrate the method of using the results in the shock-isolation-design process, two examples are presented. The values of the various physical parameters were chosen so as to simulate a realistic situation and to make possible a direct application of the results given in this report.

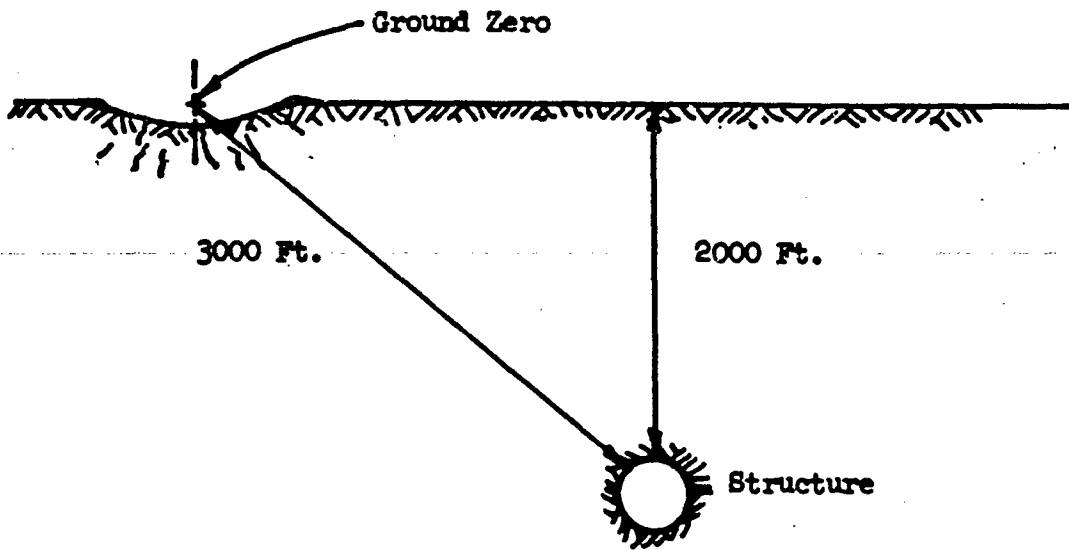


Figure 91 ILLUSTRATION OF SAMPLE PROBLEM

A circular cylindrical steel structure with a 25 foot diameter and a shell thickness of 3 inches is buried at a depth of 2,000 feet. A nuclear surface detonation of 10 MT yield is assumed to take place at a point having a slant range of 3,000 feet from the structure. It is desired to estimate the response of the interior of the structure due to the directly-transmitted shock.

Step 1 - Medium Parameters

The following values, representing typical limestone, are assumed,

$$\rho_m = 160 \text{ g lb-sec}^2/\text{ft}^4$$

$$c = 7600 \text{ ft/sec}$$

Thus, the medium modulus is

$$B = \rho_m c^2 = 2.0 \times 10^6 \text{ psi}$$

The density ratio is

$$\mu = \frac{\rho_s}{\rho_m} = \frac{490}{160} = 3.07$$

Step 2 - Shock Parameters

From Equation (5) obtain the pulse pressure, (note change to psi)

$$P = \frac{Eg}{L^3}$$

$$= (1.45)(10^{10})(10^{1/3})(2000.) / 3000.^3 = 2320 \text{ psi}$$

From Equation (7) obtain upper and lower bounds to the pulse duration,

$$\Delta t_{upper} = L/2c = 3000. / (2)(7600.) = .2 \text{ sec.}$$

$$\Delta t_{lower} = .05 W^{1/3} = (.05)(10^{1/3}) = .108 \text{ sec.}$$

Assume, therefore,

$$\Delta t = .12 \text{ sec.}$$

From the definition of the pulse length obtain,

$$t = \frac{X}{R} = \frac{c\Delta t}{R} = (7600.)(12)/12.5 = 73$$

The particle velocity is

$$u = \frac{P}{\rho_m c} = (2320)(144)g/(160)(7600)$$
$$= 9 \text{ ft/sec}$$

Step 3 - Shell Parameters

The thickness ratio is

$$H = \frac{h}{R} = \frac{.25}{12.5} = .02$$

The static displacement of the shell is

$$q_{st} = PR/E_s H = (2320)(12.5)(12)/(3)(10^7)(.02) = .58 \text{ inch}$$

Step 4 - Velocity Response

From Figure 24 obtain

$$v_{o \text{ peak}} = \frac{d(q_o/q_{st})}{dt} = .25$$

From Figure 26 obtain

$$v_{1 \text{ peak}} = .4$$

From Figure 28 obtain

$$v_{2 \text{ peak}} = .3$$

From Figure 30 obtain

$$v_{3 \text{ peak}} = .2$$

From Figure 32 obtain

$$v_{4 \text{ peak}} = .13$$

Using the root-mean-square approach, the velocity due to the deformatinal modes is

$$v_{\text{elastic}} = \left[(.25)^2 + (.3)^2 + (.2)^2 + (.13)^2 \right]^{1/2} = .45$$

Dimensionally, this becomes

$$\begin{aligned}\tilde{v}_{\text{elastic}} &= v_{\text{elastic}} \cdot q_{st} \cdot c/R \\ &= (.45)(.58)(7600)/(12.5)(12) = 13 \text{ ft/sec}\end{aligned}$$

The total velocity, due to all modes, is

$$v_{\text{total}} = v_1 + v_{\text{elastic}} = .4 + .45 = .85$$

or

$$\tilde{v}_{\text{total}} = (.85)(.58)(7600)/(12.5)(12) = .25 \text{ ft/sec}$$

Step 5 - Displacement Response

From Figure 87, obtain

$$Q_0 \text{ peak} = 1.25$$

From Figures 88 and 89 obtain

$$(Q_1)_{\tau=2} = .8$$

$$Q_1 \text{ peak} = 2(Q_1)_{\tau=2} + v_1(\tau-2) = (2)(.8) + (.4)(70) = 29.6$$

From Figure 90 obtain

$$Q_2 \text{ peak} = .3$$

From Figure 19 obtain

$$Q_3 \text{ peak} = .1$$

$$Q_4 \text{ peak} = .03$$

The displacement due to deformational modes becomes

$$Q_{\text{elastic}} = \left[(1.25)^2 + (.3)^2 + (.1)^2 + (.03)^2 \right]^{1/2} = 1.29$$

Dimensionally, this becomes

$$\tilde{Q}_{\text{elastic}} = (1.29)(.58) = .75 \text{ inch}$$

The total displacement, including rigid-body mode, is

$$Q_{\text{total}} = Q_1 + Q_{\text{elastic}} = 29.6 + .75 = 30.4$$

or

$$\tilde{Q}_{\text{total}} = (30.4)(.58) = 17.6 \text{ inches}$$

It is evident that as far as the displacement response is concerned, the major contribution is that of the rigid-body mode, whereas contributions to the velocity response are made by all modes to relatively the same extent.

The medium particle velocity and displacement are 9 ft/sec and 13 inches, respectively. An estimate of the total shell displacement based on the medium displacement may therefore be justified. However, it is clear that a similar estimate is erroneous for the velocity response.

It should be noted, however, that the rigid-body velocity and displacement values given here should be considered as upper limits, the values for the medium being considered as alternatives. This question is discussed more fully in Appendix B.

Step 6 - History

The velocity histories may be obtained using Figures 24, 26, 28, 30 and 32. The displacement histories may be obtained using Figures 13, 15, 17 and

19. The modal data thus obtained may then be approximately superposed, depending on the particular shell location.

As an illustration of how the problem may be solved when the parameter values are beyond the limits of the graphs, consider the same geometrical configuration and weapon, but a different medium.

Step 1 - Medium Parameters

The following values are assumed,

$$\rho_m = 120/\text{g lb-sec}^2/\text{ft}^4$$

$$c = 3000 \text{ ft/sec}$$

Thus, the medium modulus is

$$B = \rho_m c^2 = .23 \times 10^6 \text{ psi}$$

The density ratio is

$$\mu = \frac{\rho_s}{\rho_m} = \frac{490}{120} = 4.08$$

Step 2 - Shock Parameters

From Equation (5) obtain the pulse pressure, (note change to psi)

$$P = \frac{F L}{L^3}$$

$$= (1.45)(10^{10})(10^{1/3})(2000.)/3000.^3 = 2320 \text{ psi}$$

From Equation (7) obtain upper and lower bounds to the pulse duration,

$$\Delta t_{upper} = L/2c = 3000. / (2)(3000.) = .5 \text{ sec.}$$

$$\Delta t_{lower} = .05 W^{1/3} = (.05)(10^{1/3}) = .108 \text{ sec.}$$

Assume, therefore

$$\Delta t = .3 \text{ sec.}$$

From the definition of the pulse length obtain

$$l = \frac{X}{R} = \frac{c\Delta t}{R} = (3000.)(.3)/12.5 = 72$$

Step 3 - Shell Parameters

The thickness ratio is

$$H = \frac{h}{R} = \frac{.25}{12.5} = .02$$

The static displacement of the shell is

$$q_{st} = PR/E_s H = (2320)(12.5)(12)/(3)(10^7)(.02) = .58 \text{ inch}$$

Step 4 - Velocity Response

From Figures 23 and 24 extrapolate to obtain

$$v_o \text{ peak} = \frac{d(q_o/q_{st})}{d\tau} = .8$$

From Figure 89 obtain

$$v_1 \text{ peak} = 3.5$$

From Figures 27 and 28 extrapolate to obtain

$$v_3 \text{ peak} = 2.0$$

From Figures 29 and 30 extrapolate to obtain

$$v_3 \text{ peak} = 1.6$$

From Figures 31 and 32 extrapolate to obtain

$$v_4 \text{ peak} = 1.0$$

Using the root-mean-square approach, the velocity due to the deformational modes is

$$v_{\text{elastic}} = [(.8)^2 + (2.0)^2 + (1.6)^2 + (1.0)^2]^{1/2} = 2.75$$

Dimensionally, this becomes

$$\tilde{V}_{\text{elastic}} = V_{\text{elastic}} \cdot q_s \cdot c/R$$
$$= (2.75)(.58)(3000.)/(12.5)(12) = 32 \text{ ft/sec}$$

The total velocity, due to all modes, is

$$V_{\text{total}} = V_1 + V_{\text{elastic}} = 3.5 + 2.75 = 6.25$$

or

$$\tilde{V}_{\text{total}} = (6.25)(.58)(3000.)/(12.5)(12) = 72 \text{ ft/sec}$$

Step 5 - Displacement Response

From Figure 87 obtain

$$q_0 \text{ peak} = 1.0$$

From Figures 88 and 89 obtain

$$(q_1)_{T=2} = 7.5$$

$$q_1 \text{ peak} = 2 (q_1)_{T=2} + V_1(T-2) = (2)(7.5) + (3.5)(70) = 245$$

From Figure 90 obtain

$$q_2 \text{ peak} = 2.8$$

From Figures 18 and 19 extrapolate to obtain

$$q_3 \text{ peak} = .6$$

$$q_4 \text{ peak} = .3$$

The displacement due to deformational modes becomes

$$q_{\text{elastic}} = [(1.0)^2 + (2.8)^2 + (.6)^2 + (.3)^2]^{1/2} = 3.05$$

Dimensionally, this becomes

$$\tilde{q}_{\text{elastic}} = (3.05)(.58) = 1.77 \text{ inch}$$

The total displacement, including rigid-body mode, is

$$Q_{\text{total}} = Q_1 + Q_{\text{elastic}} = 245 + 3.05 = 248$$

or

$$\tilde{Q}_{\text{total}} = (248)(.58) = 144 \text{ inches}$$

TABLE I
TYPICAL SOIL AND ROCK PROPERTIES^{6, 34}

Soil or Rock Type	Approximate Density - lb/ft ³	Approximate Compressive Wave Velocity Range - ft/sec
Top soil, dry or moist silty loam	100 - 110	650 - 2000
Sand - loose	100 - 110	650 - 2000
Sand - well compacted	110 - 120	2000 - 4500
Saturated clay	120	3000
Sandstone - loose	140 - 150	4500 - 6000
Sandstone - well cemented	150 - 160	6000 - 10000
Limestone - soft	155 - 160	4500 - 10000
Limestone - hard	160	6000 - 16000
Granite - fractured	160 - 165	7500 - 12000
Granite	169	12000 - 18000

APPENDIX A

DUHAMEL INTEGRAL COMPUTER PROGRAM

The response of a single-degree-of-freedom system to an arbitrary forcing function may be computed knowing the system response to a step pulse. Each mode of a continuous system may be separately treated as such. Applying Duhamel's integral to the modal response of the system;

Let $A(t)$ = system response to a step pulse*

$F(t)$ = arbitrary forcing function

$x(t)$ = response of the system to $F(t)$

then

$$x(t) = F(0) A(t) + \int_0^t \frac{dF}{d\tau} A(t-\tau) d\tau$$

which, for numerical evaluation may be written as

$$x(t) = F(0) A(t) + \sum_{\tau=\Delta\tau}^{t=\Delta\tau} \frac{\Delta F}{\Delta\tau} A(t-\tau) \Delta\tau$$

If F and A are evaluated at regular intervals of t then the above expression is further reduced to

$$x(t) = F(0) A(t) + \sum_{\tau=\Delta\tau}^{t=\Delta\tau} \Delta F A(t-\tau)$$

A computer program has been written to evaluate this expression. Input data are: Δt , the interval at which $x(t)$ is to be evaluated. $F(t)$, the values of the forcing function to be taken at the midpoint of regular intervals of Δt . $A(t)$, the values of the response to a unit step pulse, to be taken at the midpoint of regular intervals of Δt . The latter two lists of data are to be ended

*Notation contained herein deviates from that defined in the table of notation and is defined above.

with 10^8 , or any arbitrarily larger number as an indication of end of data.

Output data consists of tabulated values of T, F, A, and RESPONSE.

Following is a FORTRAN LISTING OF THE PROGRAM FOR THE IBM 1620 COMPUTER.

```
c      DUHAMEL INTEGRAL    RWK 10 APRIL 64
4      DIMENSION F(200),A(200)
      READ 7,DT
      PRINT 10
      DO 1 I=1,200
      READ 7,F(I)
      IF(F(I)-1.E08)1,11,11
1      CONTINUE
11     KF=I-1
      DO 12 I=1,200
      READ 7,A(I)
      IF(A(I)-1.E08)12,13,12
12     CONTINUE
13     KA=I-1
      IF(KA-KF)14,14,15
14     K=KA
      GO TO 16
15     K=KF
16     T=DT*.5
      Z=F(1)
      DO 2 I=1,K
      X=Z*A(I)
      IF(I-1)5,5,9
5      F(I-1)=F(I)-F(I-1)
      M=I-1
      DO 3 J=1,M
      L=1-J
      X=X+F(J)*A(L)
3      PRINT 8,T,F(I),A(I),X
5      PR 1NT 8,T,F(I),A(I),X
2      T=T+DT
      GO TO 4
7      FORMAT(F16.8)
8      FORMAT(F8.3,F12.8,F12.8,F12.8)
10     FORMAT(4X1H9X1HF11X1HA8X8HRESPONSE)
      END
```

APPENDIX B

TERMINAL VELOCITIES OF RIGID-BODY-MODE RESPONSE

(Notation is the same as in the main body of the report. Equation numbers and figure numbers used refer to the main body of the report.)

The limiting value of the rigid-body velocity can be determined directly from the exact equations of motion of the shell (Equation 14). This value can be shown to be:²²

$$v_{\infty} \equiv \lim_{t \rightarrow \infty} \left(\frac{dq_1}{dt} \right) = \frac{P}{\rho_m c} \left(\frac{2}{\xi_1 + 1} \right) \quad (B-1)$$

Since the magnitude of the particle velocity behind the incoming wave is given by $P/\rho_m c$, it can be seen that it is possible to obtain values of the terminal velocity of the shell which exceed the magnitude of the particle velocity of the free-field behind the incoming wave when $\xi_1 < 1$. According to the definition of ξ_n , it may be represented as

$$\xi_1 = 2H\mu \quad (B-2)$$

Since, for a steel shell, a reasonable range of the parameter μ is given by $3 < \mu < 4$, it can be seen that as long as the thickness to radius ratio does not exceed the value $H = .125$ the value of ξ_1 will be less than one and shell terminal velocities in the rigid-body modes will exceed the magnitude of the medium particle velocity. It is not considered likely that shell thickness-to-radius ratios will very frequently exceed a value of .1. Moreover, such a value of H is really outside the limits of thin-shell theory. Regardless, it is apparent that for all cases investigated in this report, rigid-body terminal velocities will exceed those of the medium.

Mathematically, such a solution appears to be possible, but physically it may be open to some question. It seems highly unlikely that the terminal velocity of the rigid-body motion of the shell could possibly exceed the velocity of the surrounding medium. In fact, it seems unlikely that the rigid-body velocity of the shell could exceed the medium velocity for more than very short periods of time under any circumstances. It is probable that the reason that this occurs in this analysis is that such circumstances were not considered likely during derivation of the equations of motion. Consequently, no terms were included which would account for the drag of the shell in the medium in the case when the velocity of the shell exceeded the velocity of the medium. An examination of the literature failed to reveal such an analysis for any solution presently made to the cylinder-medium-interaction problem, in any type of medium. It is felt that further study with the aim of including a drag-type force in the analysis of the structure-medium interaction problem would be beneficial.

REFERENCES

1. Brode, H. L., Weapons Effects for Protective Design, Rand Report RM 1951.
2. Newmark, N. M., J. P. Haltwanger, Air Force Design Manual, Principles and Practices for Design of Hardened Structures, SWC TDR 62-138, 1958; Draft Revised Edition, publication pending, Civil Engineering Branch, Air Force Weapons Laboratory
3. Brode, H. L., R. L. Bjork, Cratering From a Megaton Surface Burst, Rand Report RM 2600, 1960.
4. Baron, M. L., H. H. Bleich, P. Weidlinger, Theoretical Studies on Ground Shock Phenomena, Final Technical Report Contract AF 33(600)-39852, Oct. 1960.
5. Weiner, R. S., Deduction of Shock Testing Methods and Facilities Criteria, Final Technical Report DASA 1238, 1963.
6. Morrison, T. C., Design and Shock Isolation Systems for Underground Protective Structures, TDR 63-3096, Volume I, AFSWC, 1963.
7. Cagnaird, L., Reflection and Refraction of Progressive Seismic Waves, McGraw-Hill, N.Y., 1962.
8. Pekeris, C. L., "The Seismic Buried Pulse," Proceedings of National Academy of Sciences, 41, 1955, 629-639.
9. Knopoff, L., "First Motion Methods in Theoretical Seismology," Journal of Acoustical Society of America 31, 1959, 1161-1168.
10. Love, A. E. H., "The Propagation of Wave Motion in an Isotropic Elastic Solid Medium," Proceedings of London Journal of Mathematics, Ser. 2, 1, 1903, 291-344.
11. Pekeris, C. L., H. Lifson, "Motion of the Surface of a Uniform Elastic Full Space Produced by a Buried Pulse," Journal of Acoustical Society of America, 29, 1957, 1233-1238.
12. Neidhardt, G. L., Theoretical Study of Energy Distribution in a Half Space Resulting from Dynamic Loading in a Depression at the Origin, TDR 63-3125, AFWL, 1963.
13. Courant, R., K. O. Friedrichs, Supersonic Flow and Shock Waves, Interscience, 1948.
14. Berry, D. S., "Stress Propagation in Viscoelastic Bodies," Journal of Mechanics and Physics Solids, 6, 1958, 177-185.

15. Sokolovsky, V. V., Prikladnaya Matematika i Mekhanika, (Journal of Applied Mathematics and Mechanics) 12, 1948, 261-280.
16. Fugelso, L. E., A. A. Arentz, D. A. Davidson, Mechanics of Penetration, Volume 2, Final Technical Report, Contract DA-19-129-QM-1542, 1961.
17. Chernov, L., Wave Propagation in a Random Medium, 1960.
18. Carrier, G. F., The Interaction of an Acoustic Wave and an Elastic Cylindrical Shell, Brown University Technical Report No. 4, 1951.
19. Mindlin, R. C., H. H. Bleich, "Response of an Elastic Cylindrical Shell to a Transverse, Step Shock Wave," Journal of Applied Mechanics, 20, June 1953, 189.
20. Baron, M. L., "The Response of a Cylindrical Shell to a Transverse Shock Wave," Proceedings 2nd U. S. National Congress of Applied Mechanics, 1954, 201.
21. Haywood, J. H., "Response of a Cylindrical Shell to a Pressure Pulse," Quarterly Journal of Mechanics and Applied Mathematics, 11, May 1958.
22. Baron, M. L., R. Parnes, "Diffraction of a Pressure Wave by a Cylindrical Shell in an Elastic Medium," Proceedings 4th U. S. National Congress of Applied Mechanics, 1962, 63-75.
23. Soldate, A. M., J. F. Hook, A Theoretical Study of Structure-Medium Interaction, AFSWC TN 61-6, 1961.
24. Paul, S. L., and A. R. Robinson, Interaction of Plane Elastic Waves with a Cylindrical Cavity, AFWL RDT-TDR-63-3021, June 1963.
25. Yoshihara, T., A. R. Robinson, J. L. Merritt, Interaction of Plane Elastic Waves with an Elastic Cylindrical Shell, University of Illinois, Civil Engineering Studies, Structural Research Series No. 261, January 1963.
26. Sommerfeld, A., "Mathematische Theorie der Diffraction," Mathematische Annalen, 47, 1896, 317, 374.
27. Friedlander, F. G., "Diffraction of Pulses by a Circular Cylinder," Communications on Pure and Applied Mathematics, 70, 1954, 705-732.
28. Payton, R. G., "Transient Interaction of an Acoustic Wave with a Circular Cylindrical Elastic Shell," Journal of Acoustical Society of America, 32, June 1960, 722-729.
29. Peralta, L. A., Initial Response of a Fluid Filled Elastic, Infinitely Long Circular Cylindrical Shell to a Shock Wave Traveling in the Surrounding Acoustic Medium, Ph.D. Dissertation, Northwestern University, June 1963.

30. Gilbert, F., L. Knopoff, "Scattering of Impulsive Elastic Waves by a Rigid Cylinder," Journal of Acoustical Society of America, 31, September 1959, 1169-1175.
31. Soldate, A. M., J. F. Hook, A Theoretical Study of Structure-Medium Interaction, TDR-62-30, AFSWC, March 1962.
32. Friedlander, F. G., Sound Pulses, Cambridge University Press, 1958.
33. Rinehart, J. W., J. Fortin, L. Burgin, "Propagation Velocity of Longitudinal Waves in Rocks. Effect of State of Stress, Stress Level of the Wave, Water Content, Porosity, Temperature, Stratification and Texture," Proceedings of the Fourth Symposium on Rock Mechanics, Pennsylvania State University, April 1961, 119-135.
34. Clark, G. B., and R. D. Caudle, Geologic Structure Stability and Deep Protection Construction, AFSWC TDR-61-93, Nov. 1961.

Unclassified

Security Classification

DOCUMENT CONTROL DATA - R&D

(Security classification of title, body of abstract and indexing annotation must be entered when the overall report is classified)

1. ORIGINATING ACTIVITY (Corporate author) General American Transportation Corporation Niles, Illinois		2a. REPORT SECURITY CLASSIFICATION Unclassified 2b. GROUP
3. REPORT TITLE DESIGN PROCEDURES FOR SHOCK ISOLATION SYSTEMS OF UNDERGROUND PROTECTIVE STRUCTURES Vol. II: STRUCTURE INTERIOR MOTIONS DUE TO DIRECTLY TRANSMITTED GROUND SHOCK		
4. DESCRIPTIVE NOTES (Type of report and inclusive dates) November 1963 to January 1965		
5. AUTHOR(S) (Last name, first name, initial) Finlayson, F.; Fugelso, L. E.; Shulman, Y.		
6. REPORT DATE December 1965	7a. TOTAL NO. OF PAGES 214	7b. NO. OF REPS 34
8a. CONTRACT OR GRANT NO. AF29(601)-6253 b. PROJECT NO. 5710	8b. ORIGINATOR'S REPORT NUMBER(S) RTD-TDR-63-3096, Vol. II	
c. Subtask 13.167 d.	8c. OTHER REPORT NO(S) (Any other numbers that may be assigned to report)	
10. AVAILABILITY/LIMITATION NOTICES Distribution of this document is unlimited.		
11. SUPPLEMENTARY NOTES	12. SPONSORING MILITARY ACTIVITY Air Force Weapons Laboratory (WLDC) Kirtland AFB, New Mexico 87117	
13. ABSTRACT <p>This volume presents a method for estimating the motions on the interior of a buried cylindrical shell resulting from directly-induced ground shock caused by the detonation of a nuclear device to aid in the preliminary design of shock isolation equipment. Various theoretical models for calculating the free-field waveform are reviewed and the acoustic model is recommended for this purpose. The reasons for this recommendation are enumerated and the methods for applying it are given. Methods for solving the structure-medium-interaction problem are discussed and the normal-mode analysis of the response of an elastic cylindrical shell in an acoustic medium to a specified input pulse is reviewed in detail. A discussion of ranges of parameters appropriate to realistic problems is included. A thorough explanation of the results of computer solutions for the shell response is presented, and a large number of graphs illustrating the results are included. The results are analyzed to determine the relative influence of the parameters on interior shell motion. The application of the method developed is explained and illustrated by sample problems. An appendix contains a Duhamel-integral computer program that can be used to generate results for cases not included in this volume.</p>		

Unclassified
Security Classification

14. KEY WORDS	LINK A		LINK B		LINK C	
	ROLE	WT	ROLE	WT	ROLE	WT
Shock Isolation Systems						
Underground Protective Structures						
Ground Shock						
Directly Transmitted Ground Shock						
Structure Interior Motions						
Cylindrical Shell						
Acoustic Medium						

INSTRUCTIONS

1. ORIGINATING ACTIVITY: Enter the name and address of the contractor, subcontractor, grantee, Department of Defense activity or other organization (corporate author) issuing the report.

2a. REPORT SECURITY CLASSIFICATION: Enter the overall security classification of the report. Indicate whether "Restricted Data" is included. Marking is to be in accordance with appropriate security regulations.

2b. GROUP: Automatic downgrading is specified in DoD Directive 5200.10 and Armed Forces Industrial Manual. Enter the group number. Also, when applicable, show that optional markings have been used for Group 3 and Group 4 as authorized.

3. REPORT TITLE: Enter the complete report title in all capital letters. Titles in all cases should be unclassified. If a meaningful title cannot be selected without classification, show title classification in all capitals in parenthesis immediately following the title.

4. DESCRIPTIVE NOTES: If appropriate, enter the type of report, e.g., interim, progress, summary, annual, or final. Give the inclusive dates when a specific reporting period is covered.

5. AUTHOR(S): Enter the name(s) of author(s) as shown on or in the report. Enter last name, first name, middle initial. If military, show rank and branch of service. The name of the principal author is an absolute minimum requirement.

6. REPORT DATE: Enter the date of the report as day, month, year, or month, year. If more than one date appears on the report, use date of publication.

7a. TOTAL NUMBER OF PAGES: The total page count should follow normal pagination procedures, i.e., enter the number of pages containing information.

7b. NUMBER OF REFERENCES: Enter the total number of references cited in the report.

8a. CONTRACT OR GRANT NUMBER: If appropriate, enter the applicable number of the contract or grant under which the report was written.

8b, 8c, & 8d. PROJECT NUMBER: Enter the appropriate military department identification, such as project number, subproject number, system numbers, task number, etc.

9a. ORIGINATOR'S REPORT NUMBER(S): Enter the official report number by which the document will be identified and controlled by the originating activity. This number must be unique to this report.

9b. OTHER REPORT NUMBER(S): If the report has been assigned any other report numbers (either by the originator or by the sponsor), also enter this number(s).

10. AVAILABILITY/LIMITATION NOTICES: Enter any limitations on further dissemination of the report, other than those

imposed by security classification, using standard statements such as:

- (1) "Qualified requesters may obtain copies of this report from DDC."
- (2) "Foreign announcement and dissemination of this report by DDC is not authorized."
- (3) "U. S. Government agencies may obtain copies of this report directly from DDC. Other qualified DDC users shall request through _____."
- (4) "U. S. military agencies may obtain copies of this report directly from DDC. Other qualified users shall request through _____."
- (5) "All distribution of this report is controlled. Qualified DDC users shall request through _____."

If the report has been furnished to the Office of Technical Services, Department of Commerce, for sale to the public, indicate this fact and enter the price, if known.

11. SUPPLEMENTARY NOTES: Use for additional explanatory notes.

12. SPONSORING MILITARY ACTIVITY: Enter the name of the departmental project office or laboratory sponsoring (paying for) the research and development. Include address.

13. ABSTRACT: Enter an abstract giving a brief and factual summary of the document indicative of the report, even though it may also appear elsewhere in the body of the technical report. If additional space is required, a continuation sheet shall be attached.

It is highly desirable that the abstract of classified reports be unclassified. Each paragraph of the abstract shall end with an indication of the military security classification of the information in the paragraph, represented as (TS), (S), (C), or (U).

There is no limitation on the length of the abstract. However, the suggested length is from 150 to 225 words.

14. KEY WORDS: Key words are technically meaningful terms or short phrases that characterize a report and may be used as index entries for cataloging the report. Key words must be selected so that no security classification is required. Identifiers, such as equipment model designation, trade name, military project code name, geographic location, may be used as key words but will be followed by an indication of technical context. The assignment of links, rules, and weights is optional.